SUBSTRATE SPECIFICITY AND ENGINEERING OF ZIP METAL TRANSPORTERS

By

Yuhan Jiang

A DISSERTATION

Submitted to
Michigan State University
in partial fulfillment of the requirements
for the degree of

Chemistry – Doctor of Philosophy

2024

ABSTRACT

The Zrt/Irt-like protein (ZIP) family consists of ubiquitously expressed divalent metal transporters critically involved in maintaining systemic and cellular homeostasis of zinc, iron, and manganese. As a highly diverse family, ZIPs exhibit very different substrate preference, but the molecular mechanism underlying the variations in substrate specificity has not been clarified. The ultimate goal of my research is to elucidate the mechanism of how ZIPs distinguish chemically similar *d*-block divalent metals. Here, I present an engineering method for human ZIP8, where four differentially conserved residues were rationally mutated into their counterparts in human ZIP4, creating a zinc-preferring quadruple variant (Q180H/E343H/C310A/N357H), which exhibited largely reduced transport activities towards Cd^{2+}, Fe^{2+}, and Mn^{2+} whereas increased activity toward Zn^{2+}, “turning” human ZIP8 into a human ZIP4-like transporter. Current progress is related to a conditional selectivity filter identified in the process, which appeared to be the molecular determinants of the substrate preference of ZIPs. To better biochemically study ZIPs, I developed a non-radioactive metal uptake assay by taking advantages of inductively coupled plasma mass spectrometry (ICP-MS) and rare stable isotopes. Combined with the quantification of the cell surface expression of human ZIP4 using biotinylation or surface-bound antibody, I estimated the turnover number of human ZIP4 to be 0.08-0.2 s^{-1}, clearly classifying human ZIP4 as a carrier. Zn efflux effect during the cell-based assay was evaluated to exclude the possibility that metal efflux may significantly affect

data interpretation in the cell-based metal transport assay. The potential of converting the current approach into a high-throughput format by using laser ablation (LA) ICP-MS was explored. Taking advantage of these progress, I am applying the ICP-MS method to a further study on the conditional selectivity filter, where different amino acid compositions of residues were introduced into the selectivity filter (Q180/D318/E343) to screen the change in the substrate preference. This work led to the discovery of variants with drastically increased activity and altered substrate preference. Selected variants also exhibited novel activities against metals that are not substrates of wild-type ZIP8, including Pb^{2+} and the diatomic cation VO^{2+}. I believe this research provided clearer understanding of the ZIP family and useful approaches that can be applied to the studies of metal transporters beyond the ZIP family.

ACKNOWLEDGEMENTS

I would like to express my deepest gratitude to everyone who has supported, helped, and guided me throughout my PhD journey.

First and foremost, I extend my heartfelt thanks to my advisor, Dr. Jian Hu, for his unconditional support academically, financially, and morally. Dr. Hu is an outstanding scientist himself, and it has been a great honor to be guided by him into the world of research. His extensive and profound knowledge of the field, insightful understanding of the projects, and diligent work ethic have inspired and encouraged me to strive harder and mold myself into a professional researcher just like him. He consistently reminded me to stay humble during moments of success and provided hope and direction during times of difficulty. These invaluable lessons have taught me the importance of focusing on unanswered questions and persevering through challenges, for better and for worse. I am deeply privileged to be Dr. Hu's student and will be forever grateful for his mentorship.

I would like to thank Dr. Dexin Sui for leading me and teaching me almost all the techniques that I know today. Dr. Sui was the senior technician in the lab who has been working in the department even before I was born. I was always amazed by how well he knows about biochemistry and molecular biology, and I was always wondering how many more tricks (experimental techniques) he hid up in his sleeves. His rigorous working style, not only for experiments but also for things going from lab arrangements

to tube labeling all left deep marks on me. I feel extremely fortunate to have learned from the best at the start of my career. Now that he is retired, I wish him a happy and fulfilling retirement.

Dr. Chi Zhang was another person that I can't thank enough for their guidance to me. She was a former post-doc and we sat back-to-back in the lab. She selflessly shared her extensive experimental knowledge and experiences with me. Her warm and kind personality was just like a warm spring breeze that touched everyone around her, and we shared many moments of laughter. I am grateful to have her in my journey and now she is not only a professor but also a mom, I wish her a successful career and life-long happiness.

I would also like to acknowledge the current members of the Hu lab. Dr. Yao Zhang is a post-doc in the lab who is not only doing outstanding research but also is like a big brother to everyone. He is warm-hearted and reliable, and we all feel lucky to have him aboard. Dr. Santhosh Gatreddi, another post-doc, is an incredibly hardworking individual whom I look up as a role model. Tianqi Wang, a third-year graduate student, is extremely bright and also brings a vibrant and energetic atmosphere to the lab. Michael Nikolovski, a post-undergraduate technician, is meticulous and industrious in his research work, also contributed a lot to our collaborative projects. I am grateful to have shared this extraordinary journey with such exceptional colleagues, and I sincerely wish them all the best in their future endeavors.

Finally, I want to express my deepest gratitude to my parents. I would not have made it this far without their unwavering support, guidance, and sacrifices. Their love and encouragement have been my most precious treasures and the source of my strength. Supporting me through graduate school in a foreign country has been challenging, especially since I couldn’t visit home for four consecutive years. The same goes for my grandparents as well, who have always been there for me growing up. I apologize for not being the son and grandson they deserve, and I dedicate this thesis to them. Thank you all for always being my driving force.

TABLE OF CONTENTS

LIST OF ABBREVIATIONS

AE	Acrodermatitis enteropathica
BMC	Binuclear metal center
DC	Dendritic cell
DCR	Differentially conserved residues
DPBS	Dulbecco's Phosphate Buffered Saline
EC system	Enzyme Commission system
ECD	Extracellular domain
EDS	Ehlers-Danlos Syndrome
ER	Endoplasmic reticulum
FBS	Fetal bovine serum
HEK	Human embryonic kidney cells
HRD	Helix-rich domain
ICP-MS	Inductively coupled plasma-mass spectrometry
IFC	Inward facing conformation
IL	Intracellular loop
LA-ICP-MS	Laser ablation-inductively coupled plasma-mass spectrometry
MD	Molecular dynamics
MRE	Metal responsive element

MT	Metallothionein
OFC	Outward facing conformation
PCD	PAL-motif containing domain
SLC	Solute carrier family
TM	Transmembrane
TMD	Transmembrane domain
TOF	Time-of-flight
ZnT	Zinc transporter
ZIP	Zrt/Irt-like protein

CHAPTER 1: INTRODUCTION

1.1 Introduction of Zn

Zinc (Zn) is a greyish, light blue metal, with a density of 7.140 g/cm^3 and a melting point of 692.68 K (419.53 ℃). Under room temperature Zn is brittle. It is occupying 0.0075% of the Earth's crust and is therefore ranked 24th in the most abundant element[1]. There are two possibilities of the origin of the name zinc. The first one is that it derived from a Persian word “seng” or “sing”, meaning stone, while the second one was from a 16th century book *Liber Mineralium II*, written by a German alchemist Paracelsus, where the word was referred to as "zincum" or "zinken"[2].

Since the first recognition of the physiological significance of Zn in lives[3], many early studies have revealed the necessity of Zn for the growing of plants[4], rats[5] and birds[6]. The significance of Zn in human was not remarked however, until 1961, when Zn was recognized as a necessary micronutrient for human[7]. In modern biological studies, the great significance and essential roles of Zn have been constantly proven in all kingdoms of lives, including animals[8–12], plants[13] and microorganisms[14].

In human body, Zn is an indispensable element and is also the second most abundant trace, only after iron[15]. Because of its full *d* shell orbitals, Zn is different from other biologically important transition metals such as Fe and Cu, as it is not involved in redox reactions. Main roles for Zn in lives including catalytic, structural and signaling[16,17]. The great importance of Zn to lives lies not only in the multiple facets of roles it is playing, but also the broad range of processes it is involved in.

As the second most abundant trace element in human, there is about 2-3 grams of Zn in an adult's body, distributed mostly in skeletal muscle (60%), followed by bone (30%), liver and skin (5%, combined), other major organs including brain (1.5%), kidney (0.7%) and heart (0.4%)[18,19]. Such wide range of distribution provides supporting evidence from the tissue level that it is vital for our body to maintain a strictly controlled Zn homeostasis. In fact, early studies in rats demonstrated that dietary uptake of Zn ranging from 10 to 100 mg/kg did not alter whole body Zn amount of the testing subjects, which was maintained a constant around ~30 mg/kg, suggesting a robust homeostatic system[20].

Bioinformatic studies have pointed out that about 2800 human proteins are potentially Zn-binding proteins, taking up 10% of the human proteome[15]. However, Zn did not always have such deep and wide involvement in lives, and it was probably a gift from the shift of Earth's early environment. Studies on Earth's early atmosphere and oceans pointed out that Zn was not easily accessible until the geochemical shift that turned the ancient sulfide-rich ocean into the modern sulfate-rich ocean[21,22]. The shift from sulfide to sulfate not only represented the ocean oxygenation, but also suggested the release of Zn, providing foundations of the rise for Zn-bound protein structures such as Zn fingers. This is without doubt one of the biggest turning points in the development of early life forms and is even considered prerequisite for the appearance of eukaryotes[23].

1.2 Physiological roles of Zn

Zn plays numerous roles in living organisms, which can be categorized into structural, catalytic and signaling roles.

1.2.1 Structural role of Zn

The structural role of Zn associated with proteins was first revealed in a very early crystallography study about insulin[24]. Since then, more studies were published on structural Zn and the role it is playing has been clearer to the community. The structural role of Zn in a protein is in a way similar to that provided by disulfide bonds[25]. The stable coordination of Zn in the complexes ensures the stability of the protein, both locally and globally. In structural Zn sites, Zn is usually coordinated by four residues in a tetrahedral geometry. Among all the residues coordinated to Zn, cysteine is the most commonly observed one, followed by histidine, and aspartate as well[26,27].

Zinc finger motif is one of the most important structural roles that Zn is playing. It is a small motif that features in coordinating one or more Zn ions and therefore stabilizing the protein structure. Zinc finger motif was firstly identified in African clawed frog (*Xenopus laevis*), in a study on transcription factor IIIA. It was by then considered a special DNA-binding motif only presented in *Xenopus laevis* until later when people found out that this structure can be ubiquitously found in a vast amount of different protein structures[28–30].

C2H2 (Cys2-His2) Zn finger is one of the most commonly found domains in transcription factors of eukaryotes and it is also the best characterized class of zinc finger

proteins (**Figure 1.1A**). The classical C2H2 domain has 28-30 amino acids, forming a β-hairpin (two β-strands in the antiparallel orientation with a linker in between) and a α-helix and therefore a ββα fold. The Zn coordination site is made up of two conserved cysteine residues from the end of the β-strand and two histidine residues at the C-terminus of the α-helix. Within this C2H2 domain, the two cysteine and histidine residues as well as the residues forming the hydrophobic core of the α-helix are conserved while the remaining parts could be variable[31,32]. Mammalian Zif268 is one of the first characterized and also best characterized proteins in this class. Within this DNA-binding protein, there are three zinc fingers forming a semicircle structure to bind the major DNA groove and are usually spaced at 3-bp intervals. The α-helix within the structure act as recognition helix that can make sequence-specific contacts to DNA bases and therefore provide guidance to the protein[33].

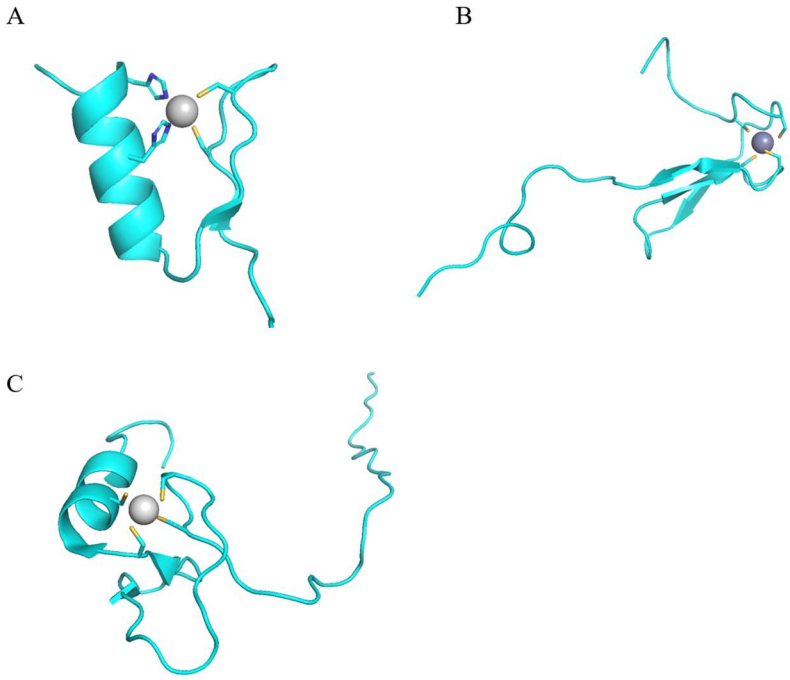

Figure 1.1. Zinc finger motifs. Zinc ions were shown in sphere, coordinated residues to the Zn ions were shown in stick mode. **(A)** C2H2 zinc finger motif from the TFIIIA in Xenopus laevis (PDB ID 1TF3)[34]. **(B)** Zinc ribbon domain in the N-terminal domain of TFIIB from Pyrococcus furiosus, (PDB ID 1PFT)[35]. **(C)** Treble clef domain from the human MYM-type protein 5 (PDB ID 2DAS)[36].

Zinc ribbon is structurally simpler than other major groups of zinc finger motif but is also considered as the largest fold group. It is usually made up of two β-hairpins and the Zn ion in this structure is coordinated to 4 cysteine residues, two from each hairpin structure (**Figure 1.1B**). Many transcription factors adopt this motif, including TFIIS, TFIIB, RNA polymerase II subunit 9 RPB9 and Topoisomerase I and III[35,37–39]. Another example of zinc ribbon domain in a protein is protein kinase CK2, where the zinc ribbons do not just form zinc coordination sites but are also in contact with each other and form homodimers through hydrophobic interactions[40].

Treble clef zinc fingers are a large group of protein whose functions vary greatly. The core of a treble clef zinc finger is complicated, including a zinc knuckle, a loop, a β-hairpin and a α-helix, in the order from N- to C- terminal (**Figure 1.1C**). The zinc knuckle refers to a conserved "CPXCG" motif and can be regarded as a shorter and tighter β-hairpin. The coordination site of Zn is normally made up of two residues from the zinc knuckle and two from the first turn of the helix[39,41]. Studies have constantly pointed out that treble clef is very versatile in its function and can possess different structural modifications. For example, RING domain of RAG1 has an additional zinc ion sharing chelating residues with the coordinated Zn to form a metal cluster[36].

1.2.2 Catalytic role of Zn

The first identification of the catalytic role of Zn can be dated back to 1939 when erythrocyte carbonic anhydrase was found to be a Zn-dependent enzyme[42]. Since then, more and more catalytic roles of Zn have been found and explored.

A catalytic Zn refers to a Zn ion that is right at the active site of an enzyme and is directly reacting with the substrates and therefore part of the catalysis and reaction. Different from structural Zn, a catalytic Zn usually has an open coordination sphere, which means in the usual four coordination geometry, at least one of the ligands is a water molecule[43–47]. However, in some cases such as adenosine deaminase where the catalytic Zn is adopting a trigonal bipyramidal geometry, the Zn ion is coordinating with 4 amino acid side chains and a water molecule[48,49]. The most commonly seen and the

predominant residues coordinating to Zn at catalytic Zn site is histidine. Glutamate, aspartate and cysteine are also seen at the catalytic site[44,50].

There are a total six classes of enzymes that were defined in the enzyme commission (EC) system, that is hydrolases, transferases, oxidoreductases, ligases, isomerases and lyases. Zn can be found in all six of them. Granted Zn also plays some other roles in these enzymes, the catalytic Zn in most of these classes is over 75%. With all the Zn enzymes, hydrolase is the biggest class, taking up 59% of the total Zn enzymes. Consistently, Zn enzyme is also a significant part of the hydrolases, where 25% of the hydrolases have Zn and 21% have Zn that plays a catalytic role[50,51]. Zn can play two roles in hydrolases, including formatting a hydroxide ion from the water molecule it coordinated to for attacking substrates, and also promoting electrophilicity of the substrate through polarization of C-O or P-O bond by coordinating to the oxygen atom. In the case of carboxypeptidase A[52] and thermolysin[53], only one Zn was required for both jobs, whereas for other cases such as alkaline phosphatase[54,55] and phospholipase C[56] two or even three Zn centers were required.

Catalytic mechanism outside of the hydrolases is very different from what previously described. It usually involved transfer of a proton to an active site, triggered by zinc binding and the increase of the acidity of the proton. This proton transfer will promote electronic rearrangement of the substrate and is the most commonly seen mechanism in non-hydrolytic enzymes (87% of the cases), enzymes such as 3-dehydroquinate

synthase adopts similar mechanism[57]. In oxidoreductases, similar electron rearrangement can also be seen. Structural studies on the super family of alcohol dehydrogenases demonstrated that Zn could shift from multiple coordination modes during the reaction cycle to participation in the redox reaction[58].

In transferases and ligases, Zn usually plays a structural role instead of catalytic role. In these enzymes, there is usually only one Zn ion whose main job is to stabilize the protein structure. This could be right next to the active site of the enzyme such as the case shown in galactose-1-phosphate uridylyl transferase[59] or within the zinc finger motif within the protein like CREB-binding protein[60].

1.2.3 Zn and cell signaling

Other than structural and catalytic roles, another crucial part that Zn is playing in cells is regarding cell signaling. The significance of Zn as a signaling molecule has been emphasized and commented as “Zinc is the calcium of the 21st century”[61]. The modulating and signaling work were achieved due to fluctuations of the Zn concentration, which regulates many physiological processes and is also often connected to pathological events. In chemical signaling, Zn acts as a signaling molecule in endocrine, paracrine, and autocrine systems; in the nervous system, Zn is released by presynaptic neurons and participates in synaptic transmission[61–63]. Some cell surface proteins can bind to Zn and further regulate downstream activities, including G protein-coupled receptor 39

(GPR39)[64,65]. Zn can also suppress insulin degradation and therefore connected to glucose and insulin metabolism[66,67].

Within cells, Zn acts as a second messenger[68,69], which can come from either outside or inside of the cells. In fact, Zn release from subcellular organelles such as endoplasmic reticulum (ER) was referred to the source of “zinc wave” and it has been considered as an indispensable part for the signaling functions[70,71].

Another important part of the intracellular release is from the cytosolic Zn-bound proteins. A well-known example for that is metallothionein (MT), which is a protein family sensitive to oxidation and will release Zn upon oxidative stimulation, and therefore is often involved in Zn signaling[72,73]. In many organisms including mammals, MT is regulated by the zinc-responsive transcription factors. MTs are small and cysteine-rich metal binding proteins that can bind to zinc, copper, cadmium and other heavy metal ions. Because their expression levels correlate with zinc amount, it can therefore bind to excess zinc when there is too much zinc in the system. In the meantime, MT can also donate zinc to the zinc-binding site of other zinc-coordinated proteins. These protective and delivering roles represent a buffering effect of MT in the cytosolic environment.

Zn-responsive transcription factors can be ubiquitously found in all kingdoms of life and play significant roles in signaling and zinc homeostasis. They can generally be divided into two classes, one protects cells from zinc deficiency and promote expression or gene related to Zn uptake while the other protects cells from zinc overload and activate

processes including Zn efflux and storage. One of the well-studied Zn-responsive transcription factors is MTF-1, whose main role is to protect cells from excessive amount of Zn. In mammals, MTF-1 usually binds to metal responsive elements (MREs) in the promoters of the target genes, which will be followed by the target gene expression[74]. There are also exceptions, such as the in the case of *Zip10*, which plays a vital role in cellular Zn uptake in hepatocytes. MTF-1 binds to the MRE downstream to the transcriptional start site of *Zip10* and the binding of MTF-1 prohibits the progression of the RNA polymerase II and therefore suppress the expression of *Zip10*[75]. Zn-responsive transcription factors like MTF-1 are actively regulating Zn homeostasis within our bodies.

Zn signaling can be further categorized as “fast” or “early” signaling and “late” signaling. “Fast” or “early” signaling refers to those that happen immediately after stimulation within seconds or minutes and more importantly without the need for protein synthesis[71,76]. “Late” signaling, on the other hand, requires change in gene expression and can affect a series of downstream processes, which could happen hours after the stimulation[77]. In general, Zn signaling affects a various of enzymes, including phosphodiesterase (PDEs)[78,79], protein tyrosine phosphatases (PTPs)[80,81], calcineurin[82], and a series of kinases including protein kinase C (PKC) and mitogen-activated protein kinase (MAPK) [83,84]. Furthermore, it is noteworthy that free Zn^{2+} concentrations required for signaling via these enzymes are low, with the IC_{50}/EC_{50} values of low nanomolar level[85,86].

1.3 Zn transporters

1.3.1 Identification of the Zn transporters

The first Zn transporter protein was identified in yeast cells. In 1989, a DNA fragment isolated from yeast genome library was found capable to confer Zn and Cd resistance to yeast cells, the protein was later named as Zn resistance conferring protein or Zrc1[87]. Later on, more proteins that share similar sequence to Zrc1 were identified, including COT1 from *S. cerevisiae*[88] and CzcD from *Alcaligenes eutrophus*[89]. These proteins, similar to Zrc1, can confer metal resistance to the cells against Zn, Co, Mn and Cd, and they also shared significant similarities with Zrc1. A few years later in 1995, the first ZnT transporter (Zn transporter) was isolated and identified from a rat kidney cDNA library. Through a series of experiments, functional role of ZnT-1 to export Zn out of cells was established[90]. A total 10 ZnT transporters were then quickly identified (ZnT1-10) and they were assigned as Solute Carrier family 30A (SLC30A)[91].

The story for ZIP family was a little more complicated. The first identified protein in the ZIP family was iron-regulated transporter or IRT1 from *Arabidopsis thaliana*. When expressed in yeast cells, it demonstrated Fe(II) uptake activity which can be strongly inhibited by Cd[92]. Enlightened by the discovery of IRT1, two zinc-regulated transporters (Zrt1 and Zrt2) from yeast were quickly identified as well due to high sequence similarities to IRT1[93,94]. In fact, Zrt1 and Zrt2 were reported in the same year as IRT1. The family was

therefore named by the three (or two kinds) of its founding members as Zrt/Irt-like protein, or ZIP.

On the other side of the story, ZIP6, which was firstly called as LIV-1, was identified in 1988, which was even earlier than both ZRT and IRT. Originally it was found to be involved in estrogen-regulated growth of ZR-75-1 human breast cancer cells[95]. It was not until more than 10 years later did the Zn transport ability of ZIP6 or LIV-1 was identified[96,97]. Closer look at the ZIP6 sequence revealed a unique motif CHEXPHEXGD which was also carried by a series of later identified ZIPs, therefore making ZIP6 the founding member of the largest subfamily in ZIP, which was named as the LIV-1 subfamily[97,98]. With the development of construction on human genome sequence, more ZIPs were identified until the total number of human ZIPs stopped at 14 (ZIP1-14). The ZIP family was also called as Solute Carrier family 39A (SLC39A)[99,100]. In the InterPro database (https://www.ebi.ac.uk/interpro/), the entry of IPR003689 with the title of “Zinc/Iron Permease” records approximately 69,000 sequences belonging to this ancient family from more than 18,000 species across all kingdoms of life, indicative of a fairly large family with a long history of evolution.

1.3.2 Classification and Evolution of ZIPs

Being a huge transporter family and ubiquitous in all kingdoms of lives, the ZIP family is a transporter family that’s of ancient history and great research interests. The ZIP family can be further divided into 4 subfamilies, ZIPI, ZIPII, LIV-1 and gufA basing on sequence

similarities[16,96,97]. Initially the idea of classification was to divide ZIPs into two subfamilies where subfamily I covers protein originate from plants and fungi while subfamily II covers mammalian, nematode and insects ZIPs[71]. It was later proposed that two more subfamilies, gufA and LIV-1, should be added on top of the original two subfamilies[16,102]. The name of the gufA subfamily came directly from the gufA gene from *Myxococcus xanthus* and LIV-1 is related to the estrogen-regulated gene *liv-1*, the protein encoded by which was later renamed into ZIP6[97].

For human ZIPs, ZIPI and gufA subfamilies only include one member respectively, which are ZIP9 and ZIP11; ZIPII has three members, including ZIP1, ZIP2 and ZIP3; the remaining 9 ZIPs all belong to LIV-1 subfamily, which is the biggest subfamily of the ZIP family.

In a recent elaborative phylogenetic analysis including 77 eukaryotic ZIPs and 122 prokaryotic ZIPs, all 199 ZIPs were primarily divided into 3 regions[102]. The first region was mainly prokaryotic ZIPs yet human ZIP11 was one of the few eukaryotic ZIPs within this region. ZIP11 is the only gufA ZIP and protein similarity network analysis have shown that human ZIP11 is actually closely related to several different kinds of bacterial ZIPs, including the founding protein of the gufA subfamily, MxGufA (*Myxococcus xanthus*). Phylogenetic analysis has also revealed that ZIP11 is indeed orthologous with prokaryotic ZupT proteins, suggesting a prokaryotic ancestry of the human ZIP11 protein[16,103].

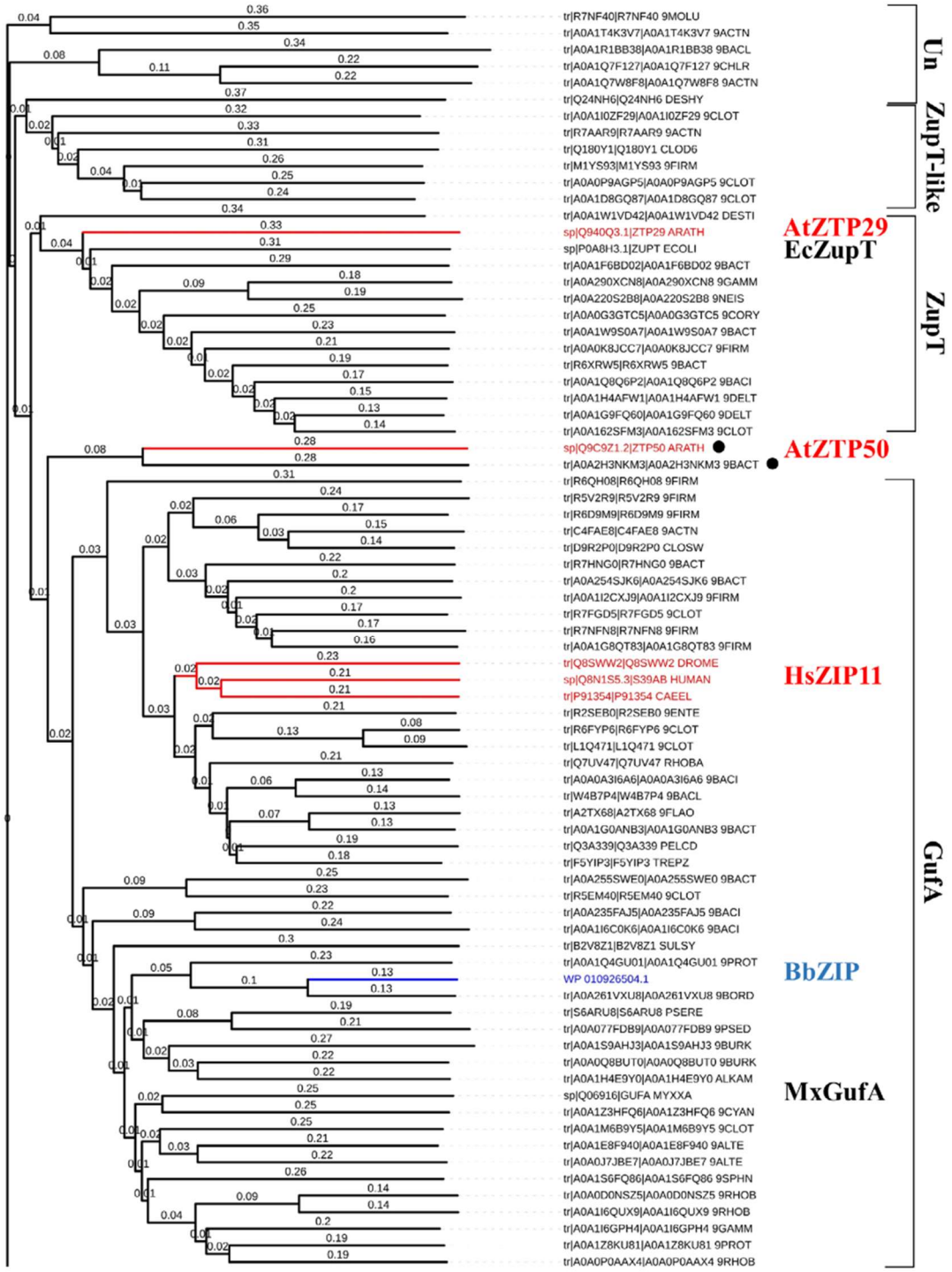

Figure 1.2. Phylogenetic tree of the ZIPs in Region I[102]. Figure is adapted from reference 102.

In the second region, the eukaryotic ZIPs were mainly from the LIV-1 subfamily. It was also worth noting the division between vesicular ZIPs (human ZIP7 and ZIP13) and

plasma membrane ZIPs (remaining LIV-1 ZIPs)[102]. The plasma membrane ZIPs could be further divided into three subgroups, basing on their extracellular domain[104]. The extracellular domain (ECD) in human ZIP4 and ZIP12 contain both helix-rich domain (HRD) and PAL-motif containing domain (PCD); human ZIP8 and ZIP14 only have PCD but no HRD; human ZIP5, ZIP6 and ZIP10 also only have PCD, but they have a long and histidine-rich loop. Sequence alignment also revealed the “structural icon” for the LIV-1 protein that is highly conserved throughout the species. In α4 and α5 there are motifs of “DGxHNFxDG” and “HExPHExGD”, respectively. These two motifs are one of the biggest hallmarks for LIV-1 protein and the latter was considered as the zinc metalloprotease motif[96,97], although there is no evidence supporting hydrolysis activity for any LIV-1 proteins.

In human ZIP8 and ZIP14, however, the α5 motif was different as the first histidine residue was replaced by glutamic acid residue. This is probably due to the needs of conferring substrate preference difference between the two close paralogs human ZIP8 and ZIP14 and all the other LIV-1 ZIPs[105].

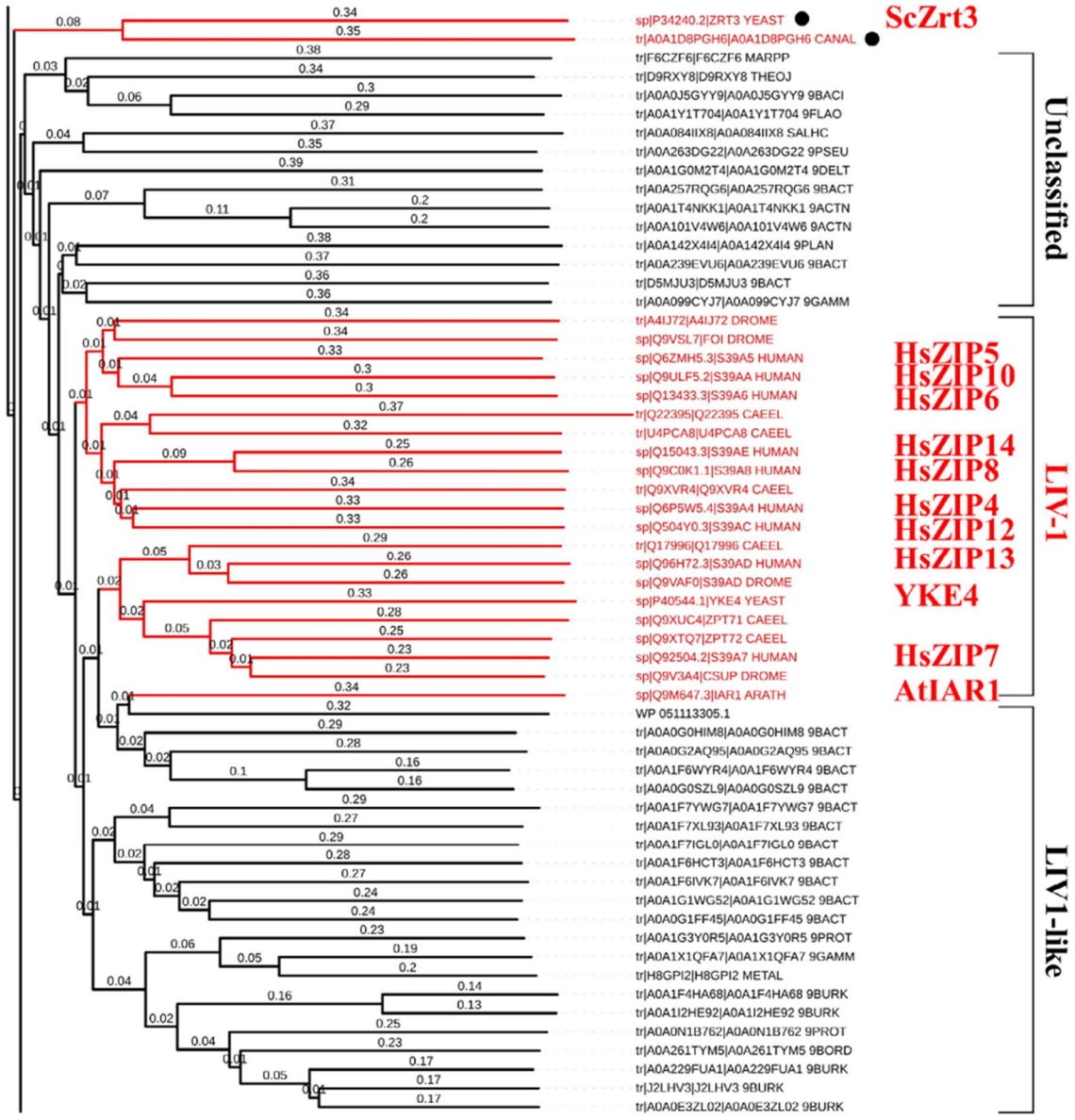

Figure 1.3. Phylogenetic tree of the ZIPs in Region II[102]. Figure is adapted from reference 102.

In the last region, the eukaryotic ZIPs can be divided into three branches. ZRT1 and IRT1, the founding members of the ZIP family, can be found in branch of the ZIPI subfamily. It is characterized with motifs at the binuclear metal center (BMC) of “HSxxIG” and “HQxFEG”. Interestingly, the isoleucine residue in the first motif was highly conserved in ZIPI subfamily while the corresponding residues in other ZIPs were either aspartate or

glutamate residues, differentiating ZIPI from other ZIPs. ZIPII subfamily, including human ZIP1-3, was also within this region three. The motif at metal binding site was “H(S/E)xFEG” and they are unlikely to have the second metal-binding site due to a positively charged lysine residue. Of great interest, human ZIP9, which was originally classified into ZIPI subfamily, was distant from ZIPI subfamily in this phylogenetic study[102,106,107]. Previous studies have also demonstrated similar results as well as a different motif at the BMC compared to ZIPI subfamily. It has been therefore suggested that ZIP9 could be considered as an independent ZIP9 subfamily[102].

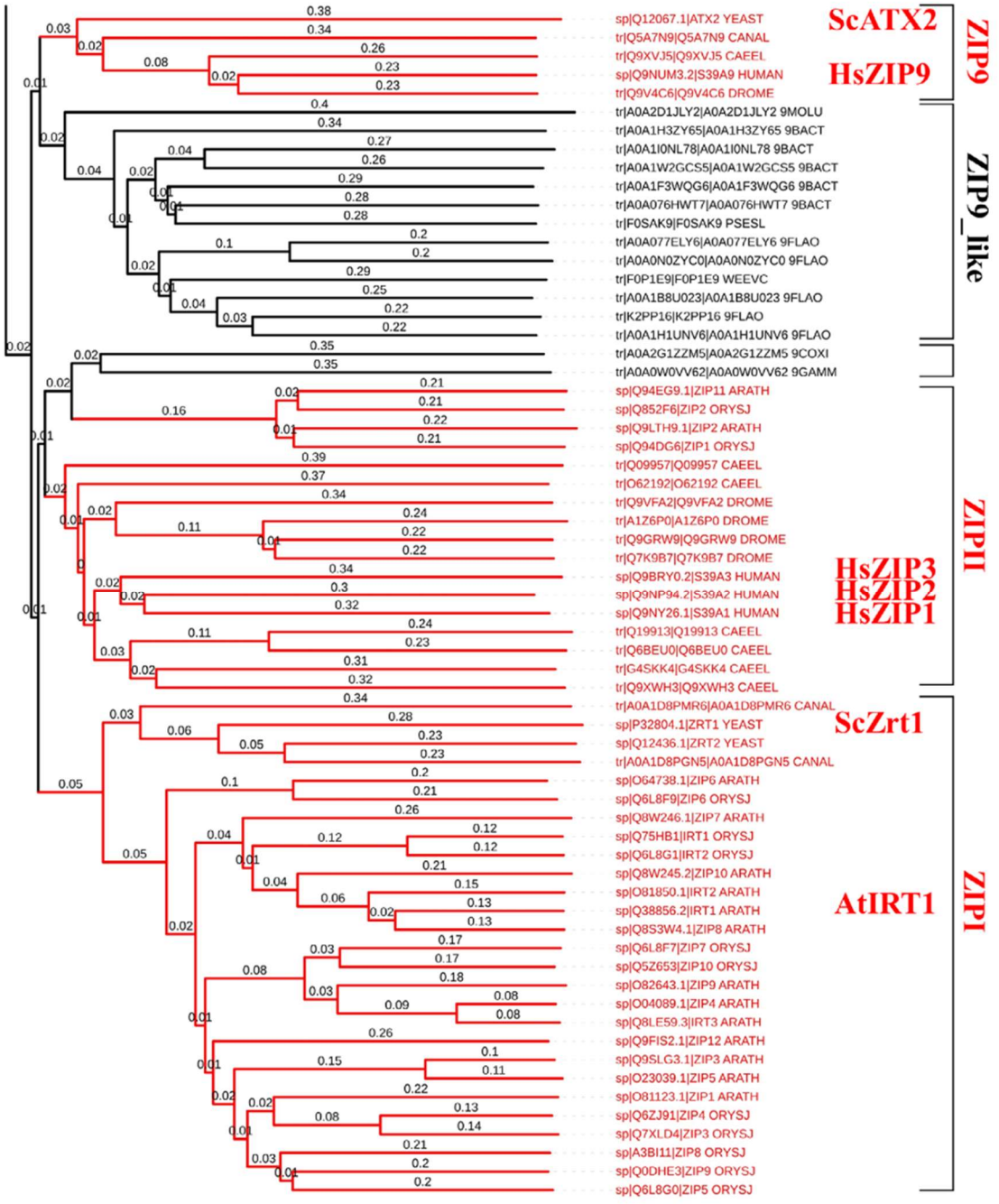

Figure 1.4. Phylogenetic tree of the ZIPs in Region III[102]. Figure is adapted from reference 102.

1.3.3 Structure of ZIPs

In most of the ZIPs, it is predicted that there are eight transmembrane (TM) domains, a long loop between TM3 and TM4 (intracellular loop 2 or IL2) that is usually histidine-

rich, and additional domains at N- and C- termini. TM4 and TM5 are amphipathic and more conserved throughout the species, suggesting a formation of metal transport pathway (**Figure 1.5A**)[108]. Later structural biology studies confirmed these early speculations. In the first crystal structure of the ZIP family, BbZIP (*Bordetella bronchiseptica*) demonstrated eight TMs and they clearly formed a tight bundle, within which an inner bundle was formed by TM2, TM4, TM5 and TM7 (**Figure 1.5B**). A pore was clearly seen in the middle of these four helices, and it was also where the metal binding sites were located, suggesting it is a metal transport pathway[109]. Newer structures of BbZIP, however, revealed a flexible extra N-terminal TM (TM0), showing the possibilities that an extra TM exists in some of the ZIP members (**Figure 1.5C**). Because it is a rare component and the amino acid composition is highly variable, it is unlikely that TM0 plays a key role in transport, but more of an activity regulation role[110,111].

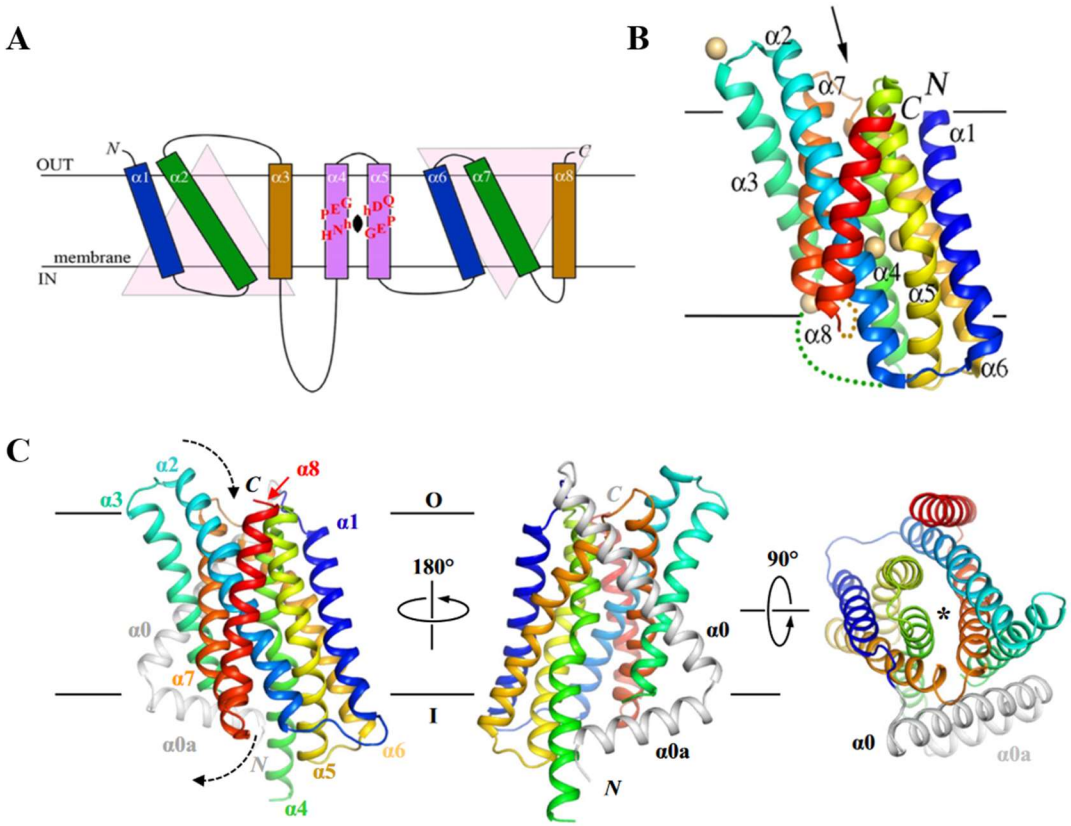

Figure 1.5. BbZIP structure. **(A)** Membrane topology for BbZIP, a representation of the ZIP family[102]. **(B)** Side view of the crystal structure of BbZIP. Coordinated metals (Cd) were shown in yellow sphere and potential metal transport pathway was pointed by black arrow[102]. **(C)** Crystal structure of the apo-form BbZIP, demonstrating an additional α0[112]. Figures in **(A)**, **(B)** were adapted from reference 102 and figures in **(C)** were adapted in reference 112.

The ZIP structure was also characterized with symmetry. There are two pairs of inverted repeats that are symmetrical correlated with an axis parallel to the membrane surface. The two pairs were TM1-3 vs. TM6-8 and TM4 vs. TM5, where TM4 and TM5 were in the middle of TM1-3 and TM6-8, like a sandwich, forming the "3+2+3" fold[102] (**Figure 1.6**).

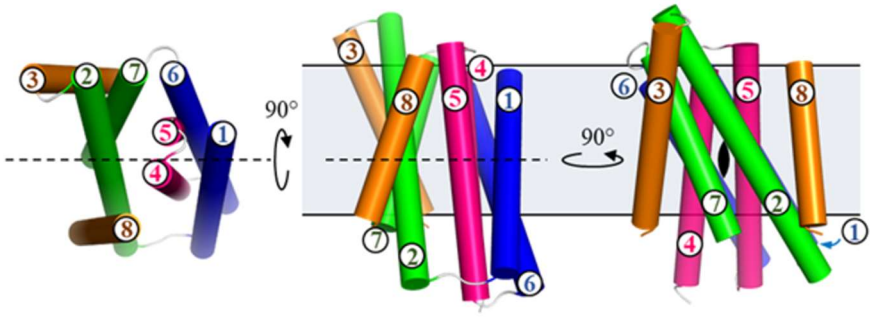

Figure 1.6. Internal symmetry as revealed in the BbZIP structure (PDB: 5TSB). The TMs are depicted as cylinders and the symmetrically related TM pairs are in the same color. The two inverted repeats (TM1-3 vs. TM6-8 and TM4 vs. TM5) are symmetrically related by a two-fold symmetrical axis shown as the dash lines (top view: *left*; side view 1: *middle*) or a symmetry sign (side view 2: *right*). Figure was adapted from reference 102.

One of the most important things identified in this first BbZIP structure was the BMC. Due to the presence of cadmium during the process of crystallization, the BMC coordinates to two cadmium ions halfway in the transport pathway through highly conserved motifs ^{177}HNhPEG^{182} from TM4 and ^{207}QD/NhPEG^{212} from TM5. The two metal centers (M1 and M2) were only 4.4Å apart, bridged by E181 from TM4[109]. Bioinformatics study covering over 17000 ZIPs the BMC is present in many ZIP members from a broad range of species, suggesting it is playing a critical role[113].

Functional studies in human ZIP4 have shown that M1 was essential for metal transport in ZIP4, without which the Zn transport ability of the protein was totally abolished; M2 however was not necessary but did affect maximum capacity of the ZIP4 and it was suggested to be involved in maintaining a stable activity across a broad pH range[113]. Indeed, a lysine residue can be found in M2 in both prokaryotic and eukaryotic ZIPs, especially for animal ZIPs, about 30% of which have the lysine residue. The positively

charged lysine residue will very likely block M2 and it is speculated that the positive charge will aid in regulating metal binding/release properties at the M1 site[113]. Functional study of human ZIP2 showed that the lysine residue, which is highly conserved in ZIP2 from different species, is crucial for transport activity[114]. It was proposed that eliminating the lysine residue may lead to a distorted geometry of the M1 site and as such impairs the transport activity. In BbZIP, eliminating the M2 site by replacing the metal chelating residues with alanine residues did not abolish Cd^{2+} binding at the M1 site[113]. In ZupT from E. coli, it was shown that the M2 site was used for the binding and transport of Fe^{2+}, but not for Zn^{2+} or Cd^{2+}, suggesting that the M2 site can be authentic transport site in some cases for certain metal substrate(s)[115].

The N-terminal of the ZIPs (extracellular domain for plasma membrane ZIPs and luminal portion for vesicular ZIPs) is extremely variable. Some of the ZIP members, especially for eukaryotic ZIPs, have large and complicated N-terminal domain which could be even conserved in subfamilies, whereas prokaryotic ZIPs usually lack this complexity and only have short and often unstructured segments. One example for folded N-terminal domain or ECD in ZIPs is human ZIP4. ZIP4-ECD has been a focus of research partially due to Acrodermatitis enteropathica (AE), as half of the AE-causing mutations occur within the ZIP4-ECD[116]. ZIP4-ECD was also of great functional role as ZIP4 mutants with part of the ECD and no ECD lost about 50% and 75% of the metal uptake ability, respectively[104]. Studies on the ECD of *Pteropus alecto* ZIP4 (pZIP4-ECD) demonstrated

that pZIP4-ECD formed a homodimer through the "PAL" motif-containing domain or PCD. This PAL motif was at the center of dimerization and is highly conserved in most of the LIV-1 ZIPs, except for ZIP7 and ZIP13[104].

A histidine-rich loop was identified within the PCD in the ZIP4 structure model, which appears to be right above the metal transport pathway. Biochemistry studies on the histidine-rich loop revealed that this dynamic loop binds to two zinc ions with an affinity at micromolar level. Alanine mutants on the loop had moderately decreased Zn transport activity compared to the wild type protein[117]. ZIP7, which is also a LIV-1 ZIP but expressed mostly on endoplasmic reticulum (ER), has a very different ECD compared to ZIP4. It doesn't have a PCD, instead, ZIP7 has tens of clustered histidine residues. With over 30% of the extracellular residues being histidine, ZIP7 has several times more histidine in the ECD than other ZIPs and is also conserved through different species. Further exploration is needed to reveal the significance of such amount of histidine residues[118,119].

The intracellular loop between the α3 and α4 is named as intracellular loop 2 or IL2. It is not conserved even within the subfamily, but is considered playing important regulation role[102]. Many efforts have been made towards understanding the IL2 from human ZIP4. Binding affinity between histidine in IL2 and the two zinc ions were nanomolar level, but NMR study suggested highly dynamic binding sites. It is then speculated that IL2 probably functions as a Zn sensor which is connected to zinc-dependent endocytosis in a high-zinc environment[120,121].

1.3.4 ZIPs and diseases

Even till these days, zinc deficiency is still a major challenge for global public health, which could lead to symptoms of growth retardation, hypogonadism, skin abnormalities, mental lethargy and severe anemia[7]. It is pointed out that 4% of the global morbidity and mortality of young children is due to zinc deficiency especially in the developing world[122]. Cases have proven that by supplementing Zn in people's daily dietary can decrease diarrhea mortality in children. Infection will be less potentially due to improved immune functions[122–125]. In general Zn is considered safe yet if used in excessive amount it could still be toxic. One example for that would be suppressing copper uptake[126].

Zn has long been found to be connected to immunodeficiency or autoimmunity. Dynamic changes in expression levels of zinc transporters were observed during dendritic cell (DC) maturation, including decrease in ZIP6 and ZIP10 expression and increase in several ZnT transporters, leading to decrease in free zinc concentration in DC[77]. ZIPs are also involved in interferon regulation. ZIP8 is highly expressed in T cells and knockdown of ZIP8 causes significantly reduce in IFN-γ secretion, which is an indicator for T cell activation. On the other hand, overexpression of ZIP8 leads to enhanced activation of T cells[82]. ZIP8 is also related to inflammation and can facilitate cytoprotection in lungs. It has been shown that ZIP8 expression in lungs is upregulated under the influence of inflammatory mediators such as LPS and TNF-α[127]. Without the expression of ZIP8 there reduces Zn in the cytosol and eventually results in cell death[128]. ZIP8's closest homolog

ZIP14 is also involved in inflammation, which is connected to the pro-inflammatory cytokine IL-6. ZIP14 expression was significantly upregulated under inflammation and IL-6 knockout mice didn't exhibit similar upregulation[129].

ZIP7 is mainly expressed on ER and with a role of maintaining the Zn homeostasis in ER, which was found to be an important piece of puzzle for B-cell development[130,131]. However, although ZIP7 is indispensable for the maturation of the B-cells, partial loss can also be tolerated and rescued, suggesting there are other related pathways and that ZIP7 is a potential target for B-cell proliferative diseases.

One of the most well-known genetic diseases linked to ZIP family is AE, which is caused by loss of function mutations that occur in human *zip4* gene. ZIP4 is expressed mainly on apical surface of enterocytes, making it at the front line of dietary Zn uptake. Therefore, it can be imagined that with ZIP4 lost functions, AE is a sever Zn deficiency syndrome with symptoms including eczematous dermatitis, alopecia, and diarrhea and can potentially be life threatening. AE can be treated by oral Zn supplements[132–134].

A novel subtype of Ehlers-Danlos Syndrome (EDS), which is a group of inherited disorders that affect connective tissues including skin, joints and blood vessel walls[135], is caused by mutations in ZIP13. This new subtype is named as spondylocheiro dysplastic-EDS (SCD-EDS) and is characterized with skeletal dysplasia especially in the spine and hands region. Mice with ZIP13 knockout demonstrated similar symptoms as SCD-EDS patient[136,137].

As Zn is playing a vast number of roles in different enzymes, an unbalanced zinc homeostasis can be involved in angiogenesis, cell proliferation, and metastasis of cancer. Therefore, it can be anticipated that abnormalities of ZIPs expression can be seen in many cancers[138].

It is well-established that hyperaccumulation of Zn is linked to breast cancer, and an increase in expression level of ZIP6, ZIP7 and ZIP10 have also been seen in breast cancer[139]. Since its identification, ZIP6 was known to be an estrogen-responsive factor that is overly expressed in breast cancer. Abnormal upregulation of ZIP6 was not only seen in breast cancer, but also in colorectal cancer[140], gastric adenocarcinoma[141], prostate cancer[142] and hepatocellular carcinoma[143]. It is worth mentioning that ZIP6 can form a heteromer with its closest homolog ZIP10[144,145], which is also playing complicated roles in cancers such as renal cell carcinoma[146] and breast cancer[147]. ZIP7 was also proposed to be a target against breast cancer[148,149].

Pancreatic cancer, which is a very deadly disease even after researchers' years of effort, is observing a significant increase in ZIP4 expression[150–153], which was reportedly through mediating the IL-6/STAT3 pathway[153]. Considering ZIP4 is a high-affinity zinc transporter playing a critical role in dietary zinc uptake and zinc reabsorption from urine, it is reasonable to see that the aberrant upregulation of ZIP4 can provide enough zinc to support the growth and proliferation of cancer cells. In fact, upregulation of ZIP4 has been seen in many other cancers including glioma[154], ovarian cancer[155], lung cancer[156],

nasopharyngeal carcinoma[157], hepatocellular carcinomas[158] and oral squamous cell carcinoma[159]. Supporting evidence from the opposite side was also seen as ZIP4-knockdown cancer cells were more sensitive to Zn-depleted environment and is more prone to zinc-depletion induced apoptosis[160]. All these ZIP4 studies in oncology exhibited the broad expression and significance of ZIP4 in different kinds of cancers, yet physiological localization of ZIP4 is specifically expressed mainly in intestine and kidney, making ZIP4 a potential anti-cancer target. ZIP4-containing exosomes in blood samples have also been used as biomarkers for diagnosis of pancreatic cancer[161].

Reduction of Zn concentration is also not uncommon in cancer. A decrease in Zn accumulation was observed during the development of prostate cancer, which is probably due to decreased expression of ZIP1 and abnormal distribution of ZIP3 to lysosomes[162–164]. Low level of Zn caused by downregulation of ZIP3 was found linked to pancreatic adenocarcinoma as well[165,166].

Efforts in therapeutic development targeting ZIPs have been made. A ZIP7 inhibitor targeting the Notch pathway was identified and its mechanism was found to be inducing ER stress-mediated apoptosis through affecting Notch trafficking. This inhibitor binds to ZIP7 within the metal transport pathway and because of the similarities of the transmembrane domain (TMD) among the ZIP members, this work could inspire the inhibitor development of other ZIP members[167].

Antibodies targeting ZIP members were also under study. It was demonstrated that ZIP6 and ZIP10 antibodies could block mitosis of culture cells[145]. Another work on a conjugated ZIP6 antibody was demonstrated efficient in suppressing and treating metastatic breast cancer[168].

1.3.5 Mechanism of the ZIPs

An energy-independent transport mechanism has been revealed in human ZIP1 and ZIP2 right after these two transporters were identified[169,170]. Early experiments have pointed out that when treated with HCO_3^-, Zn uptake by human ZIP2 was significantly increased by over 50%. Moreover, Zn transport by human ZIP2 was inhibited by lower pH (pH<7) but was stimulated as pH increases, which could be explained as higher HCO_3^- concentration. These suggested a Zn^{2+}-HCO_3^- cotransport mechanism for ZIP2. Similar effects were not seen in human ZIP1[169,170], but $Zn^{2+}/[HCO_3^-]_2$ or $Cd^{2+}/[HCO_3^-]_2$ symport mechanism was proposed in human ZIP8 as well as its closet homolog human ZIP14, where human ZIP14 demonstrated a more than three times increase in metal uptake compared to negative control when treated with bicarbonate[171,172]. A totally different mechanism however was proposed for a bacterial ZIP. It is claimed that this BbZIP is adapting a non-saturable channel-like mechanism[173].

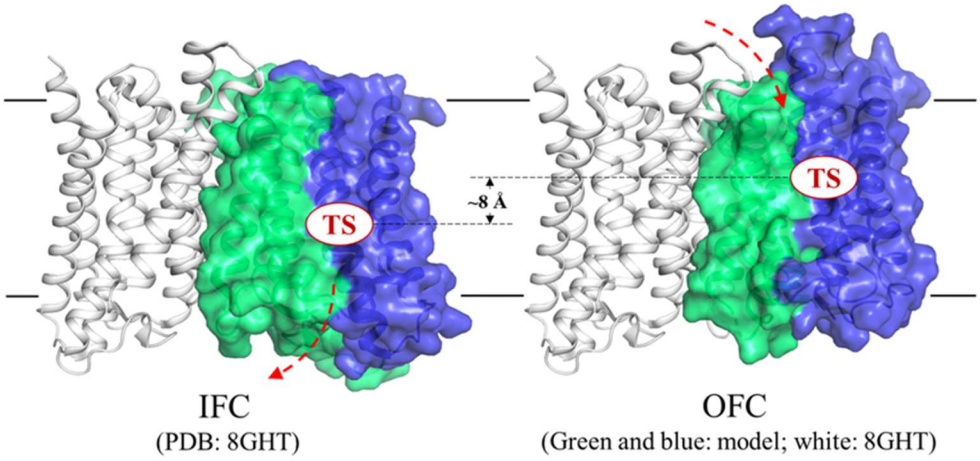

Figure 1.7. Elevator transport mode. Proposed elevator motion. On the left is inward facing conformation (IFC), on the right is the outward facing conformation (OFC). One protomer of the BbZIP dimer is shown in cartoon mode (white) and the other protomer is shown in the surface mode with the scaffold domain in green and the transport domain in blue. The dashed arrows indicate metal binding/release to/from the transport site (TS). The rigid-body motion of the transport domain relative to the scaffold domain and the vertical displacement of the transport site support an elevator mode.

Despite of distinct transport mechanisms suggested by biochemical studies, systematic study combined structural, biochemical, and computational studies strongly indicate that the ZIP family members share a same transport mode, i.e. the elevator mode (**Figure 1.7**), which is one of the three major transport modes for solute carrier proteins[174]. The evidence supporting the elevator transport mode are elaborated below:

Two-domain architecture. The experimental data supporting the elevator mode all came from the study of BbZIP. Analysis of the first BbZIP structure led to a speculation that the eight TMs of BbZIP be composed of two domains: a helix bundle formed by TM1/4/5/6 and a flat helix sheet formed by TM2/3/7/8[109]. It was also hypothesized that the relative movement of the two domains would lead to alternating access. The two-

domain architecture was later confirmed by the structures of BbZIP in the apo state[110,112]. Comparison with the structures in the cadmium bound state revealed a two-domain architecture and the relative rigid-body movement between the domains – a helix bundle (TM1/4/5/6) and a wall-like helix sheet (TM2/3/7/8). Evolutionary covariance analysis further supported the presence of two independent domains and also showed that many of the predicted interdomain interactions are not consistent with the experimentally solved IFC, suggesting the presence of an alternative conformation that would match the prediction better.

Experimentally validated outward-facing conformation model. The apparent internal symmetry of the BbZIP structure (**Figure 1.6**) allowed the generation of an OFC model by using repeat-swap homology modeling, a computational approach has been used to study many other transporters. This OFC model has been biochemically validated by cysteine accessibility assay and chemical crosslinking. Structural comparison of the OFC model with the experimentally solved IFC unraveled an upward movement of the helix bundle (transport domain) relative to the helix sheet (scaffold domain). This result not only confirmed the two-domain architecture but also revealed a vertical displacement of the transport site, which is exclusively located in the transport domain, by approximately 8 angstroms.

Dimerization mode. It has been known that ZIPs form homo- or heterodimers[104,173,175,176]. Although the early crystal structures of BbZIP only showed a

monomeric state, probably due to the unstable dimerization in detergent micelles, a later crystal structure of BbZIP solved at a low pH revealed a potential dimerization interface between the neighboring asymmetric unit[110], which was also predicted by evolutionary covariance analysis and validated by chemical crosslinking[112]. This dimerization interface was later experimentally confirmed by the cryo-EM structure of BbZIP[177]. Consistent with the proposed elevator mode, BbZIP forms a dimer exclusively through the scaffold domain and oligomerization of the scaffold domain is believed to promote the overall stability of the transporter.

AlphaFold predicted structure models. AlphaFold 2.0 works particularly well for the protein families with a large number of family members, such as the ZIP family, because the performance heavily depends on multiple sequence alignment to generate restrains for structure construction. Indeed, a folded IL2 loop in BbZIP has been predicted by AlphaFold even before the cryo-EM structure reported this novel structure feature. Using a modified version of the AlphaFold algorithm, both IFC and OFC conformations of human ZIPs were obtained computationally[178]. Comparison of the IFC and OFC structures consistently supported the elevator-like movement. Of great interest, the fourteen human ZIPs are predicted to be in different conformational states (https://alphafold.ebi.ac.uk/), and structural comparison with the BbZIP structures revealed a continuous spectrum of conformational states ranging from IFC to OFC[112] (**Figure 4B**), strongly suggesting that

the proposed elevator mode is likely applicable to many, if not all, members of the ZIP family.

1.4 Selectivity of the ZIPs

The ZIP family is a big family with 14 members, although as a Zn transporter family they can all transport Zn, there is different substrate preference among some of the ZIP members. The substrate preferences of the ZIP members are summarized below.

			substrates		references
			direct measurement	competition	
ZIP II subfamily	ZIP1	Human	Zn(II)	Fe(III), Ni(II), Cu(II), Cd(II)	[170]
		Mouse	Zn(II)	Ni(II)	[179]
		Mouse	Zn(II)	Fe(II), Ni(II), Cd(II), Co(II), Cu(II)	[180]
	ZIP2	Human	Zn(II)	Mn(II), Fe(III), Co(II), Cu(II), Cd(II)	[170]
		Human	Zn(II)	Mn(II), Fe(III), Co(II), Cu(II), Cd(II)	[169]
		Human	Cd(II)	Cu(II), Zn(II), Co(II)	[181]
		Mouse	Zn(II)	Ni(II)	[179]
	ZIP3	Mouse	Zn(II)	Mg(II), Mn(II), Ni(II), Co(II), Cu(II), Ag(II), Cd(II)	[179]
LIV-1	ZIP4	Mouse	Zn(II)		[182]
		Human	Zn(II), Cu(II), Ni(II)	Cu(II), Ni(II)	[183]
	ZIP5	Mouse	Zn (II)		[184]
		Human	Zn(II), Mn(II), Co(II), Ni(II), Cu(II)		[185]
	ZIP6	Human	Zn(II)		[186]
	ZIP7	Human	Zn(II)		[187]
		Human	Zn(II)		[188]
	ZIP8	Mouse	Cd(II)		[189]
		Mouse	Cd(II), Mn(II)	Mn(II), Hg(II)	[190]
		Mouse	Zn(II), Cd(II), Fe(II)	Hg(II), U(II), Pt(II)	[191]
		Human	Zn(II), Cd(II), Fe(II), Mn(II)		[105]
		Human and Mouse	Se(IV)		[192]
		Human	Zn(II), Cd(II), Mn(II), Se(IV)		[193]
	ZIP10	Rat	Zn(II)	Cd(II)	[194]
		Human, dog, fly	Zn(II)		[195]
		Human	Zn(II), Cu(II), Ni(II)		[185]

Table 1.1 Summary of the substrate selectivity in the ZIP family.

Table 1.1 (cont'd)

	ZIP12	Mouse	Zn(II)		196
		Mouse	Zn(II)		197
		Human	Zn(II)		198
	ZIP13	Human	Zn(II)		175
		Human	Zn(II)		199
		Fly	Fe(II)		200
	ZIP14	Human	Zn(II)		201
		Mouse	Zn(II)		129
		Mouse	Zn(II), Fe(II)		202
		Mouse	Cd(II), Mn(II)	Zn(II), Cu(II)	172
		Mouse	Zn(II), Cd(II), Mn(II), Fe(II)		203
		Human	Cd(II)		204
		Mouse	Zn(II), Cd(II), Fe(II)	Co(II), Cd(II), Ni(II), Mn(II), Pb(II)	191
		Human	Zn(II), Cu(II), Mn(II), Fe(II), Co(II), Ni(II)		185
ZIP II subfamily	ZIP9	Croaker	Zn(II)		107
		Human	Zn(II)		205
GufA	ZIP11	Mouse	Zn(II), Cu(II)		206
		Human	Zn(II)		207,208
	BbZIP	*Bordetella bronchiseptica*	Zn(II), Cd(II)		173
	ZupT	E. Coli	Zn(II)		209
		E. Coli	Fe(II), Co(II)		210
		E. Coli	Zn(II), Mn(II), Co(II), Cd(II)		211
	IRT1	*A. thaliana*	Fe(II)		92
		A. thaliana	Mn(II)	Zn(II), Cu(II), Fe(II), Cd(II)	212
		A. thaliana	Fe(II), Zn(II), Mn(II), Co(II), Cd(II)		213
	Zrt1	*Saccharomyces cerevisiae*	Zn(II)		93

Table 1.1 (cont'd)

	Zrt1	*Saccharomyces cerevisiae*	Cd(II)		214,215
	Zrt2	*Saccharomyces cerevisiae*	Zn(II)	Fe(II), Cu(II)	94

Among the earliest characterization of ZIP1 people found that ZIP1 transfected human K562 erythroleukemia cells can transport Zn into the cells and this process was inhibited by the presence of 6-time Ni (50%), Cu(II) (25%), Fe(III) (50%), Cd (25%), but not by Co, Mg, Mn[170]. Further testing on mouse ZIP1(mZIP1) showed quite different result, however, where Zn uptake was not inhibited/slightly inhibited by Cu, Cd, Mn, Co, Ag, Mg, Fe, but inhibited by Ni[179]. Detailed radioactive competition assays were done on mZIP1 to obtain deeper understanding of the competitors against Zn, revealing that Fe and Ni completely inhibited Zn uptake while Cd and Co showed a non-competitive inhibition towards Zn uptake in mZIP1 transfected HEK293T cells. The affinities of these tested metals towards mZIP1 were in the order of, basing on their K_i and K_m values, Fe>Zn>Ni=Cd>Co. Cu(II) was shown able to inhibit Zn uptake as well[180].

human ZIP2 was characterized in similar ways as human ZIP1, finding that Zn uptake was significantly inhibited by 6-time Mn(II), Fe(III), Co(II), Cu(II), Cd(II), but not by Ni(II), different from human ZIP1[1,169]. With only Zn uptake being directly measured in these early characterizations, Cd uptake by human ZIP2 was directly studied in recent years taking advantage of a Cd dye, confirming Cd can also be transported by human ZIP2. Competition against Cd showed completely inhibition in the presence of 50-time Zn, 75% and 25% inhibition by Cu(II) and Co(II), respectively. No significant inhibition was seen for Mn(II) and Ba(II). Radioactive ^{55}Fe was also used to evaluate iron transport, showing no difference compared to negative control[181]. Cd uptake by ZIP2 is also supported by

plant ZIPs studies. Yeast cells expressing a plant ZIP, *S. plumbizincicola* ZIP2 (SpZIP2) showed much higher Cd sensitivity and direct measurement by ICP-MS demonstrated a 20% increase compared to negative control[216]. For mouse ZIP2, competition assay against Zn showed only modest inhibition by all tested metals including Cu, Cd, Mn, Co, Ag, Mg, Ni and Fe, with Ni having the strongest inhibition, suggesting mouse ZIP2 is specific to Zn[179].

Specificity of ZIP3 is less known compared to other members from the subfamily. Competition assay on mouse ZIP3 showed that Zn activity was greatly inhibited by almost all tested metals including Cu, Cd, Mn, Co, Ag, Mg, Ni, but not inhibited Fe. This suggested that ZIP3 might be a more promiscuous transporter compared to its close paralogs ZIP1 and ZIP2[179].

ZIP4 is well known for its Zn specificity and its connection with AE, a sever Zn deficiency syndrome. In several different early studies, Zn transport activity by mouse ZIP4 was directly studied and clearly demonstrated by radioactive ^{65}Zn assays[182,217,218]. Its substrate specificity was also studied by competition assays and Zn uptake by mouse ZIP4 was not inhibited by any of the tested metals, including Cu, Cd, Mn, Co, Ag, Mg, Ni, Fe, in the excess amount of 10 or 50 folds[182]. This suggested that ZIP4 highly prefers Zn over other metals. A later study, however, proposed that ZIP4 can also transport Cu and Ni. By overexpressing human ZIP4 in *Xenopus laevis* oocytes and combined with radioactive isotopes, Antala and Dempski confirmed Cu and Ni activities by both

competition assays and direct measurements. Notably, 200-fold Cu(II) was able to suppress Zn activity for over 95% and direct measurements showed a K_m of 1.2 ± 0.09 μM. Ni(II) also had a low micromolar K_m of 2.9 ± 0.3 μM, suggesting Cu(II) and Ni(II) are substrates of human ZIP4[183].

ZIP5 was also firstly characterized as a Zn-specific transporter. Competition assays conducted on mouse ZIP5 against Zn showed no inhibition by Mn, Co, Ag, Mg, Ni and Fe, about 50% inhibition by 50-fold excess of Cu and Cd[184]. A more recent study taking advantage of ICP-MS however, pointed out the selective Cu transport ability in human ZIP5. When a mixture of metals of almost same ratio applied to cells, an over 16-time difference was seen between ZIP5 expressing cells and negative control. Mn, Co, Ni and Zn also demonstrated 2-4 times increase. Moreover, in one-to-one ratio Cu was able to significantly suppress Zn uptake but Zn did not affect Cu transport by human ZIP5 back in the same way, suggesting Cu is a substrate for human ZIP5 and a good or even better competitor compared to Zn[185].

ZIP6, which is also often referred to as LIV-1 in literature, was firstly identified in 1988 as a novel gene related to estrogen treatment and breast cancer[95]. This is also where the name for the subfamily derived. Substrate specificity for human ZIP6 requires further studies, yet people have demonstrated its role as a Zn transporter. In human neuroblastoma cells, when ZIP6 expression level has been suppressed down by siRNA,

Zn uptake under resting condition decreased by 68% and 75% for a 15- and 45-minutes culture comparing to the negative control, respectively[186].

ZIP7 was firstly referred to as HKE4 protein, derived from its homology of mouse KE4 gene. The first characterization of human ZIP7 in mammalian cells with free zinc dye Newport Green diacetate showed that ZIP7-expressing cells had a 5-time fluorescent intensity compared to negative control, and 20-30% stronger than the positive control LIV-1 (ZIP6)[187]. ZIP7 is also special in its subcellular localization, being mostly expressed on intracellular membrane such as ER[187,188] with a role to efflux Zn out from the intracellular compartment into the cytosol. This was confirmed in ZIP-knockout human MG-3 cells, where ZIP7$^{-/-}$ cells demonstrated a significantly increase of Zn concentration in ER and decrease in cytosol[188]. Another study generated a hypomorphic ZIP7 in mouse showed similar results and also identified blocked B cell development[130].

Different from most of the other ZIPs, ZIP8 was firstly identified not for Zn, but its Cd transport activity. Mouse fetal fibroblasts expressing mouse ZIP8 were over 30 times more sensitive to environmental Cd compared to negative control. Moreover, Cd uptake by mouse ZIP8 showed a time and dose dependent pattern, suggesting its Cd transport ability[189]. Followed up study further revealed Cd transport of mouse ZIP8 can be significantly inhibited by Mn. 50% and 80% of the Cd transport activity could be inhibited by the presence of 4- and 64-time excess of Mn, respectively. Hg could also inhibit over 50% of the activity for 64-time excess amount. Kinetic parameters for both Cd and Mn

were also determined. K_m for Cd was 0.62 μM and Mn was 2.2 μM. Such low micromolar K_m highly suggested both Cd and Mn are substrates to ZIP8, and Mn is very likely to be the physiological substrate[190]. Other than Cd and Mn, Zn and Fe transport ability of mouse ZIP8 was also proposed and characterized, supported by both direct measurement using radioactive isotopes and competition assays against Zn and Cd[105,191] . Other than Hg, heavy metals like U and Pt were also revealed to be able to inhibit Zn and Cd transport through competition assay, whether these heavy metals are substrates to ZIP8 requires further clarification[191]. Selenium (Se), another essential trace element was also proposed to be a substrate of human ZIP8. Studied in various systems including human and mouse cells and transgenic mouse lines, Se uptake was tightly correlated to ZIP8 expression level and the abundance of Zn^{2+} and HCO_3^- [192]. ZIP8-knockout HeLa cells demonstrated a decrease in Se amount after incubation in 4 μM of Na_2SeO_3 for 12 hours compared to wild-type HeLa cells while cells overexpressing ZIP8 showed doubled activities compared to negative control[193]. Being a promiscuous transporter, it is well established that ZIP8 can transport physiological transition metals such as Zn, Mn and Fe. Newer studies suggested that Se is also one of its substrates and it is clear that ZIP8 is responsible for transportation and accumulation of the unnecessary and toxic metal Cd.

In 2014, a novel androgen receptor was identified in Atlantic croaker ovaries and sequence alignment showed 81-93% identity to ZIP9 members, indicating this androgen receptor was in fact a ZIP9. In cells stably transfected with croaker ZIP9, a testosterone

related concentration-dependent increase in intracellular free Zn concentrations was observed. Moreover, this reaction to testosterone and Zn increase was abrogated by transfecting cells with SiRNA to knockdown ZIP9 expression[107]. Similarly, in chicken Zip9-knockout DT40 cells, intracellular Zn concentration was dependent on the expression of human ZIP9[205]. Another earlier study on vertebrate cells in 2009 pointed out ZIP9 regulates Zn homeostasis in the secretory pathway[219].

ZIP10 is a Zn transporter localized at the apical membrane of renal proximal tubules, revealed in studies on rats. Direct measurement showed more than 60% accumulation of Zn in rat ZIP10 transfected cells compared to negative control, and the uptake was dose-dependent and saturable, with a K_m of 19.6 μM. This Zn uptake by rat ZIP10 could be partially inhibited by Cd, suggesting Cd was also a potential substrate[194]. A more recent study showed conserved Zn transport ability of ZIP10 across species, demonstrating ZIP10 from human, fly and dog can all significantly increase Zn uptake in radioactive cell assays[195]. Interesting results from Polesel and Manolova et al showed that, like they demonstrated in the case of ZIP5, Cu was also a substrate for ZIP10. Cu uptake in ZIP10 transfected cells was over 4 times higher than controls and this Cu activity was not inhibited by the presence of same amount of Zn. Moderate increase in Ni was also seen in this study[185].

ZIP11 is the only member of the GufA subfamily and is primarily found in nucleus and Golgi apparatus. Frist functional characterization was conducted on mouse ZIP11. Taking

advantage of ICP-MS, mZIP11 transfected cells showed significant increases in Zn uptake compared to negative control, similar to the positive control mZIP14. A minor Cu uptake was also observed in this study[206]. Most recently studies have confirmed the functional role of ZIP11 to maintain the Zn homeostasis in nucleus, where ZIP11-knockdown HeLa cells demonstrated accumulations in nuclei, and this accumulation was reversed by expressing wild-type ZIP11 but not the functional-compromised mutants[207,208].

ZIP12 was found to be highly expressed in human brain and proven to be a high affinity Zn transporter[51,196]. Functional characterization or radioactive cell assays on mouse ZIP12 displayed that it is a Zn transporter with an apparent K_m of 6.6 nM. Competition assays were also conducted yet most of the tested metals, including Mg, Fe, Mn, Ni and Pb, didn't inhibit Zn uptake. Minor inhibition, however, was seen for Cu and Cd[196]. Another study in mouse spermatogonial stem cells also exhibited correlation between ZIP12 expression level and intracellular Zn concentration[197]. Being a close homolog to mouse ZIP12, human ZIP12 was determined to be a Zn transporter as well[198].

ZIP13 was characterized as a Zn specific transporter. Cell assays using expression level of metallothionein MT1A as an indicator of intracellular Zn level showed that ZIP13 transfected cells were having a much higher Zn level compared to negative control. This was confirmed by experiments using Zn specific dye FluoZin-3[175]. Radioactive Zn assays as well as the competition assays proved ZIP13 was Zn-specific. With an apparent K_m of

2 μM, the Zn uptake of ZIP13 was not inhibited by most of the tested metals. Its role in promoting vesicular Zn efflux was also implied[199]. Very interestingly, Guiran Xiao and Bing Zhou et al suggested that *Drosophila melanogaster* ZIP13 (dZIP13) was not only involved in Fe homeostasis, but also functioned as an Fe exporter. When dZIP13 was knocked down or over-expressed in flies, whole body amounts of Fe had significant decrease and increase respectively. Functions of dZIP13 was also tested in the system of E. Coli and isolated ER/Golgi (where the dZIP13 is mostly expressed) from Drosophila larvae, both indicating dZIP13 can export Fe out of the cells. Analogy between dZIP13 and human ZIP13 was shown and discussed, suggesting human ZIP13 might function similarly as an Fe exporter as well[200].

ZIP14 is the closest paralog of ZIP8 and not surprisingly shares a similar wide substrate preference like ZIP8. Human ZIP14's Zn preference was first characterized in 2005, cell assays with Zn dye Newport Green clearly exhibited Zn activity for human ZIP14[201]. Zn function for mouse ZIP14 was also illustrated in 2005, in both fluorescent and radioactive experiments[129]. These findings were soon followed by the identification of Fe transport in mouse ZIP14, where mouse ZIP14 overexpression led to significant Fe and Zn accumulation in cells and mouse ZIP14 knockdown in mouse hepatocyte AML12 cells showed reduced Fe and Zn[202]. Similarity in substrate preference between ZIP14 and ZIP8 was further explored, as mouse ZIP14 was demonstrated to be able to transport Cd and Mn, where Cd transport could be greatly inhibited by Zn and followed by Cu,

suggesting Cu was also a potential substrate for ZIP14[172]. Newer studies confirmed that ZIP14 can transport Zn, Cd, Mn, Fe[203,204,220], with some pointed out that ZIP14 might also involve in Ni and Co transport[185,191].

Prokaryotes have different Zn transporter systems. Take *Escherichia coli* as an example, three Zn transport systems were firstly found and they were P-type ATPase ZntA, cation diffusion facilitator ZitB and ABC transporter ZnuABC[209,221–224]. Inspired by the speculation that ZIP family was not only present in eukaryotes but also in bacteria[16], ZupT was identified and its Zn transport ability was portrayed with radioactive assays[209]. Similar experiments were conducted to prove that ZupT was also involved in transport of Fe and Co, and possibly Mn as well[210]. Mn transport of ZupT was later confirmed, with a K_m of 1.16 ± 0.29 μM; K_m for Zn and Co was calculated to be 0.71 ± 0.14 μM and 0.91 ± 0.09 μM, respectively, reaffirmed transport ability for these two metals. Notably, Cd transport for ZupT was reported as well, as ZupT expressed cells were showing growth defect when Cd was added to the culture[211]. Development in structural biology revealed two metal binding sites within prokaryotic ZIPs[109], and closer look at the ZupT metal binding sites showed that Zn and Cd bind to M1 where Fe binds to M2, providing evidence in molecular level for the substrate preference of this bacterial transporter[115].

Another important prokaryotic ZIP is *Bordetella bronchiseptica* ZIP (BbZIP, or ZIPB). To date it is the only member of the ZIP family that has solved structure[109,112]. Functional

reconstitution of BbZIP into proteoliposomes showed both Zn and Cd activities, implying these two metals were substrates to the protein[173].

IRT1 was first identified in 1996 when the gene of IRT1 was isolated from *A. thaliana*. The expression of IRT1 in a Fe deficiency yeast strain successfully demonstrated the Fe transport ability of this new transporter. The Fe uptake by IRT1 was measured to saturable with an apparent K_m of 6 ± 1 μM. This uptake of Fe (II) could be significantly inhibited by 10-time excess of Cd[92]. IRT1 was then found to be involved in Mn transport, with an apparent K_m of 9 ± 1 μM. In competition assay, the Mn uptake was inhibited by Fe(II), Cd, Zn and Cu, suggesting these metals are all potential substrate of the transporter[212]. Evidence, including experiments done in plants, concluded that IRT1 can mediate Cd uptake from the environment as well as the transport for Fe, Zn, Mn and Co[101,213].

Zrt1 and Zrt2 were both first identified in 1996 as the two separate systems in *Saccharomyces cerevisiae* for Zn uptake[93,94]. Zrt1 was characterized as the high-affinity uptake system, with a K_m of 0.6 ± 0.1 μM for Zn in Zn-replete cells[93]. On the other hand, Zrt2 was identified as a low-affinity Zn uptake system, with an apparent K_m for 10 μM and was implied to be active in the Zn-replete environment. Substrate specificity for both systems were also tested, showing Zn uptake by high-affinity system (Zrt1) was not inhibited by any tested metals while low-affinity system (Zrt2) had significant decrease in the presence of Fe(II) and Cu(II)[94]. Early study on Zrt1 deleted cells suggested that Cd

was also a potential substrate to Zrt1[214], which was consistent with newer study that ΔZrt1 cells showed about 50% decrease in Cd uptake compared to wild type and ΔZrt2 didn't show much difference[215]. Interestingly, Al(III) was suggested to be a substrate to Zrt2 as addition of Al(III) into the media of ΔZrt1 restored cell growth to similar level as WT, but ΔZrt1Zrt2 didn't show this growth improvement due to Al(III) addition[225].

1.5 Molecular determinates of the substrate preference in ZIPs

Although the ZIPs are classified as Zn transporters, their diverse substrate preferences within the family and the difference between the members was not well studied. Sequence alignment demonstrated a relative conserved TMD in the ZIP family, which was considered as the main part of the protein that plays role in substrate determination and transport. How are the high similarities within the TMD led to different choices of substrate? What are the molecular determinates of the substrate preferences? Efforts have been made to try to answer these questions for two decades since the identification of the ZIP family.

Zn transporters like the ZIPs can be considered as a special kind of Zn-binding proteins or enzymes. Indeed, many parameters originate from enzymology have been adopted to transporter studies such as K_m or K_{cat}. For Zn binding protein, or transition metal binding protein in general, the recognition between the metal and protein was mainly through a series of physical and chemical nature, which is going to determine what and how the ions coordinate[46].

As described in Pauling's rule, the size ratio between the metal ions and the ligands would directly affect the coordination[226]. Although metal ions usually try to coordinate as many ligands as possible, minimizing steric effects and repulsion between the ligands are also necessary. A good demonstration for this would be Zn and Cd. As elements from the same column in periodic table, Zn and Cd share a lot of similarities but not in the ionic sizes, where Zn^{2+} is 0.74 Å and Cd^{2+} is 0.97 Å[46]. Meanwhile, the most commonly seen coordination number for Zn is four while Cd is six, corroborating the great effect ionic sizes have on coordination[227].

The chemical nature of the metal ions as well as the donor atoms are also important for determining the coordination patterns. Developed in 1963, the hard and soft acids and bases theory (HSAB) has been widely used to evaluate the donor preferences for the metals[228]. As an easy and straightforward theory, it categorizes Lewis acids and bases that are small and with high charge density as "hard" and those that are large and with relatively low charge density as "soft". As predicted by the HSAB theory, hard acids prefer hard bases and soft acids prefer soft bases. Detailed classification is shown in the **Table 1.2**[229].

Hard Lewis acids	Borderline acids	Soft acids
H^+, Li^+, Na^+, K^+, Be^{2+}, Mg^{2+}, Ca^{2+}, Sr^{2+}, Ti^{4+}, Zr^{4+}, Cr^{3+}, Al^{3+}, Ga^{3+}, La^{3+}, Gd^{3+}, Co^{3+}, Fe^{3+}	Fe^{2+}, Co^{2+}, Ni^{2+}, Cu^{2+}, Zn^{2+}, Pb^{2+}, Bi^{3+}, Rh^{3+}, Ir^{3+}	Cu^+, Au^+, Ag^+, Tl^+, Hg^+, Pb^{2+}, Cd^{2+}, Pt^{2+}, Hg^{2+}
Hard Lewis bases	Borderline bases	Soft bases
F^-, OH^-, H_2O, ROH, Cl^-, RO^-, R_2O, $CH_3CO_2^-$, NH_3, RNH_2, NH_2NH_2, CO_3^{2-}, NO_3^-, O_2^-, SO_4^{2-}, PO_4^{3-}, ClO_4^-	NO_2^-, Br^-, N_3^-, N_2, C_6HNH_2, pyridine, imidazole	RSH, RS^-, R_2S, S_2^-, CN^-, RNC, CO, I^-, R_3As, R_3P, C_2H_4, H_2S, HS^-, R^-

Table 1.2 Summary of the classification of the hard and soft acid and base. Table adapted from reference 229.

As shown in the table, Zn^{2+} is a borderline acid, meaning that it could easily coordinate to the “softer” atoms such as nitrogen and sulfur as well as the “harder” atom oxygen. This prediction is consistent with the results of a bioinformatic study covering 18491 X-ray crystallography structure of zinc proteins, where Zn coordinates to 6102 cysteine (S) and 5716 histidine (N). These two residues were followed by 2026 aspartate, 1753 water molecule and 1293 glutamate (O)[230].

Coordinating geometry is another key factor in metal coordination. Basing on the number of valence *d* electrons, metal ions have different preferences on binding geometries, which was described in ligand field theory. Transition metals ions such as Fe^{3+} and Fe^{2+} prefer an octahedral or a distorted octahedral geometry as the structures are stabilized by the ligand field effect. Cu^{2+} and Cu^+ can also adopt an octahedral geometry with a distortion on the axis due to the Jahn-Teller effects. This was because

of the d^9 electron configuration of the Cu ions, the *eg* orbitals were further split, leading to distortion and global stabilization of the complex. Zn, however, has a d^{10} electron configuration and because of these full *d* orbitals, it is not affected by ligand field effects and therefore the change from octahedral to a tetrahedral ligand field is not energetically unfavorable. Bioinformatic study on the geometries of zinc protein revealed more than half of the protein are indeed adopting tetrahedral geometry.

Guided by these theoretical considerations, researchers have identified key residues important for ZIP functions.

Early biochemistry study explored the functional roles of two residues in human ZIP1, H190 and H217. These two residues are within the metal transport pathway and conserved in all ZIPII subfamily. By comparing to other ZIP members, H190 is corresponding to H177 in BbZIP, which is at the exit of the pathway, and H217 is corresponding to Q207 in BbZIP, which is within one of the metal binding sites. Alanine mutations at these two sites abolish Zn transport for human ZIP1, reiterate their importance for function[231].

It was previously demonstrated that Zn transport in human ZIP2 is pH sensitive[232]. Residues speculated to be involved were tested. H63A, E67A and E106A all showed decrease in metal transport while E70A and E106Q demonstrated increase. Interestingly, H63 and E67 in human ZIP2 correspond to Q180 and E184 in human ZIP8, which were at the focus of my projects. The bacterial counterpart S108 and P110 in BbZIP have also

been drawing a lot of attention[114] Alanine mutations at the metal transport site, including H175, E179 and H202 all led to abolished transport activity, suggesting indispensable role of this metal site to transport. Indeed, human ZIP2 only has one metal transport site while the second was blocked by a lysine residue. As for substrate selectivity, H202E (corresponding to E343 in human ZIP8) and F269A seems to had broader selectivity as Mn might be a substrate to these ZIP2 variants now, and Cd transport was also inhibited by Ba^{2+} for H202E[114].

Another study on human ZIP2 identified a series of residues, including residues along the metal transport pathway, H63, E67, E70, E106; residues possibly from the metal binding site basing on the structure model, H175, H202, E179 and residues that are in the proximity including F269 and S176. Among these variants H63A and E67A and to a lesser extent E106A showed a decrease Cd activity, while E70A and E106Q demonstrated increased Cd transport. H175A and H202A abolished function, suggested their significant role in transport; E179A had moderate Cd transport (~40% compared to WT) where E179Q was functional dead. E276 was identified in this work, as E276Q showed significantly changed selectivity, the mutant prefers Cd more in the excess of Zn, Cu and Co. Kinetics showed similar V_{max} but 3-fold higher K_m. This change might be due to a weaker coordination towards the substrates[114].

In human ZIP4, functional role of a series histidine residues in the TMD were tested. Alanine screening showed that mutations on H379, H507 and H536 all led to great

decrease on the Zn activity, suggesting these residues are important for transport. Another histidine in TM8 was of interest, as a glutamate residue is highly conserved in LIV-1 but replaced by histidine in ZIP4. Competition assay revealed that Mn^{2+}, Fe^{2+} and Co^{2+} can now compete with Zn^{2+} in the case of H624Q but direct measurement for iron uptake showed an even worse Fe^{2+} activity than wild type. H536A, however, demonstrated a significantly improved Fe activity. It is not surprising as H536 is within BMC and many studies on the counterparts of this residue in other ZIPs constantly revealed its significance. By mutating histidine into alanine, spatial and coordination limitation are both potentially removed therefore may facilitate a broader selectivity[233].

The roles of two metal binding sites within the BMC was also evaluated. The corresponding residues within the two metal binding sties were mutated into alanine in turns to generate M1 (H507A/H536A/H540A) and M2 (N508A/E537A) mutant. In the functional assay, Zn activity for M1 was totally abolished, suggesting the residues were indispensable for maintaining the function of ZIP4. M2 was not greatly affected, with only a moderate decrease in the Zn transport capacity. Moreover, competing assay was carried out on M2, where Cd, Co, Cu, Fe, Mn and Ni all failed to inhibit Zn transport. This work implied that although M2 (N508 and E357) can affect Zn transport, they were not indispensable and did not determine selectivity[113].

ZIP8 due to its multiple substrate preferences, has been the focus of the molecular determinates studies. A391 in human ZIP8 was also found to be of great interest. Mutant

A391T was found to be linked to systemic impairment of Mn homeostasis while not affecting Zn homeostasis[234,235]. Moreover, a few other ZIPs also have an alanine residue at the corresponding site, including ZIP9[102,219], whose homolog in *Saccharomyces cerevisiae* Atx2p (antioxidant 2) was found to be important to Mn transport and also has an alanine at the site[236]. Pathology studies revealed that human ZIP mutations are connected to congenital disorders through abnormal Mn homeostasis[237,238]. Mutations G38R, I340N have been identified and tested in HeLa cells, showing much lower Mn activity than wild-type ZIP8[239].

Another study tested the relationship between diseases related mutations and Se transport on human ZIP8. It demonstrated that variant G38R had expression level issue, which was much lower than WT, but if calibrated the Se transport might be about 6 times higher than wild type ZIP8, suggesting this G to R mutation is beneficial to selenium transport. Similar case was seen in C113S, which was about 2 times higher than wild type after calibration. G204 showed no significant difference and S335T expressed in similar level as wild type but with almost abolished activity[193].

Other than the diseases causing mutations, a conserved motif in TM5 has constantly be mentioned in substrate preference studies of ZIPs. This HEXXH motif is conserved in all the human ZIPs except for ZIP8 and ZIP14, which are known for their multiple substrate preferences. In these two proteins, the motif changes into EEXXH, raising interests in this H to E mutation. It was shown that when the glutamate residue was

mutated into histidine and alanine, both ZIP8 mutants lost its Cd and Mn activity, suggesting great roles of the glutamate in determining substrate preference[240].

In ZIP11, functional roles of diseases related and metal binding residues were studied by reintroducing these mutants to ZIP11 knockdown cells. Diseases related mutants A26S, A234P, and P243S all rescued the abnormal Zn level from the ZIP11 knockdown, implying normal or similar ZIP11 function. A89V, however, failed to do so, suggesting a crucial role of A89 in ZIP11 function. Mutations on the metal binding sites (H204A, E208A, E244A) all compromised ZIP11 function as well[208].

A study in Drosophila ZIP13 (dZIP13) pointed out an interesting motif swap. It was previously revealed that dZIP13 can transport Fe, and sequence alignment manifested that while dZIP13 has a DNXXH motif at the BMC, all the other LIV-1 members have a highly conserved HNXXD. The dZIP13 motif is also conserved through species and was tested crucial for the Fe function. Similar experiment in dZIP7, close homolog to dZIP13 showed the HNXXD motif is important for its Zn activity[241].

Mutations on human ZIP14 have been found to be related to diseases such as parkinsonism-dystonia symptoms through impaired ZIP14 function and accumulation of Mn. F98V, G383R and N469K were predicted to affect Mn transport in human ZIP14, suggesting their functional role[242].

Study in bacteria ZIP ZupT might shed some light on the mechanism of the ZIPs. ZupT also has a binuclear metal center (BMC), and it is found that M1 binds Zn, Cd and

Fe while M2 binds Fe only, with a higher affinity than M1.In both in vivo and in vitro study Zn was shown to be transported through M1 while Fe is transported through M2, which doesn't inhibit Zn transportation[115]. E123D (D318 in hZIP8) showed lost activity for Co, Fe, Zn and Mn while keeping an intermediate Cd activity. E123A showed intermediate Zn activity but lost the ability to transport other metals[211].

In a simulation study conducted on bacterial BbZIP, Zn ion was passed down BbZIP through a relay of a series residues including S106, A102, P199, A203 and L200 to the metal transport site. The kind of metals that can be coordinated to and passed down from these residues are therefore potential substrates of the protein[243].

In IRT1, H96, D100, E103 and C109A are at the loop between TM2 and TM3. Mutating H96, D100 and D136 into alanine led to Fe and Zn activities that were close to empty vector. Mutant C109A showed a slightly decreased Zn activity (70%) and a 120% Fe activity compared to wild type IRT1. E103A however, demonstrated interesting feature where Zn activity was lost but maintained a 120% Fe activity compared to the wild type[244].

1.6 Specific aims

Although playing crucial physiological roles, the ZIP family still remains mysterious to humans in many aspects, one of which is how ZIPs differentially distinguish substrates from non-substrate metals. Combining the first crystal structure of BbZIP our group solved in 2017[109] and the recently proposed and validated outward-facing conformation by our and another group[110,112], the progress on the BbZIP structural biology study have

revealed a clearer picture on the elevator transport mechanism. This is therefore a perfect timing to study the difference in substrate preference of the ZIPs and decipher the underlying mechanism. My thesis work has been focused on the molecular mechanism of substrate specificity of ZIPs. As ZIP8 is a well-established promiscuous metal transporter, my study on substrate specificity has centered on this protein because promiscuity is the starting point for natural or directed evolution. I have also used ZIP4 as an established model to develop a non-radioactive transport assay. The three specific aims are listed below.

1.6.1 Specific aim 1: Rationally engineering human ZIP8 and explore the molecular determinates of the substrate preference

Human ZIP8 and human ZIP4 are two LIV-1 ZIPs that exhibit a large difference in substrate preference, the former being promiscuous while the latter being zinc specific. Sequence alignment revealed differentially conserved residues that are likely to be involved in substrate selection. We hypothesize that swapping these differentially conserved residues will greatly alter the substrate preferences. The success of this aim will provide knowledge for rational engineering and elucidation of the molecular mechanisms of substrate specificity of ZIPs. To achieve this aim, we will:

1. Identify key residues that are differentially conserved in ZIP8 and ZIP4, because these residues are likely to be important in determining the substrate preference.
2. Rationally engineer human ZIP8 to alter its substrate preference by systematically

replacing the differentially conserved residues in ZIP8 by the corresponding residues in human ZIP4.

3. Screen the variants using the cell-based radioactive metal transport assay.
4. Rationale for the altered substrate specificity by using combined bioinformatics and structural information.

1.6.2 Specific aim 2: Development and application of non-radioactive metal assays

To avoid the potentially dangerous radioactive method, the community has long expected to develop a non-radioactive method. We hypothesize that by combining ICP-MS and rare stable isotopes, an easy-to-use method can be developed and applied to biochemical studies of the ZIPs. To achieve this aim, we will:

1. Develop an ICP-MS-based ^{70}Zn transport assay for human ZIP4 expressed in HEK293T cells.
2. Apply this non-radioactive assay to determine the turnover number of human ZIP4; determine the roles of the ZIP4-ECD; and evaluate Zn efflux during the assay.
3. Explore the potential of converting this approach into a high-throughput format by using laser ablation-ICP-MS (LA-ICP-MS) to detect samples on a solid surface.

1.6.3 Specific aim 3: Explore the specificity filter

During the studies on specific aim 1, a conditional selectivity filter was identified, which we believe determines the substrate preference of the protein. Although the filter existed in most of the ZIPs, the amino acids composition of the filter varies greatly. We

hypothesized that the different amino acid composition of the selectivity filter leads to the differences in substrate preference. To test this hypothesis, we will:

1. Systematically replace the residues (Q180, E318, and E343 in ZIP8) forming the selectivity filter with polar and/or charged residues to generate a library. We focus on human ZIP8 because we have established a highly reliable transport assay for this protein.
2. Screen the library against metal mixtures containing substrate and/or non-substrate metals using ICP-MS and cell-based transport assay.
3. Rationale for the altered and expanded substrate spectrum as a guidance for later engineering practice.

CHAPTER 2: Rational engineering of an elevator-type metal transporter ZIP8 reveals a conditional selectivity filter critically involved in determining substrate specificity

Yuhan Jiang[1], Zhen Li[1], Dexin Sui[2], Gaurav Sharma[1], Tianqi Wang[2], Keith MacRenaris[3], Hideki Takahashi[2], Kenneth Merz[1,2], Jian Hu[1,2]

[1]Department of Chemistry,

[2]Department of Biochemistry and Molecular Biology,

[3]Department of Microbiology & Molecular Genetics, Michigan State University, MI 48824

Published in Communicational biology, July 2023, Volume 6

This work was led by me under the guidance of Dr. Jian Hu and accomplished through collaborations. Dr. Jian Hu, Dr. Dexin Sui and I did the sequence alignment and picked the residues of interests (Figure 2.3, 2.5). Dr. Sui and I designed primers (Table 2.1) and conducted mutagenesis. Dr. Sui conducted early metal uptake assays (Figure 2.3) and I conducted the rest of the metal uptake assays, including Zn, Cd, Fe and Mn assays and kinetic assays (Figure 2.6-2.9). I conducted Western blot, Tianqi Wang provided Immunofluorescence data (Figure 2.4, 2.7, 2.13). Dr. Hu performed the bioinformatic studies (Figure 2.10). Zhen Li and Dr. Gaurav Sharma from Dr. Kenneth Merz's group carried out the computational study (Figure 2.11 and 2.12). Dr. Keith MacRenaris from

Dr. Thomas O'Halloran's group and I conducted the ICP-MS study (Table 2.2 and Figure 2.9). I conducted the swapping experiment in human ZIP4 (Figure 2.13). Dr. Hideki Takahashi was involved in manuscript writing and editing.

2.1 Summary

Engineering of transporters to alter substrate specificity as desired holds great potential for applications, including metabolic engineering. However, the lack of knowledge on molecular mechanisms of substrate specificity hinders designing effective strategies for transporter engineering. Here, we applied an integrated approach to rationally alter the substrate preference of ZIP8, a Zrt-/Irt-like protein (ZIP) metal transporter with multiple natural substrates and uncovered the determinants of substrate specificity. By systematically replacing the differentially conserved residues with the counterparts in the zinc transporter ZIP4, we created a zinc-preferring quadruple variant (Q180H/E343H/C310A/N357H), which exhibited largely reduced transport activities towards Cd^{2+}, Fe^{2+}, and Mn^{2+} whereas increased activity toward Zn^{2+}. Combined mutagenesis, modeling, covariance analysis, and computational studies revealed a conditional selectivity filter which functions only when the transporter adopts the outward-facing conformation. The demonstrated approach for transporter engineering and the gained knowledge about substrate specificity will facilitate engineering and mechanistic studies of other transporters.

2.2 Introduction

Transporter engineering has gained traction in recent years because of its great potential in broad applications, particularly in metabolic engineering[245–247]. As membrane transporters govern the fluxes of substrates, intermediates, or products across the cell

and organellar membranes, transporter engineering has been viewed as a promising strategy to control the kinetics of reactions inside the biofactories. Metal transporters hold a unique position in dealing with beneficial and/or toxic metal uptake, distribution, accumulation, and extrusion. Engineering of metal transporters may reduce contamination of toxic metals in foods, enable biofortification, or facilitate phytoremediation[248]. Albeit these potentials, there were only limited trials on a few metal transporters to alter substrate specificity. These early studies were either only focused on a small set of residues or based on error-prone PCR facilitated random mutations[244,249–251].

One prominent target for transporter engineering is the Zrt-/Irt-like protein (ZIP) family (SLC39A), which selectively transports divalent d-block metals. Recent structural, biochemical, and computational studies have provided evidence supporting that the ZIP metal transporters utilize an elevator-type transport mode to achieve alternating access[110,111,178]. In the two-domain architecture of a representative ZIP from Bordetella bronchiseptica (BbZIP), the only ZIP whose transmembrane domain structure has been solved to date, transmembrane helices (TMs) 2/3/7/8 form the static and dimeric scaffold domain whereas TM1/4/5/6 form the transport domain which slides vertically as a rigid body against the scaffold domain during transport. As the transport sites (M1 and M2) are nearly exclusively located in the transport domain, they are alternatingly exposed to either side of the membrane when the transport domain shuttles across the membrane.

Although several structures representing the inward-facing conformation (IFC) of BbZIP have been reported, an experimentally solved outward-facing conformation (OFC) of BbZIP is still missing. Nevertheless, an OFC model of BbZIP was generated by using the approach of repeat-swap homology modeling, which has been validated by biochemical approaches[111]. As an ancient protein family ubiquitously expressed in all kingdoms of life, the ZIPs are diverse in multiple aspects, including substrate specificity. Even with the gradually elucidated elevator transport mechanism, which is believed to be applicable to most if not all members of the ZIP family, how ZIPs selectively transport certain d-block metals while repelling the others remains elusive. Some ZIP family members appear to be specific toward zinc ions (Zn^{2+}), but the broader substrate spectrum of other family members allows them to function as multi-metal transporters capable of transporting a panel of divalent d-block metal ions. For instance, while most of the fourteen human ZIPs are reported to transport Zn^{2+} and play roles in Zn homeostasis and Zn signaling[138,252–254], ZIP8 and its close homolog ZIP14 transport not only Zn^{2+} but also ferrous ions (Fe^{2+}), manganese ions (Mn^{2+}), and cadmium ions (Cd^{2+}), and as such are critically involved in Fe and Mn homeostasis and are responsible for cellular Cd uptake and toxicity[172,202,238,255–264]. In Arabidopsis thaliana, Cd accumulation can be partially attributed to the Cd^{2+} transport activity, in addition to the activities toward Zn^{2+}, Fe^{2+}, and Mn^{2+}, of the root-expressing IRT1, a founding member of the ZIP family[213,265,266]. So far, the underlying mechanisms of substrate specificity of the ZIPs are largely unknown. Note

that although the exact metal species that is transported by ZIPs has not been fully established, M^{2+} is used to indicate that the ZIPs transport divalent metal substrates.

In this work, we applied a systematic approach to rationally alter the substrate specificity of a multi-metal transporter, ZIP8 from human, initially aiming to increase the preference toward Zn^{2+} over Cd^{2+} (described Zn/Cd selectivity hereafter). The quadruple variant of ZIP8 created in this study (Q180H/E343H/C310A/N357H) exhibited drastically increased preference of Zn^{2+} over not only Cd^{2+} but also Fe^{2+} and Mn^{2+}, which are the other two physiological substrates of ZIP8 besides Zn^{2+}. Structural modeling, evolutionary covariance analysis, and computational studies revealed a residue pair (Q180 and E343) that forms a selectivity filter at the entrance of the transport pathway only when ZIP8, an elevator-type transporter, adopts the outward-facing conformation, providing the structural and biochemical basis of the strong epistasis among the mutations introduced in the quadruple variant. The results of reverse substitution experiments performed on human ZIP4 confirmed the importance of the proposed selectivity filter in determining substrate preference.

2.3 Materials and Methods

2.3.1 Genes, plasmids, and mutagenesis

The complementary DNA of human ZIP4 (GenBank access number: BC062625) and human ZIP8 (GenBank access number: BC012125) from Mammalian Gene Collection were purchased from GE Healthcare. The ZIP4 coding sequence was inserted into a

modified pEGFP-N1 vector (Clontech) in which the downstream EGFP gene was deleted, and an HA tag was added at the C-terminus. The ZIP8 coding sequence was inserted into the pcDNA3.1 vector (Invitrogen). The ZIP8 construct consists of the N-terminal signal peptide of ZIP4 (amino acid residues 1-22) followed by a GSGS linker and a FLAG tag, the ZIP8 coding sequence (residue 23-460), and a HA-tag at the C-terminus. Site-directed mutagenesis of ZIP8 was conducted using QuikChange mutagenesis kit (Agilent, Cat#600250). All mutations were verified by DNA sequencing. The primers used in this work are listed in **Table 2.1**.

Name	Sequence (5'-3') [a]
ZIP8	
E343H	ACTTCCATAGCAATCCTATGTCACGAGTTTCCCCACGAGTTAGGA
C374L	CTATTCAACTTCCTTTCTGCATTGTCCTGCTATGTTGGGCTAGCT
C374L/C376A	CTATTCAACTTCCTTTCTGCATTGTCCGCTTATGTTGGGCTAGCTTT TGGC
Q180H	CTTTTTTCAAATGCAATTTTCCACCTTATTCCAGAGGCATTTGGA
Q180H/E343H/N176D	GCTATTGGGACTCTTTTTTCAGATGCAATTTTCCACCTTATTCCA
Q180H/E343H/E184K	GCAATTTTCCACCTTATTCCAAAGGCATTTGGATTTGATCCCAAA
Q180H/E343H/D189H	ATTCCAGAGGCATTTGGATTTCACCCCAAAGTCGACAGTTATGTT
Q180H/E343H/C310A	ATTGCCTGGATGATAACGCTCGCTGATGCCCTCCACAATTTCATC
Q180H/E343H/S325A	GATGGCCTGGCGATTGGGGCTGCTTGCACCTTGTCTCTCCTTCAG
Q180H/E343H/Q332T	TCCTGCACCTTGTCTCTCCTTACAGGACTCAGTACTTCCATAGCA
Q180H/E343H/N357H	GGAGACTTTGTGATCCTACTCCACGCAGGGATGAGCACTCGACAA
Q180H/E343H/P392E	TTGGTGGGCAACAATTTCGCTGAGAATATTATATTTGCACTTGCT
Q180H/E343H//T451S	ACTGGAAGAAAAACCGATTTCTCATTCTTCATGATTCAGAATGCT
ZIP4	
H379Q	CTCACTGGGGACGCTGTCCTGCAACTGACGCCCAAGGTGCTGGG G
H536E	ACCTCGCTGGCCGTGTTCTGCGAAGAGTTGCCACACGAGCTGGG G
G503C	CTGCCCTATATGATCACTCTGTGTGACGCCGTGCACAACTTCGCC
H550N	GGGGACTTCGCCGCCTTGCTGAACGCGGGGCTGTCCGTGCGCCA A

Table 2.1. The primers for mutagenesis.

[a] Only the forward primers are shown. The reverse primers are reversely complimentary to the sequences of the forward primers.

[b] The Q180H/E343H/C310A/N357H variant was generated by using the primers for the Q180H/E343H/C310A and N357H variants.

2.3.2 Mammalian cell culture, transfection, and Western blot

Human embryonic kidney cells (HEK293T, ATCC, Cat#CRL-3216) were cultured in Dulbecco's modified eagle medium (DMEM, Thermo Fisher Scientific, Invitrogen, Cat#11965092) supplemented with 10% (v/v) fetal bovine serum (FBS, Thermo Fisher Scientific, Invitrogen, Cat#10082147) and Antibiotic-Antimycotic solution (Thermo Fisher Scientific, Invitrogen, Cat# 15240062) at 5% CO_2 and 37°C. Cells were seeded on the polystyrene 24-well trays (Alkali Scientific, Cat#TPN1024) for 16 h in the basal medium and transfected with 0.8 µg DNA/well using lipofectamine 2000 (Thermo Fisher Scientific, Invitrogen, Cat# 11668019) in DMEM with 10% FBS.

For Western blot, samples were mixed with the SDS sample loading buffer and heated at 96°C for 10 min before loading on SDS-PAGE gel. The proteins separated by SDS-PAGE were transferred to PVDF membranes (Millipore, Cat#PVH00010). After blocking with 5% (w/v) nonfat dry milk, the membranes were incubated with anti-FLAG antibody (Agilent, Cat# 200474-21) or anti β-actin (Cell Signaling, Cat# 4970S) at 4°C overnight, which were detected with HRP-conjugated goat anti-rat immunoglobulin-G at 1:5000 dilution (Cell Signaling Technology, Cat# 7077S) or goat anti-rabbit immunoglobulin-G at 1:3000 dilution (Cell Signaling Technology, Cat# 7074S) respectively using the chemiluminescence reagent (VWR, Cat#RPN2232). The images of the blots were taken using a Bio-Rad ChemiDoc Imaging System.

2.3.3 Metal transport assay

2.3.3.1 Internal competition for Zn^{2+} and Cd^{2+}

Twenty hours post transfection, cells were washed with the washing buffer (10 mM HEPES, 142 mM NaCl, 5 mM KCl, 10 mM glucose, pH 7.3) followed by incubation with Chelex-treated culture media (DMEM plus 10% FBS). ICP-MS analysis indicated that the treatment with Chelex-100 reduced Zn content by more than 97%, whereas had little effects on the contents of Fe and Mn (**Table 2.2**).

(μM)	Mn	Fe	Zn
Before	0.059	3.988	3.637
After	0.043	3.702	0.091

Table 2.2. ICP-MS analysis of some *d*-block metals in the culture media (DMEM+10% FBS) before and after the treatment with the Chelex-100 resin.

The Chelex-treated culture media used for transport assay already contains 0.091 μM Zn, 3.702 μM Fe, and 0.043 μM Mn. Indicated amount of metals, including the radioactive isotopes, were added into this culture media to initiate transport. To reduce the systematic errors caused by variations in transporter expression level and in cell number during transfer and wash among different samples, we added both Zn^{2+} and Cd^{2+} to the same cell sample by taking the advantage of ^{65}Zn and ^{109}Cd emitting gamma ray at different energy levels (1100 keV and 88 keV for Zn and Cd, respectively). A diagram is shown in **Figure 2.1** to illustrate the experiment process. Accordingly, we were able to measure the two isotopes simultaneously when two detection windows were used in the gamma counter (800-1500 keV for Zn window and 30-150 keV for Cd window). As ^{65}Zn also emits gamma rays within the Cd window, a calibration was performed to determine

the signal solely derived from ^{109}Cd by subtracting the contribution of ^{65}Zn from the reading recorded within the Cd window. To do so, the signals of a series of ^{65}Zn standard samples (0-20 μM) were measured within both the Zn-window and the Cd-window. The resulting slope of the linear correlation 0.235 was used to calibrate the readings recorded within the Cd window to obtain the signals specific to Cd (**Figure 2.1**).

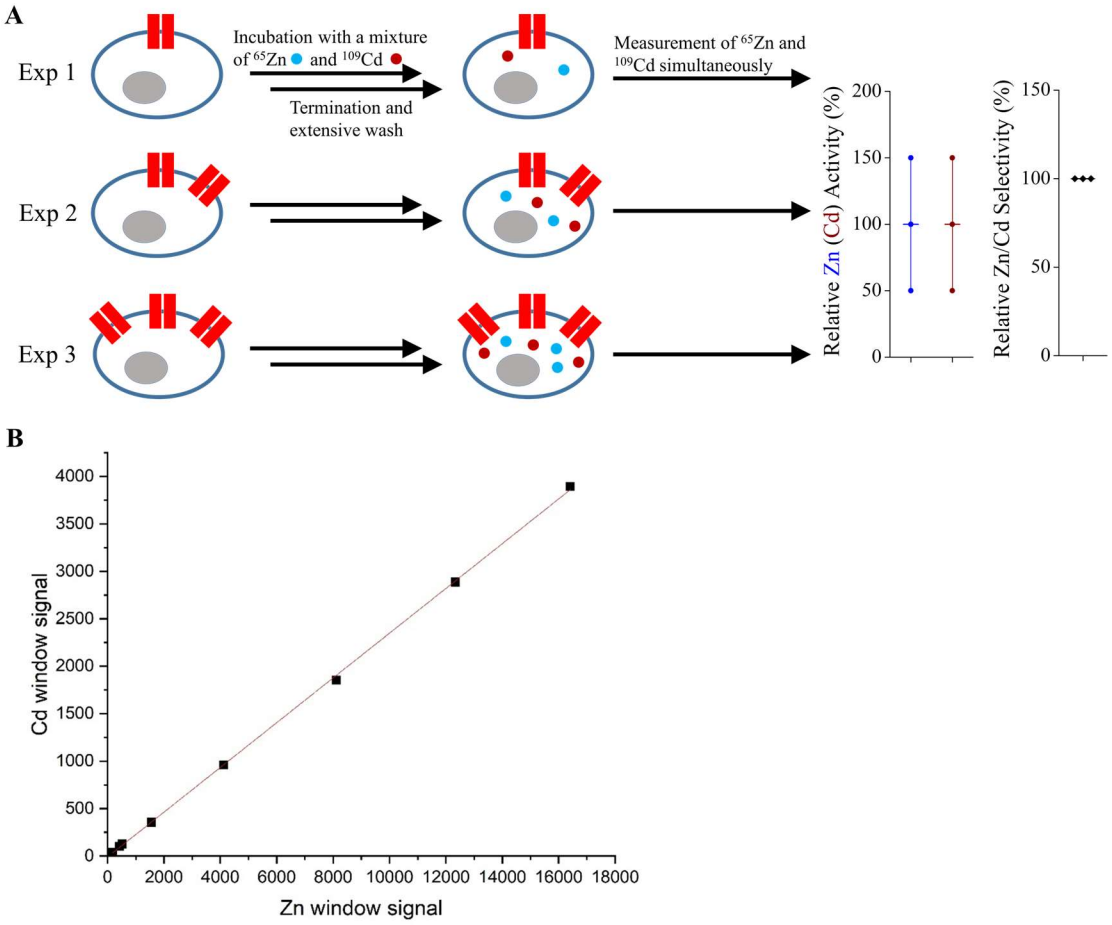

Figure 2.1. Internal competition transport assay and data processing. (**A**) Illustration of the experimental procedure. Cells expressing different levels of ZIP8 (shown as red channels) in three independent experiments (Exp 1-3) are incubated with a mixture of ^{65}Zn and ^{109}Cd under the same experimental conditions, followed by termination with an ice cold EDTA-containing solution and extensive wash. Radioactivities of ^{65}Zn and ^{109}Cd associated with the cells were simultaneously quantified by using a gamma counter in two detection windows (800-1500keV for Zn and 30-150keV for Cd). As demonstrated in the simulated experiments, although the Zn (or Cd) transport activity may have a large

Figure 2.1. (cont'd)
deviation due to varied expression levels of the transporter in different experiments, the ratios of the transport activities of Zn to Cd (the Zn/Cd selectivity) are essentially the same. (**B**) Calibration of the signals recorded in the Cd window. Radioactivities of a series of ^{65}Zn standard samples (0-20 μM) recorded in the Cd window are plotted against the readings recorded in the Zn window. The slope of the curve (0.235) means that, for any given sample containing ^{65}Zn and ^{109}Cd, 23.5% of the reading recorded in the Zn window contributes to the reading in the Cd-window. Therefore, to calibrate the readings in the Cd window, 23.5% of the reading in the Zn window was subtracted from the reading recorded in the Cd window to determine the radioactivity truly derived from ^{109}Cd. ^{109}Cd does not contribute to the reading in the Zn window.

In the experiments shown in **Figure 2.3**, 5 μM $ZnCl_2$ (0.05 μCi/well) and 5 μM $CdCl_2$ (0.05 μCi/well) were used in the substrate mixture. In the experiments shown in **Figures 2.6 and 2.13**, as the variants of ZIP8 or ZIP4 and its variants exhibited low Cd transport activity, more Cd (15 μM Cd^{2+}, 0.15 μCi/well) was used while Zn^{2+} concentration was kept the same as before. After incubation at 37°C for 30 min, the plates were transferred on ice and an equal volume of the ice-cold washing buffer containing 1 mM EDTA was added to the cells to terminate metal uptake[93,104,109,111,113,117,260,267–269]. The cells were washed twice and pelleted through centrifugation at 75 x *g* for 5 min before lysis with 0.5% Triton X-100. A Packard Cobra Auto-Gamma counter was used to measure radioactivity. The Zn (or Cd) transport activity was determined by subtracting the radioactivities of ^{65}Zn (or ^{109}Cd) associated with the cells transfected with the empty vector from those associated with the cells transfected with metal transporters.

For kinetic studies, equal amount of Zn^{2+} and Cd^{2+} were mixed in the media at the indicated concentrations with the following radioactivity: 0.01 μCi/μM for Cd^{2+} and 0.005 μCi/μM for Zn^{2+}. The remaining procedure was the same as described above.

2.3.3.2 Fe^{2+} transport assay

Twenty hours post transfection, cells were washed with the washing buffer (10 mM HEPES, 142 mM NaCl, 5 mM KCl, 10 mM glucose, pH 7.3) followed by incubation with Chelex-treated DMEM plus 10% FBS. Indicated amount of $FeCl_3$, including the radioactive $^{55}Fe^{3+}$ (0.1 μCi/μM), were added into the media supplemented with 2 mM freshly prepared ascorbic acid (to reduce Fe^{3+} to Fe^{2+}) to initiate transport[29,40]. The other procedures were the same as the Zn transport assay except that the cell lysates were mixed with the Ultima Gold cocktail (PerkinElmer, Cat# L8286) and ^{55}Fe associated with the cells was quantified using a liquid scintillation counter (LS 6500 Multi-Purpose Scintillation Counter).

2.3.3.3 Mn^{2+} transport assay

Twenty hours post transfection, cells were washed with the washing buffer (10 mM HEPES, 142 mM NaCl, 5 mM KCl, 10 mM glucose, pH 7.3) followed by incubation with Chelex-treated DMEM plus 10% FBS. $MnCl_2$ was added to the media to the final concentration of 50 μM. The other procedures were the same as the Zn transport assay except that the cell lysates were digested with nitric acid and applied to Mn measurement using ICP-MS. More specifically, 75 μL of the cell lysate was mixed with 100 μL of 70% nitric acid (Fisher chemical, Cat# A509P212) in 15 mL metal-free tube (Labcon, Cat# 3134-345-001-9). The samples were heated in 60°C water bath for 1 h to make sure the sample is fully digested. After incubation each sample was diluted to 3 ml using MilliQ

water to a final solution of 2.33% nitric acid (v/v). Samples were analyzed using the Agilent 8900 Triple Quadrupole ICP-MS equipped with the Agilent SPS 4 Autosampler. Instrument calibration was accomplished by preparing standards and internal controls. The standard was IV-ICPMS-71A (Inorganic Ventures), standard concentrations were 100, 50, 25, 12.5, 6.25, 3.125 ng/ml for each element. IV-ICPMS-71D (Inorganic Ventures) was used for internal control. The relative level of Mn was expressed as the molar ratio of Mn and phosphorus[270].

2.3.3.4 Time course experiments

To determine the optimal incubation time, time course experiments were conducted at the indicated time in the range of 0-90 minutes. In these experiments, the concentrations of Zn^{2+}, Cd^{2+}, and Fe^{2+} were 5 μM, 5 μM, and 20 μM respectively. The result is shown in **Figure 2.2**.

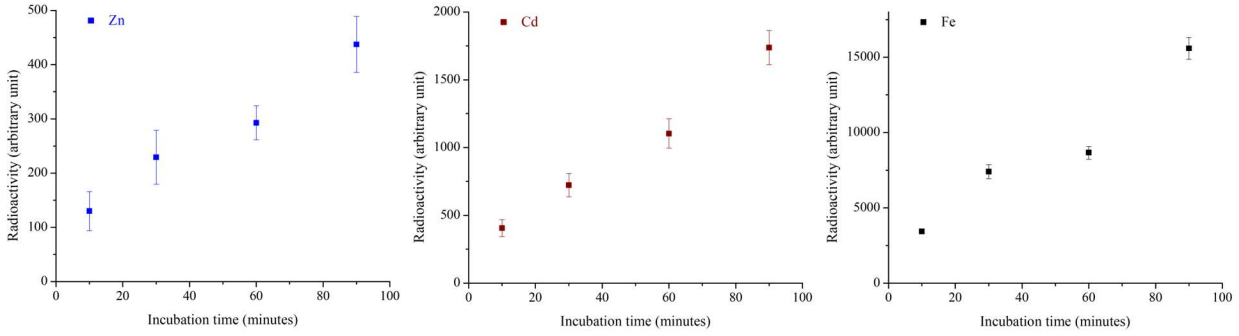

Figure 2.2. Time courses of metal transport by the wild type ZIP8. *left*: Zn^{2+}; m*iddle*: Cd^{2+}; *right*: Fe^{2+}. Metal substrates were detected using a gamma counter (for ^{65}Zn and ^{109}Cd) or a liquid scintillation counter (for ^{55}Fe). The concentrations of Zn^{2+}, Cd^{2+}, and Fe^{2+} were 5 μM, 5 μM, and 20 μM respectively.

2.3.3.5 Competition assay with Fe^{2+} or Mn^{2+}

For competition assay using Fe^{2+} or Mn^{2+}, all the procedure was the same as described above, except that the incubation buffer (Chelex-treated culture media containing DMEM plus 10% FBS) contained 5 μM Zn (0.05 μCi/well) with 100 μM $FeCl_3$ plus 2 mM ascorbic acid or 100 μM $MnCl_2$.

2.3.4 Immunofluorescence imaging

HEK293T cells were grown in 24-well trays for 16 h on Poly-D-Lysine (Corning, Cat#354210) coated coverslips and transfected with plasmids harboring ZIP8 gene or the 4M variant using lipofectamine 2000. To visualize cell surface expressed ZIP8 or the 4M variant, cells were washed by Dulbecco's phosphate-buffered saline (DPBS) after 24 h transfection and then fixed for 15 min at room temperature by using 4% formaldehyde. The cells were washed by DPBS for three times and then incubated in 2% BSA in DPBS for 1 h. The cells were incubated with 4 μg/mL anti-FLAG antibody diluted with 2% BSA in DPBS at 4ºC overnight. After washing three times by DPBS, the cells were incubated with Alexa-488 goat anti-rat antibodies at 1:200 (Thermo Fisher Scientific, Cat#A11006) diluted in DPBS with 2% BSA for 1 h. After three times washing by DPBS, coverslips were mounted on the slides with fluoroshield mounting medium with DAPI (Abcam, Cat# ab104139). Images were taken with a 40x objective using Nikon C2 confocal microscope. To detect the overall expression of ZIP8 and the 4M variant, after fixation by 4% formaldehyde, cells were permeabilized and blocked for 1 h with DPBS containing 2%

BSA and 0.1% Triton X-100 and then were incubated with 4 μg/mL anti-FLAG antibody diluted with 2% BSA in PBST with 0.1% Tween-20 (ThermoFisher Scientific, Cat# 85113) at 4 ºC overnight. The other procedures were the same as those for the non-permeabilized cells.

2.3.5 Bioinformatics and structural modeling

Multiple sequence alignment was conducted using Clustal Omega (https://www.ebi.ac.uk/Tools/msa/clustalo/). A threshold of 50% sequence identity was used as the cutoff to select orthologs of ZIP8, ZIP14, and ZIP4. Structure models were generated by SWISS MODEL (https://swissmodel.expasy.org/interactive). The structural model of human ZIP8 in the IFC was generated using the BbZIP structure (PDB: 5TSB) as the template. The models of ZIP8 in the OFC were created using either the OFC model of BbZIP[111] or the AlphaFold predicted human ZIP13 (https://alphafold.ebi.ac.uk/entry/Q96H72) as the template. Other ZIPs were modeled using the AlphaFold predicted human ZIP13 as the template. Evolutionary covariance analysis was conducted by using EVcouplings (https://v2.evcouplings.org/). To study the amino acid composition at the positions where Q180 and E343 are located in ZIP8, the protein sequences of the PF02535 family in the Pfam database (https://pfam.xfam.org/family/Zip) were retrieved, classified, and analyzed using the approach described previously[253]. The aligned sequences in each subfamily were analyzed in Jalview.

2.3.6 MD simulation and free energy calculation

MD simulations were performed using AMBER20[271]. The system was prepared using CHARMM-GUI[272], in which the box dimension was 101×101×126 Å containing one ZIP8 protein, 262 1,2-dilauroyl-sn-glycero-3-phosphocholine (DLPC) molecules, and 25973 OPC water molecules. Minimization was done in five stages with a gradient of restriction from protein backbone to side chain, each step yield 10, 000 steps of steepest descendent and 10, 000 steps of conjugate gradient methods; then 36 ns of NVT heating was performed with the temperature increasing gradually from 0 to 300 K. Then another 3 μs of simulation was performed to equilibrate the system in the NPT ensemble. Finally, a seven-window thermodynamic integration was conducted on the equilibrated system, each window yielded 300 ns. For every 50 ps the snapshot was saved to the trajectory file, yielding 420, 000 snapshots for the Gaussian Quadrature analysis. 10 Å cutoff was used for the non-bonded interaction. PME method and PBC were used for the simulations, and the Langevin algorithm with a 2.0 ps^{-1} friction coefficient was used for maintaining the temperature[273]. Berendsen barostat was used for pressure control with a relaxation time of 1.0 ps[274]. The time step was 1.0 fs with SHAKE used to constrain the bonds containing hydrogen atoms[275].

To compare free energy changes upon metal ions binding to the selectivity filter involving the side chains of H180, H343, D318, and E184 in the 4M variant, a modified 12-6-4 Lennard-Jones (m-12-6-4-LJ) non-bonded model was introduced to consider the

induced dipole effect between the metal ion and coordinating atoms during simulation[276]. Since the induced dipole effect is highly dependent on the polarizability of coordinating atoms, all parametrized polarizabilities used in this research was provided by the table in Figure S5A. Because the m-12-6-4-LJ model mainly yields strongly localized interactions, only the residues at the metal binding sites were applied with modified polarizabilities and m-12-6-4-LJ potentials.

2.3.7 Statistical analysis

Statistical analysis was conducted using the Student's *t*-test.

2.4 Results

2.4.1 Identification of the differentially conserved residues (DCRs)

ZIP8 is a member of the LIV-1 subfamily including nine human ZIPs, in which ZIP8 and ZIP14 are multi-metal transporters mediating influx of Zn^{2+}, Fe^{2+}, Mn^{2+}, and Cd^{2+} from the extracellular space[138,203]. The other LIV-1 proteins, including ZIP4, prefer Zn^{2+} over other biologically relevant divalent metal ions. Accordingly, the LIV-1 subfamily can be divided into two groups with distinct substrate specificities. Multiple sequence alignment of human LIV-1 proteins allowed us to identify two residues, Q180 and E343 (residue numbers in ZIP8), which are invariable in ZIP8 and ZIP14 but replaced by histidine residues in the Zn-preferring LIV-1 proteins (**Figure 2.3A**). We named the residues with these features differentially conserved residues (DCRs), as they are conserved in the orthologs (or close paralogs) sharing the same substrate specificity but non-

conservatively replaced with the amino acids conserved in the paralogs with different substrate specificity. As it has been demonstrated that isozyme-specific residues are crucial in determining substrate specificity of enzymes[277–279], these two DCRs were postulated as key residues defining the substrate spectrum of the LIV-1 proteins.

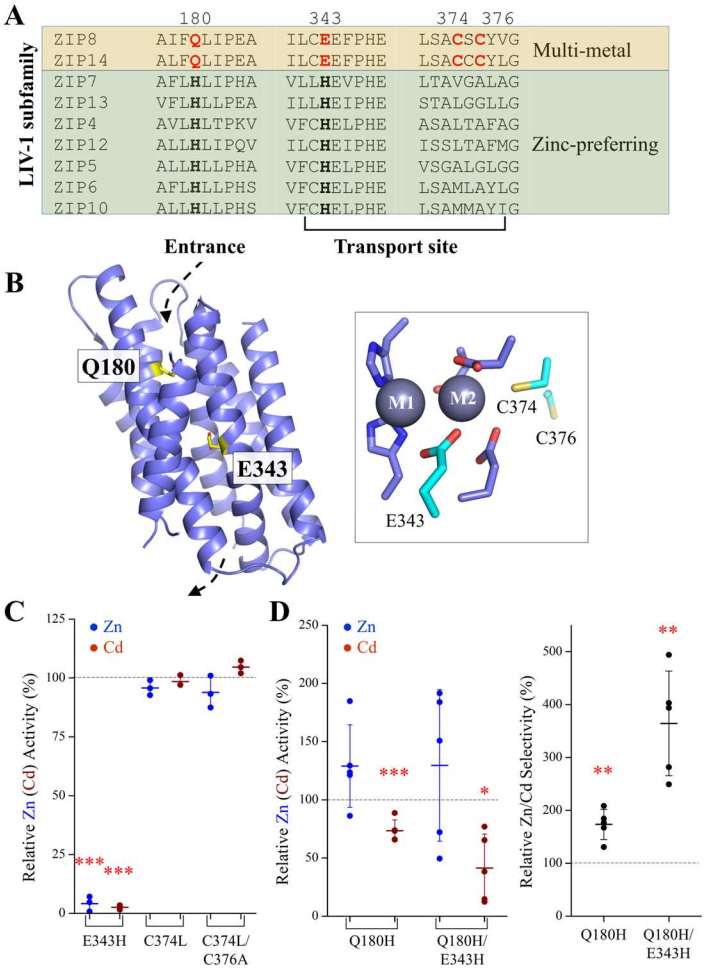

Figure 2.3. Epistatic interaction between Q180 and E343 involved in determining transport activity and substrate preference of human ZIP8. (**A**) Sequence alignment of human LIV-1 proteins to identify the uniquely conserved residues (in red) in the transport site and the pore entrance of ZIP8 and ZIP14. (**B**) The structure model of ZIP8 with the residues Q180 and H343 highlighted in stick mode. The dashed arrows indicate the entrance and the exit of the transport pathway. The transport site of ZIP8 with bound metal substrates (M1 and M2, grey spheres) is shown in the framed box, and the residues uniquely conserved in ZIP8 and ZIP14 are shown in cyan. (**C**) Zn^{2+} and Cd^{2+} transport activities of the variants with mutated transport site. The transport activities of the variants are expressed as percentages of the corresponding activities

Figure 2.3. (cont'd)
of the wild type ZIP8. The Zn^{2+} (or Cd^{2+}) transport activity was determined by subtracting the radioactivities of ^{65}Zn (or ^{109}Cd) associated with the cells transfected with the empty vector from those associated with the cells transfected with the vector that contains the DNA encoding the wild type ZIP8 or the variants. The shown data are from one representative experiment with three replicates. The short horizontal bars represent ±S.D., and the long horizontal bars indicate means. (**D**) The Q180H mutation rescued the transport dead E343H variant and increased the Zn/Cd selectivity. *Left*: The Zn^{2+} and Cd^{2+} transport activities of the variants of Q180H and Q180H/E343H. *Right*: The relative Zn/Cd selectivity of the variants of Q180H and Q180H/E343H. The Zn/Cd selectivity is defined as the ratio of the Zn^{2+} transport activity over the Cd^{2+} transport activity, and the relative Zn/Cd selectivity of a variant is expressed as percentage of the Zn/Cd selectivity of the wild type ZIP8. Each solid dot represents the mean of at least three replicates in one individual experiment. The shown data are the combined results of five independent sets of experiments conducted for each variant. The asterisks indicate the significant differences between the variants and the wild type ZIP8 (Student's *t*-tests: * $P \leq 0.05$; ** $P \leq 0.01$; *** $P \leq 0.001$).

Notably, E343 is located in the transport site (the M1 site according to the BbZIP structures), whereas Q180 is predicted to be at the entrance of the transport pathway according to the ZIP8 structure model where the transporter adopts an inward-facing conformation (IFC) (**Figure 2.3B**). In later experiments, we replaced Q180 and E343 with histidine and tested the substrate preference of the resulting variants. Sequence comparison also revealed two uniquely conserved metal-chelating residues (C374 and C376) in the putative M2 site of ZIP8, so we also tested the role of these residues by replacing them with the corresponding residues in ZIP4, a well-characterized zinc transporter[104,113,117,121,218,267,280,281].

2.4.2 Internal competition transport assay to precisely measure the Zn/Cd selectivity

Our initial focus was put on the Zn/Cd selectivity because the two metals, both in the IIB column of the periodic table, share similar properties in coordination chemistry. Indeed,

the previous studies have indicated that Zn^{2+} and Cd^{2+} use the same transport pathway through multi-metal ZIPs[115,203], and distinguishing them requires a delicate but less understood mechanism. To precisely measure small kinetic isotope effect of an enzyme, a commonly used approach is the internal competition assay in which a mixture of two competing substrates labeled with light and heavy isotopes respectively is applied to the enzyme for processing[282]. Similarly, we applied an internal competition transport assay by adding a mixture of radioactive $^{65}Zn^{2+}$ and $^{109}Cd^{2+}$ to the cells transiently expressing the wild type ZIP8 or the variants. After incubation and washing, radioactivity associated with the cells were measured to quantify ^{65}Zn and ^{109}Cd simultaneously by taking the advantage of different energy levels of the gamma rays emitted by the two radioisotopes (^{65}Zn: 800-1500 keV; ^{109}Cd: 30-150 keV). Under the optimal experimental conditions (**Figure 2.2**), the calculated radioactivity ratio of ^{65}Zn over ^{109}Cd would represent the ratio of the transport rates of the two competing substrates (*i.e.*, the Zn/Cd selectivity). An illustration of the internal competition transport assay is shown in **Figure 2.1**.

2.4.3 Identification of a double variant with a greatly increased Zn/Cd selectivity

The metal chelating residues in the transport site, including E343 in the M1 metal binding site as well as C374 and C376 in the M2 metal binding site[109,113], were tested in the first round. As shown in **Figure 2.3C**, the mutations on the cysteine residues (C374L and C374L/C376A) yielded no change in Zn^{2+} (or Cd^{2+}) transport activity, whereas the E343H variant exhibited no transport activity toward either substrate. This result was

unexpected because the E343H mutation leads to a binuclear metal center with metal chelating residues identical to ZIP4, so it is unlikely that this mutation completely disrupts metal binding at the transport site. The abolished transport activity of the E343H variant could not be explained by misfolding either because the mutation did not cause a drastically reduced expression as indicated in Western blot (**Figure 2.4**).

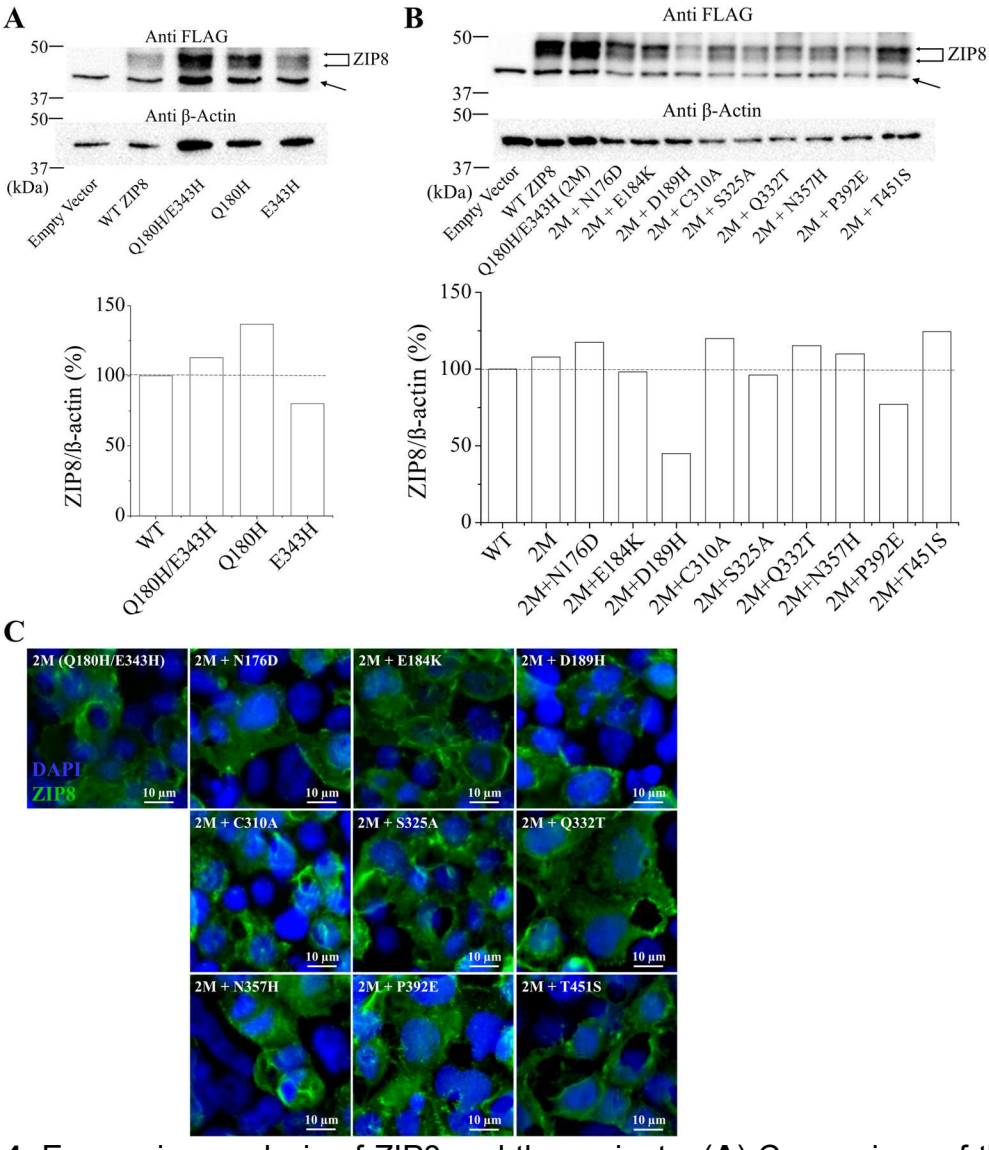

Figure 2.4. Expression analysis of ZIP8 and the variants. (**A**) Comparison of the single and double variants with the wild type ZIP8 by Western blot (upper panel) and quantification analysis using ImageJ (lower panel). (**B**) Comparison of triple variants with

Figure 2.4. (cont'd)
the wild type ZIP8 and the Q180H/E343H (2M) variant by Western blot (upper panel) and quantification analysis using ImageJ (lower panel). N-FLAG ZIP8 and β-actin were detected using anti-FLAG and anti-actin antibodies, respectively. The expression level of a variant is expressed as the percentage of the ratio of the wild type ZIP8 over β-actin. The shown result is from a representative experiment. (**C**) Immunofluorescence analysis of cell surface expressed ZIP8 variants. The procedure is the same as indicated in the legend of Figure 4A.

We then tested the effects of the mutation of Q180 which is located at the entrance of the transport pathway. Of interest, the Q180H variant exhibited an increase in the Zn/Cd selectivity by nearly two folds when compared with the wild type ZIP8 (**Figure 2.3D**). More importantly, the Q180H mutation rescued the transport dead E343H variant, and the resulting Q180H/E343H double variant (the 2M variant hereafter) exhibited a nearly four-fold increase in the Zn/Cd selectivity relative to the wild type ZIP8 and a two-fold increase on top of the Q180H variant, indicative of strong synergistic effect between the two residues. Close inspection of the data showed that the increased Zn/Cd selectivity was achieved primarily through suppressing the Cd^{2+} transport activity (**Figure 2.3D**), whereas the Zn^{2+} transport activity was modestly increased but with no statistical significance.

2.4.4 Identification of additional mutations that further improve the Zn/Cd specificity

By comparing the amino acid sequences among ZIP8, ZIP14, and ZIP4 homologs from multiple species (**Figure 2.5**), many additional DCRs were identified. We chose ZIP4 to compare ZIP8 and ZIP14 is because ZIP4 shares the highest sequence identity with

ZIP8/14 than other LIV-1 members and also it is a well-characterized zinc transporter. Mapping a total of 35 DCRs on the structure model of ZIP8 revealed a distinguishable pattern that many DCRs, particularly those potentially involved in metal chelation, are located along or at the entrance of the transport pathway (**Figures 2.5** & **2.6A**).

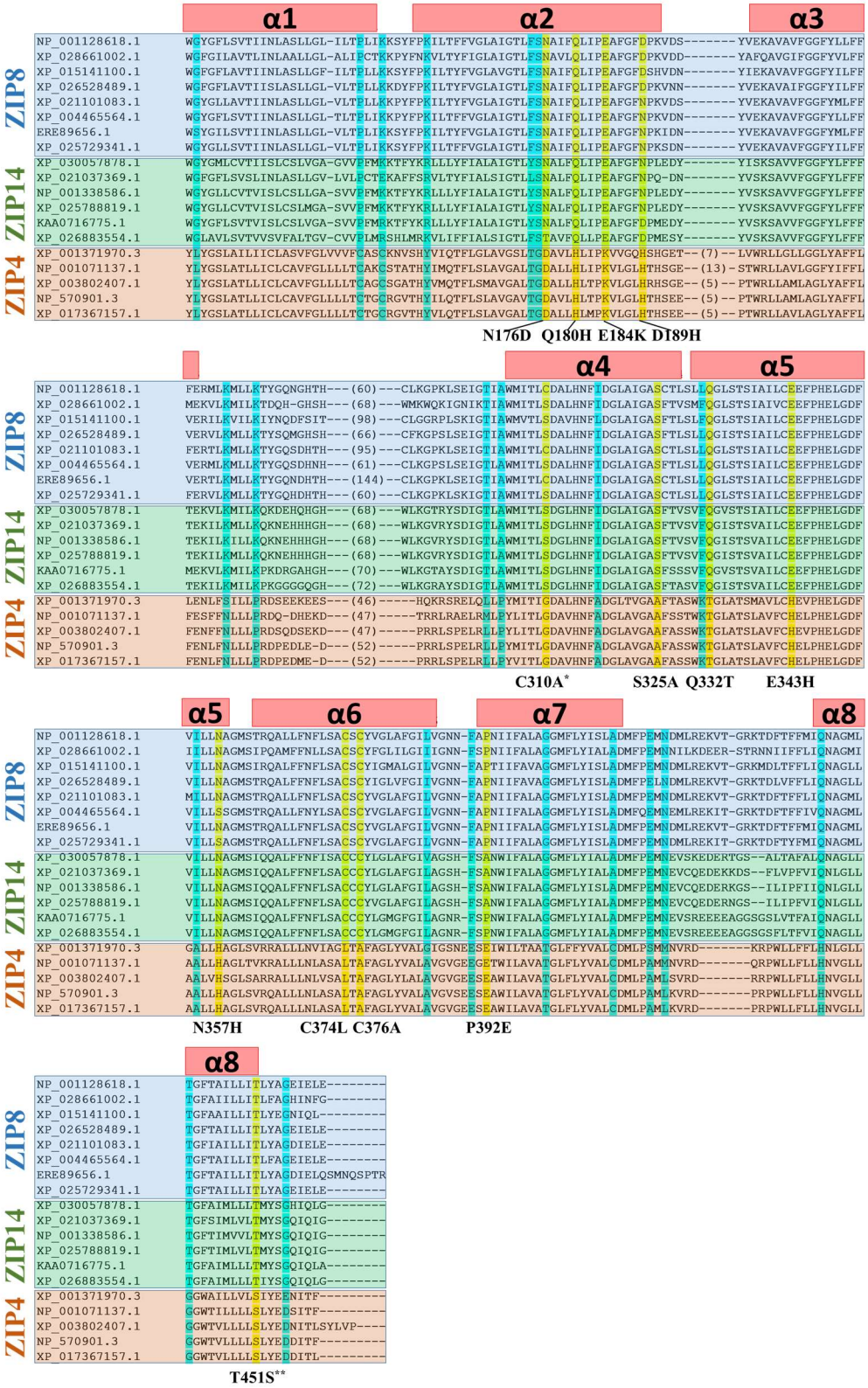

Figure 2.5. Sequence alignment of the transmembrane domains of the paralogs of ZIP8 (with blue background), ZIP14 (green), and ZIP4 (pink). ZIP8s: NP_001128618.1

Figure 2.5. (cont'd)
(*Homo sapiens*), XP_028661002.1 (*Erpetoichthys calabaricus*), XP_015141100.1 (*Gallus gallus*), XP_026528489.1 (*Notechis scutatus*), XP_021101083.1 (*Heterocephalus glaber*), XP_004465564.1 (*Dasypus novemcinctus*), ERE89656.1 (*Cricetulus griseus*), XP_025729341.1 (*Callorhinus ursinus*). ZIP14s: XP_030057878.1 (*Microcaecilia unicolor*), XP_021037369.1 (*Mus caroli*), NP_001338586.1 (*Homo sapiens*), XP_025788819.1 (*Puma concolor*), KAA0716775.1 (*Triplophysa tibetana*), XP_026883554.1 (*Electrophorus electricus*). ZIP4s: XP_001371970.3 (*Monodelphis domestica*), NP_001071137.1 (*Rattus norvegicus*), XP_003802407.1 (*Otolemur garnettii*), NP_570901.3 (*Homo sapiens*), XP_017367157.1 (*Cebus imitator*). The DCRs along or at the entrance of the transport pathway are highlighted in yellow and the others are in cyan. The tested DCRs are potential metal chelating residues (before or after substitution) along the transport pathway or at the pore entrance. The mutations derived from DCR swapping are listed below the alignment. The transmembrane helices (α1-α8) are shown as the red bars above the sequences. *C310 was substituted with alanine to avoid potential structural disruption caused by glycine substitution. **T451S is a conservative replacement, but it was tested because T451 is spatially close to other selected DCRs.

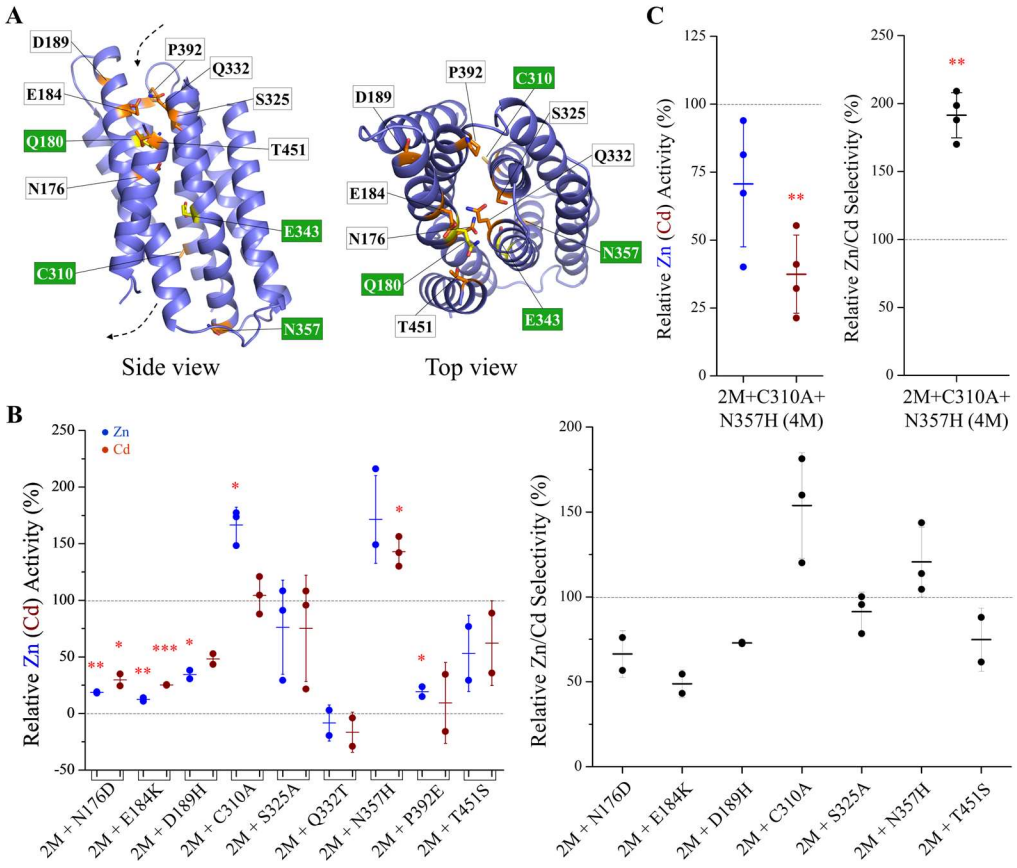

Figure 2.6. Generation of a quadruple variant with further improved Zn/Cd selectivity. (**A**) Mapping of the selected DCRs on the structure model of ZIP8. The selected DCRs are

Figure 2.6. (cont'd)
labeled and shown in stick mode – Q180 and E343 are in yellow, and the others are in orange. The residues substituted in the quadruple variant are labeled in white on a green background. (**B**) Screening of the triple variants with mutations on the selected DCRs. The Zn^{2+} (Cd^{2+}) transport activities (*left*) and the Zn/Cd selectivity (*right*) are expressed as percentage relative to the Q180H/E343H double variant (2M). Each solid dot represents the mean of at least three replicates in one individual experiment. The shown data are the combined results of 2-3 independent sets of experiments conducted for each variant. The short horizontal bars represent S.D., and the long horizontal bars indicate means. (**C**) Comparison of the Zn (Cd) transport activity (*left*) and the Zn/Cd selectivity (*right*) of the quadruple variant (4M) with those of the 2M variant. The Zn (Cd) transport activities (*left*) and the Zn/Cd selectivity (*right*) are expressed as the percentage values relative to the 2M variant. Each data point represents the mean of three replicates in one experiment and the results of four independent sets of experiments are shown. The asterisks indicate the significant differences between the 2M and the triple variants or between the triple and the quadruple (4M) variants (Student's *t*-tests: * $P \leq 0.05$; ** $P \leq 0.01$).

Based on the structure model, we postulate that, compared with the DCRs facing lipids or involved in TM packing, the metal chelating DCRs in the transport pathway are most likely to play a role in distinguishing metal substrates. We therefore examined whether replacing these DCRs in ZIP8 with the corresponding amino acids in ZIP4 would further increase the Zn/Cd selectivity on top of the 2M variant (**Figure 2.6B**). The nine generated triple variants exhibited quite different properties: Some variants lost most (for the variants of 2M+N176D and 2M+E184K) or nearly all (for the variants of 2M+Q322T and 2M+P392E) of the transport activity toward both Zn^{2+} and Cd^{2+}. The variant of 2M+D189H also exhibited reduced activity, but it can be attributed to the lower expression level (**Figure 2.4B**). The variants of 2M+S325A and 2M+T451S showed no change in Zn^{2+} or Cd^{2+} transport when compared with the 2M variant, whereas the mutations of C310A and N357H seemed to increase the activity toward Zn^{2+} more than Cd^{2+}. We then

examined whether combining the C310A and N357H mutations with the 2M variant would improve the Zn/Cd selectivity. As shown in **Figure 2.6C**, the resulting quadruple variant (Q180H/C310A/E343H/N357H, the 4M variant hereafter) exhibited a two-times greater Zn/Cd selectivity than the 2M variant, which can be attributed to a significantly reduced Cd^{2+} transport activity and a small (but statistically insignificant) decrease in Zn^{2+} transport activity (**Figure 2.6C**). When compared with the wild type ZIP8, the 4M variant achieved an approximately 7-8 times enhancement in the Zn/Cd selectivity.

2.4.5 Transport kinetic study of the 4M variant toward the multiple substrates of ZIP8

Expression analysis showed that the 4M variant was expressed in HEK293T cells with similar total and cell surface expression levels when compared with the wild type ZIP8 (**Figure 2.7A**), indicating that the combined mutations did not affect folding or intracellular trafficking of the transporter.

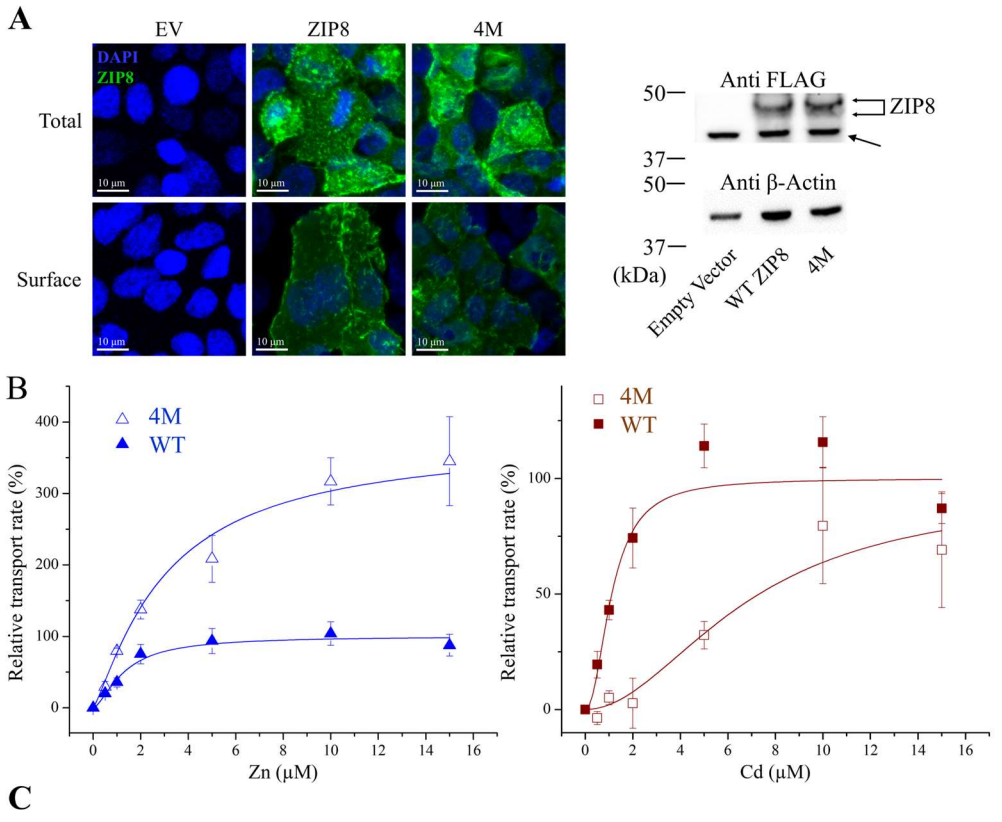

C

	Zn				Cd			
	K_M (μM)	Relative V_{max} (%)	Hill coefficient	V_{max}/K_M of 4M relative to WT ZIP8 (%)	K_M (μM)	Relative V_{max} (%)	Hill coefficient	V_{max}/K_M of 4M relative to WT ZIP8 (%)
WT ZIP8	1.3±0.3	100±10	1.2±0.2	160	1.1±0.2	100±10	2.1±1.0	15
4M variant	3.1±1.2	375±71	1.6±0.4		6.9±4.5	94±57	2.0±1.0	

Figure 2.7. Transport kinetics of the 4M variant in comparison with that of the wild type ZIP8. (**A**) Expression analysis of the wild type ZIP8 and the 4M variant in HEK293T cells. *Left*: Immunofluorescence images of the cells expressing the wild type ZIP8 or the 4M variant. The total expression and the surface expression of the N-FLAG ZIP8 (or the 4M variant) were detected by an anti-FLAG antibody and then an Alexa-488 labeled secondary antibody in permeabilized and non-permeabilized cells, respectively. The scale bar represents 10 μm. *Right*: Western blot of the wild type ZIP8 and the 4M variant. β-Actin was used as loading control. A non-specific signal is indicated by the arrow. (**B**) Transport of Zn^{2+} (*left*) and Cd^{2+} (*right*) by the 4M variant (open symbols) and the wild type ZIP8 (solid symbols). The shown data are from one representative experiment with 3-4 replicates for each data point. The error bars indicate ±S.D. The curves were fitted using the Hill model in Origin™. The transport rates are expressed as percentages of the V_{max} value of the wild type ZIP8. (**C**) The kinetic parameters of the 4M variant and the wild type ZIP8. The errors are the S.E. generated in curve fitting.

To understand the biochemical basis of the increased Zn/Cd selectivity, we measured Zn^{2+} and Cd^{2+} uptake and compared the kinetic parameters of the wild type ZIP8 and the 4M variant. As shown in **Figure 2.7B**, the 4M variant transported Zn^{2+} with a nearly fourfold increase in V_{max} but also a more than twofold increase in K_M, which led to a 1.6-times increase in V_{max}/K_M when compared to the wild type ZIP8. When transporting Cd^{2+}, the 4M variant exhibited a sixfold increase in K_M with no significant change in V_{max}, resulting in a 6-7 times reduction in V_{max}/K_M. The cooperativity as indicated by the Hill coefficients (n=1-2) may result from the M1 and M2 metal binding sites in the transport site and/or from the interactions between the two monomers of the ZIP dimer. Dimerization seems to be a common feature among the ZIP family members[104,110,111,283,284]. Together, the mutations in the 4M variant led to a moderate increase in specificity constant for Zn^{2+} but a large reduction for Cd^{2+}, which accounted for the greatly enhanced Zn/Cd selectivity. In addition, the transport kinetics of the 4M variant was reminiscent of that of ZIP4 that transports Zn^{2+} much more efficiently than Cd^{2+} under the same experimental conditions (**Figure 2.8**). However, the residual Cd^{2+} transport activity of the 4M variant suggests that there are additional unidentified mechanism(s) to allow the 4M variant to transport Cd^{2+}.

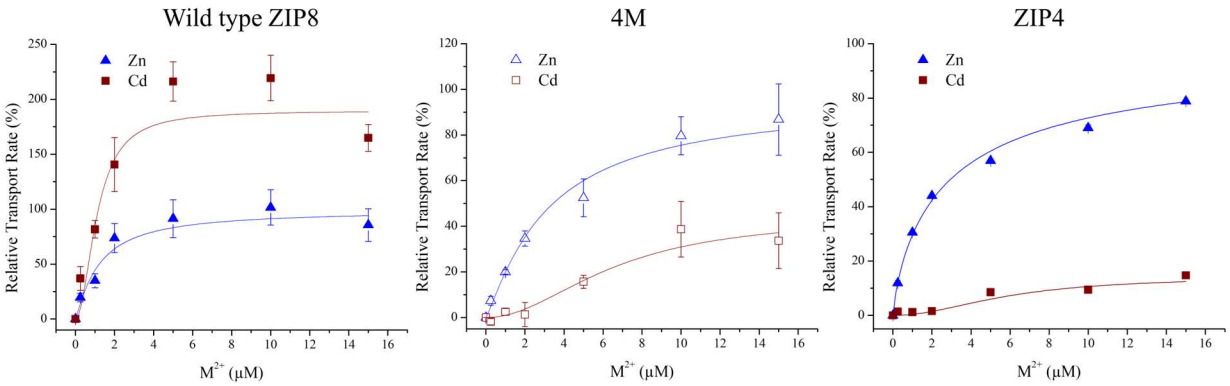

Figure 2.8. The Zn and Cd transport activities of the wild type ZIP8 and the 4M variant (*left*) in comparison with human ZIP4 (*right*). The same data shown in Figure 3B are presented differently for better comparison with ZIP4. The transport rates are expressed as the percentages of the V_{max} for Zn^{2+}.

Fe^{2+} and Mn^{2+} are also natural substrates of ZIP8 and known to compete with other metals[238,257,259,260]. To examine whether the 4M variant exhibits altered transport activities toward these two metals, we compared the Zn^{2+} transport activities of the wild type ZIP8 and the 4M variant in the presence and absence of an excess amount of Fe^{2+} or Mn^{2+}. As for the Zn^{2+}/Fe^{2+} competition, Zn^{2+} transport at the concentration of 5 μM significantly decreased for the wild type ZIP8 when 100 μM Fe^{2+} was added (**Figure 2.9A**).

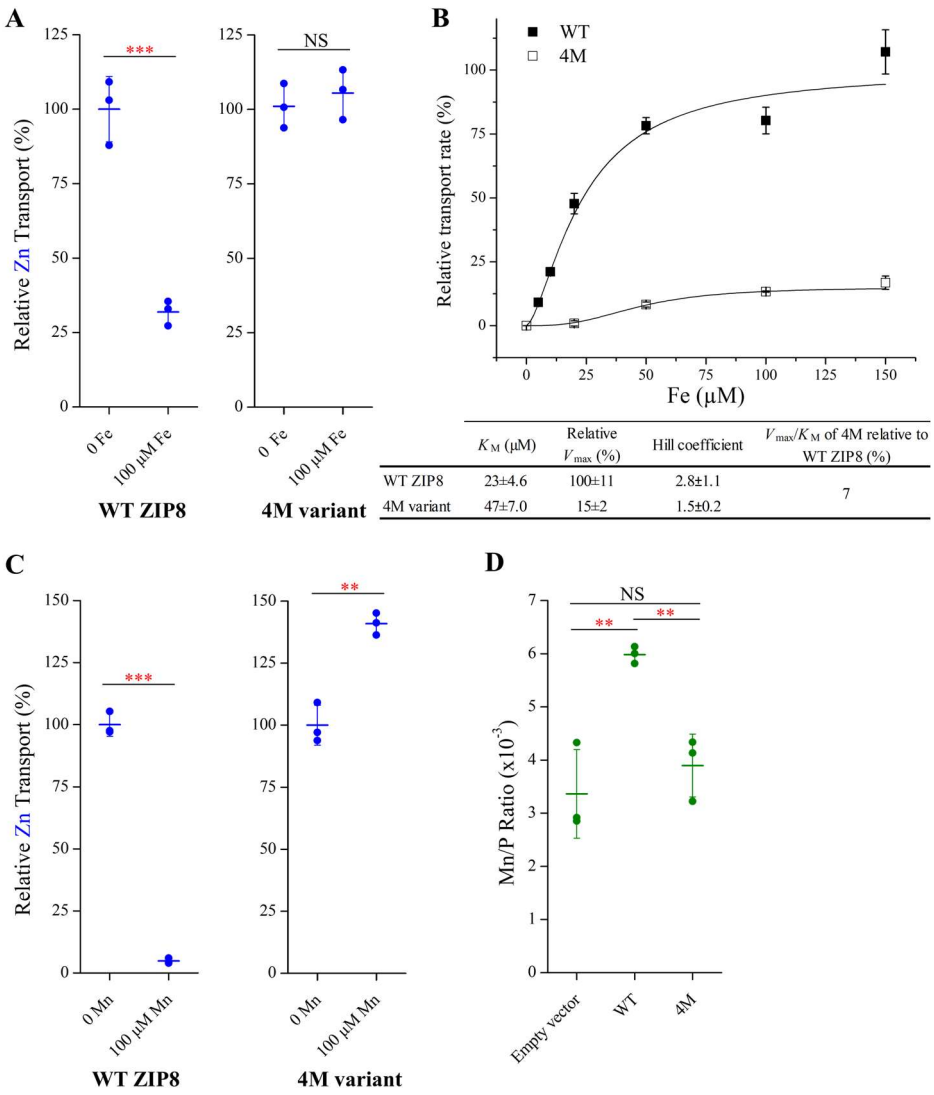

	K_M (μM)	Relative V_{max} (%)	Hill coefficient	V_{max}/K_M of 4M relative to WT ZIP8 (%)
WT ZIP8	23±4.6	100±11	2.8±1.1	7
4M variant	47±7.0	15±2	1.5±0.2	

Figure 2.9. Reduced Fe^{2+} and Mn^{2+} transport activity of the 4M variant. (**A**) Inhibition of Zn^{2+} transport of the wild type ZIP8 and the 4M variant by 100 μM of Fe^{2+}. The shown data are from one representative experiment with three replicates for each condition. (**B**) Fe^{2+} transport kinetics of the wild type ZIP8 and the 4M variant. The shown data are from one representative experiment with three replicates for each condition. The error bars indicate ±S.D. The curves were fitted using the Hill model in Origin™. The transport rates are expressed as percentages of the V_{max} of the wild type ZIP8. The kinetic parameters of the 4M variant and the wild type ZIP8 are listed in the table and the errors are the S.E. generated in curve fitting. (**C**) Inhibition of Zn^{2+} transport of the wild type ZIP8 and the 4M variant by 100 μM of Mn^{2+}. The shown data are from one representative experiment with three replicates for each condition. (**D**) Mn^{2+} transport assay of the wild type ZIP8 and the 4M variant. After incubation with Mn^{2+} (50 μM) for 30 min, the cells were washed and digested by nitric acid for ICP-MS measurement. The intracellular Mn levels were expressed as the molar ratios of Mn and phosphorus in the same sample. The shown

Figure 2.9. (cont'd)
data are from one representative experiment with three replicates for each condition. In (A), (C), and (D), the short horizontal bars represent S.D., and the long horizontal bars indicate means. The asterisks indicate the significant differences (Student's *t*-tests: ** P≤0.01; *** P≤0.001; NS, not significant).

In contrast, the 4M variant showed no sign of Zn^{2+} transport inhibition by 100 μM Fe^{2+}, suggesting that the 4M variant may have lost most of the transport activity toward Fe^{2+}. Consistently, the 4M variant showed a V_{max}/K_M that is more than ten times lower than that for the wild type ZIP8 with V_{max} being reduced by seven folds and K_M being increased by two folds (**Figure 2.9B**). For Mn^{2+}, the presence of Mn^{2+} at the concentration of 100 μM efficiently blocked Zn^{2+} transport of the wild type ZIP8 by more than 90% but had no inhibitory effect on the Zn^{2+} transport activity of the 4M variant (**Figure 2.9C**). Rather, a ~40% increase in Zn^{2+} uptake was observed, indicative of a putative allosteric activation. Next, we measured the Mn^{2+} transport activities of the wild type ZIP8 and the 4M variant by using inductively coupled plasma mass spectrometry (ICP-MS). The Mn/phosphorus (Mn/P) molar ratio of the wild type ZIP8 sample was significantly increased, whereas no change in the Mn/P ratio was observed for the 4M variant sample when compared with the control group (**Figure 2.9D**). These results strongly indicated that the 4M variant has lost the Mn^{2+} transport activity.

Collectively, by substituting four DCRs of the multi-metal transporter ZIP8 with the amino acids at the corresponding positions of the Zn transporter ZIP4, we were able to create a ZIP8 variant with a drastically increased substrate preference toward Zn^{2+} over

Cd^{2+}, Fe^{2+}, and Mn^{2+} due to the enhanced Zn^{2+} transport and the greatly diminished transport for the other metals.

2.4.6 A conditional selectivity filter that is formed and functions only in the outward-facing conformation (OFC)

In order to understand the structural and biochemical basis of the strong epistatic interaction between Q180 and E343 (**Figure 2.6**), we conducted structural modeling, evolutionary covariance analysis, and phylogenetic analysis, which revealed a conditional selectivity filter that functions only in the OFC.

Using the IFC structure and the OFC structure model of BbZIP as templates, we generated the homology models of human ZIP8 in two conformational states (**Figure 2.10A**). We noticed that AlphaFold predicts the structures of human ZIPs in distinct conformations with several ZIPs being in the OFC state[111]. Using the predicted structure of ZIP13, which represents the most outward open state, as the template, we generated an additional ZIP8 structural model in the OFC (**Figure 2.10A**).

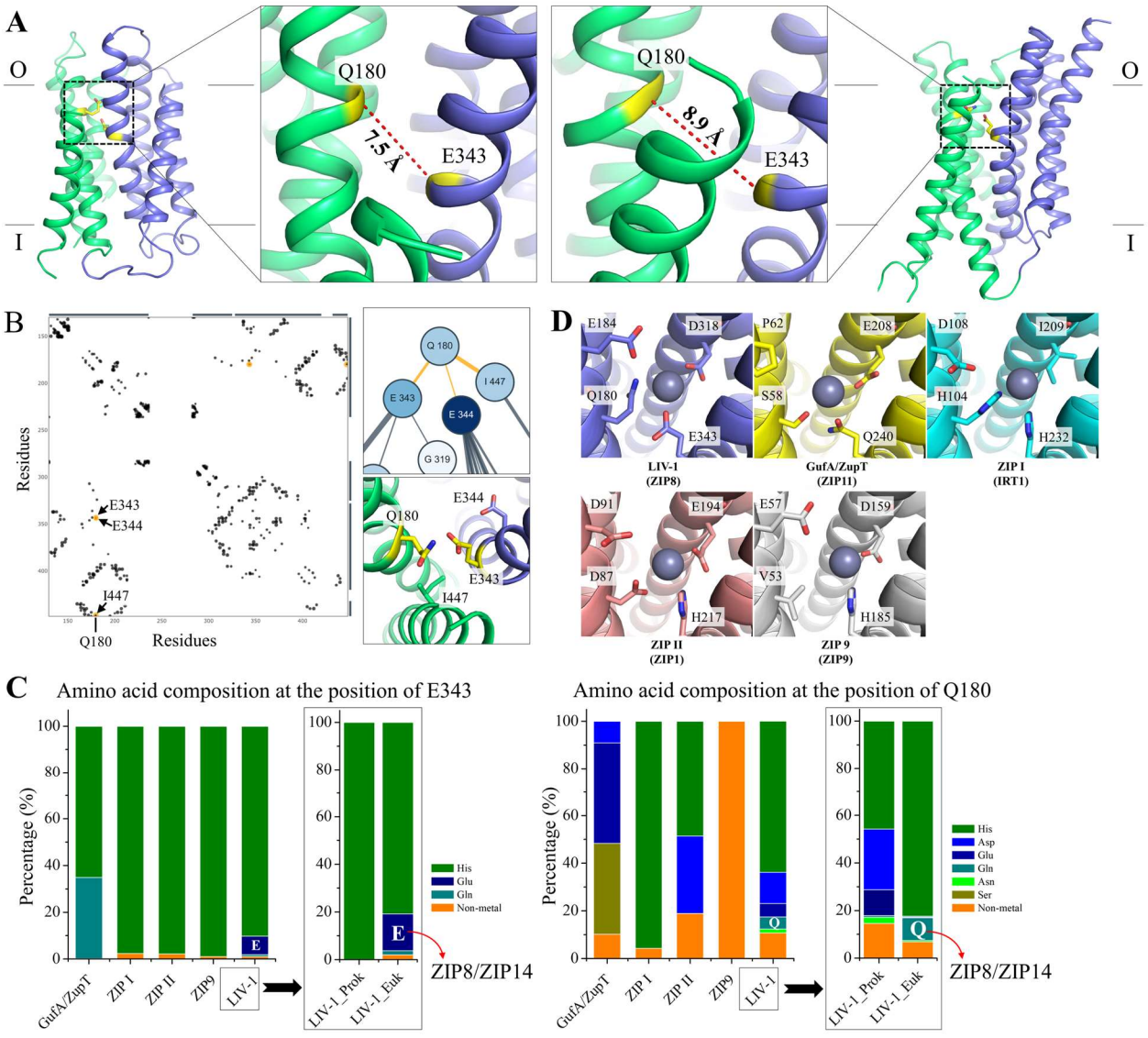

Figure 2.10. Identification of a conditional selectivity filter at the entrance of the transport pathway. (**A**) ZIP8 structural models in the OFC. The structural models were generated using either the OFC model of BbZIP (*left*) or the AlphaFold predicted human ZIP13 (*right*) as the template in homology modeling. As shown in the zoomed-in views, Q180 and E343 are close and face to each other in both structural models with the distances between the C_αs being labeled. The scaffold domain is colored in green and the transport domain in blue. (**B**) Predicted contacting residues of ZIP8 in an evolutionary covariance analysis by EVcouplings. Interactions involving Q180 are highlighted in orange in the interaction diagram (*left*). E343, E344, and I447 are predicted to interact with Q180, which is consistent with the structural model of ZIP8 in the OFC (*right*). (**C**) Amino acid composition at the positions of E343 (*left*) and Q180 (*right*) in major ZIP subfamilies. Analysis of prokaryotic and eukaryotic ZIPs in the LIV-1 subfamily is shown in the frames. The amino acid sequences retrieved from the PF02535 family in the Pfam database, including 2599

Figure 2.10. (cont'd)
in GufA/ZupT subfamily, 1200 in ZIP I subfamily, 716 in ZIP II subfamily, 5955 in LIV-1 subfamily, and 1033 in ZIP9 subfamily, were aligned and analyzed in Jalview. (**D**) The selectivity filter of ZIPs (in parentheses) from the major subfamilies. The structural models were generated using the AlphaFold predicted human ZIP13 as the template in homology modeling. The residues potentially involved in metal binding in ZIP8 and the corresponding residues in other ZIPs are labeled and shown in stick mode. Some side chains were adjusted to better accommodate a zinc ion (grey sphere).

Remarkably, although the C_α atoms of Q180 and E343 are 14.9 Å apart in the IFC model, they approach one another in both OFC models where they are 7.5 Å and 8.9 Å apart, respectively. Consistently, Q180 and E343 are predicted to form a direct interaction according to an evolutionary covariance analysis of ZIP8 (**Figure 2.10B**). As these metal chelating residues are close in space and face each other, they likely form a metal binding site at the entrance of the transport pathway.

Next, we conducted a phylogenetic analysis of the Q180-E343 pair in the entire ZIP family. Sequence analysis of more than 11,000 ZIPs from the major subfamilies of the ZIP revealed that the topologically equivalent residue of E343 of ZIP8 is histidine in most of the subfamilies, while glutamate occupies this position only in a small fraction of the eukaryotic LIV-1 proteins (**Figure 2.10C**). At the position equivalent to Q180 of ZIP8, a glutamine, which is exclusively present in the eukaryotic members of the LIV-1 subfamily, always copresents with a glutamate at the position equivalent to E343 of ZIP8, suggesting that the functions of the two residues are strongly coupled, which is consistent with the strong epistasis as revealed in the mutagenesis study (**Figure 2.6**).

Taken together, given the short distance between Q180 and E343 in the OFC models and their functional coupling in determining substrate preference and activity, Q180 and E343 are likely involved in a selectivity filter at the entrance of the transport pathway. As Q180 and E343 approach only when the transporter adopts an OFC, we call it a conditional selectivity filter. Close inspection of the OFC models suggested that D318 from the transport site may also join Q180 and E343 to better coordinate metal ions at the pore entrance (**Figure 2.10D**) and the nearby E184 is another candidate involved in metal recruitment. Indeed, the E184K mutation reduced the activity of the 2M variant by 80-90% (**Figure 2.6**). Sequence analysis of the entire ZIP family and modeling studies suggested that this conditional selectivity filter may be present in most of the ZIP family members, although the amino acid composition of this metal binding site may vary in different subfamilies (**Figure 2.10D**).

2.4.7 Free energy calculation of metal binding to the selectivity filter

Substitution of Q180 and E343 by histidine residues introduced two imidazole groups in the selectivity filter (**Figure 2.11A**), generating a metal binding site preferring Zn^{2+} over Fe^{2+} and Mn^{2+} according to the previously determined free energies of metal binding with small molecule ligands (**Figure 2.12A**)[285,286].

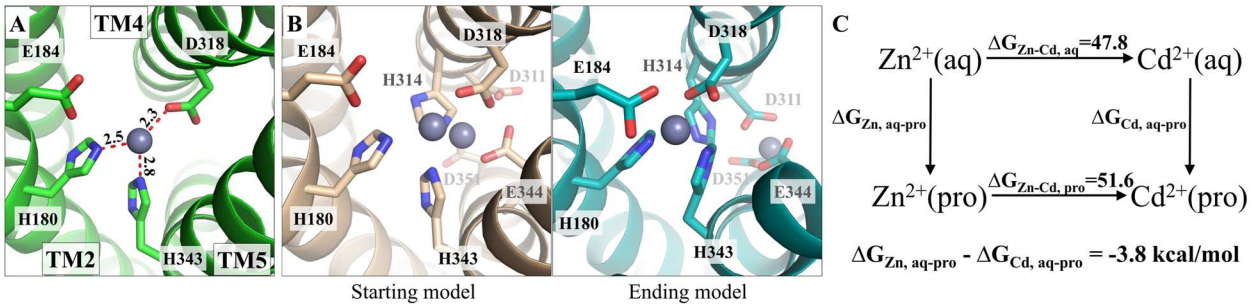

Figure 2.11. Computational characterization of the interactions of the 4M variant with metal substrates at the selectivity filter. (**A**) Structural model of the 4M variant with a zinc ion bound (grey sphere) at the selectivity filter. The structural model was generated by homology modeling using the human ZIP13 structure predicted by AlphaFold as the template. The metal ion is coordinated with H180, D318, and H343 with the metal-ligand distances labeled in angstrom. (**B**) MD simulations of the 4M variant with two bound zinc ions. *Left*: the starting model. One zinc ion was placed at the selectivity filter and the other at the transport site to prevent the former from entering the channel. *Right*: the ending model. The metal ion initially placed at the selectivity filter was stabilized by four residues, including E184, whereas the second one in the transport site moved down the transport pathway to a deeper position where two aspartate residues (D311 and D351, highly conserved in the LIV-1 subfamily) joined E344 to form a new metal binding site. (**C**) Free energy calculation of Zn^{2+} and Cd^{2+} binding to the selectivity filter (with E184 included) of the 4M variant. M^{2+}(aq) and M^{2+}(pro) indicate Zn^{2+} (or Cd^{2+}) in aqueous solution or bound at the selectivity filter, respectively. The free energy change resulting from the mutation of Zn^{2+} to Cd^{2+} in aqueous solution ($\Delta G_{Zn\text{-}Cd,\ aq}$) or at the selectivity filter ($\Delta G_{Zn\text{-}Cd,\ pro}$) was calculated using thermodynamic integration and the results are expressed in kcal/mol.

However, this estimation cannot satisfactorily explain why histidine replacement also improved the Zn/Cd selectivity since the free energy reduction upon ligand replacement with imidazole is similar for Zn^{2+} and Cd^{2+}. To address this issue, we conducted molecular dynamics (MD) simulations on the 4M variant in the OFC with a bound metal ion at the selectivity filter to obtain an energy-minimized structural model, which will be subsequently used for free energy calculation of metal binding using thermodynamic integration[285–291]. In the first trial, only after 10 ns of MD simulation, the Zn^{2+} initially

located at the selectivity filter moved to a deeper place within the transport pathway where the metal ion was coordinated by the residues from both M1 and M2 sites (**Figure 2.12B**).

A

Metal ion	Imidazole (His)			Acetate (Asp and Glu)		
	logK	Energy (kcal/mol)	Polarizability on coordinating nitrogen	logK	Energy (kcal/mol)	Polarizability on coordinating oxygen
Zn^{2+}	2.55	-3.48	2.71	1.58	-2.16	0.77
Fe^{2+}	1.80	-2.46	N/A	1.40	-1.91	N/A
Mn^{2+}	1.20	-1.64	N/A	1.40	-1.91	N/A
Cd^{2+}	2.66	-3.63	3.20	1.93	-2.63	1.17

B

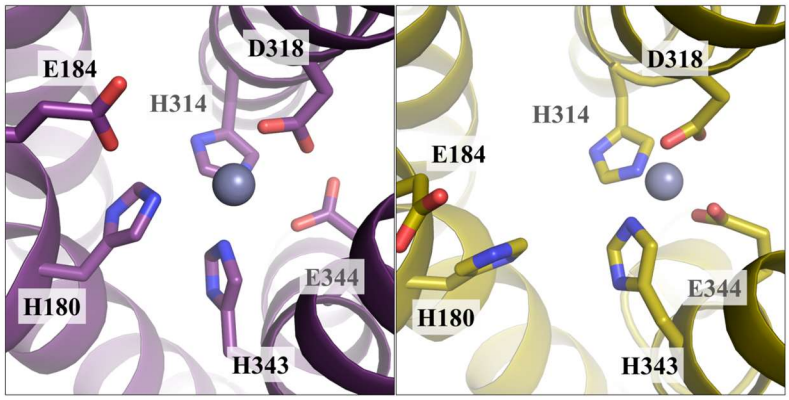

Figure 2.12. Computational characterization of metal binding at the selectivity filter. (**A**) Free energy changes of metal ion binding with small molecule ligands (refs 41&42). (**B**) The initial trial of MD simulation. The zinc ion initially located at the selectivity filter (*left*) moved to the transport site in the ending model (*right*) where it is coordinated with the residues from M1 (H314, H343), M2 (E344), and a bridging residue involved in both M1 and M2 (D318).

To prevent metal ion translocation to the transport site, a second metal ion was added in the starting model at the position which would otherwise be occupied by the metal ion at the selectivity filter. As expected, the metal ion bound at the selectivity filter was stabilized throughout a 3 μs MD simulation only with a small displacement (**Figure 2.11B**). Notably, E184, which was not included in metal chelation in the starting model, was found

to join the metal binding site with H180, H343, and D318 during the MD simulations, likely improving metal binding at the selectivity filter. Meanwhile, due to the repulsion between the two metal ions in the starting model, the second metal ion added in the transport site moved further down the transport pathway and then stabilized by three carboxylic acid residues (E344, D311, and D351). Using this energy-minimized and structure-stabilized ending model, we calculated and compared the free energy changes of Zn^{2+} and Cd^{2+} binding at the selectivity filter. As shown in **Figure 2.11C**, the selectivity filter (with E184 being included) of the 4M variant prefers binding Zn^{2+} over Cd^{2+} by 3.8±0.3 kcal/mol (n=3). Overall, the results of free energy calculation supported that the amino acid composition of the identified selectivity filter critically determines the substrate preference and that metal screening at the selectivity filter is a crucial step of distinguishing metal substrates.

2.4.8 Characterization of the ZIP4 variants containing the reverse substitutions

To test the importance of the selectivity filter in another ZIP, we chose human ZIP4 to perform reverse substitution on the residues that are topologically equivalent to those that were mutated in the 4M variant of ZIP8. As shown in **Figure 2.13A**, for Zn^{2+} and Cd^{2+} transport, the results indicated that: (1) The H379Q mutation (the reverse substitution of Q180H in ZIP8) showed little effect on Zn^{2+} or Cd^{2+} transport activity; (2) The H536E mutation (the reverse substitution of E343H in ZIP8) completely abolished the Zn^{2+} transport activity but retained a marginal activity toward Cd^{2+}; (3) Combining the H379Q and H536E mutations (the reverse substitutions of the 2M variant) partially restored Zn^{2+}

and Cd^{2+} transport activities and the Zn/Cd selectivity was significantly reduced by more than 60%, mirroring the effect of the 2M variant of ZIP8 that exhibits an increased Zn/Cd selectivity; and (4) Incorporation of additional two mutations (G503C and H550N, the additional two reverse substitutions of the 4M variant) with the H379Q/H536E variant abrogated Zn^{2+} and Cd^{2+} transport activities. Importantly, the partial restoration of Zn^{2+} and Cd^{2+} activities of the H536E variant by the H379Q mutation suggests an epistatic interaction, consistent with the proposed structural model where residues at these two positions are in close proximity when the transporter is in the OFC (**Figure 2.10**).

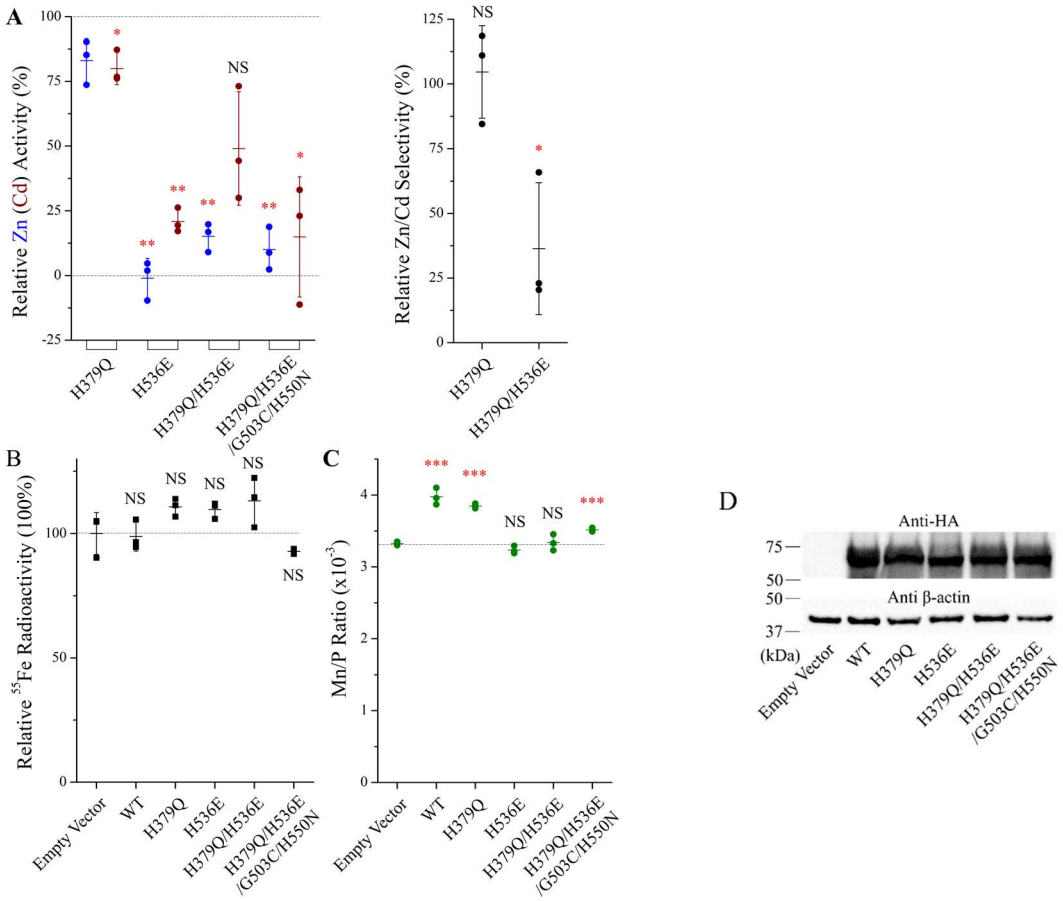

Figure 2.13. Characterization the substrate specificities of human ZIP4 and its variants. (**A**) The Zn^{2+} (Cd^{2+}) transport activities (*left*) and the Zn/Cd selectivity (*right*) are expressed as percentage relative to the wild-type ZIP4. Each solid dot represents the

Figure 2.13. (cont'd)
mean of three replicates in one individual experiment. The shown data are the combined results of three independent sets of experiments conducted for each variant. The short horizontal bars represent S.D., and the long horizontal bars indicate means. (**B**) Fe^{2+} transport assay of the wild-type ZIP4 and the variants. The ^{55}Fe radioactivity associated with the cells transfected with the empty vector was set as 100%. The shown data are from one representative experiment with three replicates for each condition. (**C**) Mn^{2+} transport assay of the wild-type ZIP4 and the variants. After incubation with Mn^{2+} (50 μM) for 30 min, the cells were washed and digested by nitric acid for ICP-MS measurement. The intracellular Mn levels were expressed as the molar ratios of Mn and phosphorus in the same sample. The shown data are from one representative experiment with three replicates for each condition. The asterisks indicate the significant differences between the wild-type ZIP4 and the variants (for Zn and Cd) or between the empty vector group and the transporter groups (for Fe and Mn). Student's *t*-tests: * P≤0.05; ** P≤0.01; *** P≤0.001. The expression of the HA-tagged ZIP4 and the variants were analyzed by Western blots. (**D**) Expression analysis of ZIP4 and the variants by Western blot. Human ZIP4 with a C-terminal HA tag and β-actin were detected using anti-HA and anti-β-actin antibodies, respectively.

The significantly reduced Zn/Cd selectivity of the H379Q/H536E variant reinforces the notion that these two residues at the selectivity filter play a role in determining substrate specificity. As the H379Q mutation had little effect on Zn^{2+} or Cd^{2+} transport activity, it seems that the H536E mutation is responsible for the reduced Zn/Cd selectivity. Indeed, the single H536E mutation did not completely abrogate Cd^{2+} transport activity as it did for Zn^{2+} transport. While we could not detect Fe^{2+} transport activity for any of the tested constructs of ZIP4, a Mn^{2+} transport activity was detected for the wild-type ZIP4 and the H379Q variant (**Figures 2.13B** & **C**). The Mn^{2+} transport activity was diminished by the H536E mutation but could not be restored by the H379Q mutation. Interestingly, the quadruple variant (H379Q/H536E/G503C/H550N) exhibited a partially restored Mn^{2+} activity. Overall, the mutagenesis study on ZIP4 confirmed the importance of the

selectivity filter in determining substrate preference, whereas the other two mutations along the transport pathway appeared to function differently from their counterparts in ZIP8.

2.5 Discussion

Engineering of metal transporters with altered substrate specificity can be strategized for potential applications in agriculture and environmental protection. In this work, we developed and applied an approach to rationally alter the substrate specificity of a multi-metal ZIP transporter, human ZIP8. We created a zinc-preferring ZIP8 variant by combining four designed mutations on selected residues at the entrance or along the transport pathway, demonstrating that these mutations increased the Zn^{2+} transport activity while largely suppressed the activities toward Cd^{2+}, Fe^{2+}, and Mn^{2+} (**Figures 2.3-2.7**). To apply this approach on a transporter of interest, it is crucial to identify a close homolog (referred to as the reference) with a distinct substrate spectrum. ZIP4 was chosen as the reference of ZIP8 because it strongly prefers Zn^{2+} over Cd^{2+} (**Figure 2.8**)[113,267,268]. One can identify the DCRs through multiple sequence alignment of the homologs of the target and the reference, map them on the structure (or structure model) of the transporter, and find specific residues located at the entrance or along the transport pathway. Then, the selected DCRs are replaced with the amino acids in the corresponding positions of the reference transporter. The resulting variants are subjected to internal competition transport assay to identify the mutations which confer a desired

substrate specificity to the variants. Finally, the beneficial mutations can be combined for greater fitness improvement. This approach is likely applicable to other transporters, and it can also be combined with directed evolution. For instance, optimization of the amino acids at the key residues identified from the DCR swapping study can be pursued by multi-site saturation mutagenesis.

More importantly, the mutagenesis and functional studies conducted in this work unraveled key molecular determinants of substrate specificity of ZIP8, in particular a conditional selectivity filter. Among the four residues substituted in the 4M variant, only E343 participates in metal binding at the M1 site which is the primary transport site of the ZIPs[109,115,183,244]. Previous multiple sequence analysis has predicted E343 as a key residue involved in determining substrate specificity[253,254], but its role was evidenced only when the transport dead E343H variant was rescued by the Q180H mutation in the 2M variant (**Figure 2.3**). The importance of the equivalent residue of Q180 in other ZIPs, including H104 in IRT1[244], H379 in ZIP4[109,283], and S106 in BbZIP[110], were documented, and it has been proposed that the residue at this position is at the very frontline in interacting with metal substrates[109,283]. Consistently, this work finds that Q180 in ZIP8 plays a pivotal role in determining substrate preference. Structural modeling, covariance analysis, phylogenetic analysis, and free energy calculation provided the structural and physicochemical basis of the epistatic interaction and synergy of Q180 with E343, strongly indicating that Q180 and E343 not only jointly exert functions in selecting

substrates but also physically interact at the entrance of the transport pathway in the OFC (**Figures 2.9** & **2.10**). Physical contact of the involved residue pair is one of many reasons that explain the epistasis of two compensatory mutations[292]. The importance of this residue pair in determining substrate preference and a similar epistatic interaction between these two residues have been confirmed through the corresponding reverse substitutions in ZIP4 (**Figure 2.13**), a zinc transporter in the same LIV-1 subfamily. Compared with other known elevator transporters, ZIP8 (and possibly many other ZIPs as well as) is unique in that Q180 in the scaffold domain approaches E343 in the transport domain to screen metal substrates (**Figure 2.10A**). This is a prominent example showing that the scaffold domain of an elevator transporter may actively participate in substrate selection. Different from the pre-formed selectivity filters in ion channels transporting alkaline and alkaline earth metal ions, the selectivity filter of ZIP8, which is a likely carrier according to the saturable kinetic profile (**Figures 2.7** & **2.9**), is formed in a conformation dependent manner, which therefore represents an unprecedented conditional selectivity filter. Also unlike the selectivity filters of canonical ion channels, the proposed selectivity filter of ZIP8 must not be the only mechanism that determines substrate specificity, since residues in the transport site and along the transport pathway (see below) are the obvious candidates involved in discriminating metal substrates.

The other two mutations in the 4M variant (C310A and N357H) are distant from the transport site or the entrance of the transport pathway. Rather, they are located at the

interface between the transport domain and the scaffold domain. Although each mutation had very modest effects, combination of the two mutations significantly improved the Zn/Cd selectivity on top of the 2M double variant (**Figures 2.5** & **2.6**). One possible explanation is that these mutations at the domain interface alter the dynamics of the elevator-type transporter, *i.e.*, the sliding of the transport domain against the scaffold domain. It has been shown that the mutations at the domain interface of a prototypic elevator transporter UapA drastically changed the substrate spectrum[293]. In addition, mutations of metal chelating residues may also alter the dynamic interactions of metal substrate with the transporter along the transport pathway. This is consistent with the notion that substrate translocation dynamics is as crucial as modification of the transport site in defining the substrate spectrum of a sugar transporter[294]. Accordingly, the entire process of multiple dynamic interactions between substrate molecule and transporter along and at the entrance of the conduit, rather than the mere substrate binding at the high-affinity transport site, is vital for substrate recognition and selection. Uniquely for metals, their interactions with a variety of ligands in solution (water, counterions, and other small molecule ligands) should also be considered, as the ligand exchange rates of metal-ligand complexes can affect metal selectivity as well.

Taken together, we demonstrated in this work that substitution of four rationally selected residues was sufficient to convert human ZIP8 that transports multiple metal substrates into a zinc-preferring transporter. Importantly, a conditional selectivity filter that

is formed and functions only when the transporter adopts the OFC was identified by using combined approaches. As the 4M variant is a zinc-preferring transporter with similar total and cell surface expression as the wild type ZIP8 (**Figure 2.7A**), it can be applied to knock-out/knock-in experiments to determine whether certain biological functions of ZIP8 are attributed to the transport activity toward Zn^{2+} and/or other natural substrates (Fe^{2+} and Mn^{2+}). Given the high sequence identity between ZIP8 and ZIP14 (48%), the same mutations in ZIP14 may generate similar effects on substrate specificity. After all, the importance of the proposed selectivity filter has been confirmed in ZIP4 (**Figure 2.13**), which shares a lower sequence identity (31%). Whether or not the identified residue pair plays a similar role in ZIPs with longer evolutionary distance needs to be tested in future study.

2.6 Conclusion

In this work, we identified a series of differentially conserved residues through sequence alignment and residue mapping. In vivo functional metal uptake assays studied these mutants and one variant, 4M, stood out during the screening for change in Zn/Cd preferences. Kinetics studies on Zn and Cd validified the dramatic change Zn and Cd change in the mutants compared to the wild type was achieved through slightly increased Zn preference and greatly decreased Cd activity. Fe and Mn activity was abolished for 4M as well. This work combined suggested a successful method for rational engineering, potentially applicable to other transporter families.

A conditional selectivity filter was also identified during the process. Consistent with the recent structural biology development in the ZIP family[111], the Q180 and E343 residue in human ZIP8 will came to each other's proximity to form a filter and further determine the substrate preference of the protein. Further clarification on the role of this filter will be of great interests.

2.7 Acknowledgements

I thank Dr. Jian Hu for the instruction and intelligent input in this project. I thank Dr. Dexin Sui, as well as Dr. Chi Zhang for the guidance, especially for the technical instruction and support. I thank our great collaborator Dr. Kenneth Merz and Dr. Thomas O'Halloran for their group's outstanding work. I thank Dr. Keith MacRenaris and Dr. Aaron Sue from the O'Halloran group for instructing me on ICP-MS. I thank Dr. Hideki Takahashi for manuscript drafting and editing.

This work is supported by NIH GM129004 and GM140931.

CHAPTER 3: Determination of metal ion transport rate of human ZIP4 using stable zinc isotopes

Yuhan Jiang[1], Keith MacRenaris[1,2,3,5], Thomas V. O'Halloran[1,2,3,5,*], Jian Hu[1,4,*]

[1]Department of Chemistry, Michigan State University, East Lansing, MI, USA

[2]Department of Microbiology and Molecular Genetics, Michigan State University, East Lansing, MI, USA

[3]Elemental Health Institute, Michigan State University, East Lansing, MI, USA.

[4]Department of Biochemistry and Molecular Biology, Michigan State University, East Lansing, MI, USA

[5]Quantitative Bio Element Analysis and Mapping (QBEAM) Center, Michigan State University, East Lansing, MI, USA

Under review in Journal of Biological Chemistry.

This work was led by me under the guidance of Dr. Jian Hu and Dr. Thomas V. O'Halloran. I and Dr. Keith MacRenaris did preliminary exploration of the 70Zn protocol, (Table 3.1, Figure 3.3, 3.4, 3.5, 3.6, 3.9, 3.11), where I conducted cell assays and Dr. MacRenaris and I conducted the ICP-MS measurement. I conducted all the western blot experiments. All four authors were involved in manuscript writing and editing.

3.1 Summary

The essential microelement zinc is absorbed in the small intestine mainly by the zinc transporter ZIP4, a representative member of the Zrt/Irt-like protein (ZIP) family. ZIP4 is reportedly upregulated in many cancers, making it a promising oncology drug target. To date, there have been no reports on the turnover number of ZIP4, which is a crucial missing piece of information needed to better understand the transport mechanism. In this work, we used a non-radioactive zinc isotope, ^{70}Zn, and inductively coupled plasma-mass spectrometry (ICP-MS) to study human ZIP4 (hZIP4) expressed in HEK293 cells. Our data showed that ^{70}Zn can replace the radioactive ^{65}Zn as a tracer in kinetic evaluation of hZIP4 activity. This approach, combined with the quantification of the cell surface expression of hZIP4 using biotinylation or surface-bound antibody, allowed us to estimate the apparent turnover number of hZIP4 to be in the range of 0.08-0.2 s^{-1}. The turnover numbers of the truncated hZIP4 variants are significantly smaller than that of the full-length hZIP4, confirming a crucial role for the extracellular domain in zinc transport. Using ^{64}Zn and ^{70}Zn, we measured zinc efflux during the cell-based transport assay and found that it has little effect on the zinc import analysis under these conditions. Finally, we demonstrated that use of laser ablation (LA) ICP-TOF-MS on samples applied to a solid substrate significantly increased the throughput of the transport assay. We envision that the approach reported here can be applied to the studies of metal transporters beyond the ZIP family.

3.2 Introduction

As an essential trace element, zinc ions play catalytic, structural, and regulatory roles in biological systems[295], including cell signaling[296–298] and cell cycle control during meiosis and mitosis[299–306]. Zinc fluxes are also associated with numerous physio-pathological processes[297,299,303,307–313]. In humans, dietary zinc is absorbed in the small intestine where its transport is primarily mediated by ZIP4, a zinc transporter belonging to the Zrt/Irt-like protein (ZIP) metal transporter family[138,253,254,314]. The pivotal role of ZIP4 in zinc uptake is manifested by ZIP4 dysfunctional mutations that lead to acrodermatitis enteropathica (AE), a life-threatening recessive genetic disorder[133,218,267,268,315]. Remarkably, aberrant expression of ZIP4 has been found in many types of cancer and knockdown of ZIP4 in cancer cells significantly reduces cell proliferation and metastasis[151,158,161,316–322]. Limited tissue distribution under normal conditions and aberrant upregulation in cancer suggest that ZIP4 is a promising cancer biomarker and anti-tumor drug target.

The mechanism of zinc ion transport by ZIP-family proteins is not well understood. Recent structural and biochemical studies of a bacterial ZIP from *Bordetella bronchiseptica* have suggested that the ZIP transporters use an elevator mode as the common transport mechanism[110,111] (**Figure 3.1**). As elevator transporters can act as either carriers or channels to achieve substrate translocation across the membrane, it is important to determine the transport mechanism of the ZIPs of interest by characterizing their kinetic properties. Proteoliposome-based studies showed that the bacterial ZIPs may

behave as carriers or ion channels[115,284,323], but the cell-based assays have suggested that the ZIPs act as carriers. Early studies on a ZIP homolog from *E.coli*, ZupT, showed that the transporter behaved as a carrier in an *E.coli* strain where several endogenous metal transporters have been knocked out[211,324]. Due to the difficulties in protein production, liposome reconstitution, and the transporters' sensitivity to lipid composition[325], eukaryotic ZIPs have only been studied in the cell-based transport assay[93,94,104,109,113,117,183,184,265,283,326,327]. However, one concern with the cell-based assay is that metal efflux during the transport assay, which is due to the activities of metal exporters on the plasma membrane, may lead to an underestimation of the imported metal substrate, resulting in a distorted dose curve and incorrectly determined kinetic parameters. Therefore, it is necessary to evaluate the effect of metal efflux on the transport assay.

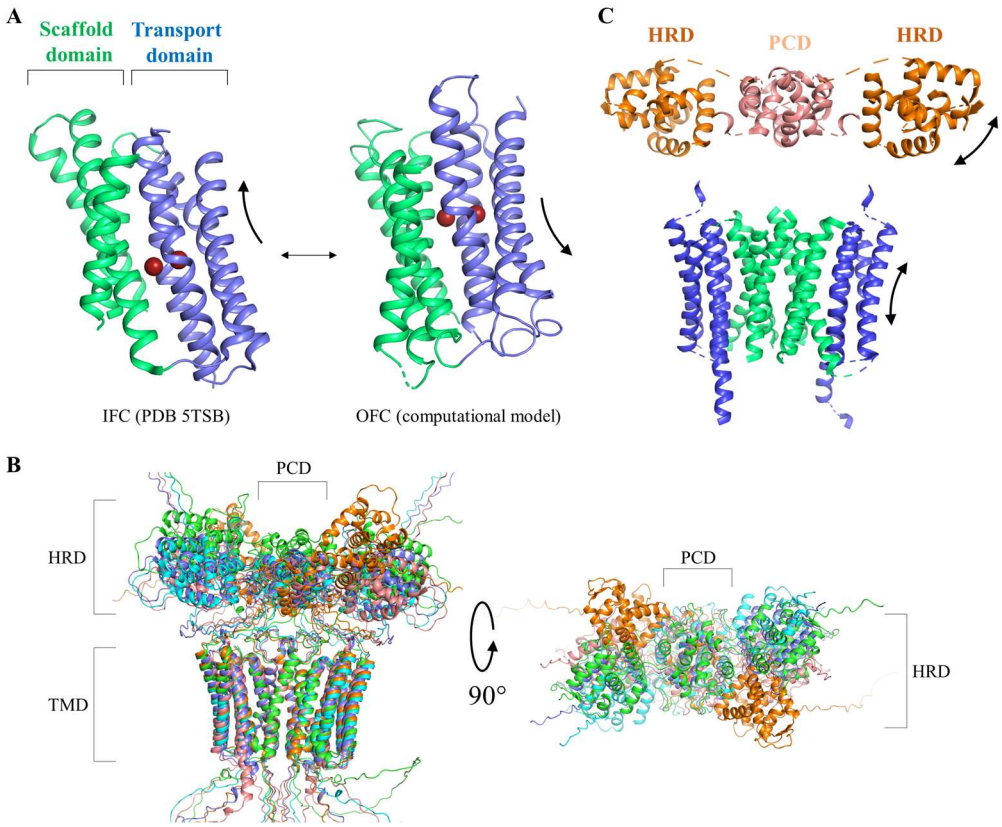

Figure 3.1. Proposed elevator-type transport mechanism. (**A**) The elevator motion of BbZIP. The interconversion of the inward-facing and outward-facing conformations is achieved by vertical sliding of the transport domain (blue) against the static scaffold domain (green) that is involved in dimerization (not shown). The computational model for the outward-facing conformation was reported in ref 40. (**B**) Five AlphaFold 2.0 predicted structures of mouse ZIP4 dimer in the side (*left*) and top (*right*) views. The transmembrane domains (TMD) are structurally superimposed to reveal the flexibility of the HRD and PCD domains. (**C**) A putative interaction between the HRD (orange) and the transport domain (blue). The TMD is colored as for BbZIP in (A). For clarity, the predicted loops have been trimmed. Considering that the elevator motion of the transport domain and the flexibility of the HRD domain, as indicated by the curved arrows, it is plausible that the interaction of the HRD with the transport domain may promote the formation and stabilization of the outward-facing conformation and thereby facilitate zinc transport.

So far, the radioactive ^{65}Zn is the most commonly used substrate in the cell-based transport assays for the ZIPs because of the high intracellular zinc level in mammalian cells (up to 250 μM). However, the inclusion of radioactive metals in the transport assay limits the application of this approach to the extent necessary to thoroughly characterize

these important metal transporters. An alternative approach is to use a low-abundance stable isotope of zinc so that the high natural background issue can be largely relieved. Indeed, ^{70}Zn, which takes only 0.6% of naturally present zinc, has been used in the cell-based transport assay[328], demonstrating the potential to study transport kinetics of metal transporters.

In this work, we used a modified ^{70}Zn-based approach to study the transport kinetics of hZIP4 which is expressed in HEK293 cells. Quantification of ^{70}Zn by ICP-MS and the cell surface expression level of the transporter allowed us to report, for the first time, the turnover number of hZIP4. Using this approach, we re-examined the role of the extracellular domain (ECD) for ZIP4 function and confirmed the crucial role of the ECD for optimal zinc transport. Using two stable zinc isotopes, ^{64}Zn and ^{70}Zn, we found that although zinc efflux is detectable it has little effect on the results of the transport assay under our experimental conditions. Taken together, these results lead us to conclude that hZIP4 most likely functions as a carrier, rather than an ion channel. We also demonstrated that the application of laser ablation (LA) ICP-MS can significantly increase the throughput of isotope measurement to study the cell samples loaded on a glass slide.

3.3 Materials and Methods

3.3.1 Gene, plasmids, and reagents

The complementary DNA of human ZIP4 (GenBank access number: BC062625) from Mammalian Gene Collection were purchased from GE Healthcare. The hZIP4 coding

sequence was inserted into a modified pEGFP-N1 vector (Clontech) in which the downstream EGFP gene was deleted, and an HA tag was added at the C-terminus. ZIP4 variants (ΔHRD-hZIP4-HA and ΔECD-hZIP4-HA) were generated as previously described[104]. All mutations were verified by DNA sequencing. For the hZIP4 construct for purification, a FLAG tag is added immediately after the signal peptide to generate the final FLAG-hZIP4-HA construct[121]. ^{64}ZnO and ^{70}ZnO were purchased from American Elements (Product# ZN-OX-01-ISO.064I, Lot#1871511028-400 and ZN-OX-01-ISO.070I, Lot#1871511028-401, respectively). 30 mg of zinc oxide powder was dissolved in 5 ml of 1 M HCl and then diluted with ddH2O to make the stock solution at the concentration of 50 mM. The ^{64}Zn sample was certified as 98% abundance while ^{70}Zn isotope in the other sample corresponded to an abundance of 72%. Other reagents were purchased from Sigma-Aldrich or Fisher Scientific.

3.3.2 Cell culture, transfection, and Western blot

Human embryonic kidney cells (HEK293T, ATCC, #CRL-3216) were cultured in Dulbecco's modified eagle medium (DMEM, Thermo Fisher Scientific, Invitrogen, Cat#11965092) supplemented with 10% (v/v) fetal bovine serum (FBS, Thermo Fisher Scientific, Invitrogen, Cat#10082147) and Antibiotic-Antimycotic solution (Thermo Fisher Scientific, Invitrogen, Cat# 15240062) at 5% CO_2 and 37°C. The polystyrene 24-well trays (Alkali Scientific, Cat#TPN1024) were treated with 300 µl Poly-D-Lysine (Corning, Cat#354210) for each well overnight, after which cells were seeded in the DMEM plus

medium. After 16 hours of incubation cells were transfected with 0.8 µg DNA/well using lipofectamine 2000 (Thermo Fisher Scientific, Invitrogen, Cat# 11668019) in DMEM plus 10% FBS.

For Western blot, samples were mixed with the SDS sample loading buffer and heated at 96 °C for 10 min before loading on SDS-PAGE gel. The proteins separated by SDS-PAGE were transferred to PVDF membranes (Millipore, Cat#PVH00010). After blocking with 5% (w/v) nonfat dry milk, the membranes were incubated with mouse anti-HA antibody (Thermo Fisher Scientific, Cat# 26183) or rabbit anti-β-actin (Cell Signaling, Cat# 4970 S) at 4 °C overnight, which were detected with HRP-conjugated horse anti-mouse immunoglobulin-G antibody at 1:5000 dilution (Cell Signaling Technology, Cat# 7076) or goat anti-rabbit immunoglobulin-G antibody at 1:3000 dilution (Cell Signaling Technology, Cat# 7074) respectively using the chemiluminescence reagent (VWR, Cat#RPN2232). The images of the blots were taken using a Bio-Rad ChemiDoc Imaging System.

3.3.3 Treatment of the culture media with Chelex-100

100 ml of the culture media (DMEM+10% FBS) was mixed with 5 g Chelex-100 resin (Sigma-Aldrich, Cat# C7901) in a column and placed on a gyratory rocker overnight. The resin can be regenerated for further treatment after following process: washed by one column volume of water, incubate with one column volume of 1 M hydrochloric acid for

one hour, wash with one column volume of water, incubate with one column volume of 1 M sodium hydroxide for one hour, wash with two column volumes of water.

3.3.4 Zinc transport assay

Twenty hours post transfection, cells were washed with the washing buffer (10 mM HEPES, 142 mM NaCl, 5 mM KCl, 10 mM glucose, pH 7.3) followed by incubation with Chelex-treated culture media. ^{70}Zn was added to initiate the transport. In the experiments shown in Figures 1A, 1B and 4B, 5 μM of ^{70}Zn was added. In the experiments shown in Figures 2 and 3, 12 μM of ^{70}Zn (about 5-10 times of the apparent K_M) was added. After incubation at 37°C for 30 min, the plates were put on ice and an equal volume of the ice-cold washing buffer containing 1 mM EDTA was added to the cells to terminate metal uptake, followed by three times of washing with ice-cold washing buffer.

3.3.5 Estimation of cell surface expression level by biotinylation

Cell surface protein biotinylation and isolation was done with the cell surface protein biotinylation and Isolation kit (Thermoscientific, Cat#A44390). 20 hours post transfection, the cells from six wells in a 24-well tray were washed by phosphate-buffered saline (PBS, 200 μl per well) and subjected to amine labelling of the membrane proteins at cell surface with Sulfo-NHS-SS-Biotin in PBS (200 μl per well) as described in the manual. After incubation at room temperature for 10 minutes, the labelling solution was removed and cells were washed with the ice-cold tris(hydroxymethyl)aminomethane-buffered saline (TBS, 200 μl per well) to terminate the reaction. Cells were then harvested in TBS (200

μl per well) and lysed. The lysate was applied to the NeutrAvidin agarose column to purify the labeled proteins. The labelled proteins were collected in the elution buffer containing 10 mM DTT. The samples were then mixed with 2xSDS loading buffer with a 1:1 volume ratio. hZIP4 with an N-FLAG tag and C-HA tag (FLAG-hZIP4-HA) was purified as reported[121] and used as the standard to generate a standard curve. The samples from cells and the standards were subjected to Western blot.

3.3.6 Estimation of cell surface expression level by surface bound antibody

Twenty hours post transfection, cell culture media was removed and cells were washed with Dulbecco's phosphate-buffered saline (DPBS). Cells were then fixed with 4% formaldehyde for 10 minutes at room temperature, followed by three times of washing with DPBS to remove formaldehyde. To detect the HA-tagged hZIP4 expressed at cell surface, cells were incubated in DPBS solution with 5% BSA (Sigma-Aldrich, Cat# A2153) and 3 μg/ml anti-HA antibody (Invitrogen, Cat# 26183) for one hour and a half at room temperature. The solution was then removed and the cells were washed five times with DPBS. Each time the plate was put on a gyratory rocker for 5 minutes of gentle shaking. The sample was subjected to Western blot together with the known amount of anti-HA antibody. The latter was used to generate a standard curve to estimate the cell surface bound anti-HA antibody. To detect the cell surface bound anti-HA antibodies, the HRP-conjugated horse anti-mouse immunoglobulin-G antibody at 1:5000 dilution (Cell Signaling Technology, Cat# 7076) was directly applied to the PVDF membrane in the

Western blot experiment, followed by signal visualization using the chemiluminescence reagent (VWR, Cat#RPN2232).

3.3.7 Zinc isotope replacement experiment and estimation of zinc efflux

HEK293T cells were seeded into poly-D-lysine treated polystyrene 24-well plates as described previously and allowed to grow in the regular culture media (DMEM plus 10% FBS) for 16 hours. The culture media were then removed as much as possible and the metal supplemented ^{64}Zn-enriched culture media was added. The metal supplemented ^{64}Zn-enriched culture media is the Chelex-treated culture media (DMEM plus 10% FBS) supplemented with Mg, Ca, Cu, and ^{64}Zn to restore these metals back to the levels in the untreated culture media. The calculation was based on the ICP-MS data in **Table 3.1** At the designed time points, the ^{64}Zn enriched culture media was removed and cells were washed with the washing buffer for three times. The cells were digested in nitric acid for ICP-MS analysis.

	^{24}Mg	^{43}Ca	^{54}Fe	^{55}Mn	^{63}Cu	^{64}Zn
Before treatment	782.463±9.836	1705.372±32.952	3.048±0.343	0.070±0.011	0.236±0.002	4.037±0.138
After treatment	9.778±7.494	24.857±15.512	3.141±0.631	0.068±0.031	0.137±0.052	0.369±0.235
Residual metal (%)	1.25	1.46	103.05	97.64	58.2	9.14

Table 3.1. Changes of divalent metal concentrations (in μM) in the cell culture media before and after Chelex-100 treatment. Data from three independent experiments are expressed as mean±S.D.

3.3.8 Determination of zinc efflux during the transport assay

After being cultured in the ^{64}Zn enriched culture media for three passages in a poly-D-lysine treated polystyrene 24-well plate, HEK293T cells were transfected with the

plasmid encoding hZIP4. 20 hours post transfection, the cells were treated with or without the ^{70}Zn-enriched culture media containing 5 μM ^{70}Zn. Six replicates from different wells were included in each group (the treated cells or the untreated cells). After incubation at 37°C for 30 minutes, the cells in both groups were treated in the same way as described in the section of zinc transport assay. ^{64}Zn and ^{70}Zn associated with the cells were quantified by ICP-MS and calibrated with ^{31}P in the same sample by using the Zn/P count ratio. A cartoon illustration explaining the following equations is shown in **Figure 3.11B**. The efflux of ^{64}Zn during the transport assay was determined accordingly.

$$^{64}Zn_{initial} = {}^{64}Zn_{edg,\ rt} + {}^{64}Zn_{edg,\ ef} \quad (1)$$

$$^{64}Zn_{end} = {}^{64}Zn_{edg,\ rt} + {}^{64}Zn_{if,\ rt} \quad (2)$$

$$^{70}Zn_{initial} = {}^{70}Zn_{edg,\ rt} + {}^{70}Zn_{edg,\ ef} \quad (3)$$

$$^{70}Zn_{end} = {}^{70}Zn_{edg,\ rt} + {}^{70}Zn_{if,\ rt} \quad (4)$$

$$^{64}Zn_{if,\ rt} / {}^{70}Zn_{if,\ rt} = C_{64/70} \quad (5)$$

where the subscripts *initial* and *end* represent states of cells before and after the assay, respectively. *edg* represents the endogenous zinc; *rt* represents the zinc retained after the assay; *ef* represents the zinc exported during the assay; *if* represents the zinc imported during the assay.

$^{64}Zn_{initial}$ and $^{70}Zn_{initial}$ were determined in the untreated cells, and $^{64}Zn_{end}$ and $^{70}Zn_{end}$ were determined in the treated cells. $C_{64/70}$ refers to the ^{64}Zn/^{70}Zn molar ratio in the ^{70}Zn stock solution, which was experimentally determined to be 0.123. As shown in the dataset

in **Figure 3.11B**, $^{70}Zn_{initial}$ is two orders of magnitude smaller than $^{70}Zn_{end}$, which is because the cells were grown in the ^{64}Zn-enriched culture media. Since $^{70}Zn_{edg,\ ef}$ is a portion of $^{70}Zn_{initial}$, it can be ignored in (4), yielding

$$^{70}Zn_{if,\ rt} \approx {}^{70}Zn_{end}$$

substitute $^{70}Zn_{if,\ rt}$ into equation (5), $^{64}Zn_{if,\ rt} = {}^{70}Zn_{if,\ rt} \times C_{64/70}$

substitute $^{64}Zn_{if,\ rt}$ into equation (2), $^{64}Zn_{edg,\ rt} = {}^{64}Zn_{end} - {}^{64}Zn_{if,\ rt}$

substitute $^{64}Zn_{edg,\ rt}$ into equation (1), $^{64}Zn_{edg,\ ef} = {}^{64}Zn_{initial} - {}^{64}Zn_{edg,\ rt}$

Accordingly, percentage of endogenous ^{64}Zn efflux = $^{64}Zn_{edg,\ ef} / {}^{64}Zn_{initial} \times 100\%$.

3.3.9 ICP-MS experiment

All standards, blanks, and cell samples were prepared using trace metal grade nitric acid (70%, Fisher chemical, Cat# A509P212), ultrapure water (18.2 MΩ·cm @ 25 °C), and metal free polypropylene conical tubes (15 and 50 mL, Labcon, Petaluma, CA, USA). For cell samples in polystyrene 24-well cell culture plates, 200 µl of 70% trace nitric acid was added to allow for initial sample digestion. Following digestion, 150 µl of the digested product was transferred into metal free 15 mL conical tubes. For liquid samples, 50 µl of liquid samples were added to metal free conical tubes followed by addition of 150 µl of 70% trace nitric acid. All cell and liquid samples were then incubated at 65°C in a water bath for one hour followed by dilution to 5 ml using ultrapure water. These completed ICP-MS samples were then analyzed using the Agilent 8900 Triple Quadrupole ICP-MS (Agilent, Santa Clara, CA, USA) equipped with the Agilent SPS 4 Autosampler, integrate

sample introduction system (ISiS), x-lens, and micromist nebulizer. Daily tuning of the instrument was accomplished using manufacturer supplied tuning solution containing Li, Co, Y, Ce, and Tl. Global tune optimization was based on optimizing intensities for ^{7}Li, ^{89}Y, and ^{205}Tl while minimizing oxides ($^{140}Ce^{16}O/^{140}Ce$ < 1.5%) and doubly charged species ($^{140}Ce^{++}/^{140}Ce^{+}$ < 2%). Following global instrument tuning, gas mode tuning was accomplished using the same manufacturer supplied tuning solution in KED mode (using 100% UHP He, Airgas). Specifically, intensities for ^{59}Co, ^{89}Y, and ^{205}Tl were maximized while minimizing oxides ($^{140}Ce^{16}O/^{140}Ce$ < 0.5%) and doubly charged species ($^{140}Ce^{++}/^{140}Ce^{+}$ < 1.5%) with short term RSDs < 3.5%. ICP-MS standards were prepared from a stock solution of NWU-16 multi-element standard (Inorganic Ventures, Christiansburg, VA, USA) that contains As, Ca, Cd, Co, Cr, Cu, Fe, K, Mg, Mn, Ni, Se, V, Zn that were diluted with 3% (v/v) trace nitric acid in ultrapure water to a final element concentration of 1000, 500, 250, 125, 62.5, 31.25, and 0 (blank) ng/g standard. Internal standardization was accomplished inline using the ISIS valve and a 200 ng/g internal standard solution in 3% (v/v) trace nitric acid in ultrapure water consisting of Bi, In, ^{6}Li, Sc, Tb, and Y (IV-ICPMS-71D, Inorganic Ventures, Christiansburg, VA, USA). The isotopes selected for analysis were ^{31}P, ^{64}Zn, ^{66}Zn, ^{67}Zn, ^{68}Zn, ^{70}Zn and ^{6}Li, ^{45}Sc, and ^{89}Y for internal standardization. Continuing calibration blanks (CCBs) were run every 10 samples and a continuing calibration verification standard was analyzed at the end of every run for a 90-110% recovery.

3.3.10 LA-ICP-TOF-MS experimental protocol

Cell samples were lysed with 0.25% Triton X-100 plus 10% Coomassie blue. 5 µl of cell lysate was carefully dropped onto a siliconized glass slide which was then transferred into a 200°C oven to let the droplets dry completely. To siliconize glass slides, we used 25 x 75 x 1.0 mm microscope slides (Alkali Scientific, Cat# SM2551) that were washed thoroughly with hand soap and water. After leaving on bench top for drying, the slides were placed in a beaker to which siliconization solution (Supelco, Cat# 85126) was added, and the slides were submerged covered for 30 minutes at room temperature (about 25°C) in a hood. The glass slides were then carefully removed from the beaker and dried overnight at room temperature. The slides were then rinsed briefly with ultrapure deionized water and placed in an oven (45°C) overnight. The slides need to be preheated before samples are added to minimize the coffee stain effect and for sufficient drying of the droplet.

3.3.11 LA-ICP-TOF-MS instrument setup and sample parameters

Glass slides were loaded into a Bioimage 266 nm laser ablation system (Elemental Scientific Lasers, Bozeman, MT, USA) which is equipped with an ultra-fast low dispersion TwoVol3 ablation chamber and a dual concentric injector (DCI3) and is coupled to an icpTOF S2 (TOFWERK AG, Thun, Switzerland) ICP-TOF-MS. Daily tuning of the LA-ICP-TOF-MS settings was performed using NIST SRM612 glass certified reference material (National Institute for Standards and Technology, Gaithersburg, MD, USA). Optimization

for torch alignment, lens voltages, and nebulizer gas flow was based on high intensities for ^{140}Ce and ^{55}Mn while maintaining low oxide formation based on the $^{232}Th^{16}O+/^{232}Th+$ ratio (< 0.5).

Sample loaded glass slides were tested on the LA system using multiple laser powers and spot sizes to determine optimum parameters for ablation. Due to the sample dye, we needed higher LA power to ablate through the sample with enough energy density while still minimizing ablation of glass. The optimized laser parameters were 80% laser power (9.5-10.5 J/cm^2 laser fluence, 0.1-0.15 mJ sample energy) with a 40 μm spot size (circular) and repetition rate of 50 Hz (single pulse response was tested daily with values between 4-5 ms) with no overlap between the adjacent laser spots. Ablation of the glass slide was analyzed using ^{27}Al and ^{140}Ce elemental maps to ensure minimal glass ablation but complete sample ablation. Following ablation of the entire droplet and concurrent analysis (**Figure 3.2**), we sped up the process by ablating five parallel lines across each droplet with 120 μm spacing between two adjacent lines. This provided sufficient data points for statistical analysis with minimal differences between analyses (**Figure 3.2**). Because of the coffee stain effect, cell lysate was not evenly distributed within a sample droplet. For each ablation line, the ^{31}P counts were used to identify and exclude the data from the ablation points where the cell lysate content is very low. Then, the counts of ^{31}P and ^{70}Zn from the five ablation lines for each sample droplet were summed up respectively and used to calculate the $^{70}Zn/^{31}P$ count ratio.

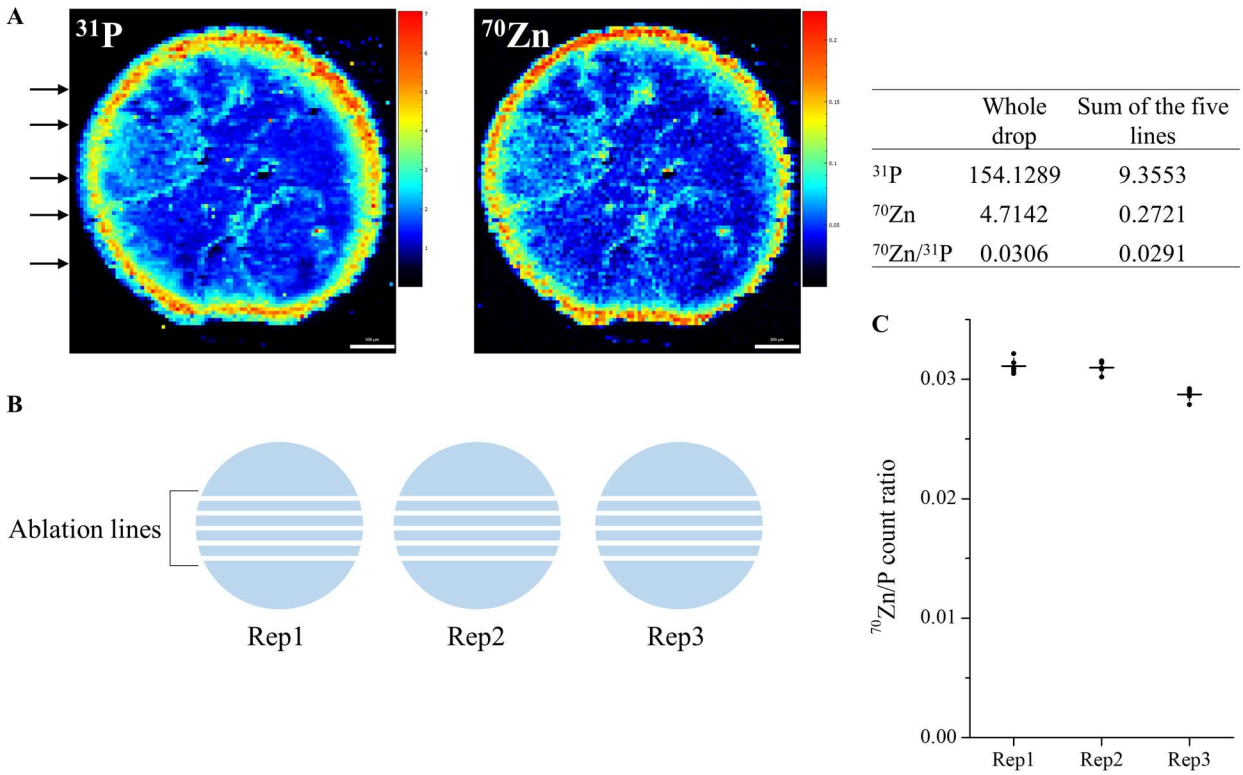

	Whole drop	Sum of the five lines
^{31}P	154.1289	9.3553
^{70}Zn	4.7142	0.2721
$^{70}Zn/^{31}P$	0.0306	0.0291

Figure 3.2. Comparison of the ^{70}Zn/P count ratios at different locations within sample drops. **(A)** Imaging of ^{31}P and ^{70}Zn of a drop of cell lysate on glass slide by LA-ICP-MS. The arrows indicate the rough positions of the five ablation lines randomly selected for analysis. The scale bars indicate 500 μm. The table shows that the determined ^{70}Zn/^{31}P count ratios for the whole drop and the sum of the five lines are nearly identical. (**B**) Cartoon illustration of ablation of three replicates. The white lines represent the ablation lines. For each drop, ablation was conducted along five parallel lines with a distance of 120 micrometers between the adjacent lines. (**C**) Comparison of the ^{70}Zn/P count ratios of the five lines within the and between the sample drops. The shown data are the three replicates of the sample for which the hZIP4-expressing HEK293 cells were treated with the ^{70}Zn-enriched culture media containing 17 μM total zinc. Each dot represents the ^{70}Zn/P count ratio of one ablation line, which was determined by LA-ICP-MS. The relative SD for the five lines in each replicate is approximately 2%, indicating that the ^{70}Zn/P count ratios at different locations in one sample drop are highly consistent.

3.3.12 Statistics

We assumed a normal distribution of the samples and significant difference were examined using Student's *t* test. Uncertainties are reported as standard deviation or standard error of the mean, as indicated.

3.4 Results

3.4.1 Preparation of the ^{70}Zn-enriched culture media for the cell-based zinc transport assay

Due to the high concentration of zinc in mammalian cells[295], it is critical to distinguish between zinc imported from the extracellular space (exogenous zinc) and that already present in the cells prior to the assay (endogenous zinc). The use of the radioactive zinc isotope ^{65}Zn is a well-established solution, but this long-lived and high-energy gamma emitter also raises safety concerns for the researchers performing the experiments. Therefore, the use of a non-radioactive metal substrate becomes an attractive option. In an early study, transport assays employed the stable isotope ^{70}Zn (natural abundance=0.6%)[328]. The ^{70}Zn-enriched culture media was prepared in two steps: total zinc concentration in the culture media was first decreased by treatment with the zinc-specific S100A12 protein immobilized on agarose followed by supplementation with salts containing ^{70}Zn[329]. It was shown that the cellular ^{70}Zn concentration was significantly increased after the cells were incubated with the ^{70}Zn-enriched media and that the cells expressing ZIP transporters accumulated more ^{70}Zn in a two-hour incubation than control cells, providing the proof-of-concept of using ^{70}Zn in the cell-based transport assay.

Using an analogous approach, we treated the cell culture media containing FBS with the metal ion chelating resin Chelex-100 to lower the zinc concentration. Chelex-100 has relatively high selectivity toward zinc ions over the transition metals (manganese, iron,

cobalt, nickel and copper)[330] and has been employed to prepare metal-deficient mammalian cell culture media[331]. We tested whether a treatment of a commonly used mammalian culture media (DMEM+10% FBS) with Chelex-100 would be sufficient to remove most of the naturally present zinc so that the natural background of zinc would be low enough to allow for a sensitive analysis. As shown in **Table 3.1**, the results of inductively coupled plasma mass spectrometry (ICP-MS) analysis indicated that the Chelex-100 treatment removed approximately 90-95% of the zinc naturally present in the culture media. We then added the desired amounts of ^{70}Zn (72% enrichment) to the Chelex-treated media to generate the ^{70}Zn-enriched media for the cell-based transport assay. Consistent with the previous reports[329,331], the Chelex-treated media contain 43% less copper, 99% less calcium, 99% less magnesium when compared with the media without the treatment. These changes in metal content did not affect the activity of hZIP4 (**Figure 3.3**).

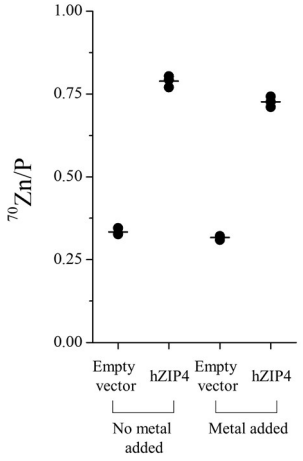

Figure 3.3. Comparison of hZIP4 activity in the Chelex-treated culture media with and without supplementing Mg, Ca, and Cu. These metal elements were found to be removed by Chelex-100 (**Table 3.1**).

3.4.2 Zinc transport assay of hZIP4 using the ^{70}Zn-enriched culture media

To measure the transport activity of hZIP4, the ^{70}Zn-enriched culture media was applied to HEK293 cells transiently expressing hZIP4. After incubation at 37 °C, the reaction was terminated with an ice-cold buffer containing 1 mM EDTA, followed by extensive wash using a phosphorous-free wash buffer. Concentrated nitric acid was then added to digest the cells and the resulting samples were subjected to ICP-MS analysis. To control for the variation in cell number between samples, we normalized the counts per second of ^{70}Zn using the count ratio of ^{70}Zn and ^{31}P (^{70}Zn/P) following the approach of Lane et al.[270]. This calibration simplifies the procedure as there is no need to count cell numbers or measure protein concentrations of the samples. As shown in **Figure 3.4A**, incubation with the ^{70}Zn-enriched culture media resulted in a higher level of the ^{70}Zn/P ratio for the cells expressing hZIP4 than that for the cells transfected with an empty vector, indicating that the activity of hZIP4 can be tracked using the stable isotope ^{70}Zn. Based on the time course experiments, an incubation time of 30 minutes was chosen for later experiments (**Figure 3.4B**). Since the ^{70}Zn/P ratios after background subtraction are linearly correlated with the cell surface expression levels of hZIP4 (**Figure 3.5**), the calculated ^{70}Zn/P ratio represents the transport activity of hZIP4 expressed in HEK293T cells. Under the optimized conditions, a dose-dependent experiment was performed, and the dose curve was fitted with the Hill model commonly used in steady-state kinetic study

(**Figure 3.4C**). The apparent K_M is 1.1±0.3 μM with the Hill coefficient of ~1, which agrees with our previously reported values when ^{65}Zn was used in the transport assay[104,109].

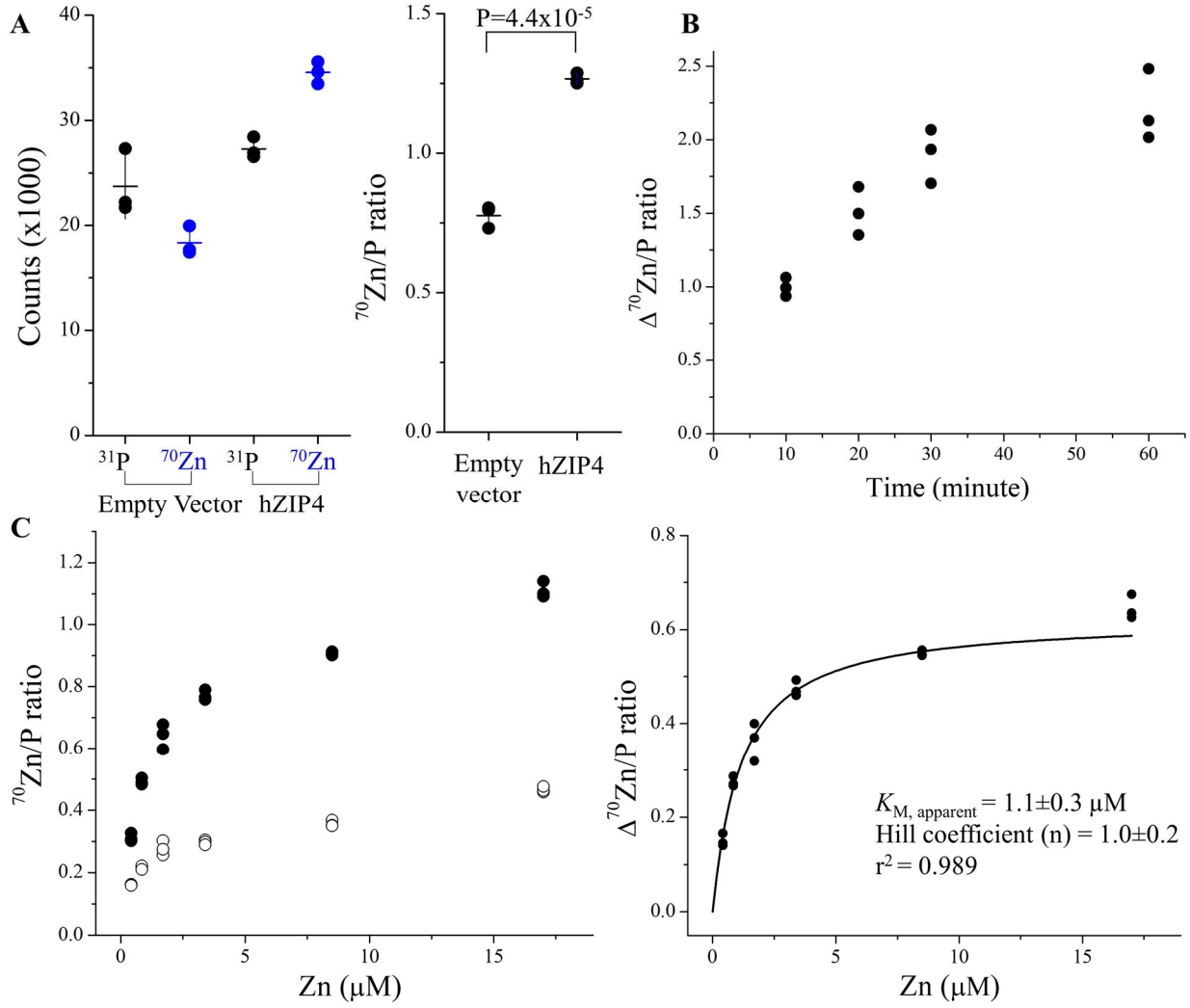

Figure 3.4. Cell-based kinetic study of hZIP4 using the stable isotope ^{70}Zn as the substrate. (**A**) Counts (per second, detected in ICP-MS) of ^{31}P and ^{70}Zn in the cells with and without expressed hZIP4 (*left*) and the $^{70}Zn/P$ count ratios (*right*). The error bars represent the standard deviation of the mean. The Student's *t* test was performed to examine the statistically significant difference. (**B**) Time course of hZIP4-mediated ^{70}Zn transport. Three replicates were performed at each time point. (**C**) Dose curve of hZIP4-mediated ^{70}Zn transport. *Left*: The $^{70}Zn/P$ count ratios of the cells with (solid circle) and without (open circle) expressing hZIP4 at the indicated concentrations of total zinc in the extracellular space. *Right*: Kinetic analysis of hZIP4. The activity of hZIP4 was calculated by subtracting the $^{70}Zn/P$ count ratio of the cells transfected with the empty vector from that of the cells expressing hZIP4. The curve was fitted with the Hill model. Three

Figure 3.4. (cont'd)
replicates were performed for each condition. The extracellular zinc consists of ^{70}Zn (with an enrichment of 72%) and other zinc isotopes. The shown data are from one of three independent experiments in which similar results were obtained.

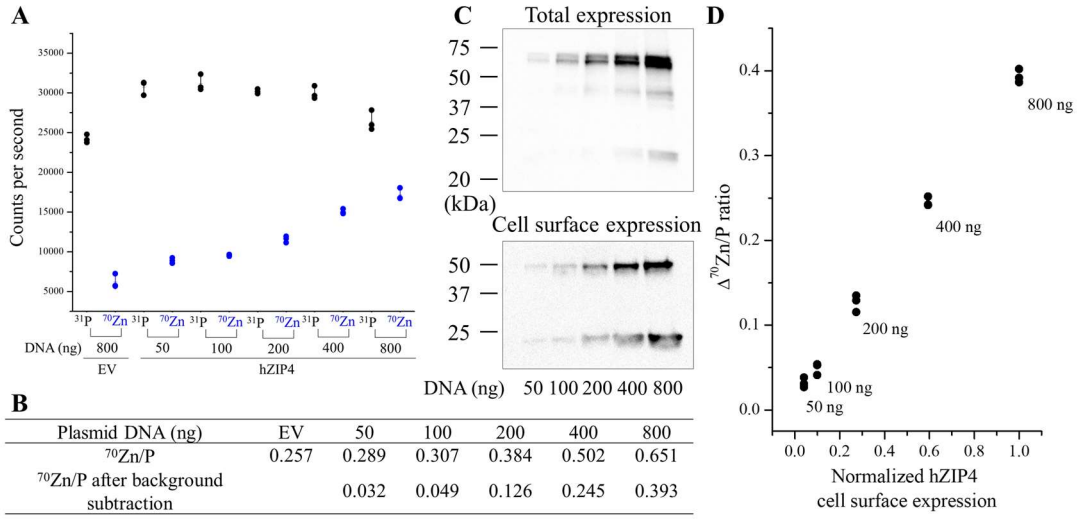

B

Plasmid DNA (ng)	EV	50	100	200	400	800
$^{70}Zn/P$	0.257	0.289	0.307	0.384	0.502	0.651
$^{70}Zn/P$ after background subtraction		0.032	0.049	0.126	0.245	0.393

Figure 3.5. Correlation between the zinc transport activity of hZIP4 and its cell surface expression level. (**A**) Counts (per second, detected in ICP-MS) of ^{31}P and ^{70}Zn in the HEK293T cells transfected with empty vector (EV, 800 ng) or the indicated amounts of plasmid DNA encoding hZIP4-HA (50-800 ng). The error bars represent the standard deviation of the mean. (**B**) $^{70}Zn/P$ count ratios before and after subtracting the background. (**C**) Total and cell surface expression of hZIP4. Cells in each well of a 24-well plate were transfected with the indicated amounts of plasmid DNA with a fixed ratio of 400 ng DNA per μL of Lipofectamine 2000. Total expression of hZIP4 was detected in Western blot using an anti-HA antibody, and cell surface expression of hZIP4 was determined by the surface bound anti-HA antibody, which was detected in Western blot using an HRP-conjugated horse anti-mouse IgG antibody. (**D**) Correlation of the $^{70}Zn/P$ ratios (after background subtraction) and the cell surface expression levels of hZIP4.

3.4.3 Determination of the turnover number of hZIP4 and re-examination of the role of the ECD

While the turnover number is a useful gauge for understanding transport mechanisms, there are no reports of such values to date for eukaryotic ZIP transporters. The turnover number of a transporter is commonly evaluated using experimentally determined values

for V_{max} and the number of transporters expressed at the cell surface. V_{max} can be determined in the ICP-MS experiment that reports the total transport rate (number of zinc ions per second) of hZIP4 when zinc concentration is saturating (**Figure 3.4**)[104,117]. To determine the cell surface expression level of a membrane protein, biotinylation followed by Western blot is a commonly used approach[332,333]. We applied this approach to the cells expressing hZIP4-HA and estimated the number of hZIP4-HA expressed at the cell surface by comparison with the purified hZIP4 tagged with an N-FLAG and C-HA (FLAG-hZIP4-HA) in the Western blot experiment (**Figure 3.6A**). We also performed the ^{70}Zn transport assay on the hZIP4-HA-expressing cells which were transfected at the same time as the cells used for the analysis of the hZIP4-HA surface expression (**Figure 3.6B**). Although the expression levels of hZIP4-HA may vary in different independent experiments, hZIP4-HA expression in the same batch of transfection are very similar (**Figure 3.7**). These results allowed us to estimate the apparent turnover number of hZIP4 to be 0.08±0.02 s^{-1} (mean±standard error, S.E., n=3). The slow transport rate and the saturable kinetics both suggest that hZIP4 is best characterized as a carrier.

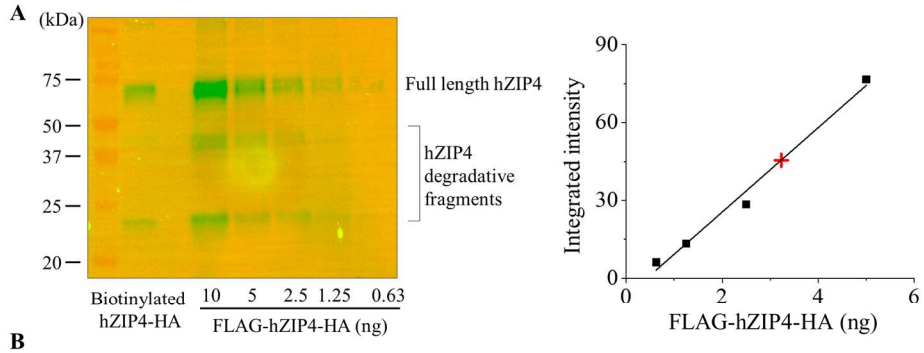

B

	^{70}Zn transported by hZIP4 (nanomole/well)	All zinc isotopes transported by hZIP4 [a] (nanomole/well)	Zinc transport rate of hZIP4 [b] (picomole/s/well)	Cell surface expressed hZIP4 (picomole/well)	Apparent turnover number (s^{-1})
Exp1	0.022	0.030	0.017	0.32	0.05
Exp2	0.023	0.031	0.017	0.31	0.06
Exp3	0.014	0.019	0.014	0.12	0.1
Mean±S.E.					0.08±0.02

[a] The enrichment of ^{70}Zn is 72%.
[b] The transport assays were conducted for 30 minutes.

Figure 3.6. Determination of the turnover number of hZIP4. (**A**) Estimation of the surface expression level of hZIP4-HA by biotinylation and Western blot. The purified FLAG-hZIP4-HA was used as the standard. Degradative fragments were found in both biotinylated hZIP4-HA and FLAG-hZIP4-HA. In the standard curve, the black squares represent the standards and the red cross represents the biotinylated hZIP4-HA in the sample. Biotinylated sample was loaded into the gel with 50% dilution. The shown data are from one of three independent experiments. (**B**) Calculation of the turnover number of hZIP4 from three independent experiments.

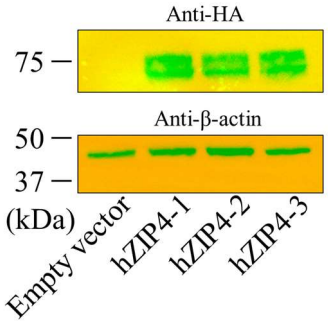

Figure 3.7. Comparison of hZIP4 transient expression in the cells grown in different wells in the same experiment. Western blot was performed to detect the HA-tagged hZIP4 and β-actin.

We then extended this ^{70}Zn-based assay to further evaluate the role of ZIP4-ECD in zinc transport function. ZIP4 has a large ECD among human ZIPs but the exact function

of this domain has not been fully elucidated. In our early study where ^{65}Zn was used in transport assays[104], we showed that deletion of the N-terminal-most HRD subdomain resulted in a 50% loss of activity and deletion of the entire ECD, which consists of the HRD and the PCD subdomains, resulted in approximately 75% loss of activity compared to the full-length hZIP4, indicating that the ECD is important for optimal zinc transport. However, a recent study reported that ECD deletion of hZIP4 with a C-terminal eGFP tag did not significantly affect the zinc transport activity when compared with the full-length hZIP4-eGFP[176]. To clarify this point, we compared the apparent turnover numbers of hZIP4 variants with a C-terminal HA tag including the full-length transporter (hZIP4-HA), the ΔHRD variant (ΔHRD-hZIP4-HA), and the ΔECD variant (ΔECD-hZIP4-HA). The previous study has shown that the truncated variants did not affect the apparent K_M[104], so we focused only on the turnover number. The number of moles of ^{70}Zn associated with the cells expressing hZIP4-HA or the variants were quantified by using ICP-MS as described above. In this study, we did not use biotinylation to estimate the cell surface expression levels of these constructs because they have different numbers of the lysine residues at the extracellular side and accessibility of the lysine residues differs according to a structure model predicted by AlphaFold (**Figure 3.8**).

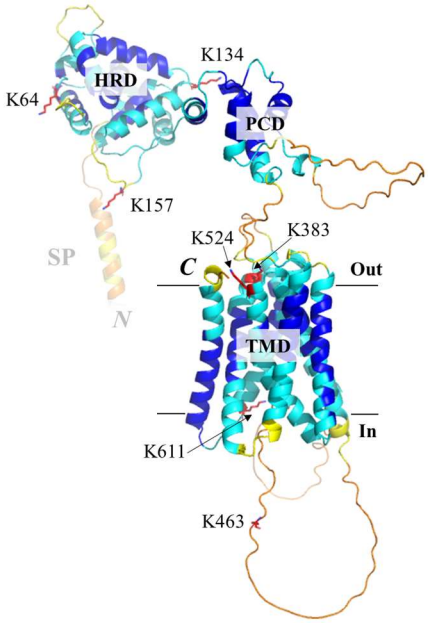

Figure 3.8. Lysine residues in hZIP4. The AlphaFold predicted structure of hZIP4 (UniProt ID: Q6P5W5) is shown in cartoon mode and colored with the confidence score (pLDDT). hZIP4 consists of the ECD and the TMD, and the former is composed of the very N-terminal HRD subdomain and the PCD subdomain. All the seven lysine residues are shown in stick mode, labeled, and colored in red, out of which five are exposed to the extracellular side – three are fully exposed in the HRD and two appear to be partially buried in the TMD. SP: signal peptide.

Instead, we determined the surface expression levels of hZIP4-HA and its variants by quantifying the anti-HA antibody bound at the surface of fixed but non-permeabilized cells. The use of a surface-bound antibody to evaluate the cell surface expression of a membrane protein is a well-established approach[334] and has been used in prior studies of ZIP4[218,335]. To quantify the cell surface-bound anti-HA antibodies, a standard curve was generated by applying the serially diluted anti-HA antibodies in a Western blot experiment **(Figure 3.9A)**. After calibrating the transport data with the cell surface expression levels of the HA-tagged transporter constructs (**Figure 3.9B**), the determined apparent turnover number of hZIP4-HA (0.2±0.03 s^{-1}, mean±S.E., n=3, **Figure 3.9C**) was

found to be generally consistent with that obtained from the biotinylation experiment (0.08±0.02 s^{-1}, **Figure 3.6**). Consistent with our previous report[104], the cell surface expression levels of the two truncated variants are significantly higher than that of the full-length hZIP4-HA and the calculated apparent turnover numbers (0.05±0.01 s^{-1} for ΔHRD-hZIP4-HA, mean±S.E., n=3, and 0.03±0.01 s^{-1} for ΔECD-hZIP4-HA, mean±S.E., n=3) are significantly lower than that of the full-length hZIP4-HA. The difference in cell surface expression levels also agree with the different total expression levels for these constructs (**Figure 3.10**). Collectively, these results reinforce the notion that ZIP4-ECD is crucial for optimal zinc transport activity of hZIP4 and the HRD subdomain plays a more important role in supporting an efficient zinc transport than the PCD subdomain.

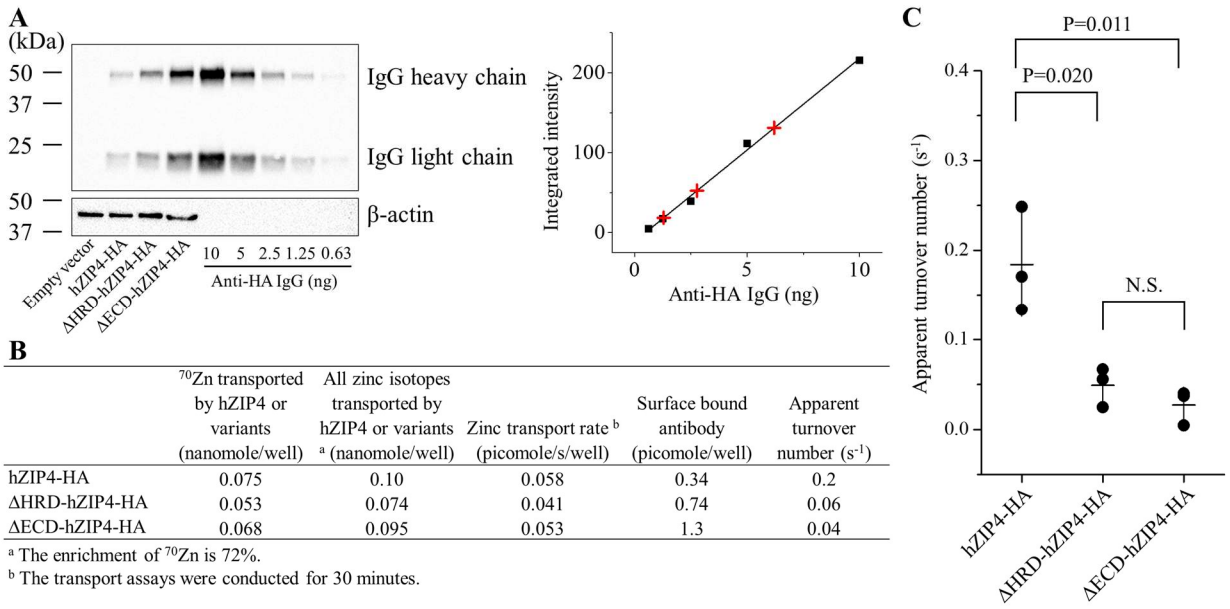

B

	^{70}Zn transported by hZIP4 or variants (nanomole/well)	All zinc isotopes transported by hZIP4 or variants [a] (nanomole/well)	Zinc transport rate [b] (picomole/s/well)	Surface bound antibody (picomole/well)	Apparent turnover number (s^{-1})
hZIP4-HA	0.075	0.10	0.058	0.34	0.2
ΔHRD-hZIP4-HA	0.053	0.074	0.041	0.74	0.06
ΔECD-hZIP4-HA	0.068	0.095	0.053	1.3	0.04

[a] The enrichment of ^{70}Zn is 72%.
[b] The transport assays were conducted for 30 minutes.

Figure 3.9. Comparison of the apparent turnover numbers of hZIP4-HA and the truncated variants (ΔHRD-hZIP4-HA and ΔECD-hZIP4-HA). (**A**) Estimation of the cell surface bound anti-HA antibodies. *Left*: Western blot of the cell surface bound anti-HA antibodies. The samples containing the indicated amount of anti-HA antibody were used as the standards. A HRP-conjugated horse-anti-mouse antibody was used to detect the mouse anti-HA

Figure 3.9. (cont'd)
antibodies. *Right*: Quantification of the cell surface bound anti-HA antibodies in the cell samples. The black squares represent the standards and the red plus signs represent the surface bound anti-HA antibody in the samples. (**B**) Calculation of the apparent turnover numbers using the data from one representative experiment. The shown data are from one of three independent experiments in which similar results were obtained. (**C**) Comparison of the apparent turnover numbers of hZIP4-HA, ΔHRD-hZIP4-HA, and ΔECD-hZIP4-HA. Each data point represents the mean of one of three independent experiments. Three replicates were performed in one experiment. The error bars represent the standard deviations of the mean. The Student's *t* test was performed to examine statistically significant difference.

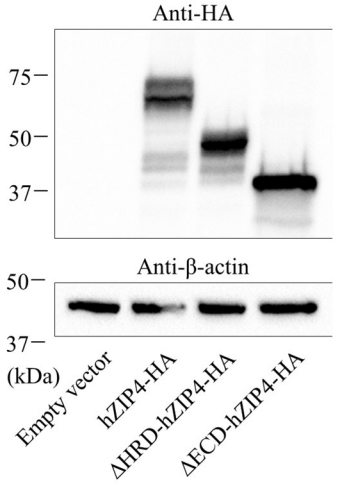

Figure 3.10. Comparison of total expression of hZIP4 and the truncated variants. Western blot was performed to detect the HA-tagged proteins and β-actin.

3.4.4 Estimation of zinc efflux during the transport assay

One concern with the cell-based transport assay is that while substrate is being transported into the cells by the importer of interest, some of the imported substrate may be expelled from the cells due to the activity of exporters at the plasma membrane. If this happens, it will lead to an underestimation of the influx rate and thus inaccuracy in the determination of the kinetic parameters. To evaluate possible effects of zinc efflux on the

zinc transport assay for hZIP4, we designed the isotope exchange experiment. First, we determined how long it takes to replace the naturally present cellular zinc (endogenous zinc) with ^{64}Zn (98% enrichment) added in the extracellular space. To do this, the cells growing in the regular culture media (DMEM plus 10% FBS, contains the naturally present zinc isotopes with natural abundance) were incubated with the ^{64}Zn-enriched culture media and the levels of cellular ^{70}Zn (as an indicator of the endogenous zinc in cells) and ^{64}Zn were measured using ICP-MS at different time points. As shown in **Figure 3.11A**, after incubation for 48 hours without culture media replacement, the replacement of ^{70}Zn by ^{64}Zn reached equilibrium. The decrease in the $^{70}Zn/^{64}Zn$ count ratio fit well with the one-phase decay model, indicating that the imported ^{64}Zn exchanged with a single intracellular zinc pool.

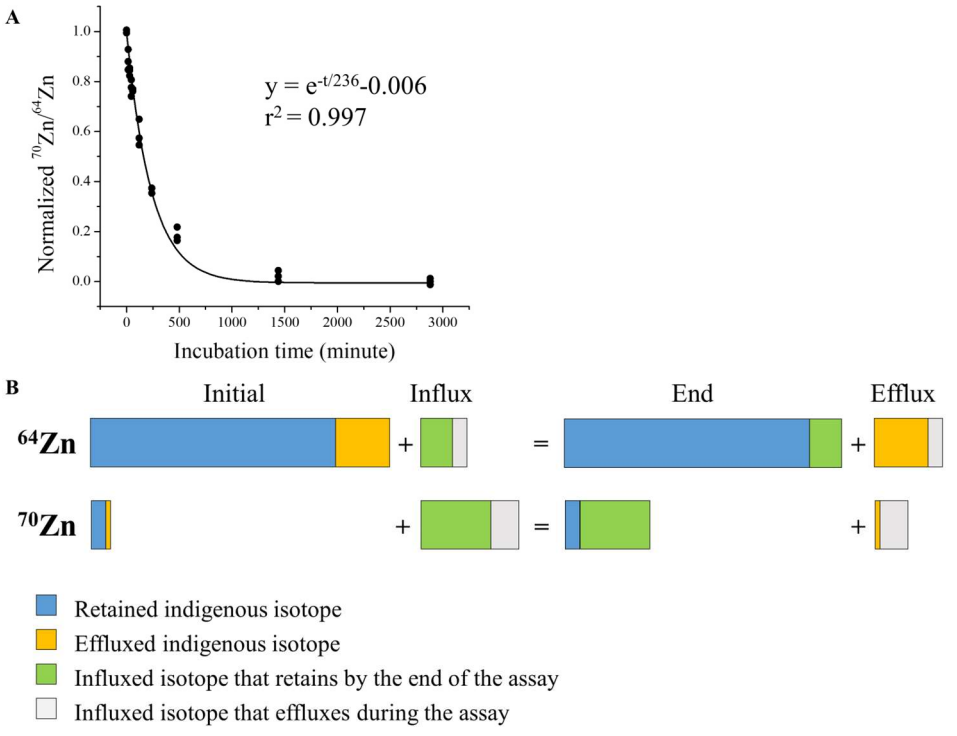

	Initial	End	Influxed isotope that retains	Endogenous isotope that retains	Endogenous isotope that effluxes	Percentage of exported endogenous isotope (%)
$^{64}Zn/P$	2.522±0.039[a]	2.402±0.089[a]	0.042±0.002	2.360±0.089	0.162±0.098	6.4±3.9
$^{70}Zn/P$	0.004±0.000[a,b]	0.336±0.013[a]	0.336±0.013			

[a]Determined experimentally.
[b]Ignored in calculation.

Figure 3.11. Evaluation of zinc efflux during the transport assay. (**A**) Time course of ^{70}Zn replacement by ^{64}Zn. Cells growing in the regular culture media with naturally present zinc isotopes were incubated with the ^{64}Zn-enriched culture media. At the indicated time points, cells were digested for ICP-MS analysis. The $^{70}Zn/^{64}Zn$ count ratios were normalized and plotted against the reaction time, and the curve was fitted using the one-phase decay model. (**B**) Estimation of zinc efflux during the transport assay. The hZIP4-expressing cells growing in the ^{64}Zn-enriched culture media were washed and then incubated with the ^{70}Zn-enriched culture media for 30 minutes. The $^{64}Zn/P$ and $^{70}Zn/P$ count ratios were determined by ICP-MS before and after the transport assay. *Upper*: The diagram illustrating the changes of ^{64}Zn and ^{70}Zn due to influx and efflux during the assay. *Lower*: Calculation of zinc efflux in one of three independent experiments in which similar results were obtained. Six replicates were performed for each condition. The calculations are described in detail in *Experimental procedures*.

Next, we cultured the cells in the ^{64}Zn-enriched media for three passages (3 days per passage) to ensure a complete replacement and then transferred the cells to the same

^{70}Zn-enriched media used in the zinc transport assay for a 30-min incubation. After termination by addition of EDTA followed by extensive washing, the amounts of ^{64}Zn and ^{70}Zn associated with the cells were determined by ICP-MS. As presented in **Figure 3.11B**, our calculation showed that 6.4±3.9% of the endogenous ^{64}Zn was expelled from the cells during the 30 min transport assay. The calculations are detailed in *Experimental procedures*. Given that the imported zinc ions rapidly exchange with a single pool of the endogenous zinc (**Figure 3.11A**), it can be deduced that the same percentage of ^{70}Zn imported during the assay has been expelled from the cells through the same pathway as the endogenous ^{64}Zn. This result indicates that a small fraction of zinc ions from the endogenous zinc pool (^{64}Zn) and those from the extracellular space (mainly ^{70}Zn) are exported from the cells during the transport assay, and therefore the hZIP4 activity (determined by the imported ^{70}Zn) is indeed underestimated. Given that only ~6% of the influxed zinc was exported during the assay, we conclude that zinc efflux would not significantly affect the transport kinetic study of hZIP4 under the current experimental conditions. Consistently, a fit of the data in **Figure 3.11A** indicates that an approximate half-life for zinc loss from the cells was 3 hours (i.e. 164 min), providing further support for this conclusion. It has been reported that mammalian cells handle light and heavy zinc isotopes differently, resulting in a 0.2-0.4‰ difference in their transport[336], which is two orders of magnitude smaller than the ~6% zinc efflux determined in this work. Therefore, the kinetic isotope effect may have little effect on data interpretation. Nevertheless, our

data also suggest that care should be taken in the experimental design to minimize the effect of substrate efflux on the activity measurement of an importer.

Collectively, it is very unlikely that the determined slow transport rate (0.08-0.2 s^{-1}) is due to a significant zinc efflux during the transport assay. We speculate that in order to acquire an adequate amount of zinc using a slow zinc transporter like ZIP4, cells must express a large number of transporter molecules at the cell surface, thus allowing the mechanisms that regulate the cell surface expression level of the transporter[121,217,337] to efficiently fine tune the overall zinc transport capacity at the plasma membrane. Whether endogenously expressed hZIP4, other than hZIP4 overexpressed in HEK293T cells, exhibits a similar transport rate and whether other mammalian ZIPs are also slow transporters warrant future investigation.

3.4.5 LA-ICP-MS assisted zinc transport assay with an increased throughput

It takes approximately three minutes to analyze one sample by ICP-MS in the liquid mode. A higher throughput is required for many applications, including inhibitor screening for drug discovery and directed evolution for transporter engineering. We explored the possibility of increasing the speed of isotope measurement by using LA-ICP-MS. For this purpose, cells were lysed after the ^{70}Zn-based transport assay, and the cell lysate was dropped onto a siliconized glass slide and dried in oven (**Figure 3.12A)**. On a standard glass slide (26 mm x 75 mm), up to 36 drops can be manually applied at a volume of 5 µl

per drop. The ^{70}Zn/P count ratio of each drop was then measured by LA-ICP-MS equipped with a time-of-flight (TOF) detector.

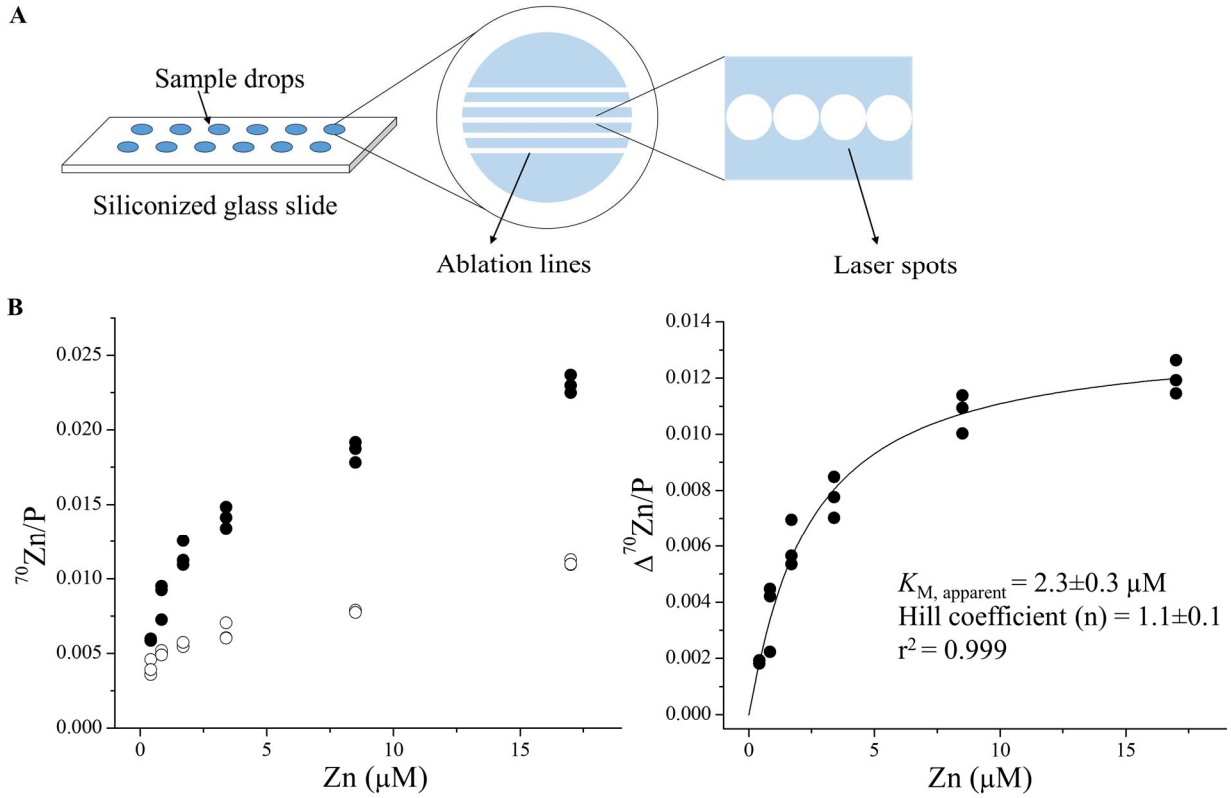

Figure 3.12. Kinetic study of hZIP4 with increased throughput by using LA-ICP-MS. (**A**) Cartoon illustration of a siliconized glass slide loaded with cell lysate samples for LA-ICP-MS detection. To increase the detection speed, five parallel lines (composed of continuous contacting spots) were ablated across each sample drop. (**B**) Dose curve of hZIP4-mediated ^{70}Zn transport using LA-ICP-TOF-MS to detect ^{70}Zn and ^{31}P. *Left*: The ^{70}Zn/P count ratios of the cells with (solid circle) and without (open circle) expressing hZIP4 at the indicated concentrations of total zinc in the extracellular space. *Right*: Kinetic study of hZIP4. The activity of hZIP4 was calculated by subtracting the ^{70}Zn/P count ratio of the cells transfected with an empty vector from that of the cells expressing hZIP4. The curve was fitted using the Hill model. Each point represents the data of the cells in one subwell. For each condition, three replicates were performed. The extracellular zinc consists of ^{70}Zn (with an enrichment of 72%) and other zinc isotopes. The shown data are from one of three independent experiments in which similar results were obtained.

Because the ^{70}Zn/P ratio remains nearly constant at different locations within one drop (**Figure 3.2**), each drop was scanned by five parallel lines across the drop, rather

than the entire area of the drop, to speed up the process. Accordingly, it took less than half a minute to scan one drop, reducing the analysis time by a factor of six when compared with the assays conducted in the liquid mode. Although the absolute amount of ^{70}Zn associated with the cells are not established under the current protocol, a dose curve of hZIP4-mediated zinc transport can be generated by using the determined $^{70}Zn/P$ ratios. As shown in **Figure 3.12B**, the $^{70}Zn/P$ ratios in the hZIP4-expressing cells are significantly higher than those in the cells transfected with the empty vector, and subtraction of the latter from the former yielded a dose curve similar to that generated by using the data collected by ICP-MS in the liquid mode (**Figure 3.4**). Curve fitting using the Hill model resulted in an apparent K_M of 2.3±0.3 μM (n=3) with the Hill coefficient of ~1 (**Figure 3.12A**), consistent with values obtained in prior studies [104,117] and in the transport assay described above (**Figure 3.4**). These results demonstrate that this LA-ICP-TOF-MS assisted approach significantly increases the throughput without compromising data quality. We expect the throughput of this approach to further increase significantly with optimization of automation of cell handling, slide preparation, and slide scanning strategy.

3.5 Discussion

Although the free Zn^{2+} concentration within cells could be extremely low even to picomolar level, the total Zn^{2+} concentration in cells is up to sub-millimolar level. Such a high concentration of cellular Zn represents a very high background readings for cell-

based Zn biochemistry studies, bring huge errors and inaccuracy. Indeed, one of the reasons why radioactive ^{65}Zn, despite its hazardous nature, is still very commonly used in the field is for its zero background in nature, along with its other features such as easy detection and the straightforwardness in experiment design. We developed a new protocol for in vivo Zn assay, and by taking advantage of the low abundance of ^{70}Zn (0.6%) the high background issue from the natural Zn has been minimized. Furthermore, to eliminate indigenous Zn from the incubation solution, people have previously reported the usage of agarose bound zinc-specific S100A12 protein[330]. Although efficient, it is not quite accessible. Here we tested and replaced it with the more commercially available ion chelating resin Chelex-100. Lastly, the detection issue was solved with ICP-MS, which is considered one of the most powerful elemental analysis methods taking into account of its low detection limit, high resolution and rapid and easy screening speed, especially when coupled with an auto-sampler. The new protocol has been tested and was capable of replacing the radioactive Zn assays, demonstrating good data quality and consistence. Taking advantage of this new system, we were able to study more biochemical features of the ZIP family and we believe it could potentially be applied to more transporter studies.

We revealed that the turnover number of the hZIP4-HA being 0.2±0.03 s^{-1} (**Figure 3.9C**), which suggested that ZIP4 is a carrier. This value is generally consistent with the turnover numbers of representative carrier proteins[338] and close to a panel of slow carriers, including VMAT1 (0.2 s^{-1})[339], MATE1 (0.4 s^{-1})[340], NET (0.11 s^{-1})[341], Tyt1 (0.4 s^{-1}) [126], and

Glt_{ph} (0.14 s^{-1})[342]. However, caution must be exercised because a low turnover number does not necessarily exclude the possibility of an ion channel, as the boundary between the two classes of membrane transport proteins can be blurred[343]. Considering that ZIP4 undergoes endocytosis[121,217,337], it is plausible that the ZIP4 surface expression level determined by biotinylation may be overestimated. However, given that the zinc ion concentration in the PBS buffer used in the biotinylation reaction is unlikely to be at micromolar or higher and that the reaction was conducted only at room temperature for 10 minutes, we don't think ZIP4 endocytosis, which is a zinc and energy dependent process, would significantly affect the estimation of ZIP4 expression at the cell surface.

We also revisit the functional role of the ZIP4-ECD, reaching the same conclusion as we previously published that ZIP4-ECD plays a crucial part in ZIP4 function. The exact function of ZIP4-ECD is still not fully understood. It has been shown that elimination of N-glycosylation of ZIP4-ECD does not affect the zinc transport activity[268]. ZIP4-ECD forms a homodimer in the crystal structure primarily through the PCD subdomain[104]. Although facilitating dimerization is a likely function of ZIP4-ECD, the fact that the HRD contributes most to promoting zinc transport (**Figure 3.9C**) suggests that the ECD must have additional function(s) beyond dimerization. It has been noted that all experimentally solved structures of BbZIP are in the inward-facing conformation, regardless of whether the transporter is in the substrate-bound or apo state[110,111,177], suggesting that the transporter in the outward-facing conformation is an energetically unfavorable state with

a small population and that promoting the formation and/or stabilization of the outward-facing conformation may therefore represent a strategy to increase the transport activity. According to the structural model of ZIP4 and the proposed elevator mechanism[110,111,253], the HRD, which shows considerable flexibility in the crystal structure of ZIP4-ECD[104] and in the AlphaFold predicted structures (**Figure 3.1B**), could transiently interact with the transport domain as the latter slides outward, thereby facilitating the formation and stabilization of the outward-facing conformation (**Figure 3.1C**). Testing this hypothesis, especially when the structure of full-length ZIP4 is available, will help to clarify the function of the HRD that is present only in ZIP4 and its close homologue ZIP12.

For the study in Zn efflux during the metal assays, given only 6% of the indigenous Zn was effluxed during the assay, it does not affect the final conclusion of the studies. But caution should be taken for similar biochemical studies. The exploration in the high-throughput potential of the LA-ICP-MS showed great possibilities that if granted with further optimization, aid of robotic machinery and customized platform, LA-ICP-MS could be a very powerful and high-throughput method for various purposes including therapeutic development.

3.6 Conclusion

In this work, we applied a modified ^{70}Zn-based approach to study the transport kinetics of hZIP4, a representative ZIP metal transporter and a promising oncology drug target. Our data showed that the low-abundance stable isotope ^{70}Zn can adequately

replace the radioactive ^{65}Zn in the cell-based transport assay. This approach, combined with quantification of the surface expression level of hZIP4, allowed us to estimate the apparent turnover number of hZIP4 to be in the range of 0.08-0.2 s^{-1}, indicating that hZIP4 is best described at this time as a carrier, rather than an ion channel. Re-examination of the role of the hZIP4-ECD reinforced the notion that the HRD subdomain is responsible for most of the function of the ECD in facilitating zinc transport. Estimation of zinc efflux during the transport assay showed that zinc efflux did not significantly affect the analysis of zinc influx. We also demonstrated that the throughput of the ^{70}Zn-based approach can be significantly increased when LA-ICP-TOF-MS was used to study the samples loaded on glass slides. This approach may be developed into an assay suitable for drug discovery targeting other ZIPs and zinc transporters from other metal transporter families. Biological metals with more than one stable isotopes, such as iron (^{54}Fe, ^{56}Fe, ^{57}Fe, and ^{58}Fe), nickel (^{58}Ni, ^{60}Ni, ^{61}Ni, ^{62}Ni, and ^{64}Ni), and copper (^{63}Cu and ^{65}Cu), can also be similarly studied using the ICP-MS-based assay presented in this work.

3.7 Acknowledgements

I thank Dr. Jian Hu for the instruction, intelligent input in this project and his unconditional support. I thank Dr. Keith MacRenaris and Dr. Aaron Sue from the O'Halloran group for instructing me on ICP-MS as well as the friendly supportive environment they provided. I thank Dr. Thomas O'Halloran for his input in the manuscript and his kindness to me. I thank the Hu group for the support.

This work is supported by NIH GM129004 and GM140931.

CHAPTER 4: Targeting the selectivity filter to drastically alter the substrate spectrum of a promiscuous metal transporter

Yuhan Jiang[1], Michael Nikolovski[1], Keith MacRenaris[2], Thomas V. O'Hallaron[2], Jian Hu[1]

[1]Department of Chemistry,

[2]Department of Biochemistry and Molecular Biology, Michigan State University, East Lansing, MI 48824

Brief introduction on the work

This work was led by me under the guidance of Dr. Jian Hu and Dr. Thomas V.O'Hallaron. I and Dr. Jian Hu designed the mutants, I conducted the cell-based assays. I, Michael Nikolovski and Dr. Keith MacRenaris conducted ICP-MS measurement.

4.1 Summary

d-block metal transporters are important for the homeostasis of life essential trace elements and also attractive targets of protein engineering for selective enrichment or exclusion of *d*-block metals from the host. However, systematic efforts in metal transporter engineering are still lacking due to the poor understanding of the transport mechanism and substrate specificity. Here, we demonstrate a strategy to alter and expand the substrate spectrum of ZIP8, a promiscuous *d*-block metal transporter, by randomizing the three residues believed to form a selective filter at the entrance of the transport pathway. Screening of the library using the cell-based transport assay and ICP-MS for simultaneous metal content measurement led to the discovery of variants with drastically increased activity and altered substrate preference. Selected variants also exhibited novel activities against metals that are not substrates of wild-type ZIP8, including the diatomic cation VO^{2+}. These findings, together with the discovery that Pb^{2+} is a new substrate of wild-type ZIP8, indicate that the ZIP fold has strong plasticity and amenability to transport a variety of metals with different physicochemical properties, and is therefore a promising platform for the creation of designer metal transporters for potential applications.

4.2 Introduction

Some *d*-block metals, such as manganese, iron, cobalt, nickel, copper, zinc, and molybdenum perform essential functions in biological systems by playing structural,

catalytic, and regulatory roles in various biomolecules[8,344–349]. The importance of these metals and the potential deleterious effects upon dysregulation underscore the need for precise regulation of their concentration and distribution in biological systems, and metal transporters, which act as selective gates to control the flux of metal ions across biological membranes, therefore play a central role in maintaining the homeostasis of these micronutrients at the cellular and systemic levels[350,351].

To harness the selective transport of metal ions, the divalent *d*-block metal transporters have been considered to be attractive engineering targets for applications such as biofortification[352,353], phytoremediation[354,355], biomining[356,357], and heavy metal exclusion from foods[358,359]. From this perspective, the Zrt/Irt-like protein (ZIP) family has gained increasing attention due to its ubiquitous expression in all kingdoms of life, its broad substrate spectrum and, in particular, its pivotal role in metal uptake from the environment[101,138,253,254,314]. Creating a ZIP with desired properties will allow the highly selective accumulation or exclusion of certain metals in the host organism, which holds great potential for the aforementioned applications. For example, engineering IRT1, a plant root-expressing iron-transporting ZIP, to eliminate Cd transport activity while retaining iron transport activity may help reduce Cd uptake by crops in contaminated soils[244].

In our previous study on ZIP8, a promiscuous ZIP that transports zinc, iron, manganese, and cadmium, we showed that a combination of four rationally designed

mutations led to a variant with increased zinc transport activity and drastically reduced activities for Cd, Fe, and Mn, demonstrating the feasibility of rational engineering of a ZIP transporter[327]. Importantly, the strong epistatic interaction between two residues chosen for mutagenesis allowed us to identify a selectivity filter located at the entrance of the transport pathway (**Figure 4.1**). Three residues (Q180, E318, and E343) approach each other when the transporter adopts an outward-facing conformation according to the proposed elevator transport mode[110,111], and form a transient metal binding site that may screen the coming metal ions before the substrate translocate to the transport site. Bioinformatic analysis of these three positions revealed that although the proposed selectivity filter is likely present in most ZIP family members, the amino acid composition is highly diverse[113,327], suggesting that ZIPs may have very different substrate preferences and that the selectivity filter represents an ideal target to alter substrate spectrum.

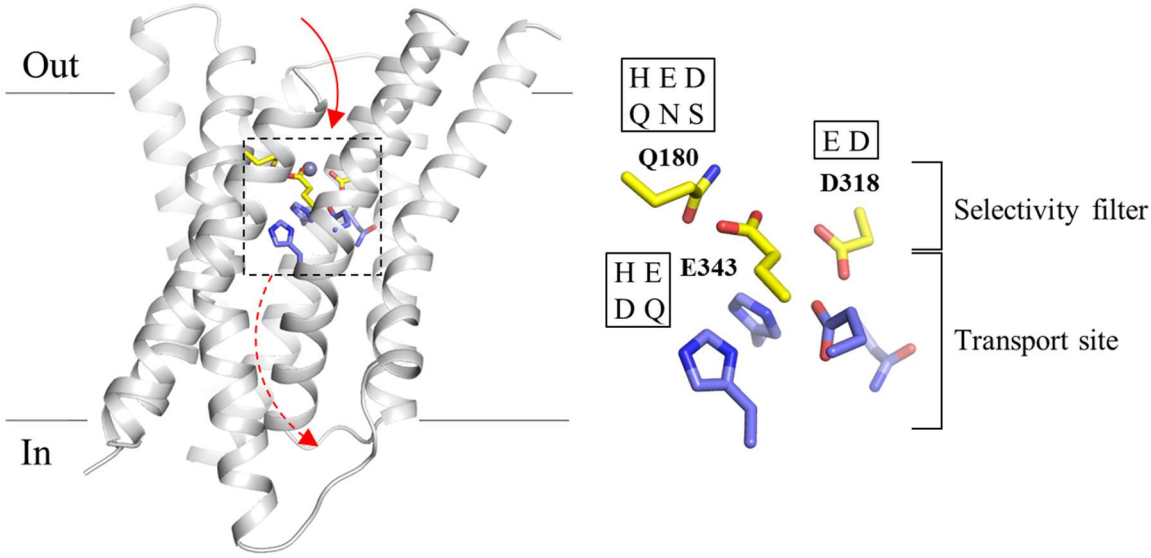

Figure 4.1. The selectivity filter and transport site of ZIP8.

Figure 4.1. (cont'd)
Left: the structural model of human ZIP8 in the outward-facing conformation. The solid red arrow indicates the pathway for metal to enter the transport site through the selectivity filter, and the dashed red arrow indicates the pathway for metal to be released to the cytoplasm when the transporter switches to the inward-facing conformation. The model was generated by homology modeling using the AlphaFold predicted ZIP13 structure as template (https://alphafold.ebi.ac.uk/entry/Q96H72). For clarity, long loops connecting transmembrane helices are trimmed. The residues at the selectivity filter are shown in yellow and the residues forming the transport site are in blue. The metal substrate is depicted as a grey sphere. D318 and E343 work at both the selectivity filter and transport site. *Right*: the zoomed-in view of the framed region. The one-letter codes of the amino acids to be introduced into the positions at the selectivity filter are shown in the frames.

In this work, we explored the extent to which the substrate spectrum of ZIP8 can be tuned by systematically altering the amino acid composition of the selectivity filter and screening the variants against a panel of divalent *d*-block metals using an ICP-MS-based transport assay. Our data showed that this strategy resulted not only in drastically altered activity and substrate preference for the known ZIP8 substrates, but also in an expansion of the substrate spectrum to include the metals that are not substrates for wild-type ZIP8. These results demonstrate the great potential of the ZIP fold to be engineered to selectively transport a variety of divalent metals, paving the way for the creation of designer metal transporters for applications.

4.3 Materials and Methods

4.3.1 Gene, plasmids, and reagents

The complementary DNA of human ZIP8 (GenBank access number: BC012125) from Mammalian Gene Collection were purchased from GE Healthcare. The ZIP8 construct consists of the N-terminal signal peptide of ZIP4 (amino acid residues 1-22) followed by

a GSGS linker and a FLAG tag, the ZIP8 coding sequence (residue 23-460), and a HA-tag at the C-terminus. Site-directed mutagenesis of ZIP8 was conducted using QuikChange mutagenesis kit (Agilent, Cat#600250). All mutations were verified by DNA sequencing. ^{70}ZnO was purchased from American Elements (ZN-OX-01-ISO.070I, Lot#1871511028-401) and $^{57}FeCl_3$ was purchased from Sigma-Aldrich (790427, Lot#MBBD4771). 30 mg of zinc oxide powder was dissolved in 5 ml of 1 M HCl and then diluted with ddH_2O to make the stock solution at the concentration of 50 mM. $^{57}FeCl_3$ was dissolved in 1 M HCl to final concentration of 100 mM. The ^{70}Zn sample was certified as 72% abundance and ^{57}Fe was 99.9%. Other reagents were purchased from Sigma-Aldrich or Fisher Scientific.

4.3.2 Cell culture, transfection, and Western blot

Human embryonic kidney cells (HEK293T, ATCC, Cat#CRL-3216) were cultured in Dulbecco's modified eagle medium (DMEM, Thermo Fisher Scientific, Invitrogen, Cat#11965092) supplemented with 10% (v/v) fetal bovine serum (FBS, Thermo Fisher Scientific, Invitrogen, Cat#10082147) and Antibiotic-Antimycotic solution (Thermo Fisher Scientific, Invitrogen, Cat# 15240062) at 5% CO_2 and 37°C. Cells were seeded on the polystyrene 24-well trays (Alkali Scientific, Cat#TPN1024) for 16 h and transfected with 0.8 μg DNA/well using lipofectamine 2000 (Thermo Fisher Scientific, Invitrogen, Cat# 11668019) in DMEM with 10% FBS.

For Western blot, samples were mixed with the SDS sample loading buffer and heated at 37°C for 20 min before loading on SDS-PAGE gel. The proteins separated by SDS-PAGE were transferred to PVDF membranes (Millipore, Cat#PVH00010). After blocking with 5% (w/v) nonfat dry milk, the membranes were incubated with anti-FLAG antibody (Agilent, Cat# 200474-21) or anti β-actin (Cell Signaling, Cat# 4970S) at 4°C overnight, which were detected with HRP-conjugated goat anti-rat immunoglobulin-G at 1:5000 dilution (Cell Signaling Technology, Cat# 7077S) or goat anti-rabbit immunoglobulin-G at 1:3000 dilution (Cell Signaling Technology, Cat# 7074S) respectively using the chemiluminescence reagent (VWR, Cat#RPN2232). The images of the blots were taken using a Bio-Rad ChemiDoc Imaging System.

4.3.3 Metal transport assay

Twenty hours post transfection, cells were washed with the wash buffer (10 mM HEPES, 142 mM NaCl, 5 mM KCl, 10 mM glucose, pH 7.3) followed by incubation with the wash buffer plus metals for 30 minutes. To screen substrate and non-substrate metals for wild-type ZIP8, the metal mixture contained 5 μM of $AuCl_3$, 5 μM $PtCl_4$ or 5 μM $(NH_4)_2Cr_2O_7$, respectively. To screen variants against metal substrates, metal mixture Set 1 is composed of 2 mM $CaCl_2$, 1 mM $MgCl_2$, 5 μM for $CdCl_2$, $CoCl_2$, $MnCl_2$, $Pb(NO_3)_2$, Na_2SeO_3, $^{57}FeCl_3$, $^{70}ZnCl_2$, and 1 mM of ascorbic acid. The metal mixture Set 2 is composed of 2 mM $CaCl_2$, 1 mM $MgCl_2$, 2 μM of $CdCl_2$, 15 μM of $MnCl_2$, 40 μM of $^{57}FeCl_3$ and 1 mM of ascorbic acid. To test novel activities toward non-substrate metals, the metal

mixture contained 2 mM $CaCl_2$, 1 mM $MgCl_2$, 2.5 μM ^{70}Zn, and 5 μM for $CuCl_2$, $VOSO_4$, $NiSO_4$, respectively.

After incubation at 37°C for 30 min, the plates were put on ice and an equal volume of the ice-cold washing buffer containing 1 mM EDTA was added to the cells to terminate metal uptake, followed by three times of washing with ice-cold wash buffer.

4.3.4 ICP-MS experiment

All standards, blanks, and cell samples were prepared using trace metal grade nitric acid (70%, Fisher chemical, Cat# A509P212), ultrapure water (18.2 MΩ·cm @ 25 °C), and metal free polypropylene conical tubes (15 and 50 mL, Labcon, Petaluma, CA, USA). For cell samples in polystyrene 24-well cell culture plates, 200 μl of 70% trace nitric acid was added to allow for initial sample digestion. Following digestion, 150 μl of the digested product was transferred into metal free 15 mL conical tubes. For liquid samples, 50 μl of liquid samples were added to metal free conical tubes followed by addition of 150 μl of 70% trace nitric acid. All cell and liquid samples were then incubated at 65°C in a water bath for one hour followed by dilution to 5 ml using ultrapure water. These completed ICP-MS samples were then analyzed using the Agilent 8900 Triple Quadrupole ICP-MS (Agilent, Santa Clara, CA, USA) equipped with the Agilent SPS 4 Autosampler, integrate sample introduction system (ISiS), x-lens, and micromist nebulizer. Daily tuning of the instrument was accomplished using manufacturer supplied tuning solution containing Li, Co, Y, Ce, and Tl. Global tune optimization was based on optimizing intensities for ^{7}Li,

^{89}Y, and ^{205}Tl while minimizing oxides ($^{140}Ce^{16}O/^{140}Ce$ < 1.5%) and doubly charged species ($^{140}Ce^{++}/^{140}Ce^{+}$ < 2%). Following global instrument tuning, gas mode tuning was accomplished using the same manufacturer supplied tuning solution in KED mode (using 100% UHP He, Airgas). Specifically, intensities for ^{59}Co, ^{89}Y, and ^{205}Tl were maximized while minimizing oxides ($^{140}Ce^{16}O/^{140}Ce$ < 0.5%) and doubly charged species ($^{140}Ce^{++}/^{140}Ce^{+}$ < 1.5%) with short term RSDs < 3.5%. ICP-MS standards were prepared from a stock solution of NWU-16 multi-element standard (Inorganic Ventures, Christiansburg, VA, USA) that contains As, Ca, Cd, Co, Cr, Cu, Fe, K, Mg, Mn, Ni, Se, V, Zn that were diluted with 3% (v/v) trace nitric acid in ultrapure water to a final element concentration of 1000, 500, 250, 125, 62.5, 31.25, and 0 (blank) ng/g standard. Internal standardization was accomplished inline using the ISIS valve and a 200 ng/g internal standard solution in 3% (v/v) trace nitric acid in ultrapure water consisting of Bi, In, ^{6}Li, Sc, Tb, and Y (IV-ICPMS-71D, Inorganic Ventures, Christiansburg, VA, USA). The isotopes selected for analysis were ^{31}P, ^{64}Zn, ^{66}Zn, ^{67}Zn, ^{68}Zn, ^{70}Zn and ^{6}Li, ^{45}Sc, and ^{89}Y for internal standardization. Continuing calibration blanks (CCBs) were run every 10 samples and a continuing calibration verification standard was analyzed at the end of every run for a 90-110% recovery.

4.3.5 Statistics

We assumed a normal distribution of the samples and significant difference were examined using two-tail Student's *t* test. Uncertainties are reported as standard deviation or standard error of the mean, as indicated.

4.4 Results

4.4.1 Generation of a library of ZIP8 variants with randomized selectivity filter

Since the selectivity filter is at the very frontline when interacting with metals, we hypothesized that changing the amino acid composition of the three residues constituting the selectivity filter will lead to altered substrate preference. To test this, we systematically introduced different polar amino acid residues at these positions based on bioinformatic analysis of the ZIP family (**Figure 4.1**). Q180 is at the pore entrance but not at the transport site and this position is mostly occupied by a polar or charged residue, including histidine, aspartate, glutamate, asparagine, glutamine, and serine[327]. E318 is one of the residues at the transport site and can be replaced by an aspartate or a histidine in other ZIPs[113]. Since a histidine at this position is only present in ZIP13, a Golgi-residing ZIP with controversial data regarding the function – it has been shown to be a zinc importer for the human protein[360] but an iron exporter for the homologous protein in *Drosophila*[200,241]. In this work, histidine was not introduced to this position because it would not be a component of the selectivity filter if ZIP13 maintains the same topology as other ZIPs but function as an exporter. E343 is another residue acting at both the

selectivity filter and the transport site. In addition to glutamate, the position of E343 can also be occupied a histidine or a glutamine in other ZIPs[327]. Given the similar property to glutamate, aspartate was also introduced to this position although it is not present at this position in any ZIP. Through site-directed mutagenesis and recombination, a library consisting of 48 constructs (wild-type ZIP8 and 47 variants) was generated for functional screen (**Table 4.1**).

Construct	Amino Acid			Metal Mixture Set 1[a]				Metal Mixture Set 2[b]	
	180	318	343	Co^{2+}	Zn^{2+}	Cd^{2+}	Pb^{2+}	Mn^{2+}	Cd^{2+}
Q180D/343D	D	D	D	67 ±19[c]	188±4[d]	137± 6	171± 52	49 ± 4	152±30
Q180E/E343D	E	D	D	179± 63	211± 4	158± 3	152± 46	64 ± 7	193±39
Q180H/E343D	H	D	D	111 ± 23	268± 5	182± 2	84 ± 28	131±10	189±36
Q180N/E343D	N	D	D	174± 30	150± 9	180±13	176± 56	95 ±22	81 ±11
Q180S/E343D	S	D	D	290± 47	197±12	200± 9	209± 68	107±17	157±24
E343D	Q	D	D	718± 90	223±14	370±26	427± 79	482±90	150±15

Table 4.1. Screening of the ZIP8 library against a panel of metal substrates.
[a] Composed of 2 mM $CaCl_2$, 1 mM $MgCl_2$, 5 μM for $CdCl_2$, $CoCl_2$, $MnCl_2$, $Pb(NO_3)_2$, Na_2SeO_3, $^{57}FeCl_3$, $^{70}ZnCl_2$, and 1 mM of ascorbic acid. SeO_3^{2-} data are not shown due to low reading.
[b] Composed of 2 mM $CaCl_2$, 1 mM $MgCl_2$, 2 μM of $CdCl_2$, 15 μM of $MnCl_2$, 40 μM of $^{57}FeCl_3$ and 1 mM of ascorbic acid. Fe^{2+} data are not shown due to low activity and large variation.
[c] Mean±S.E.M. Relative activity expressed as percentage of the activity of wild-type ZIP8. The number of independent experiments (n) for Set 1 and Set 2 is 4 and 3, respectively.
[d] Cells are color based on the following criterial: less than 15%, red; between 15% and 50%, pink; between 50% and 150%, white; between 150% and 300%, light blue; greater than 300%, dark blue.

Table 4.1 (cont'd)

Q180D	D	D	E	24 ± 9	119± 6	81 ± 6	125± 12	45 ± 7	104± 2
Q180E	E	D	E	34 ± 5	131± 5	82 ± 5	94 ± 14	54 ± 8	109± 6
Q180H	H	D	E	33 ± 13	168± 5	105± 3	34 ± 19	73 ±12	138± 7
Q180N	N	D	E	40 ± 9	91 ± 3	91 ± 6	121± 28	57 ± 3	62 ± 6
Q180S	S	D	E	80 ± 8	113± 4	93 ± 5	139± 27	58 ± 6	88 ± 8
WT	Q	D	E	100	100	100	100	100	100
Q180D/E343H	D	D	H	69 ± 14	196± 3	129± 3	195± 32	53 ± 7	153±32
Q180E/E343H	E	D	H	166± 35	232± 8	158± 2	165± 49	45 ± 5	185±45
Q180H/E343H	H	D	H	19 ± 9	213± 9	111 ± 4	30 ± 10	34 ± 7	186±89
Q180N/E343H	N	D	H	0 ± 7	19 ± 3	32 ± 5	38 ± 21	34 ±19	23 ±21
Q180S/E343H	S	D	H	25 ± 10	50 ± 2	62 ± 5	60 ± 11	24 ±13	40 ±32
E343H	Q	D	H	48 ± 29	73 ±12	135±21	71 ± 33	33 ± 2	26 ± 3
Q180D/E343Q	D	D	Q	191± 38	441±15	296±13	413±126	94 ± 9	157±23
Q180E/E343Q	E	D	Q	224± 23	538±21	477±30	593±180	161±19	217±46
Q180H/E343Q	H	D	Q	307± 59	491±29	399±34	194± 67	122±12	253±41
Q180N/E343Q	N	D	Q	66 ± 23	244±21	180±13	195± 62	57 ± 6	69 ± 8
Q180S/E343Q	S	D	Q	0 ± 42	17 ± 6	19 ± 2	28 ± 13	20 ± 4	25 ± 5
E343Q	Q	D	Q	161± 34	316±40	278±28	346± 31	78 ± 6	91 ±15
Q180D/D318E/E343D	D	E	D	16 ± 7	27 ± 2	35 ± 4	44 ± 6	56 ±23	34 ±28
Q180E/D318E/E343D	E	E	D	16 ± 5	38 ± 6	41 ± 2	57 ± 22	58 ±17	36 ±25
Q180H/D318E/E343D	H	E	D	9 ± 3	10 ± 2	6 ± 0	0 ± 63	8 ± 5	3 ± 3
Q180N/D318E/E343D	N	E	D	15 ± 6	28 ± 6	40 ± 0	50 ± 30	54 ±19	27 ±22

Table 4.1 (cont'd)

Q180S/D318E/E343D	S	E	D	13 ± 5	28 ± 5	35 ± 2	43 ± 21	47 ± 9	29 ±23
D318E/E343D	Q	E	D	0 ± 46	35 ± 4	41 ± 4	38 ± 11	45 ± 3	35 ± 7
Q180D/D318E	D	E	E	0 ± 18	25 ± 4	37 ± 7	16 ± 32	42 ± 7	21 ±14
Q180E/D318E	E	E	E	0 ± 17	20 ± 2	43 ± 6	0 ± 14	45 ± 8	12 ± 5
Q180H/D318E	H	E	E	13 ± 15	16 ± 2	25 ± 5	63 ± 22	34 ±26	11 ± 7
Q180N/D318E	N	E	E	0 ± 28	21 ± 8	45 ±11	116± 84	63 ±11	16 ± 7
Q180S/D318E	S	E	E	0 ± 19	23 ± 5	43 ± 8	33 ± 32	43 ±10	13 ± 4
D318E	Q	E	E	18 ± 14	31 ± 5	40 ± 3	125± 60	58 ±18	17 ± 7
Q180D/D318E/E343H	D	E	H	11 ± 0	31 ± 5	39 ± 5	58 ± 19	52 ±21	29 ±24
Q180E/D318E/E343H	E	E	H	17 ± 6	36 ± 2	36 ± 2	172± 54	41 ± 9	26 ±19
Q180H/D318E/E343H	H	E	H	2 ± 3	14 ± 3	14 ± 3	0 ± 73	15 ± 8	4 ± 4
Q180N/D318E/E343H	N	E	H	10 ± 3	17 ± 4	17 ± 2	0 ± 50	27 ±12	8 ± 8
Q180S/D318E/E343H	S	E	H	15 ± 3	21 ± 4	19 ± 2	52 ± 22	19 ± 5	8 ± 5
D318E/E343H	Q	E	H	0 ± 8	9 ± 1	16 ± 2	46 ± 25	25 ±13	21 ±20
Q180D/D318E/E343Q	D	E	Q	19 ± 6	30 ± 1	29 ± 3	57 ± 5	57 ±31	29 ±24
Q180E/D318E/E343Q	E	E	Q	7 ± 4	40 ± 4	37 ± 2	61 ± 22	49 ±14	28 ±19
Q180H/D318E/E343Q	H	E	Q	18 ± 2	85 ± 4	45 ± 3	0 ± 43	38 ±17	29 ±17
Q180N/D318E/E343Q	N	E	Q	15 ± 7	30 ± 3	36 ± 2	50 ± 24	53 ±16	26 ±22
Q180S/D318E/E343Q	S	E	Q	18 ± 6	33 ± 3	36 ± 2	53 ± 23	50 ±13	28 ±22
D318E/E343Q	Q	E	Q	0 ± 43	36 ± 5	39 ± 4	175±145	39 ± 2	31 ± 7

4.4.2 Identification of Pb^{2+} as a new substrate of ZIP8

In order to define the border of the substrate spectrum of wild-type ZIP8, we first screened a total of thirteen metals that include not only the known substrates of ZIP8, including Zn^{2+}, Fe^{2+}, Mn^{2+}, Co^{2+}, and Cd^{2+}, but also those that are not, including Cr^{3+}, VO^{2+}, Ni^{2+}, Cu^{2+}, Pt^{4+}, Au^{3+}, Hg^{2+}, and Pb^{2+}. Different from our previous studies where a Chelex-treated DMEM plus 10% FBS was used to dissolve metal substrates and incubate with HEK293T cells in the transport assay, we used a buffer containing 10 mM HEPES, 142 mM NaCl, 5 mM KCl and 10 mM glucose in this work to avoid metal binding to serum proteins so that the actual free metal concentrations are likely to be higher than those when a serum-containing solution was used. In the transport assay, the HEK293T cells transiently expressing ZIP8 were incubated with the solution containing the metal mixture and ICP-MS was used to detect metal levels, which are expressed as the ratio of M/^{31}P where M and ^{31}P are the metal being tested and phosphorus in the same sample, respectively. When the same of batch of cells are used in the same experiment, the resulting M/^{31}P ratios are highly precise, as shown in our previous study on ZIP4 when ^{70}Zn was used as the substrate[361]. As expected, several known ZIP substrate metals, including Zn^{2+}, Cd^{2+}, Mn^{2+} and Co^{2+}, were shown to be transported into the cells expressing ZIP8 significantly more than the cells transfected with an empty vector. No transport activity of ^{57}Fe, a stable Fe isotope with a low natural abundance, was detected because ascorbic acid, which keeps iron in the reduced state, is not compatible with Cu^{2+}

in the solution and therefore excluded from the metal mixture. Unexpectedly, although Mn activity turned out to be very low, likely due to the competition from other preferred metals, such as Zn and Cd, the transport activity for Pb^{2+} was detected as the M/^{31}P ratio for the ZIP8 group was ~20% higher than that of the control group (**Figure 4.2**). As the radius of Pb^{2+} (143 pm) is about two times compared to Zn^{2+} (74 pm), the finding that Pb^{2+} is a novel substrate of ZIP8 indicates that the transport site and selectivity filter are able to accommodate metal ions with very different size. However, the inability of wild-type ZIP8 to transport many other tested metals, including VO^{2+}, Cr^{2+}, Ni^{2+}, Cu^{2+}, Pt, Au, and Hg^{2+} indicates that, despite of promiscuity, ZIP8 still transports metals in a selective manner.

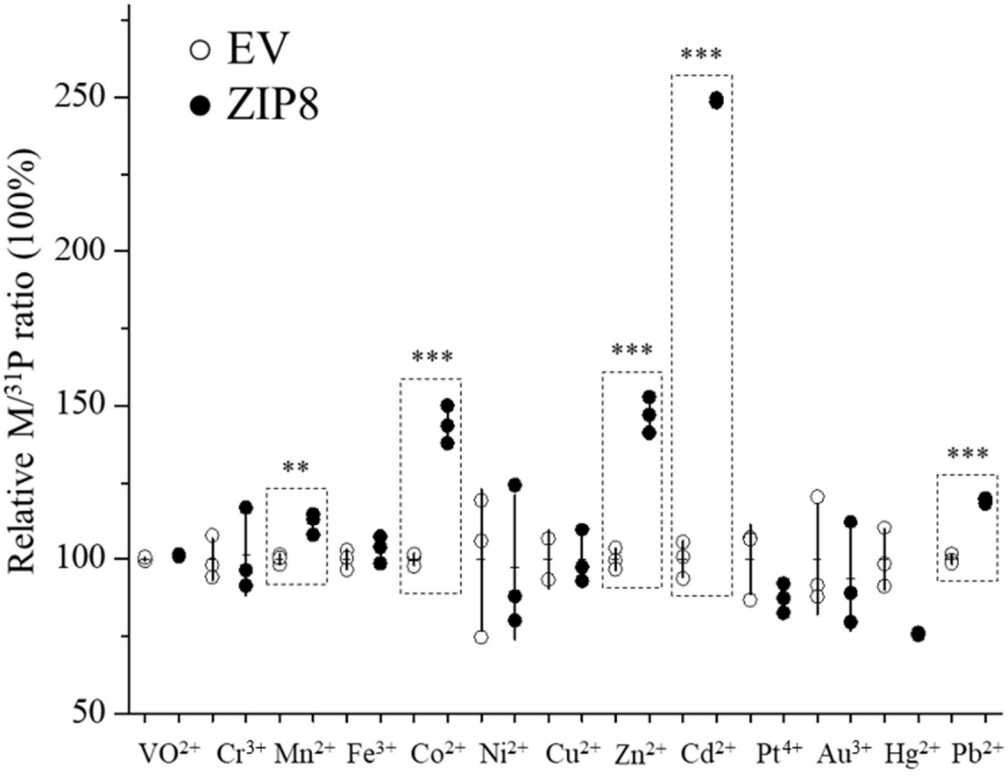

Figure 4.2. Detection of ZIP8 transport activity toward an array of metals. For each metal, the relative M/^{31}P molar ratio of the ZIP8 group is expressed as the percentage of the

Figure 4.2. (cont'd)
M/^{31}P molar ratio of the empty vector group. Fe^{3+} was not reduced to Fe^{2+} due to the lack of ascorbic acid in the sample to avoid reaction with Cu^{2+}. Each symbol (open circle for the empty vector group or solid circle for the ZIP8 group) represents the result of one replicate, and three replicates were conducted under one condition. For the result of each metal, the horizontal bar is the mean of three replicates and the vertical bar shows 1±S.D. Two tailed student's *t* test was used to test statistical significance. **: P<0.01; ***: P<0.001. The P values for Mn^{2+}, Co^{2+}, Zn^{2+}, Cd^{2+}, and Pb^{2+} are 0.006, 0.0003, 0.0003, $2x10^{-6}$, and $4x10^{-5}$, respectively.

4.4.3 Screening the library against metal substrate mixtures

Given that ICP-MS can spontaneously quantify the content of multiple metals in a sample, ICP-MS is particularly useful to study substrate specificity because the relative transport rate for each metal would not be affected by variations in expression level or cells number in different samples. In this work, in order to examine the systematic mutagenesis of the selectivity filter leads to changed substrate specificity, the constructs in the generated library were screened against a mixture of known metal substrates – Zn, Cd, Mn, Co, Fe, and Pb. However, due to the presence of competing substrates, the activity of Mn and Fe couldn't be consistently detected. To address this problem, a second set of metal mixture composed of Mn, Fe, and Cd was used to screen the library. The molar ratios of Mn, Fe, and Cd in the metal mixture have been optimized so that the activities for all three metals can be detected (**Figure 4.3**).

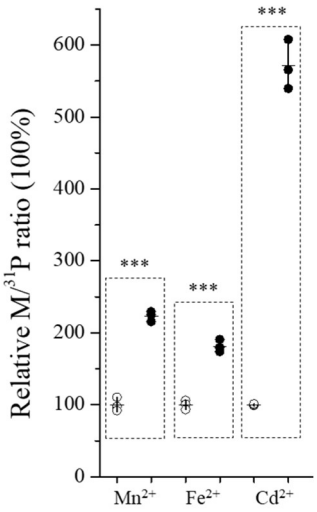

Figure 4.3. Detection of the activities for Mn^{2+}, Fe^{2+}, and Cd^{2+} under an optimized condition. For each metal, the relative $M/^{31}P$ ratio of the ZIP8 group (solid circle) is expressed as the percentage of the $M/^{31}P$ ratio of the empty vector group (open circle). Each data point represents the result of one replicate, and six replicates were conducted under one condition. For the result of each metal, the horizontal bar is the mean of three replicates and the vertical bar shows 1±S.D. Two tailed student's *t* test was used to test statistical significance. ***: $P<0.001$. The P values for Mn^{2+}, Fe^{2+}, and Cd^{2+}, are $6x10^{-5}$, 0.0002, and $2x10^{-7}$, respectively.

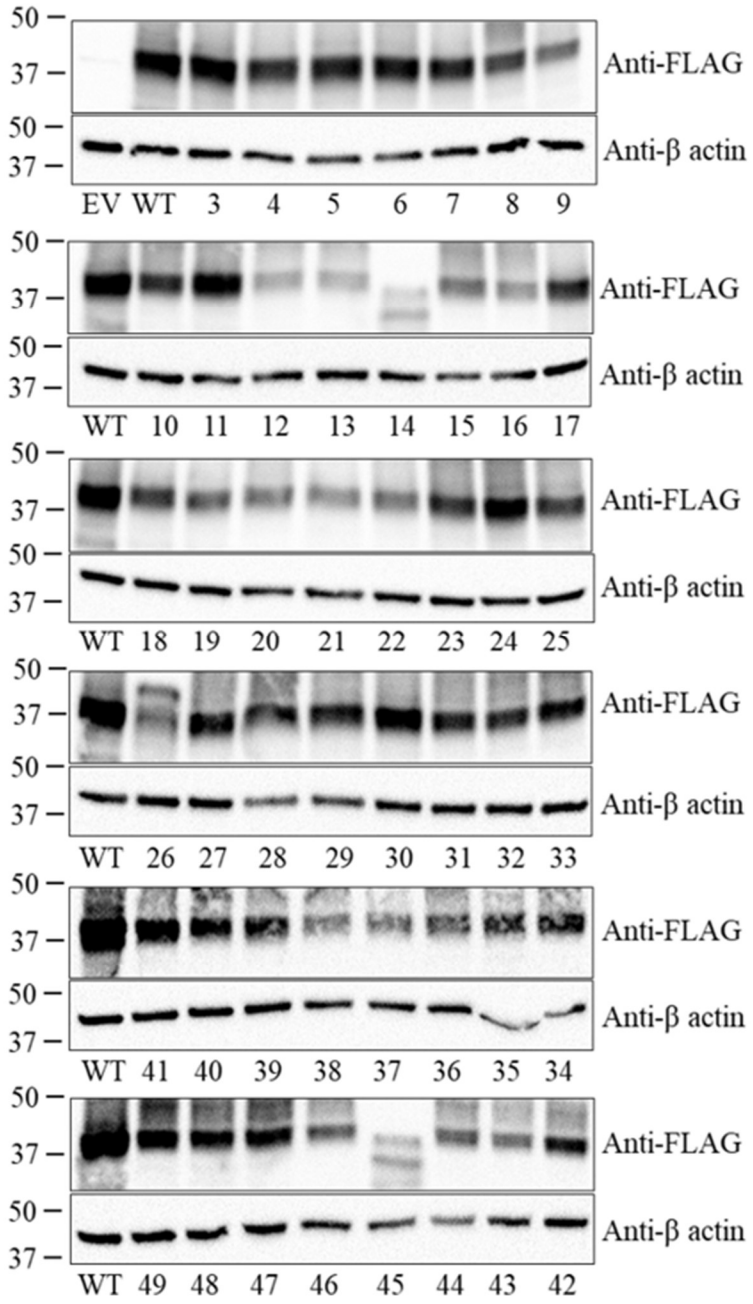

Variant#	Substitutions
3	Q180D
4	Q180E
5	Q180H
6	Q180N
7	Q180S
8	D318E
9	E343D
10	E343H
11	E343Q
12	Q180D/D318E
13	Q180E/D318E
14	Q180H/D318E
15	Q180N/D318E
16	Q180S/D318E
17	Q180D/E343D
18	Q180E/E343D
19	Q180H/E343D
20	Q180N/E343D
21	Q180S/E343D
22	Q180D/E343Q
23	Q180E/E343Q
24	Q180H/E343Q
25	Q180N/E343Q
26	Q180S/E343Q
27	D318E/E343D
28	D318E/E343Q
29	Q180D/E343H
30	Q180E/E343H
31	Q180H/E343H
32	Q180N/E343H
33	Q180S/E343H
34	D318E/E343H
35	Q180D/D318E/E343D
36	Q180D/D318E/E343Q
37	Q180E/D318E/E343D
38	Q180E/D318E/E343Q
39	Q180N/D318E/E343D
40	Q180N/D318E/E343Q
41	Q180S/D318E/E343D
42	Q180S/D318E/E343Q
43	Q180D/D318E/E343H
44	Q180E/D318E/E343H
45	Q180H/D318E/E343D
46	Q180H/D318E/E343H
47	Q180H/D318E/E343Q
48	Q180N/D318E/E343H
49	Q180S/D318E/E343H

Figure 4.4. Western blot data of the empty vector (negative control), ZIP8-WT and the variants. Western blot was performed to detect the FLAG-tagged proteins (human ZIP8 and its variants) and β-actin.

The M/^{31}P ratio of was calculated for each metal substrate and expressed as the percentage of the M/^{31}P ratio of the same metal for the wild-type ZIP8. The results are

summarized in **Table 4.1** and the activity toward each metal for each variant was classified into five categories – greatly increased (greater than 300%); modestly increased (between 150% and 300%); no significant change (between 50% and 150%); modestly reduced (between 15% and 50%); and greatly reduced (less than 15%). It should be noted that Fe data are not included in **Table 4.1** because the results of Fe transport are less reproducible with larger variations than those for other metals, probably due to the still weak activity even under the optimized condition. Analysis of the data in **Table 4.1**, including the expression analysis of the constructs by Western blot (**Figure 4.4**), led to several interesting findings.

i. D318E substitution is detrimental to the transport of all metals for nearly all the tested variants, which is not due to reduced expression of these variants according to the results of Western blot.

ii. Variants containing the combination of the E343D substitution and D318 (present in the wild-type ZIP8) favor the transport of metal substrates in most cases. The most outstanding variant is the E343D single variant that exhibits significantly increased activity for all metals with the activities for Co^{2+}, Mn^{2+}, and Pb^{2+} being increased more than those for Zn^{2+} and Cd^{2+}, indicating an altered substrate preference.

iii. When only considering the variants without the detrimental D318E substitution and with the obvious outlier E343D being excluded, there are clearly positive correlations between activities of any two tested metals (**Figure 4.5**). The greatest correlation

between Zn and Cd reflects their similar chemical properties and therefore it would be most challenging to create variants to selectively transport one while exclude the other. In contrast, the poorest correlations between Mn and Cd and between Co and Pb suggest better chances to separate the activities for each metal pair.

iv. When the Zn^{2+} activities were correlated with the activities for Cd^{2+}, Pb^{2+}, and Co^{2+}, the slopes, which were all smaller than one (**Figure 4.5**), indicate that the common effect of the mutations at the selectivity filter is to increase the preference for Zn^{2+} over other metals. Further analysis revealed several variants that exhibited significantly altered substrate preference, including: (1) the double variant Q180E/E343H that shows modestly increased activity for non-Mn^{2+} metals but a reduced activity for Mn, making it a Mn-excluding variant; (2) the double variant Q180H/E343H that behaves to be a Zn/Cd-preferred variant with reduced activities for Co^{2+}, Mn^{2+}, and Pb^{2+} and a consistent preference for Zn^{2+} over Cd^{2+} as reported[327]; (3) the double variant Q180N/D318E that appears to be a Mn-preferred variant, despite the activities for all metals were reduced; and (4) the triple variant Q180E/D318E/E343H that behaves like a Pb-preferred variant with increased Pb transport activity while reduced activities for other metals. To reveal the biochemical basis for altered activity/substrate specificity in these variants, further kinetic studies are required.

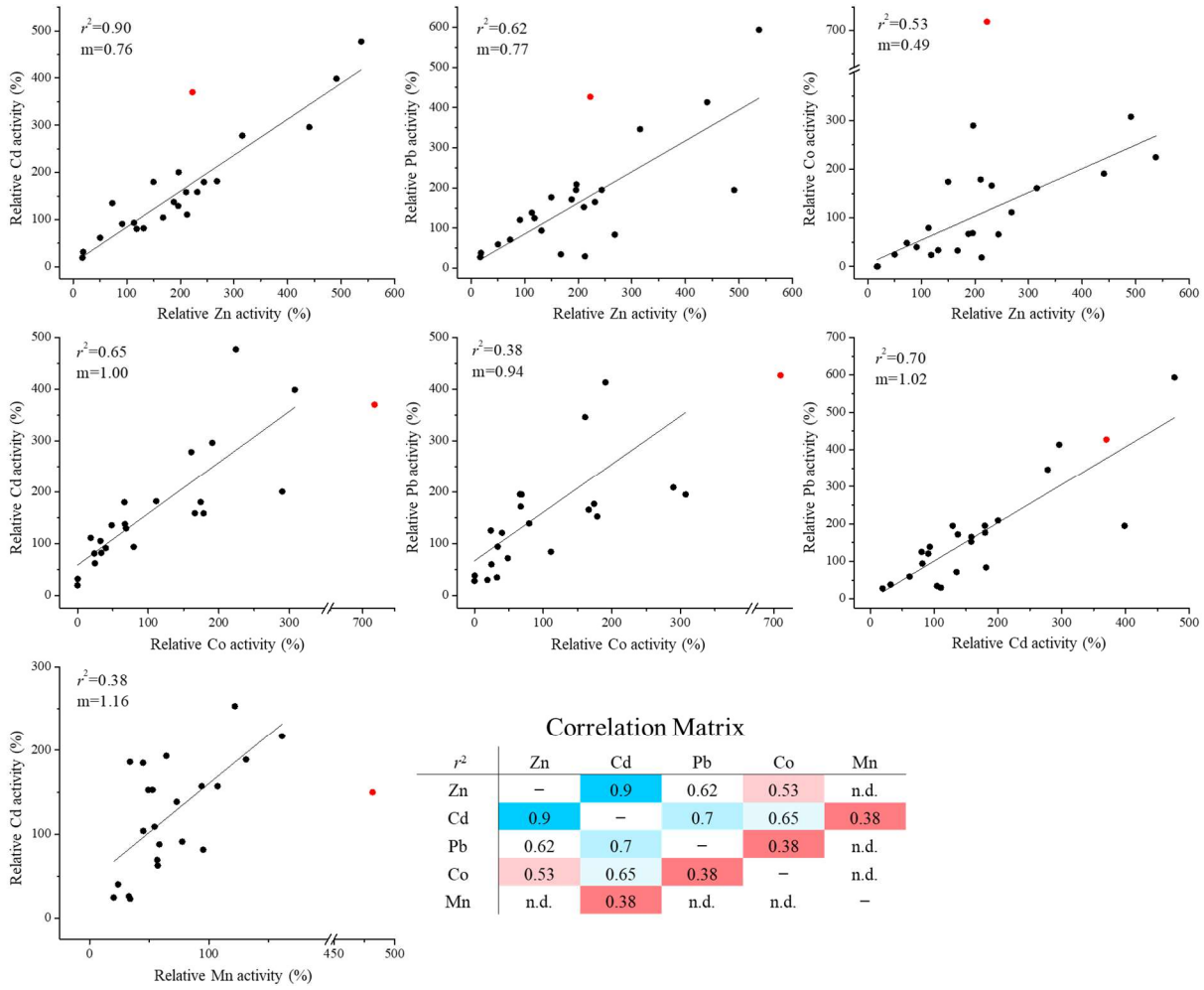

Correlation Matrix

r^2	Zn	Cd	Pb	Co	Mn
Zn	–	0.9	0.62	0.53	n.d.
Cd	0.9	–	0.7	0.65	0.38
Pb	0.62	0.7	–	0.38	n.d.
Co	0.53	0.65	0.38	–	n.d.
Mn	n.d.	0.38	n.d.	n.d.	–

Figure 4.5. Correlation analysis of the activities for different metal substrates. Activities are expressed as the percentages of the corresponding activities of wild-type ZIP8. Only the variants without the D318E substitution were analyzed due to the strong detrimental effects of the mutation on the activities for nearly all metals tested. The E343D single variant (red solid circle) was excluded from linear regression because it is an obvious outlier for nearly all correlation analysis (except for the Cd-Pb pair). The activities for Zn^{2+}, Cd^{2+}, Pb^{2+}, and Co^{2+} obtained in Metal Mixture Set 1 and the activities for Mn^{2+} and Cd^{2+} obtained in Metal Mixture Set 2 were applied to correlation analysis. The r^2 values are summarized in the correlation matrix.

4.4.4 New transport activities toward non-substrate metals

Given the significantly altered substrate specificity of the selected variants, we wondered if any of these variants is able to transport the metals which are not substrates

of wild-type ZIP8 (such as VO^{2+}, Ni^{2+}, and Cu^{2+}). We then conducted transport assay of these variants against a metal mixture containing these non-substrate divalent cations and compared the results with wild-type ZIP8. As shown in **Figure 4.6**, all tested variants exhibited transport activity for at least one of the non-substrate metals since the M/^{31}P ratios were significantly greater than those for wild-type ZIP8, i.e. two variants showed activity for VO^{2+}, four variants for Ni^{2+}, and three variants for Cu^{2+}. Of great interest, the double variant Q180N/D318E displayed activities for all three non-substrates, whereas the transport activities of this variant for Zn^{2+}, Cd^{2+}, Co^{2+}, and Mn^{2+} were shown to be reduced (**Table 4.1**). In contrast, the E343D variant, which showed drastically increased activities for all known ZIP8 substrates (**Table 4.1**), only exhibited a marginal activity toward VO^{2+} but no activity toward Ni^{2+} or Cu^{2+}. These results indicate that new transport activities can be generated by changing the amino acid composition of the selectivity filter, but at the expense of reduced activities against former substrates.

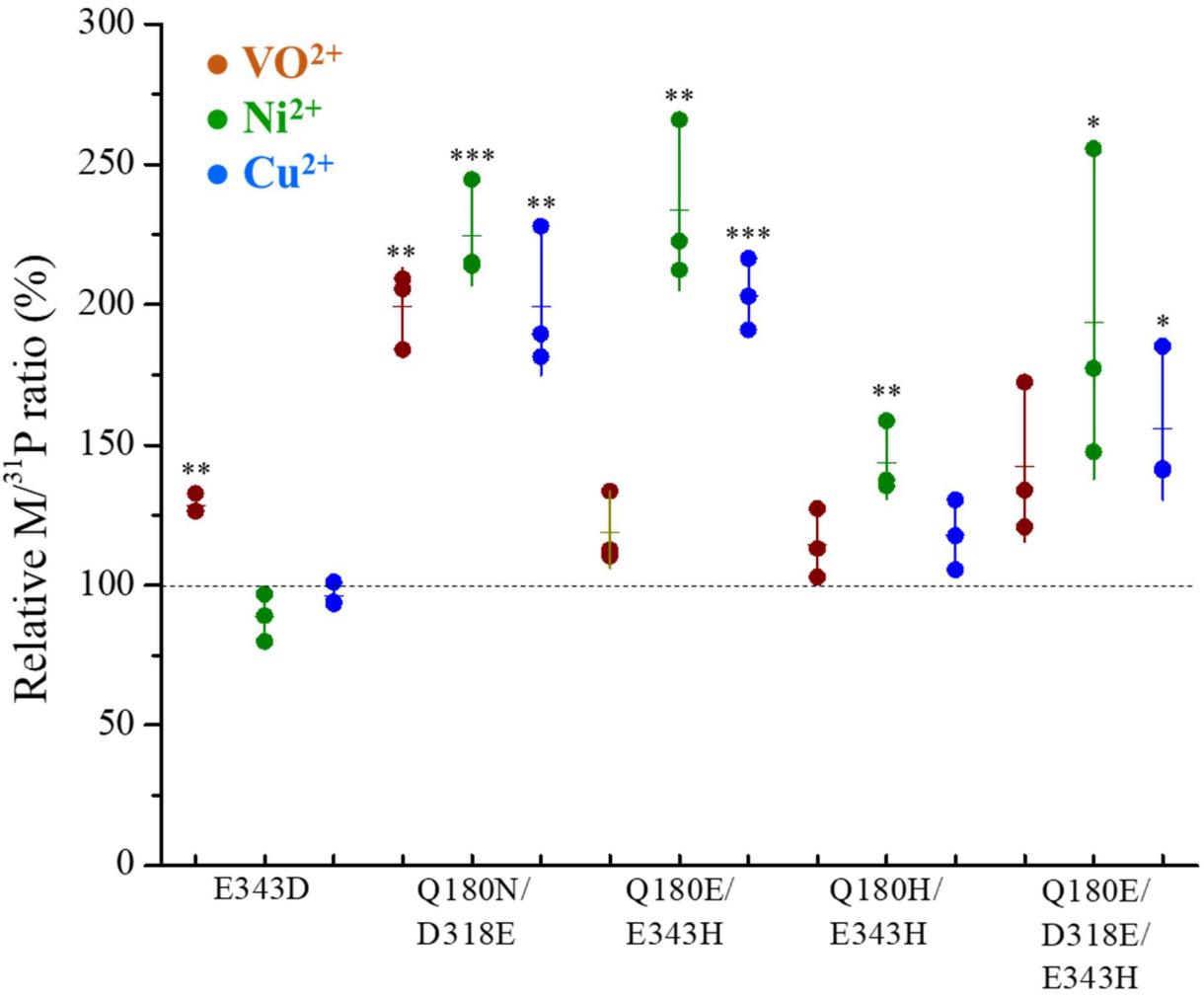

Figure 4.6. Detection of new activities toward VO^{2+}, Ni^{2+}, and Cu^{2+} for selected variants. The relative M/^{31}P ratio of a variant is expressed as the percentage of the M/^{31}P ratio of the wild-type ZIP8. Each symbol represents the result of one sample, and three replicates were conducted for one condition. The horizontal bar is the mean of three replicates and the vertical bar shows 1±S.D. Data shown are from one of three independent experiments. Two tailed student's *t* test was conducted to test statistical significance. *: P<0.05; **: P<0.01; ***: P<0.001. The P values from left to right are 0.002, 0.002, 0.0002, 0.003, 0.002, 0.0002, 0.009, 0.046, and 0.02, respectively.

4.5 Discussion

The engineering of metal transporters that allow for the enrichment or exclusion of certain metals from living organisms has great potential in applications including, but not limited to, biofortification, phytoremediation, bio-mining, and heavy metal exclusion from

food. However, the field also faces significant challenges. First, the d-block metals, which are the target metals of most interest in these applications, share similar physicochemical properties, making it difficult to create metal transporters with high selectivity. Second, our understanding of the transport mechanism and substrate specificity of *d*-block metal transporters is still in its infancy, and the poor knowledge of the dynamic *d*-block metal-protein interactions during metal translocation through the transporter significantly impedes rational engineering. Third, the lack of high-throughput assays for metal transporters hinders the application of directed evolution to metal transporter engineering. Here, we applied a metal transporter engineering approach based on our previous finding of a conditional selectivity filter at the pore entrance of the transporter ZIP8[327], a highly promiscuous transporter, was chosen as the target based on the fact that promiscuity is known to be a starting point for different specificities in natural or directed evolution[362]. Our data strongly suggest that both the transport activity and substrate specificity of ZIP8 can be altered over a wide range, demonstrating the feasibility of tuning the function of a metal transporter by targeting the selected key residues based on prior knowledge.

By randomizing the three residues forming the selectivity filter, we generated a library consisting of 48 constructs and screened them using ICP-MS to study transport activity and substrate preference by taking advantage of the simultaneous measurement of multiple elements, including the metals of interest and phosphorus used for activity calibration. The results showed that both activity and substrate preference can be

drastically altered by targeting the selectivity filter, highlighting the key role of this structural element in transport. The E343D mutation is particularly interesting because this position is very rarely occupied by an aspartate in the entire ZIP family, although the substitution is considered to be conservative. Since E343 plays a dual role in transport – a gating residue in the selectivity filter and a residue in the transport site to confer a high affinity, the greatly increased activity for all known metal substrates caused by the E343D mutation may suggest that a shorter side chain allows a faster metal binding to the transport site due to a larger pore of the selectivity filter and/or a faster release from the transport site due to a longer distance between the metal and the carboxylic acid and thus a weaker interaction. The exclusion of an aspartate from this position in natural evolution may be the result of the otherwise much higher transport rate, which would be detrimental to the tightly controlled homeostasis for *d*-block metals. Conversely, the D318E substitution drastically reduced the transporter activity across the entire spectrum of metal substrates, which could not be rescued by the E343D substitution, despite the two residues facing each other in both the selectivity filter and the transport site (**Figure 4.1**). The lack of epistatic effects of contacting residues, as observed between Q180 and E343[327], suggests that D318 and E343 have non-overlapping functions. In fact, the variants with the same amino acid composition at the selectivity filter but different distribution among the three involved residues often did not show the same activity and

substrate preference (**Figure 4.7**), indicating that the three positions in the selectivity filter are not equal in determining activity and substrate preference.

Construct	Amino Acid			Metal Mixture_Set 1				Metal Mixture_Set 2	
	180	318	343	Co	Zn	Cd	Pb	Mn	Cd
Q180E/E343D	E	D	D	179	211	158	152	64	193
Q180D	D	D	E	24	119	81	125	45	104
Q180D/D318E/E343D	D	E	D	16	27	35	44	56	34
Q180H/E343D	H	D	D	111	268	182	84	131	189
Q180D/E343H	D	D	H	69	196	129	195	53	153
E343D	Q	D	D	718	223	370	427	482	150
Q180D/E343Q	D	D	Q	191	441	296	413	94	157
Q180H	H	D	E	33	168	105	34	73	138
Q180E/E343H	E	D	H	166	232	158	165	45	185
Q180D/D318E/E343H	D	E	H	11	31	39	58	52	29
Q180H/D318E/E343D	H	E	D	9	10	6	0	8	3
WT	Q	D	E	100	100	100	100	100	100
Q180E/E343Q	E	D	Q	224	538	477	593	161	217
D318E/E343D	Q	E	D	0	35	41	38	45	35
Q180D/D318E/E343Q	D	E	Q	19	30	29	57	57	29
Q180H/D318E	H	E	E	13	16	25	63	34	11
Q180E/D318E/E343H	E	E	H	17	36	36	172	41	26
Q180H/D318E/E343Q	H	E	Q	18	85	45	0	38	29
D318E/E343H	Q	E	H	0	9	16	46	25	21
Q180H/E343Q	H	D	Q	307	491	399	194	122	253
E343H	Q	D	H	48	73	135	71	33	26
Q180E/D318E/E343D	E	E	D	16	38	41	57	58	36
Q180D/D318E	D	E	E	0	25	37	16	42	21
Q180E	E	D	E	34	131	82	94	54	109
Q180E/D318E/E343Q	E	E	Q	7	40	37	61	49	28
D318E	Q	E	E	18	31	40	125	58	17

Figure 4.7. Comparison of the constructs with the same amino acid composition at the selectivity filter. The constructs within the same frame have the same amino acid composition but different distribution at the positions of 180, 318, and 343. They often do not exhibit the same activity or substrate preference, suggestive of non-overlapping roles of these residues in transport. Data are retrieved from **Table 4.1**.

This work led to the discovery of ZIP8 variants that may help elucidate the biological functions of this promiscuous metal transporter. ZIP8 has been shown to be involved in many different physiological and pathological processes. Since ZIP8 can transport Zn, Mn and Fe under physiological conditions, it is not always easy to determine whether a particular function of ZIP8 is associated with its transport activity for which

metal substrate(s). We previously reported that the combination of two mutations, Q180H and E343H, resulted in a ZIP8 variant with an increased preference for Zn over Cd. In this work, the screening results (**Table 4.1** and **Figure 4.5**) showed that the Q180H/E343H variant indeed behaves like a Zn-preferred transporter with a substrate preference in the order Zn>Cd>>Mn~Co~Pb. A slightly different variant (Q180E/E343H) turned out to be a Mn-excluded variant, since the activities for all substrates except Mn were increased, while the activity for Mn was decreased by more than 50%. In contrast, the Q180N/D318E variant prefers Mn over Zn, although the activities for all substrates are decreased to different extents. Because these variants show drastically altered preferences for different physiological substrates, they can be used to differentiate the role of different metal activities in a physio/pathological event. Similarly, the Q180E/D318E/E343H variant could be useful to study the contribution of ZIP8 in Pb^{2+} transport and toxicity, since it strongly prefers Pb^{2+} over the other metal substrates.

Finally, our data demonstrate the great potential of the ZIP fold to transport metal ions with very different physicochemical properties. It is unexpected that Pb^{2+}, a non-*d*-block metal ion with a radius even larger than Cd^{2+}, the previous largest ZIP substrate, can be accommodated to pass through the ZIP8 transport pathway (**Figure 4.2**). Consistently, our data showed that although VO^{2+}, Ni^{2+} and Cu^{2+} are not substrates for wild-type ZIP8, new activities towards these metals were found in selected variants (**Figure 4.6**). Although Ni^{2+} and Cu^{2+} have been reported to be substrates of some

ZIPs[183,185], this is the first time that the diatomic ion VO^{2+} is found to be transported by a ZIP. Taken together, our study clearly demonstrates that the ZIP fold, which is conserved in the entire ZIP family, has a strong plasticity and amenability to transport a variety of metal ions, and thus may be an ideal platform for creating metal transporters with greatly altered and expanded substrate spectrum.

4.6 Acknowledgements

I thank Dr. Jian Hu for the instruction, intelligent input in this project and his unconditional support. I thank Dr. Keith MacRenaris and Dr. Aaron Sue from the O'Halloran group for instructing me on ICP-MS. I thank Dr. Thomas O'Halloran for his input in the project. I thank Michael Nikolovski for the great teamwork. I thank the Hu group for the support.

This work is supported by NIH GM129004 and GM140931.

CHAPTER 5: Conclusion and perspectives

This thesis project aims to better understand the molecular basis of substrate specificity and use the gained knowledge to alter the substrate spectrum of the ZIP metal transporters. To achieve these goals, I have focused on representative ZIPs including human ZIP4 and ZIP8 to answer the following questions:

1. What are the molecular determinants for substrate specificity of ZIPs? What are the roles of the residues in the identified selectivity filter?
2. Can we rationally engineer the promiscuous ZIP8 and alter its substrate preference as desired? And can we broaden the substrate spectrum of ZIPs?
3. Can we develop a non-radioactive metal assay using ICP-MS and stable isotopes to speed up engineering and also answer biochemical questions of ZIPs?

Overall, I have addressed most of these questions. In Chapter Two, I identified a series of differentially conserved residues (DCRs) by comparing the ZIPs with different substrate preference. By just mutating four selected DCRs, ZIP8 was successfully converted into a ZIP4-like and Zn-preferring transporter. Importantly, this effort led to the identification of a conditional selectivity filter which plays a key role in determining the substrate specificity. The follow-up work in Chapter Four showed that extensive mutagenesis of the selectivity filter led to drastically altered and expanded substrate spectrum of ZIP8, not only confirming the importance of the selectivity filter but also

providing a novel strategy to engineer ZIP8 and other ZIPs, since the selectivity filter is a shared structural element in most ZIPs. Engineering ZIPs requires a rapid and reliable analytical approach to measure the transport activity of variants generated in the process. To meet this requirement, in Chapter Three, I developed a non-radioactive approach by taking advantage of ICP-MS and stable rare isotopes. Using this approach, I demonstrated a 0.08-0.2 s^{-1} turnover rate for human ZIP4 expressed in HEK293T cells, indicating that ZIP4 is best described as a carrier and reaffirmed the key role of ZIP4-ECD for Zn transport activity. Metal efflux during the assay was found not to be significant, eliminating the concern that efflux may seriously interfere with data interpretation for the cell-based transport assay. The increased throughput of this approach, particularly when LA-ICP-MS was applied to study samples on a solid surface, indicated a good potential for conversion of this approach into a high-throughput format in future study.

I believe there are two prominent questions to be addressed in the field for future research.

1. Clarification of the transporter mechanism. Convincing evidence has been presented to support the elevator transport mode for BbZIP and possibly other ZIPs. However, an experimentally solved OFC structure is still not available, representing a major missing piece for the proposed transport cycle. As BbZIP in the cadmium-bound state prefers the IFC while BbZIP in the apo state is unstable in detergent micelles likely due to a high degree of dynamics, the OFC

of BbZIP needs to be stabilized by mutagenesis, chemical crosslinking, optimization of the membrane mimetics, or their combinations for structural characterization by x-ray crystallography or cryo-EM. A completely elucidated transport mechanism of ZIPs will provide a paradigm for the elevator transporter and for metal transport across biological membranes.

In addition to further establishing the universal elevator mode that is applicable to the entire ZIP family, the transport mechanisms of different ZIPs should be investigated to establish the subfamily/subgroup-specific mechanism. The low sequence similarity among the five major subfamilies and many other smaller groups strongly suggests functional diversity. This calls for a closer look at the different mechanisms among all the ZIP subfamilies.

2. Engineering of ZIPs for desired transport properties. Engineering metal transporters for desired substrate specificity and transport activity holds a huge potential for applications in agriculture and environmental protection. Our recent progress has demonstrated that rational engineering of a ZIP is feasible, but the extent to which the substrate specificity of a given ZIP can be altered and expanded towards non-substrate metals are still prominent questions. Efforts in this direction could also lead to better understanding in structure-function correlation, which may potentially lead to engineered transporters with a fully designed substrate preference or even *de novo* designer transporters.

Although these goals along with real-life applications are still a long way off, the substantial benefits of success warrant more attention for future research.

BIBLIOGRAPHY

(1) John Rieuwerts. The Elements of Environmental Pollution. **2015**. https://doi.org/10.4324/9780203798690.

(2) Fathi Habashi. Handbook of Extractive Metallurgy. **1997**.

(3) Raulin, J. Etudes Clinique Sur La Vegetation. Annales Des Science as Naturelle. *Botanique* **1869**, *11*, 93–299.

(4) Maze, P. Influences Respectives Des Elements de La Solution Gmineral Du Mais. *Ann. L'Institut Pasteur Paris* **1914**, *28*, 21–69.

(5) W. R. Todd; C. A. Elvehjem; E. B. Hart. Zinc in the Nutrition of the Rat. *Am. J. Physiol.* **1933**, *107* (1), 146–156. https://doi.org/10.1152/ajplegacy.1933.107.1.146.

(6) Boyd L. O'Dell; Paul M. Newberne; Savage, J. E. Significance of Dietary Zinc for the Growing Chicken. *J. Nutr.* **1958**, *65* (4), 503–523. https://doi.org/10.1093/jn/65.4.503.

(7) Ananda S. Prasad; Halsted, J. A.; Manucher Nadimi. Syndrome of Iron Deficiency Anemia, Hepatosplenomegaly, Hypogonadism, Dwarfism and Geophagia. *Am. J. Med.* **1961**, *31* (4), 532–546. https://doi.org/10.1016/0002-9343(61)90137-1.

(8) Wolfgang Maret; Maret, W. Zinc and Human Disease. *Met. Ions Life Sci.* **2013**, *13*, 389–414. https://doi.org/10.1007/978-94-007-7500-8_12.

(9) Astrid Sigel; Sigel, H.; Sigel, R. K. O. Interrelations between Essential Metal Ions and Human Diseases. *Met. Ions Life Sci.* **2013**. https://doi.org/10.1007/978-94-007-7500-8.

(10) Atish Prakash; Kanchan Bharti; Abu Bakar Abdul Majeed. Zinc: Indications in Brain Disorders. *Fundam. Clin. Pharmacol.* **2015**, *29* (2), 131–149. https://doi.org/10.1111/fcp.12110.

(11) Yoan Chérasse; Yoshihiro Urade; Urade, Y. Dietary Zinc Acts as a Sleep Modulator. *Int. J. Mol. Sci.* **2017**, *18* (11), 2334. https://doi.org/10.3390/ijms18112334.

(12) Ananda S. Prasad. Zinc in Human Health: Effect of Zinc on Immune Cells. *Mol. Med.* **2008**, *14* (5), 353–357. https://doi.org/10.2119/2008-00033.prasad.

(13) Grmay H. Lilay; Castro, P. H.; Feixue Liao; Liao, F.; Alexander, R. D.; Aarts, M. G. M.; Assunção, A. G. L. Arabidopsis bZIP19 and bZIP23 Act as Zinc Sensors to Control Plant Zinc Status. *Nat. Plants* **2021**, *7* (2), 137–143. https://doi.org/10.1038/s41477-021-00856-7.

(14) Barrett Sugarman. Zinc and Infection. *Clin. Infect. Dis.* **1983**, *5* (1), 137–147. https://doi.org/10.1093/clinids/5.1.137.

(15) Claudia Andreini; Banci, L.; Bertini, I.; Rosato, A. Counting the Zinc-Proteins Encoded in the Human Genome. *J. Proteome Res.* **2006**, *5* (1), 196–201. https://doi.org/10.1021/pr050361j.

(16) L. Alex Gaither; Eide, D. J. Eukaryotic Zinc Transporters and Their Regulation. *Biometals* **2001**, *14* (3), 251–270. https://doi.org/10.1007/978-94-017-3728-9_5.

(17) Klaus Hantke; Hantke, K. Bacterial Zinc Transporters and Regulators. *Biometals* **2001**, *14* (3), 239–249. https://doi.org/10.1007/978-94-017-3728-9_4.

(18) Takafumi Hara; Takeshi Takeda; Teruhisa Takagishi; Takagishi, T.; Kazuhisa Fukue; Taiho Kambe; Fukada, T. Physiological Roles of Zinc Transporters: Molecular and Genetic Importance in Zinc Homeostasis. *J. Physiol. Sci.* **2017**, *67* (2), 283–301. https://doi.org/10.1007/s12576-017-0521-4.

(19) Janet C. King; David M. Shames; Shames, D. M.; Leslie R. Woodhouse. Zinc Homeostasis in Humans. *J. Nutr.* **2000**, *130* (5). https://doi.org/10.1093/jn/130.5.1360s.

(20) M. Kirchgeßner; Kirchgessner, M. Underwood Memorial Lecture. Homeostasis and Homeorhesis in Trace Element Metabolism. **1993**, *8*, 4–21.

(21) Andrey Bekker; Heinrich Holland; Pei Ling Wang; Douglas Rumble; Holly J. Stein; Judith L. Hannah; Louis L. Coetzee; Nicolas J. Beukes. Dating the Rise of Atmospheric Oxygen. *Nature* **2004**, *427* (6970), 117–120. https://doi.org/10.1038/nature02260.

(22) Gail Lee Arnold; Ariel D. Anbar; Jane Barling; Lyons, T. W. Molybdenum Isotope Evidence for Widespread Anoxia in Mid-Proterozoic Oceans. *Science* **2004**, *304* (5667), 87–90. https://doi.org/10.1126/science.1091785.

(23) Christopher L. Dupont; Butcher, A.; Ruben E. Valas; Valas, R. E.; Philip E. Bourne; Caetano-Anollés, G. History of Biological Metal Utilization Inferred through Phylogenomic Analysis of Protein Structures. *Proc. Natl. Acad. Sci. U. S. A.* **2010**, *107* (23), 10567–10572. https://doi.org/10.1073/pnas.0912491107.

(24) Darren M. Scott; Scott, D. A.; A. M. Fisher; Fisher, A. M. THE INSULIN AND THE ZINC CONTENT OF NORMAL AND DIABETIC PANCREAS. *J. Clin. Invest.* **1938**, *17* (6), 725–728. https://doi.org/10.1172/jci101000.

(25) Bert L. Vallée; Auld, D. S. Zinc Coordination, Function, and Structure of Zinc Enzymes and Other Proteins. *Biochemistry* **1990**, *29* (24), 5647–5659. https://doi.org/10.1021/bi00476a001.

(26) Brett Lovejoy; Anne Cleasby; Anne M. Hassell; Kelly Longley; Luther, M. A.; Weigl, D.; Gerard M. McGeehan; Mcgeehan, G.; Andrew B. McElroy; David H. Drewry; Millard H. Lambert; Steven R. Jordan. Structure of the Catalytic Domain of Fibroblast Collagenase Complexed with an Inhibitor. *Science* **1994**, *263* (5145), 375–377. https://doi.org/10.1126/science.8278810.

(27) John Spurlino; Angela Smallwood; Dennis Carlton; Tracey M. Banks; Karen J. Vavra; Jeffrey S. Johnson; Ewell R. Cook; Joseph Falvo; R. Wahl; Wahl, R. C.; Pulvino, T. A.; Wendoloski, J. J.; Douglas L. Smith. 1.56 Å Structure of Mature Truncated Human Fibroblast Collagenase. *Proteins* **1994**, *19* (2), 98–109. https://doi.org/10.1002/prot.340190203.

(28) Klug, A.; Daniela Rhodes. Zinc Fingers: A Novel Protein Fold for Nucleic Acid Recognition. *Cold Spring Harb. Symp. Quant. Biol.* **1987**, *52*, 473–482. https://doi.org/10.1101/sqb.1987.052.01.054.

(29) Jay S. Hanas; Daria J. Hazuda; Daniel F. Bogenhagen; Bogenhagen, D. F.; Felicia Y.-H. Wu; Wu, C. W. Xenopus Transcription Factor A Requires Zinc for Binding to the 5 S RNA Gene. *J. Biol. Chem.* **1983**, *258* (23), 14120–14125. https://doi.org/10.1016/s0021-9258(17)43831-2.

(30) Jeremy M. Berg. Zinc Fingers and Other Metal-Binding Domains. Elements for Interactions between Macromolecules. *J. Biol. Chem.* **1990**, *265* (12), 6513–6516. https://doi.org/10.1016/s0021-9258(19)39172-0.

(31) Anna Fedotova; Artem Bonchuk; Vladic Mogila; Pavel Georgiev. C2H2 Zinc Finger Proteins: The Largest but Poorly Explored Family of Higher Eukaryotic

Transcription Factors. *Acta Naturae* **2017**, *9* (2), 47–58. https://doi.org/10.32607/20758251-2017-9-2-47-58.

(32) Carl O. Pabo; Peisach, E.; Grant, R. A. Design and Selection of Novel Cys2His2 Zinc Finger Proteins. *Annu. Rev. Biochem.* **2001**, *70* (1), 313–340. https://doi.org/10.1146/annurev.biochem.70.1.313.

(33) Nikola P. Pavletich; Carl O. Pabo. Zinc Finger-DNA Recognition: Crystal Structure of a Zif268-DNA Complex at 2.1 A. *Science* **1991**, *252* (5007), 809–817. https://doi.org/10.1126/science.2028256.

(34) Kathryn J. Brayer; Segal, D. J. Keep Your Fingers off My DNA: Protein-Protein Interactions Mediated by C2H2 Zinc Finger Domains. *Cell Biochem. Biophys.* **2008**, *50* (3), 111–131. https://doi.org/10.1007/s12013-008-9008-5.

(35) Wenlian Zhu; Zeng, Q.; Christopher M. Colangelo; Lewis, L. M.; Michael F. Summers; Scott, R. A. The N-Terminal Domain of TFIIB from Pyrococcus Furiosus Forms a Zinc Ribbon. *Nat. Struct. Mol. Biol.* **1996**, *3* (2), 122–124. https://doi.org/10.1038/nsb0296-122.

(36) Gurmeet Kaur; Subramanian, S. Classification of the Treble Clef Zinc Finger: Noteworthy Lessons for Structure and Function Evolution. *Sci. Rep.* **2016**, *6* (1), 32070–32070. https://doi.org/10.1038/srep32070.

(37) Xiuqi Qian; Shai N. Gozani; Yoon, H. S.; Jeon, C. J.; Agarwal, K.; Weiss, M. A. Novel Zinc Finger Motif in the Basal Transcriptional Machinery: Three-Dimensional NMR Studies of the Nucleic Acid Binding Domain of Transcriptional Elongation Factor TFIIS. *Biochemistry* **1993**, *32* (38), 9944–9959. https://doi.org/10.1021/bi00089a010.

(38) Bing Wang; David N. M. Jones; Jones, D. M.; Kaine, B. P.; Michael A. Weiss. High-Resolution Structure of an Archaeal Zinc Ribbon Defines a General Architectural Motif in Eukaryotic RNA Polymerases. *Structure* **1998**, *6* (5), 555–569. https://doi.org/10.1016/s0969-2126(98)00058-6.

(39) Nick V. Grishin. Treble Clef Finger—a Functionally Diverse Zinc-Binding Structural Motif. *Nucleic Acids Res.* **2001**, *29* (8), 1703–1714. https://doi.org/10.1093/nar/29.8.1703.

(40) Filhol, O.; Benítez, M. J.; Cochet, C. A Zinc Ribbon Motif Is Essential for the Formation of Functional Tetrameric Protein Kinase CK2. **2005**, 121–127. https://doi.org/10.1007/0-387-27421-9_18.

(41) Sanjeev Krishna; Majumdar, I.; Grishin, N. V. Structural Classification of Zinc Fingers: Survey and Summary. *Nucleic Acids Res.* **2003**, *31* (2), 532–550. https://doi.org/10.1093/nar/gkg161.

(42) D. Keilin; T. Mann. Carbonic Anhydrase. *Nature*. https://doi.org/10.1038/144442b0.

(43) Bert L. Vallée; Auld, D. S. Functional Zinc-Binding Motifs in Enzymes and DNA-Binding Proteins. *Faraday Discuss.* **1992**, *93* (93), 47–65. https://doi.org/10.1039/fd9929300047.

(44) Keith McCall; McCall, K. A.; Can Huang; Huang, C. C.; Carol A. Fierke; Fierke, C. A. Function and Mechanism of Zinc Metalloenzymes. *J. Nutr.* **2000**, *130* (5). https://doi.org/10.1093/jn/130.5.1437s.

(45) Bert L. Vallée; Auld, D. S. New Perspective on Zinc Biochemistry: Cocatalytic Sites in Multi-Zinc Enzymes. *Biochemistry* **1993**, *32* (26), 6493–6500. https://doi.org/10.1021/bi00077a001.

(46) D.W. Christianson. Structural Biology of Zinc. *Adv. Protein Chem.* **1991**, *42*, 281–355. https://doi.org/10.1016/s0065-3233(08)60538-0.

(47) Robert L. Jernigan; G. Raghunathan; İvet Bahar. Characterization of Interactions and Metal Ion Binding Sites in Proteins. *Curr. Opin. Struct. Biol.* **1994**, *4* (2), 256–263. https://doi.org/10.1016/s0959-440x(94)90317-4.

(48) Wilson, D. K.; Florante A. Quiocho. A Pre-Transition-State Mimic of an Enzyme: X-Ray Structure of Adenosine Deaminase with Bound 1-Deazaadenosine and Zinc-Activated Water. *Biochemistry* **1993**, *32* (7), 1689–1694. https://doi.org/10.1021/bi00058a001.

(49) D. Keith Wilson; Wilson, D. K.; Frederick B. Rudolph; Rudolph, F. B.; Florante A. Quiocho; Quiocho, F. A. Atomic Structure of Adenosine Deaminase Complexed with a Transition-State Analog: Understanding Catalysis and Immunodeficiency Mutations. *Science* **1991**, *252* (5010), 1278–1284. https://doi.org/10.1126/science.1925539.

(50) Andreini, C.; Ivano Bertini; Bertini, I. A Bioinformatics View of Zinc Enzymes. *J. Inorg. Biochem.* **2012**, *111*, 150–156. https://doi.org/10.1016/j.jinorgbio.2011.11.020.

(51) Taiho Kambe; Tsuji, T.; Hashimoto, A.; Itsumura, N. The Physiological, Biochemical, and Molecular Roles of Zinc Transporters in Zinc Homeostasis and Metabolism. *Physiol. Rev.* **2015**, *95* (3), 749–784. https://doi.org/10.1152/physrev.00035.2014.

(52) David W. Christianson; William N. Lipscomb. Carboxypeptidase A. *Acc. Chem. Res.* https://doi.org/10.1021/ar00158a003.

(53) Brian W. Matthews. Structural Basis of the Action of Thermolysin and Related Zinc Peptidases. *Acc. Chem. Res.* **1988**, *21* (9), 333–340. https://doi.org/10.1021/ar00153a003.

(54) Stec, B.; Kathleen M. Holtz; Evan R. Kantrowitz. A Revised Mechanism for the Alkaline Phosphatase Reaction Involving Three Metal Ions. *J. Mol. Biol.* **2000**, *299* (5), 1303–1311. https://doi.org/10.1006/jmbi.2000.3799.

(55) Jesse G. Zalatan; Catrina, I. E.; Mitchell, R.; Grzyska, P. K.; O'Brien, P. J.; Herschlag, D.; Hengge, A. C. Kinetic Isotope Effects for Alkaline Phosphatase Reactions: Implications for the Role of Active-Site Metal Ions in Catalysis. *J. Am. Chem. Soc.* **2007**, *129* (31), 9789–9798. https://doi.org/10.1021/ja072196+.

(56) Stephen F. Martin; Hergenrother, P. J. Catalytic Cycle of the Phosphatidylcholine-Preferring Phospholipase C from Bacillus Cereus. Solvent Viscosity, Deuterium Isotope Effects, and Proton Inventory Studies. *Biochemistry* **1999**, *38* (14), 4403–4408. https://doi.org/10.1021/bi9821216.

(57) Carpenter, E. P.; Alastair R. Hawkins; Frost, J. W.; Katherine A. Brown. Structure of Dehydroquinate Synthase Reveals an Active Site Capable of Multistep Catalysis. *Nature* **1998**, *394* (6690), 299–302. https://doi.org/10.1038/28431.

(58) Patrick J. Baker; Britton, K. L.; Fisher, M.; Esclapez, J.; Carmen Pire; María José Bonete; Ferrer, J.; Rice, D. W. Active Site Dynamics in the Zinc-Dependent Medium Chain Alcohol Dehydrogenase Superfamily. *Proc. Natl. Acad. Sci. U. S. A.* **2009**, *106* (3), 779–784. https://doi.org/10.1073/pnas.0807529106.

(59) Sandaruwan Geeganage; Frey, P. A. Significance of Metal Ions in Galactose-1-Phosphate Uridylyltransferase: An Essential Structural Zinc and a Nonessential

Structural Iron. *Biochemistry* **1999**, *38* (40), 13398–13406. https://doi.org/10.1021/bi9910631.

(60) Sonja A. Dames; Martinez-Yamout, M. A.; De Guzman, R. N.; H. Jane Dyson; Wright, P. E. Structural Basis for Hif-1 Alpha /CBP Recognition in the Cellular Hypoxic Response. *Proc. Natl. Acad. Sci. U. S. A.* **2002**, *99* (8), 5271–5276. https://doi.org/10.1073/pnas.082121399.

(61) Christopher J. Frederickson; Koh, J.-Y.; Bush, A. I. The Neurobiology of Zinc in Health and Disease. *Nat. Rev. Neurosci.* **2005**, *6* (6), 449–462. https://doi.org/10.1038/nrn1671.

(62) Stefano L. Sensi; Pierre Paoletti; Ashley I. Bush; Israel Sekler. Zinc in the Physiology and Pathology of the CNS. *Nat. Rev. Neurosci.* **2009**, *10* (11), 780–791. https://doi.org/10.1038/nrn2734.

(63) Atsüshi Takeda; Masatoshi Nakamura; Hiroaki Fujii; Tamano, H. Synaptic Zn2+ Homeostasis and Its Significance. *Metallomics* **2013**, *5* (5), 417–423. https://doi.org/10.1039/c3mt20269k.

(64) Haleli Sharir; Zinger, A.; Andrey Nevo; Israel Sekler; Michal Hershfinkel. Zinc Released from Injured Cells Is Acting via the Zn2+-Sensing Receptor, ZnR, to Trigger Signaling Leading to Epithelial Repair. *J. Biol. Chem.* **2010**, *285* (34), 26097–26106. https://doi.org/10.1074/jbc.m110.107490.

(65) Limor Besser; Ehud Chorin; Israel Sekler; William F. Silverman; Atkin, S. D.; Russell, J. T.; Hershfinkel, M. Synaptically Released Zinc Triggers Metabotropic Signaling via a Zinc-Sensing Receptor in the Hippocampus. *J. Neurosci.* **2009**, *29* (9), 2890–2901. https://doi.org/10.1523/jneurosci.5093-08.2009.

(66) Taghi Ghafghazi; Michael L. McDaniel; Lacy, P. E. Zinc-Induced Inhibition of Insulin Secretion from Isolated Rat Islets of Langerhans. *Diabetes* **1981**, *30* (4), 341–345. https://doi.org/10.2337/diab.30.4.341.

(67) Motoyuki Tamaki; Yoshio Fujitani; Akemi Hara; Toyoyoshi Uchida; Yasuaki Tamura; Kageumi Takeno; Takeno, K.; Kawaguchi, M.; Takahiro Watanabe; Takeshi Ogihara; Ayako Fukunaka; Tomoaki Shimizu; Tomoya Mita; Akio Kanazawa; Kanazawa, A.; M. Imaizumi; Imaizumi, M. O.; Abe, T.; Takaya Abe; Abe, T.; Hiroshi Kanazawa; Kiyonari, H.; Kiyonari, H.; Shintaro Hojyo; Hojyo, S.; Toshiyuki Fukada; Fukada, T.; Takeshi Kawauchi; Kawauchi, T.; Shinya Nagamatsu; Nagamatsu, S.; Toshio Hirano; Hirano, T.; Ryuzo Kawamori;

Kawamori, R.; Hirotaka Watada; Watada, H. The Diabetes-Susceptible Gene SLC30A8/ZnT8 Regulates Hepatic Insulin Clearance. *J. Clin. Invest.* **2013**, *123* (10), 4513–4524. https://doi.org/10.1172/jci68807.

(68) Toshiyuki Fukada; Fukada, T.; Satoshi Yamasaki; Yamasaki, S.; Keigo Nishida; Nishida, K.; Keigo Nishida; Masaaki Murakami; Murakami, M.; Toshio Hirano; Hirano, T. Zinc Homeostasis and Signaling in Health and Diseases: Zinc Signaling. *J. Biol. Inorg. Chem.* **2011**, *16* (7), 1123–1134. https://doi.org/10.1007/s00775-011-0797-4.

(69) Toshio Hirano; Hirano, T.; Masaaki Murakami; Murakami, M.; Toshiyuki Fukada; Fukada, T.; Keigo Nishida; Nishida, K.; Satoshi Yamasaki; Yamasaki, S.; Tomoyuki Suzuki; Suzuki, T. Roles of Zinc and Zinc Signaling in Immunity: Zinc as an Intracellular Signaling Molecule. *Adv. Immunol.* **2008**, *97*, 149–176. https://doi.org/10.1016/s0065-2776(08)00003-5.

(70) Kathryn Mary Taylor; Taylor, K. M.; Hiscox, S. E.; Nicholson, R. I.; Christer Högstrand; Kille, P. Protein Kinase CK2 Triggers Cytosolic Zinc Signaling Pathways by Phosphorylation of Zinc Channel ZIP7. *Sci. Signal.* **2012**, *5* (210). https://doi.org/10.1126/scisignal.2002585.

(71) Satoshi Yamasaki; Kumiko Sakata-Sogawa; Aiko Hasegawa; Tomoyuki Suzuki; Koki Kabu; Eriko Sato; Sato, E.; Tomohiro Kurosaki; Susumu Yamashita; Makio Tokunaga; Keigo Nishida; Toshio Hirano. Zinc Is a Novel Intracellular Second Messenger. *J. Cell Biol.* **2007**, *177* (4), 637–645. https://doi.org/10.1083/jcb.200702081.

(72) Hajo Haase; Wolfgang Maret. Protein Tyrosine Phosphatases as Targets of the Combined Insulinomimetic Effects of Zinc and Oxidants. *Biometals* **2005**, *18* (4), 333–338. https://doi.org/10.1007/s10534-005-3707-9.

(73) Mandar A. Aras; Aizenman, E. Redox Regulation of Intracellular Zinc: Molecular Signaling in the Life and Death of Neurons. *Antioxid. Redox Signal.* **2011**, *15* (8), 2249–2263. https://doi.org/10.1089/ars.2010.3607.

(74) Viola Günther; Lindert, U.; Schaffner, W. The Taste of Heavy Metals: Gene Regulation by MTF-1. *Biochim. Biophys. Acta* **2012**, *1823* (9), 1416–1425. https://doi.org/10.1016/j.bbamcr.2012.01.005.

(75) Louis A. Lichten; Moon-Suhn Ryu; Guo, L.; Embury, J. E.; Robert J. Cousins. MTF-1-Mediated Repression of the Zinc Transporter Zip10 Is Alleviated by Zinc Restriction. *PLOS ONE* **2011**, *6* (6). https://doi.org/10.1371/journal.pone.0021526.

(76) Hajo Haase; Julia L. Ober-Blöbaum; Gabriela Engelhardt; Silke Hebel; Antje Heit; Holger Heine; Lothar Rink; Rink, L. Zinc Signals Are Essential for Lipopolysaccharide-Induced Signal Transduction in Monocytes. *J. Immunol.* **2008**, *181* (9), 6491–6502. https://doi.org/10.4049/jimmunol.181.9.6491.

(77) Hiroyuki Kitamura; Hideyuki Morikawa; Hokuto Kamon; Iguchi, M.; Shintaro Hojyo; Toshiyuki Fukada; Susumu Yamashita; Tsuneyasu Kaisho; Akira, S.; Masaaki Murakami; Hirano, T. Toll-like Receptor-Mediated Regulation of Zinc Homeostasis Influences Dendritic Cell Function. *Nat. Immunol.* **2006**, *7* (9), 971–977. https://doi.org/10.1038/ni1373.

(78) Shintaro Hojyo; Fukada, T.; Shimoda, S.; Ohashi, W.; Bum-Ho Bin; Haruhiko Koseki; Hirano, T. The Zinc Transporter SLC39A14/ZIP14 Controls G-Protein Coupled Receptor-Mediated Signaling Required for Systemic Growth. *PLOS ONE* **2011**, *6* (3). https://doi.org/10.1371/journal.pone.0018059.

(79) Verena von Bülow; Lothar Rink; Haase, H. Zinc-Mediated Inhibition of Cyclic Nucleotide Phosphodiesterase Activity and Expression Suppresses TNF-α and IL-1β Production in Monocytes by Elevation of Guanosine 3′,5′-Cyclic Monophosphate. *J. Immunol.* **2005**, *175* (7), 4697–4705. https://doi.org/10.4049/jimmunol.175.7.4697.

(80) David L. Brautigan; Paul Börnstein; Byron Gallis. Phosphotyrosyl-Protein Phosphatase. Specific Inhibition by Zn. *J. Biol. Chem.* **1981**, *256* (13), 6519–6522. https://doi.org/10.1016/s0021-9258(19)69016-2.

(81) Matthew A. Wilson; Wilson, M. B.; Hogstrand, C.; Maret, W. Picomolar Concentrations of Free Zinc(II) Ions Regulate Receptor Protein-Tyrosine Phosphatase β Activity. *J. Biol. Chem.* **2012**, *287* (12), 9322–9326. https://doi.org/10.1074/jbc.c111.320796.

(82) Tolunay Beker Aydemir; Juan P. Liuzzi; Steven McClellan; Robert J. Cousins. Zinc Transporter ZIP8 (SLC39A8) and Zinc Influence IFN-γ Expression in Activated Human T Cells. *J. Leukoc. Biol.* **2009**, *86* (2), 337–348. https://doi.org/10.1189/jlb.1208759.

(83) Péter Csermely; Márta Szamel; Klaus Resch; J. Somogyi. Zinc Can Increase the Activity of Protein Kinase C and Contributes to Its Binding to Plasma Membranes in T Lymphocytes. *J. Biol. Chem.* **1988**, *263* (14), 6487–6490. https://doi.org/10.1016/s0021-9258(18)68668-5.

(84) Anders Hansson. Extracellular Zinc Ions Induces Mitogen-Activated Protein Kinase Activity and Protein Tyrosine Phosphorylation in Bombesin-Sensitive Swiss 3T3 Fibroblasts. *Arch. Biochem. Biophys.* **1996**, *328* (2), 233–238. https://doi.org/10.1006/abbi.1996.0168.

(85) Wolfgang Maret; Jacob, C.; Bert L. Vallée; Fischer, E. H. Inhibitory Sites in Enzymes: Zinc Removal and Reactivation by Thionein. *Proc. Natl. Acad. Sci. U. S. A.* **1999**, *96* (5), 1936–1940. https://doi.org/10.1073/pnas.96.5.1936.

(86) Hajo Haase; Maret, W. Intracellular Zinc Fluctuations Modulate Protein Tyrosine Phosphatase Activity in Insulin/Insulin-like Growth Factor-1 Signaling. *Exp. Cell Res.* **2003**, *291* (2), 289–298. https://doi.org/10.1016/s0014-4827(03)00406-3.

(87) Akihito Kamizono; Kamizono, A.; Masafumi Nishizawa; Nishizawa, M.; Yutaka Teranishi; Teranishi, Y.; Kousaku Murata; Murata, K.; Akira Kimura; Kimura, A. Identification of a Gene Conferring Resistance to Zinc and Cadmium Ions in the Yeast Saccharomyces Cerevisiae. *Mol. Genet. Genomics* **1989**, *219* (1), 161–167. https://doi.org/10.1007/bf00261172.

(88) Douglas S. Conklin; J. A. Mcmaster; Michael R. Culbertson; Kung, C. COT1, a Gene Involved in Cobalt Accumulation in Saccharomyces Cerevisiae. *Mol. Cell. Biol.* **1992**, *12* (9), 3678–3688. https://doi.org/10.1128/mcb.12.9.3678.

(89) Dietrich H. Nies. CzcR and CzcD, Gene Products Affecting Regulation of Resistance to Cobalt, Zinc, and Cadmium (Czc System) in Alcaligenes Eutrophus. *J. Bacteriol.* **1992**, *174* (24), 8102–8110. https://doi.org/10.1128/jb.174.24.8102-8110.1992.

(90) Richard D. Palmiter; Findley, S. D. Cloning and Functional Characterization of a Mammalian Zinc Transporter That Confers Resistance to Zinc. *EMBO J.* **1995**, *14* (4), 639–649. https://doi.org/10.1002/j.1460-2075.1995.tb07042.x.

(91) Richard D. Palmiter; Liping Huang. Efflux and Compartmentalization of Zinc by Members of the SLC30 Family of Solute Carriers. *Pflüg. Arch. Eur. J. Physiol.* **2004**, *447* (5), 744–751. https://doi.org/10.1007/s00424-003-1070-7.

(92) Eide, D. J.; Broderius, M.; Fett, J. P.; Guerinot, M. L. A Novel Iron-Regulated Metal Transporter from Plants Identified by Functional Expression in Yeast. *Proc. Natl. Acad. Sci. U. S. A.* **1996**, *93* (11), 5624–5628. https://doi.org/10.1073/pnas.93.11.5624.

(93) Hui Zhao; Zhao, H.; Hui Zhao; David J. Eide; Eide, D. J. The Yeast ZRT1 Gene Encodes the Zinc Transporter Protein of a High-Affinity Uptake System Induced by Zinc Limitation. *Proc. Natl. Acad. Sci. U. S. A.* **1996**, *93* (6), 2454–2458. https://doi.org/10.1073/pnas.93.6.2454.

(94) Hui Zhao; Hui Zhao; Zhao, H.; David J. Eide; Eide, D.; Eide, D. J.; Eide, D. J. The ZRT2 Gene Encodes the Low Affinity Zinc Transporter in Saccharomyces Cerevisiae. *J. Biol. Chem.* **1996**, *271* (38), 23203–23210. https://doi.org/10.1074/jbc.271.38.23203.

(95) David L. Manning; Manning, D. L.; Roger J. Daly; Daly, R. J.; P. G. Lord; Lord, P. G.; Kevin F. Kelly; Kelly, K. F.; C.D. Green; Green, C. D. Effects of Oestrogen on the Expression of a 4.4 Kb mRNA in the ZR-75-1 Human Breast Cancer Cell Line. *Mol. Cell. Endocrinol.* **1988**, *59* (3), 205–212. https://doi.org/10.1016/0303-7207(88)90105-0.

(96) Taylor, K. M. LIV-1 Breast Cancer Protein Belongs to New Family of Histidine-Rich Membrane Proteins with Potential to Control Intracellular Zn2+ Homeostasis. *Iubmb Life* **2000**, *49* (4), 249–253. https://doi.org/10.1080/15216540050033087.

(97) Kathryn Mary Taylor; Nicholson, R. I. The LZT Proteins; the LIV-1 Subfamily of Zinc Transporters. *Biochim. Biophys. Acta* **2003**, *1611* (1), 16–30. https://doi.org/10.1016/s0005-2736(03)00048-8.

(98) KM Taylor. The LIV-1 Subfamily of Zinc Transporters: From Origins to Present Day Discoveries. *Int. J. Mol. Sci.* **2023**, *24* (2), 1255–1255. https://doi.org/10.3390/ijms24021255.

(99) Taiho Kambe; Tomoyuki Suzuki; Nagao, M.; Yamaguchi-Iwai, Y. Sequence Similarity and Functional Relationship among Eukaryotic ZIP and CDF Transporters. *Genomics Proteomics Bioinformatics* **2006**, *4* (1), 1–9. https://doi.org/10.1016/s1672-0229(06)60010-7.

(100) Lichten, L. A.; Robert J. Cousins; Robert J. Cousins; Cousins, R.; Robert J. Cousins; Robert J. Cousins. Mammalian Zinc Transporters: Nutritional and

Physiologic Regulation. *Annu. Rev. Nutr.* **2009**, *29* (1), 153–176. https://doi.org/10.1146/annurev-nutr-033009-083312.

(101) Mary Lou Guerinot; Guerinot, M. L. The ZIP Family of Metal Transporters. *Biochim. Biophys. Acta* **2000**, *1465* (1), 190–198. https://doi.org/10.1016/s0005-2736(00)00138-3.

(102) Jian Hu; Hu, J. Toward Unzipping the ZIP Metal Transporters: Structure, Evolution, and Implications on Drug Discovery against Cancer. *FEBS J.* **2020**, *288* (20), 5805–5825. https://doi.org/10.1111/febs.15658.

(103) Laura E. Lehtovirta-Morley; Mohammad Alsarraf; Wilson, D. Pan-Domain Analysis of ZIP Zinc Transporters. *Int. J. Mol. Sci.* **2017**, *18* (12), 2631. https://doi.org/10.3390/ijms18122631.

(104) Tuo Zhang; Tuo Zhang; Tuo Zhang; Zhang, T.; Dexin Sui; Sui, D.; Jian Hu; Hu, J. Structural Insights of ZIP4 Extracellular Domain Critical for Optimal Zinc Transport. *Nat. Commun.* **2016**, *7* (1), 11979–11979. https://doi.org/10.1038/ncomms11979.

(105) Yuhan Jiang; Zhen Li; Dexin Sui; Gaurav Sharma; Tianqi Wang; Keith W. MacRenaris; Hideki Takahashi; Kenneth M. Merz; Jian Hu. Author Correction: Rational Engineering of an Elevator-Type Metal Transporter ZIP8 Reveals a Conditional Selectivity Filter Critically Involved in Determining Substrate Specificity. *Commun. Biol.* **2023**, *6* (1). https://doi.org/10.1038/s42003-023-05460-3.

(106) Peter Thomas; Aubrey Converse; André Berg; Berg, H. ZIP9, a Novel Membrane Androgen Receptor and Zinc Transporter Protein. *Gen. Comp. Endocrinol.* **2018**, *257* (1), 130–136. https://doi.org/10.1016/j.ygcen.2017.04.016.

(107) André Berg; Rice, C. W.; Rice, C. D.; Md. Saydur Rahman; Jingjing Dong; Peter Thomas; Thomas, P. Identification and Characterization of Membrane Androgen Receptors in the ZIP9 Zinc Transporter Subfamily: I. Discovery in Female Atlantic Croaker and Evidence ZIP9 Mediates Testosterone-Induced Apoptosis of Ovarian Follicle Cells. *Endocrinology* **2014**, *155* (11), 4237–4249. https://doi.org/10.1210/en.2014-1198.

(108) David J. Eide. Zinc Transporters and the Cellular Trafficking of Zinc. *Biochim. Biophys. Acta* **2006**, *1763* (7), 711–722. https://doi.org/10.1016/j.bbamcr.2006.03.005.

(109) Tuo Zhang; Tuo Zhang; Tuo Zhang; Zhang, T.; Jian Liu; Jian Liu; Jian Liu; Liu, J.; M. Fellner; Fellner, M.; Chi Zhang; Zhang, C.; Dexin Sui; Sui, D.; Jian Hu; Hu, J. Crystal Structures of a ZIP Zinc Transporter Reveal a Binuclear Metal Center in the Transport Pathway. *Sci. Adv.* **2017**, *3* (8). https://doi.org/10.1126/sciadv.1700344.

(110) Anders Wiuf; Anders Wiuf; Steffen, J. H.; Jonas Hyld Steffen; Eva Ramos Becares; Eva Ramos Becares; Christina Grønberg; Christina Grønberg; Mahato, D. R.; Dhani Ram Mahato; Søren G F Rasmussen; Søren G. F. Rasmussen; Andersson, M.; Magnus Andersson; Croll, T. I.; Tristan I. Croll; Gotfryd, K.; Kamil Gotfryd; Gourdon, P.; Pontus Gourdon. The Two-Domain Elevator-Type Mechanism of Zinc-Transporting ZIP Proteins. *Sci. Adv.* **2022**, *8* (28). https://doi.org/10.1126/sciadv.abn4331.

(111) Yao Zhang; Yuhan Jiang; Kaifu Gao; Dexin Sui; Peixuan Yu; Min Su; Guowei Wei; Jian Hu. Structural Insights into the Elevator-Type Transport Mechanism of a Bacterial ZIP Metal Transporter. *bioRxiv* **2023**, *14* (1). https://doi.org/10.1038/s41467-023-36048-4.

(112) Zhang, Y.; Jiang, Y.; Gao, K.; Sui, D.; Yu, P.; Su, M.; Wei, G.-W.; Hu, J. Structural Insights into the Elevator-Type Transport Mechanism of a Bacterial ZIP Metal Transporter. *Nat. Commun.* **2023**, *14* (1), 385. https://doi.org/10.1038/s41467-023-36048-4.

(113) Tuo Zhang; Tuo Zhang; Tuo Zhang; Zhang, T.; Sui, D.; Zhang, C.; Cole, L. E.; Hu, J. Asymmetric Functions of a Binuclear Metal Center within the Transport Pathway of a Human Zinc Transporter ZIP4. *FASEB J.* **2020**, *34* (1), 237–247. https://doi.org/10.1096/fj.201902043r.

(114) Gergely Gyimesi; Albano, G.; Fuster, D. G.; Hediger, M. A.; Jonai Pujol-Giménez. Unraveling the Structural Elements of pH Sensitivity and Substrate Binding in the Human Zinc Transporter SLC39A2 (ZIP2). *J. Biol. Chem.* **2019**, *294* (20), 8046–8063. https://doi.org/10.1074/jbc.ra118.006113.

(115) Roberts, C. S.; Ni, F.; Mitra, B. The Zinc and Iron Binuclear Transport Center of ZupT, a ZIP Transporter from Escherichia Coli. *Biochemistry* **2021**. https://doi.org/10.1021/acs.biochem.1c00621.

(116) Glen K. Andrews. Regulation and Function of Zip4, the Acrodermatitis Enteropathica Gene. *Biochem. Soc. Trans.* **2008**, *36* (6), 1242–1246. https://doi.org/10.1042/bst0361242.

(117) Tuo Zhang; Tuo Zhang; Tuo Zhang; Zhang, T.; Eziz Kuliyev; Kuliyev, E.; Eziz Kuliyev; Dexin Sui; Sui, D.; Jian Hu; Hu, J. The Histidine-Rich Loop in the Extracellular Domain of ZIP4 Binds Zinc and Plays a Role in Zinc Transport. *Biochem. J.* **2019**, *476* (12), 1791–1803. https://doi.org/10.1042/bcj20190108.

(118) John Adulcikas; Adulcikas, J.; Shaghayegh Norouzi; Shaghayegh Norouzi; Norouzi, S.; Lawrence Bretag; Bretag, L.; Sukhwinder Singh Sohal; Sohal, S. S.; Stephen Myers; Myers, S.; Stephen Myers. The Zinc Transporter SLC39A7 (ZIP7) Harbours a Highly-Conserved Histidine-Rich N-Terminal Region That Potentially Contributes to Zinc Homeostasis in the Endoplasmic Reticulum. *Comput. Biol. Med.* **2018**, *100*, 196–202. https://doi.org/10.1016/j.compbiomed.2018.07.007.

(119) Attila Kumánovics; Poruk, K. E.; Katharine A. Osborn; Diane McVey Ward; Kaplan, J. YKE4 (YIL023C) Encodes a Bidirectional Zinc Transporter in the Endoplasmic Reticulum of Saccharomyces Cerevisiae. *J. Biol. Chem.* **2006**, *281* (32), 22566–22574. https://doi.org/10.1074/jbc.m604730200.

(120) Elizabeth M. Bafaro; Mark W. Maciejewski; Jeffrey C. Hoch; Dempski, R. E. Concomitant Disorder and High-Affinity Zinc Binding in the Human Zinc- and Iron-Regulated Transport Protein 4 Intracellular Loop. *Protein Sci.* **2019**, *28* (5), 868–880. https://doi.org/10.1002/pro.3591.

(121) Chi Zhang; Zhang, C.; Dexin Sui; Sui, D.; Tuo Zhang; Tuo Zhang; Tuo Zhang; Zhang, T.; Jian Hu; Hu, J. Molecular Basis of Zinc-Dependent Endocytosis of Human ZIP4 Transceptor. *Cell Rep.* **2020**, *31* (4), 107582. https://doi.org/10.1016/j.celrep.2020.107582.

(122) Mary E. Penny. Zinc Supplementation in Public Health. *Ann. Nutr. Metab.* **2013**, *62*, 31–42. https://doi.org/10.1159/000348263.

(123) Ananda S. Prasad; Frances W.J. Beck; Bin Bao; James T. Fitzgerald; Diane Snell; Joel Steinberg; Lavoisier Cardozo. Zinc Supplementation Decreases Incidence of Infections in the Elderly: Effect of Zinc on Generation of Cytokines and Oxidative Stress. *Am. J. Clin. Nutr.* **2007**, *85* (3), 837–844. https://doi.org/10.1093/ajcn/85.3.837.

(124) Melanie J Tuerk; Fazel, N.; Nasim Fazel. Zinc Deficiency. *Curr. Opin. Gastroenterol.* **2009**, *25* (2), 136–143. https://doi.org/10.1097/mog.0b013e328321b395.

(125) Hajo Haase; Eugenio Mocchegiani; Lothar Rink; Rink, L. Correlation between Zinc Status and Immune Function in the Elderly. *Biogerontology* **2006**, *7* (5), 421–428. https://doi.org/10.1007/s10522-006-9057-3.

(126) Broun, E. R.; Greist, A.; Tricot, G.; Hoffman, R. A Reversible Cause of Sideroblastic Anemia and Bone Marrow Depression. *J. Am. Med. Assoc. JAMA* **2016**. https://doi.org/10.1001/jama.264.11.1441.

(127) Besecker, B. Y.; Bao, S.; Barbara Bohacova; Papp, A. C.; Wolfgang Sadée; Knoell, D. L. The Human Zinc Transporter SLC39A8 (Zip8) Is Critical in Zinc-Mediated Cytoprotection in Lung Epithelia. *Am. J. Physiol.-Lung Cell. Mol. Physiol.* **2008**, *294* (6). https://doi.org/10.1152/ajplung.00057.2008.

(128) Juan P. Liuzzi; Guo, L.; Chang, S.-M.; Robert J. Cousins. Krüppel-like Factor 4 Regulates Adaptive Expression of the Zinc Transporter Zip4 in Mouse Small Intestine. *Am. J. Physiol.-Gastrointest. Liver Physiol.* **2009**, *296* (3). https://doi.org/10.1152/ajpgi.90568.2008.

(129) Juan P. Liuzzi; Lichten, L. A.; Rivera, S.; Blanchard, R. K.; Aydemir, T. B.; Knutson, M. D.; Tomas Ganz; Ganz, T.; Robert J. Cousins. Interleukin-6 Regulates the Zinc Transporter Zip14 in Liver and Contributes to the Hypozincemia of the Acute-Phase Response. *Proc. Natl. Acad. Sci. U. S. A.* **2005**, *102* (19), 6843–6848. https://doi.org/10.1073/pnas.0502257102.

(130) Anzilotti, C.; Swan, D. J.; Boisson, B.; Mukta Deobagkar-Lele; Oliveira, C.; Chabosseau, P.; Engelhardt, K. R.; Xia Xu; Xu, X.-N.; Xu, X.; Chen, R.; Rui Chen; Alvarez, L.; Berlinguer-Palmini, R.; Bull, K. R.; Cawthorne, E.; Cribbs, A. P.; Crockford, T. L.; Dang, T. S.; Amy Fearn; Fenech, E. J.; de Jong, S. J.; Lagerholm, B. C.; S., C.; Sims, D.; van den Berg, B.; Xu, Y.; Cant, A. J.; Kleiner, G.; Timothy Ronan Leahy; Leahy, T. R.; de la Morena, M. T.; Puck, J. M.; Ralph Shapiro; van der Burg, M.; J. Ross Chapman; Christianson, J. C.; Davies, B.; McGrath, J. J.; McGrath, J. A.; Przyborski, S.; Koref, M. S.; Stuart G. Tangye; Tangye, S. G.; Werner, A.; Rutter, G. A.; Padilla-Parra, S.; Casanova, J.-L.; Cornall, R. J.; Conley, M. E.; Hambleton, S. An Essential Role for the Zn2+ Transporter ZIP7 in B Cell Development. *Nat. Immunol.* **2019**, *20* (3), 350–361. https://doi.org/10.1038/s41590-018-0295-8.

(131) Johanna Ollig; Ollig, J.; Veronika Kloubert; Kloubert, V.; Kathryn M. Taylor; Kathryn Mary Taylor; Taylor, K. M.; Lothar Rink; Rink, L. B Cell Activation and Proliferation Increase Intracellular Zinc Levels. *J. Nutr. Biochem.* **2019**, *64*, 72–79. https://doi.org/10.1016/j.jnutbio.2018.10.008.

(132) Sébastien Küry; Küry, S.; Küry, S.; Brigitte Dréno; Dréno, B.; Stéphane Bézieau; Bézieau, S.; Bézieau, S.; Stéphanie Giraudet; Giraudet, S.; Monia Kharfi; Kharfi, M.; R. Kamoun; Kamoun, R.; Jean-Paul Moisan; Moisan, J.-P. Identification of SLC39A4 , a Gene Involved in Acrodermatitis Enteropathica. *Nat. Genet.* **2002**, *31* (3), 239–240. https://doi.org/10.1038/ng913.

(133) Wang, K.; Zhou, B.; Kuo, Y.-M.; Jason Zemansky; Jane Gitschier. A Novel Member of a Zinc Transporter Family Is Defective in Acrodermatitis Enteropathica. *Am. J. Hum. Genet.* **2002**, *71* (1), 66–73. https://doi.org/10.1086/341125.

(134) E. J. Moynahan. ACRODERMATITIS ENTEROPATHICA: A LETHAL INHERITED HUMAN ZINC-DEFICIENCY DISORDER. *The Lancet* **1974**, *2* (7877), 399–400. https://doi.org/10.1016/s0140-6736(74)91772-3.

(135) Heather N. Yeowell; Sheldon R. Pinnell. The Ehlers-Danlos Syndromes. *Semin. Dermatol.* **1993**, *12* (3), 229–240.

(136) Cecilia Giunta; Elcioglu, N. H.; Albrecht, B.; Eich, G.; Céline Chambaz; Andreas R. Janecke; Heather N. Yeowell; Weis, M.; David R. Eyre; Marius E. Kraenzlin; Steinmann, B. Spondylocheiro Dysplastic Form of the Ehlers-Danlos Syndrome—An Autosomal-Recessive Entity Caused by Mutations in the Zinc Transporter Gene SLC39A13. *Am. J. Hum. Genet.* **2008**, *82* (6), 1290–1305. https://doi.org/10.1016/j.ajhg.2008.05.001.

(137) Toshiyuki Fukada; Civic, N.; Furuichi, T.; Shimoda, S.; Mishima, K.; Higashiyama, H.; Idaira, Y.; Yoshinobu Asada; Hiroshi Kitamura; Satoshi Yamasaki; Shintaro Hojyo; Manabu Nakayama; Osamu Ohara; Haruhiko Koseki; Heloísa G. dos Santos; Luisa Bonafé; Russia Ha-Vinh; Andreas Zankl; Sheila Unger; Unger, S.; Marius E. Kraenzlin; Kraenzlin, M. E.; Jacques S. Beckmann; Saito, I.; Carlo Rivolta; Ikegawa, S.; Andrea Superti-Furga; Hirano, T. The Zinc Transporter SLC39A13/ZIP13 Is Required for Connective Tissue Development; Its Involvement in BMP/TGF-β Signaling Pathways. *PLOS ONE* **2008**, *3* (11). https://doi.org/10.1371/journal.pone.0003642.

(138) Jeong, J.; Eide, D. J. The SLC39 Family of Zinc Transporters. *Mol. Aspects Med.* **2013**, *34* (2), 612–619. https://doi.org/10.1016/j.mam.2012.05.011.

(139) KM Taylor; Kathryn Mary Taylor; Taylor, K. M.; Helen Morgan; Morgan, H. E.; Kathryn Smart; Smart, K.; N. Mohamad Zahari; Zahari, N. M.; Sara Louise Pumford; Pumford, S. L.; Ian O. Ellis; Ellis, I. O.; J. F. R. Robertson; Robertson, J.

F. R.; Robert Ian Nicholson; Nicholson, R. I. The Emerging Role of the LIV-1 Subfamily of Zinc Transporters in Breast Cancer. *Mol. Med.* **2007**, *13* (7), 396–406. https://doi.org/10.2119/2007-00040.taylor.

(140) Vincenza Barresi; Valenti, G.; Giorgia Spampinato; Nicolò Musso; Sergio Castorina; Enrico Rizzarelli; D. F. Condorelli. Transcriptome Analysis Reveals an Altered Expression Profile of Zinc Transporters in Colorectal Cancer. *J. Cell. Biochem.* **2018**, *119* (12), 9707–9719. https://doi.org/10.1002/jcb.27285.

(141) Chen Wu; Li, D.; Li, D. Y.; Jia, W. H.; Hu, Z.; Zhou, Y.; Dianke Yu; Tong Tong; Wang, M.; Wang M; Dong Lin; Lin, D.; Lin, D.; Yan Qiao; Qiao, Y.; Qiao, Y.-L.; Yumin Zhou; Zhou, Y.; Jiang Chang; Yang, U. K.; Jiang Chang; Chang, J.; Zhai, K.; Kan Zhai; Wei, L.; Menghan Wang; Wang, M.; Tan, W.; Lixuan Wei; Shen, H.; Wen Tan; Yi-Xin Zeng; Hongbing Shen; Yi–Xin Zeng; Zeng, Y. X. Genome-Wide Association Study Identifies Common Variants in SLC39A6 Associated with Length of Survival in Esophageal Squamous-Cell Carcinoma. *Nat. Genet.* **2013**, *45* (6), 632–638. https://doi.org/10.1038/ng.2638.

(142) Hui Wen Lue; Xinggang Yang; Yang, X.; Ruoxiang Wang; Weiping Qian; Roy Z H Xu; Robert H. Lyles; Osunkoya, A. O.; Binhua P. Zhou; Zhou, B. P.; Robert L. Vessella; Majd Zayzafoon; Liu, Z.; Zhi Ren Liu; Liu, Z. R.; Haiyen E. Zhau; Chung, L. W. K. LIV-1 Promotes Prostate Cancer Epithelial-to-Mesenchymal Transition and Metastasis through HB-EGF Shedding and EGFR-Mediated ERK Signaling. *PLOS ONE* **2011**, *6* (11). https://doi.org/10.1371/journal.pone.0027720.

(143) Ruinan Shen; Shen, R.; Feng Xie; Xie, F.; Hui Shen; Shen, H.; Qu liu; Liu, Q.; Tao Zheng; Zheng, T.; Xingrui Kou; Kou, X.; De-Xian Wang; Wang, D.; Jiamei Yang; Yang, J. Negative Correlation of LIV-1 and E-Cadherin Expression in Hepatocellular Carcinoma Cells. *PLOS ONE* **2013**, *8* (2). https://doi.org/10.1371/journal.pone.0056542.

(144) Kathryn Mary Taylor; Issa A. Muraina; Brethour, D.; Gerold Schmitt-Ulms; Thirayost Nimmanon; Ziliotto, S.; Peter Kille; Christer Högstrand. Zinc Transporter ZIP10 Forms a Heteromer with ZIP6 Which Regulates Embryonic Development and Cell Migration. *Biochem. J.* **2016**, *473* (16), 2531–2544. https://doi.org/10.1042/bcj20160388.

(145) Nimmanon, T.; Silvia Ziliotto; Ogle, O.; Burt, A. L.; Gee, J. M. W.; Glen K. Andrews; Kille, P.; Christer Högstrand; Maret, W.; Kathryn Mary Taylor. The ZIP6/ZIP10 Heteromer Is Essential for the Zinc-Mediated Trigger of Mitosis. *Cell. Mol. Life Sci.* **2021**, *78* (4). https://doi.org/10.1007/s00018-020-03616-6.

(146) Devendra Pal; Pal, D.; Sharma, U.; Singh, S. K.; Prasad, R.; Prasad, R. Association between ZIP10 Gene Expression and Tumor Aggressiveness in Renal Cell Carcinoma. *Gene* **2014**, *552* (1), 195–198. https://doi.org/10.1016/j.gene.2014.09.010.

(147) Naofumi Kagara; Natsumi Tanaka; Shinzaburo Noguchi; Hirano, T. Zinc and Its Transporter ZIP10 Are Involved in Invasive Behavior of Breast Cancer Cells. *Cancer Sci.* **2007**, *98* (5), 692–697. https://doi.org/10.1111/j.1349-7006.2007.00446.x.

(148) Kathryn Mary Taylor; Petra Vichova; Jordan, N. J.; Hiscox, S. E.; Hendley, R.; Nicholson, R. I. ZIP7-Mediated Intracellular Zinc Transport Contributes to Aberrant Growth Factor Signaling in Antihormone-Resistant Breast Cancer Cells. *Endocrinology* **2008**, *149* (10), 4912–4920. https://doi.org/10.1210/en.2008-0351.

(149) Christer Högstrand; Peter Kille; Robert Ian Nicholson; Kathryn Mary Taylor. Zinc Transporters and Cancer: A Potential Role for ZIP7 as a Hub for Tyrosine Kinase Activation. *Trends Mol. Med.* **2009**, *15* (3), 101–111. https://doi.org/10.1016/j.molmed.2009.01.004.

(150) Min Li; Li, M.; Yuqing Zhang; Zhang, Y.; Uddalak Bharadwaj; Bharadwaj, U.; Qihui Zhai; Zhai, Q.; Zhai, Q. J.; Charlotte H. Ahern; Ahern, C. H.; William E. Fisher; Fisher, W. E.; F. Charles Brunicardi; Brunicardi, F. C.; Craig D. Logsdon; Logsdon, C. D.; Changyi Chen; Chen, C.; Chen, C.; Qizhi Yao; Yao, Q. Down-Regulation of ZIP4 by RNA Interference Inhibits Pancreatic Cancer Growth and Increases the Survival of Nude Mice with Pancreatic Cancer Xenografts. *Clin. Cancer Res.* **2009**, *15* (19), 5993–6001. https://doi.org/10.1158/1078-0432.ccr-09-0557.

(151) Li, M.; Zhang, Y.; Liu, Z.; Chen, C.; Bharadwaj, U.; Wang, H.; Wang, X.; Zhang, S.; Liuzzi, J. P.; Chang, S. M.; Robert J. Cousins; Fisher, W. E.; Brunicardi, F. C.; Logsdon, C. D.; Chen, C.; Yao, Q. Aberrant Expression of Zinc Transporter Zip4 (Slc39a4) Significantly Contributes to Human Pancreatic Cancer Pathogenesis and Progression. *Proc. Natl. Acad. Sci. U. S. A.* **2008**, *104* (47), 18636–18641. https://doi.org/10.1073/pnas.0709307104.

(152) Yuqing Zhang; Changyi Chen; Qizhi Yao; Yao, Q.; Min Li. ZIP4 Upregulates the Expression of Neuropilin-1, Vascular Endothelial Growth Factor, and Matrix Metalloproteases in Pancreatic Cancer Cell Lines and Xenografts. *Cancer Biol. Ther.* **2010**, *9* (3), 236–242. https://doi.org/10.4161/cbt.9.3.10749.

(153) Yuqing Zhang; Uddalak Bharadwaj; Craig D. Logsdon; Changyi Chen; Qizhi Yao; Min Li. ZIP4 Regulates Pancreatic Cancer Cell Growth by Activating IL-6/STAT3 Pathway through Zinc Finger Transcription Factor CREB. *Clin. Cancer Res.* **2010**, *16* (5), 1423–1430. https://doi.org/10.1158/1078-0432.ccr-09-2405.

(154) Yi Lin; Lin, Y.; Yong Chen; Chen, Y.; Yongzhi Wang; Wang, Y.; Jingxuan Yang; Yang, J.; Vivian F. Zhu; Zhu, V. F.; Yu-Lun Liu; Liu, Y.; Xiaobo Cui; Cui, X.; Leon Chen; Chen, L.; Wei Yan; Yan, W.; Tao Jiang; Jiang, T.; Georgene W. Hergenroeder; Hergenroeder, G. W.; Stephen Fletcher; Fletcher, S. A.; Jonathan M. Levine; Levine, J. M.; Dong H. Kim; Kim, D. H.; Nitin Tandon; Tandon, N.; Jay Jiguang Zhu; Zhu, J.-J.; Min Li; Li, M. ZIP4 Is a Novel Molecular Marker for Glioma. *Neuro-Oncol.* **2013**, *15* (8), 1008–1016. https://doi.org/10.1093/neuonc/not042.

(155) Qipeng Fan; Fan, Q.; Qingchun Cai; Cai, Q.; Pengfei Li; Li, P.; Wenyan Wang; Wang, W.; Wenyan Wang; Wang, W.; Jing Wang; Wang, J.; Emily Gerry; Gerry, E.; Tian Li Wang; Wang, T. L.; Ie Ming Shih; Shih, I. M.; Kenneth P. Nephew; Nephew, K. P.; Yan Xu; Xu, Y. The Novel ZIP4 Regulation and Its Role in Ovarian Cancer. *Oncotarget* **2017**, *8* (52), 90090–90107. https://doi.org/10.18632/oncotarget.21435.

(156) Huang, C.; Xiaobo Cui; Xiaotian Sun; Jingxuan Yang; Min Li. Zinc Transporters Are Differentially Expressed in Human Non-Small Cell Lung Cancer. *Oncotarget* **2016**, *7* (41), 66935–66943. https://doi.org/10.18632/oncotarget.11884.

(157) Qi Zeng; Liu, Y.; Liu, J.; Han, J.; Guo, J.; Shun Lü; Xuemei Huang; Yi, P.; Jinyi Lang; Peng Zhang; Zhang, P.; Chunting Wang. Inhibition of ZIP4 Reverses Epithelial-to-Mesenchymal Transition and Enhances the Radiosensitivity in Human Nasopharyngeal Carcinoma Cells. *Cell Death Dis.* **2019**, *10* (8), 588–588. https://doi.org/10.1038/s41419-019-1807-7.

(158) Benjamin P. Weaver; Weaver, B. P.; Yuxia Zhang; Zhang, Y.; Stephen Edward Hiscox; Hiscox, S. E.; Grace L. Guo; Grace L. Guo; Guo, G. L.; Guo, G. L.; Udayan Apte; Apte, U.; KM Taylor; Kathryn Mary Taylor; Taylor, K. M.; Christian T. Sheline; Christian T. Sheline; Sheline, C. T.; Li Wang; Wang, L.; Glen K. Andrews; Andrews, G. K. Zip4 (Slc39a4) Expression Is Activated in Hepatocellular Carcinomas and Functions to Repress Apoptosis, Enhance Cell Cycle and Increase Migration. *PLOS ONE* **2010**, *5* (10). https://doi.org/10.1371/journal.pone.0013158.

(159) Susumu Ishida; Ishida, S.; Atsushi Kasamatsu; Kasamatsu, A.; Yosuke Endo-Sakamoto; Endo-Sakamoto, Y.; Daisuke Nakashima; Nakashima, D.; Nao Koide; Koide, N.; Taro Takahara; Takahara, T.; Toshihiro Shimizu; Shimizu, T.; Manabu Iyoda; Iyoda, M.; Masashi Shiiba; Shiiba, M.; Hideki Tanzawa; Tanzawa, H.; Katsuhiro Uzawa; Uzawa, K. Novel Mechanism of Aberrant ZIP4 Expression with Zinc Supplementation in Oral Tumorigenesis. *Biochem. Biophys. Res. Commun.* **2017**, *483* (1), 339–345. https://doi.org/10.1016/j.bbrc.2016.12.142.

(160) Xiaobo Cui; Yuqing Zhang; Zhang, Y.; Jingxuan Yang; Xiaotian Sun; Sun, X.; John P. Hagan; Hagan, J. P.; Sushovan Guha; Li, M. ZIP4 Confers Resistance to Zinc Deficiency-Induced Apoptosis in Pancreatic Cancer. *Cell Cycle* **2014**, *13* (7), 1180–1186. https://doi.org/10.4161/cc.28111.

(161) Haoyi Jin; Jin, H.; Peng Liu; Liu, P.; Wu, Y.; Yunhao Wu; Wu, Y.; Xiangli Meng; Meng, X.; Mei Wu; Wu, M.; Jiahong Han; Jiahong Han; Han, J.; Tan, X. Exosomal Zinc Transporter ZIP4 Promotes Cancer Growth and Is a Novel Diagnostic Biomarker for Pancreatic Cancer. *Cancer Sci.* **2018**, *109* (9), 2946–2956. https://doi.org/10.1111/cas.13737.

(162) Liping Huang; Kirschke, C. P.; Zhang, Y. Decreased Intracellular Zinc in Human Tumorigenic Prostate Epithelial Cells: A Possible Role in Prostate Cancer Progression. *Cancer Cell Int.* **2006**, *6* (1), 10–10. https://doi.org/10.1186/1475-2867-6-10.

(163) Konstantin Golovine; Robert G. Uzzo; Petr Makhov; Paul L. Crispen; Kunkle, D. A.; Kolenko, V. Depletion of Intracellular Zinc Increases Expression of Tumorigenic Cytokines VEGF, IL-6 and IL-8 in Prostate Cancer Cells via NF-κB Dependent Pathway. *The Prostate* **2008**, *68* (13), 1443–1449. https://doi.org/10.1002/pros.20810.

(164) Leslie A. Johnson; Kanak, M. A.; André Kajdacsy-Balla; Joseph P. Pestaner; Bagasra, O. Differential Zinc Accumulation and Expression of Human Zinc Transporter 1 (hZIP1) in Prostate Glands. *Methods* **2010**, *52* (4), 316–321. https://doi.org/10.1016/j.ymeth.2010.08.004.

(165) Leslie C. Costello; Bernard A. Levy; Mohamed Mokhtar Desouki; Jing Zou; Bagasra, O.; Johnson, L. A.; Hanna, N.; Franklin, R. B. Decreased Zinc and Downregulation of ZIP3 Zinc Uptake Transporter in the Development of Pancreatic Adenocarcinoma. *Cancer Biol. Ther.* **2011**, *12* (4), 297–303. https://doi.org/10.4161/cbt.12.4.16356.

(166) Renty B. Franklin; Jing Zou; Leslie C. Costello. The Cytotoxic Role of RREB1, ZIP3 Zinc Transporter, and Zinc in Human Pancreatic Adenocarcinoma. *Cancer Biol. Ther.* **2014**, *15* (10), 1431–1437. https://doi.org/10.4161/cbt.29927.

(167) Erin Nolin; Sara Gans; Llamas, L.; Somnath Bandyopadhyay; Bandyopadhyay, S.; Brittain, S. M.; Bernasconi-Elias, P.; Carter, K. P.; Loureiro, J.; Thomas, J. R.; Schirle, M.; Yang, Y.; Guo, N.; Roma, G.; Schuierer, S.; Beibel, M.; Lindeman, A.; Sigoillot, F.; Chen, A.; Kevin Xie; Xie, K.; Samuel B. Ho; Ho, S. B.; Ho, S. B.; John S. Reece-Hoyes; Reece-Hoyes, J. S.; Reece-Hoyes, J. S.; W.A. Weihofen; Weihofen, W. A.; Kayla Tyskiewicz; Tyskiewicz, K.; Dominic Hoepfner; Hoepfner, D.; Richard I. McDonald; McDonald, R. I.; Nicolette Guthrie; Guthrie, N.; Abhishek Dogra; Dogra, A.; Haibing Guo; Guo, H.; Jian Shao; Shao, J.; Shao, J.; Jian Ding; Ding, J.; Stephen M. Canham; Stephen M. Canham; Canham, S. M.; Geoffrey M. Boynton; Boynton, G.; Elizabeth George; George, E.; Kang Zhao; Kang, Z. B.; Christophe Antczak; Antczak, C.; Jeffery A. Porter; Porter, J. A.; Owen B. Wallace; Wallace, O.; John A. Tallarico; Tallarico, J. A.; Amy E. Palmer; Palmer, A. E.; Jeremy L. Jenkins; Jenkins, J. L.; Rishi K. Jain; Jain, R. K.; Simon M. Bushell; Simon, B.; Christy J. Fryer; Fryer, C. Discovery of a ZIP7 Inhibitor from a Notch Pathway Screen. *Nat. Chem. Biol.* **2019**, *15* (2), 179–188. https://doi.org/10.1038/s41589-018-0200-7.

(168) Django Sussman; Smith, L. M.; Martha E. Anderson; Steven Duniho; Hunter, J. H.; Kostner, H.; Miyamoto, J. B.; Nesterova, A.; Westendorf, L.; Van Epps, H. A.; Whiting, N.; Benjamin, D. SGN-LIV1A: A Novel Antibody-Drug Conjugate Targeting LIV-1 for the Treatment of Metastatic Breast Cancer. *Mol. Cancer Ther.* **2014**, *13* (12), 2991–3000. https://doi.org/10.1158/1535-7163.mct-13-0896.

(169) La, G.; Eide, D. J. Functional Expression of the Human hZIP2 Zinc Transporter. *J. Biol. Chem.* **2000**, *275* (8), 5560–5564. https://doi.org/10.1074/jbc.275.8.5560.

(170) L. Alex Gaither; Eide, D. J.; Eide, D. J. The Human ZIP1 Transporter Mediates Zinc Uptake in Human K562 Erythroleukemia Cells. *J. Biol. Chem.* **2001**, *276* (25), 22258–22264. https://doi.org/10.1074/jbc.m101772200.

(171) Zhiwei Liu; Hong Li; Soleimani, M.; Girijashanker, K.; Jodie M. Reed; He, L.; Dalton, T. P.; Nebert, D. W. Cd2+ versus Zn2+ Uptake by the ZIP8 HCO3--Dependent Symporter: Kinetics, Electrogenicity and Trafficking. *Biochem. Biophys. Res. Commun.* **2008**, *365* (4), 814–820. https://doi.org/10.1016/j.bbrc.2007.11.067.

(172) Girijashanker, K.; He, L.; Soleimani, M.; Reed, J. M.; Li, H. C.; Hong Li; Zhiwei Liu; Liu, Z.; Wang, B.; Wang, B.; Dalton, T. P.; Nebert, D. W. Slc39a14 Gene Encodes ZIP14, A Metal/Bicarbonate Symporter: Similarities to the ZIP8 Transporter. *Mol. Pharmacol.* **2008**, *73* (5), 1413–1423. https://doi.org/10.1124/mol.107.043588.

(173) Wei Lin; Chai, J.; Love, J. D.; Love, J.; Dax Fu. Selective Electrodiffusion of Zinc Ions in a Zrt-, Irt-like Protein, ZIPB. *J. Biol. Chem.* **2010**, *285* (50), 39013–39020. https://doi.org/10.1074/jbc.m110.180620.

(174) Evan P. Campbell; Ahmed Abdallah Abushawish; Lauren A Valdez; Miriam Bell; Melita Haryono; Padmini Rangamani; Brenda L. Bloodgood. Electrical Signals in the ER Are Cell Type and Stimulus Specific with Extreme Spatial Compartmentalization in Neurons. *Cell Rep.* **2023**, *42* (1), 111943–111943. https://doi.org/10.1016/j.celrep.2022.111943.

(175) Bum-Ho Bin; Fukada, T.; Hosaka, T.; Yamasaki, S.; Wakana Ohashi; Hojyo, S.; Miyai, T.; Nishida, K.; Yokoyama, S.; Hirano, T. Biochemical Characterization of Human ZIP13 Protein: A Homo-Dimerized Zinc Transporter Involved in the Spondylocheiro Dysplastic Ehlers-Danlos Syndrome. *J. Biol. Chem.* **2011**, *286* (46), 40255–40265. https://doi.org/10.1074/jbc.m111.256784.

(176) Liu, Y.; Bafaro, E. M.; Cowan, A. E.; Dempski, R. E. The Transmembrane Domains Mediate Oligomerization of the Human ZIP4 Transporter in Vivo. *Sci Rep*, 2022, *12*, 21083. https://doi.org/10.1038/s41598-022-24782-6.

(177) Changxu Pang; Jinling Chai; Zhu Ping; John Shanklin; Qun Liu. Structural Mechanism of Intracellular Autoregulation of Zinc Uptake in ZIP Transporters. *Nat. Commun.* **2023**, *14* (1). https://doi.org/10.1038/s41467-023-39010-6.

(178) Andrea Pasquadibisceglie; Adriana Leccese; Fabio Polticelli. A Computational Study of the Structure and Function of Human Zrt and Irt-like Proteins Metal Transporters: An Elevator-Type Transport Mechanism Predicted by AlphaFold2. *Front. Chem.* **2022**, *10*. https://doi.org/10.3389/fchem.2022.1004815.

(179) Jodi Dufner-Beattie; S. Joshua Langmade; Wang, F.; Eide, D. J.; Glen K. Andrews. Structure, Function, and Regulation of a Subfamily of Mouse Zinc Transporter Genes. *J. Biol. Chem.* **2003**, *278* (50), 50142–50150. https://doi.org/10.1074/jbc.m304163200.

(180) Shohei Segawa; Makiko Shibamoto; Mikayo Ogawa; Saori Miyake; Kaho Mizumoto; Akihiro Ohishi; Kazuhiro Nishida; Kohei Nagasawa. The Effect of Divalent Metal Cations on Zinc Uptake by Mouse Zrt/Irt-like Protein 1 (ZIP1). *Life Sci.* **2014**, *113* (1), 40–44. https://doi.org/10.1016/j.lfs.2014.07.030.

(181) Marie C. Franz; Pujol-Giménez, J.; Nicolas Montalbetti; Fernandez-Tenorio, M.; DeGrado, T. R.; Niggli, E.; Romero, M. F.; Hediger, M. A. Reassessment of the Transport Mechanism of the Human Zinc Transporter SLC39A2. *Biochemistry* **2018**, *57* (26), 3976–3986. https://doi.org/10.1021/acs.biochem.8b00511.

(182) Jodi Dufner-Beattie; Jodi Dufner-Beattie; Dufner-Beattie, J.; Fudi Wang; Wang, F.; Yien–Ming Kuo; Kuo, Y.-M.; Jane Gitschier; Gitschier, J.; David J. Eide; David Eide; Eide, D. J.; Eide, D. J.; Glen K. Andrews; Glen K. Andrews; Andrews, G. K. The Acrodermatitis Enteropathica Gene ZIP4 Encodes a Tissue-Specific, Zinc-Regulated Zinc Transporter in Mice. *J. Biol. Chem.* **2003**, *278* (35), 33474–33481. https://doi.org/10.1074/jbc.m305000200.

(183) Antala, S.; Dempski, R. E. The Human ZIP4 Transporter Has Two Distinct Binding Affinities and Mediates Transport of Multiple Transition Metals. *Biochemistry* **2012**, *51* (5), 963–973. https://doi.org/10.1021/bi201553p.

(184) Fudi Wang; Wang, F.; Byung-Eun Kim; Kim, B.-E.; Michael J. Petris; Petris, M. J.; David J. Eide; Eide, D. J.; Eide, D. J. The Mammalian Zip5 Protein Is a Zinc Transporter That Localizes to the Basolateral Surface of Polarized Cells. *J. Biol. Chem.* **2004**, *279* (49), 51433–51441. https://doi.org/10.1074/jbc.m408361200.

(185) Marcello Polesel; Ingles-Prieto, A.; Christodoulaki, E.; Ferrada, E.; Cédric Doucerain; Patrick Altermatt; Michelle Knecht; Michael Kuhn; Anna-Lena Steck; Maria Wilhelm; Vania Manolova. Functional Characterization of SLC39 Family Members ZIP5 and ZIP10 in Overexpressing HEK293 Cells Reveals Selective Copper Transport Activity. *Biometals* **2022**. https://doi.org/10.1007/s10534-022-00474-6.

(186) Winyoo Chowanadisai; Bo Lönnerdal; Shannon L. Kelleher. Zip6 (LIV-1) Regulates Zinc Uptake in Neuroblastoma Cells under Resting but Not Depolarizing Conditions. *Brain Res.* **2008**, *1199* (1199), 10–19. https://doi.org/10.1016/j.brainres.2008.01.015.

(187) Kathryn Mary Taylor; Morgan, H. E.; Johnson, A.; Nicholson, R. I. Structure-Function Analysis of HKE4, a Member of the New LIV-1 Subfamily of Zinc

Transporters. *Biochem. J.* **2004**, *377* (1), 131–139. https://doi.org/10.1042/bj20031183.

(188) Grace Woodruff; Christian G. Bouwkamp; Femke M.S. de Vrij; Timothy W. Lovenberg; Pascal Bonaventure; Kushner, S. A.; Anthony Harrington. The Zinc Transporter SLC39A7 (ZIP7) Is Essential for Regulation of Cytosolic Zinc Levels. *Mol. Pharmacol.* **2018**, *94* (3), 1092–1100. https://doi.org/10.1124/mol.118.112557.

(189) Timothy P. Dalton; Dalton, T. P.; Lei He; He, L.; Bin Wang; Wang, B.; Wang, B.; Marian L. Miller; Miller, M. L.; Jin Li; Jin, L.; Keith F. Stringer; Stringer, K. F.; Xiaoqing Chang; Chang, X.; C. Stuart Baxter; Baxter, C. S.; Daniel W. Nebert; Nebert, D. W. Identification of Mouse SLC39A8 as the Transporter Responsible for Cadmium-Induced Toxicity in the Testis. *Proc. Natl. Acad. Sci. U. S. A.* **2005**, *102* (9), 3401–3406. https://doi.org/10.1073/pnas.0406085102.

(190) Lei He; Girijashanker, K.; Dalton, T. P.; Reed, J. M.; Li, H. C.; Hong Li; Soleimani, M.; Daniel W. Nebert. ZIP8, Member of the Solute-Carrier-39 (SLC39) Metal-Transporter Family: Characterization of Transporter Properties. *Mol. Pharmacol.* **2006**, *70* (1), 171–180. https://doi.org/10.1124/mol.106.024521.

(191) Daniel W. Nebert; Marina Gálvez-Peralta; Everett B. Hay; Li, H. C.; Erika Johansson; Yin, C.; Bin Wang; He, L.; Soleimani, M. ZIP14 and ZIP8 Zinc/Bicarbonate Symporters in Xenopus Oocytes: Characterization of Metal Uptake and Inhibition. *Metallomics* **2012**, *4* (11), 1218–1225. https://doi.org/10.1039/c2mt20177a.

(192) Joseph McDermott; Xiangrong Geng; Lan Jiang; Marina Gálvez-Peralta; Fei Chen; Daniel W. Nebert; Zijuan Liu. Zinc- and Bicarbonate-Dependent ZIP8 Transporter Mediates Selenite Uptake. *Oncotarget* **2016**, *7* (23), 35327–35340. https://doi.org/10.18632/oncotarget.9205.

(193) Zhan-Ling Liang; Tan, H. W.; Jia-Yi Wu; Chen, X.-L.; Wang, X.-Y.; Xu, Y.-M.; Andy T. Y. Lau. The Impact of ZIP8 Disease-Associated Variants G38R, C113S, G204C, and S335T on Selenium and Cadmium Accumulations: The First Characterization. *Int. J. Mol. Sci.* **2021**, *22* (21), 11399. https://doi.org/10.3390/ijms222111399.

(194) P. Kaler; Rajendra Prasad. Molecular Cloning and Functional Characterization of Novel Zinc Transporter rZip10 (Slc39a10) Involved in Zinc Uptake across Rat

Renal Brush-Border Membrane. *Am. J. Physiol.-Ren. Physiol.* **2007**, *292* (1). https://doi.org/10.1152/ajprenal.00014.2006.

(195) Greg M. Landry; Eva Furrow; Furrow, E.; Heather L. Holmes; Terumitsu Hirata; Hirata, T.; Kato, A.; Paige Williams; Strohmaier, K.; Christopher J R Gallo; Min Chang; Chang, M.-H.; Pandey, M. K.; Hongde Jiang; Jiang, H.; Aditya Bansal; Bansal, A.; Marie Christine Franz; Montalbetti, N.; Alexander, M. P.; Pablo Cabrero; Julian A. T. Dow; Timothy R. DeGrado; Michael F. Romero; Romero, M. F. Cloning, Function, and Localization of Human, Canine, and Drosophila ZIP10 (SLC39A10), a Zn2+ Transporter. *Am. J. Physiol.-Ren. Physiol.* **2019**, *316* (2). https://doi.org/10.1152/ajprenal.00573.2017.

(196) Winyoo Chowanadisai; David M. Graham; Carl L. Keen; Mark A. Messerli. Neurulation and Neurite Extension Require the Zinc Transporter ZIP12 (Slc39a12). *Proc. Natl. Acad. Sci. U. S. A.* **2013**, *110* (24), 9903–9908. https://doi.org/10.1073/pnas.1222142110.

(197) Xinye Zhu; Chengxuan Yu; Wangshu Wu; Lei Shi; Chuanwen Jiang; Jiang, C.; Li Wang; Zhide Ding; Liu, Y. Zinc Transporter ZIP12 Maintains Zinc Homeostasis and Protects Spermatogonia From Oxidative Stress During Spermatogenesis. *Reprod. Biol. Endocrinol.* **2021**. https://doi.org/10.21203/rs.3.rs-800872/v1.

(198) Elizabeth Scarr; Udawela, M.; Greenough, M.; Jaclyn Neo; Mi Hae Seo; Seo, M. S.; Money, T. T.; Upadhyay, A.; Bush, A. I.; Everall, I. P.; Thomas, E. A.; Dean, B. Increased Cortical Expression of the Zinc Transporter SLC39A12 Suggests a Breakdown in Zinc Cellular Homeostasis as Part of the Pathophysiology of Schizophrenia. *Npj Schizophr.* **2016**, *2* (1), 16002–16002. https://doi.org/10.1038/npjschz.2016.2.

(199) Jeong, J.; Walker, J. M.; Wang, F.; Park, J. G.; Palmer, A. E.; Giunta, C.; Rohrbach, M.; Beat Steinmann; Steinmann, B.; Eide, D. J. Promotion of Vesicular Zinc Efflux by ZIP13 and Its Implications for Spondylocheiro Dysplastic Ehlers–Danlos Syndrome. *Proc. Natl. Acad. Sci. U. S. A.* **2012**, *109* (51), 201211775. https://doi.org/10.1073/pnas.1211775110.

(200) Guiran Xiao; Guiran Xiao; Xiao, G.; Zhaohui Wan; Wan, Z.; Qiangwang Fan; Fan, Q.; Xiaona Tang; Tang, X.; Bing Zhou; Bing Zhou; Zhou, B. The Metal Transporter ZIP13 Supplies Iron into the Secretory Pathway in Drosophila Melanogaster. *eLife* **2014**, *3*. https://doi.org/10.7554/elife.03191.

(201) Kathryn Mary Taylor; Morgan, H. E.; Johnson, A.; Nicholson, R. I. Structure-Function Analysis of a Novel Member of the LIV-1 Subfamily of Zinc Transporters, ZIP14. *FEBS Lett.* **2005**, *579* (2), 427–432. https://doi.org/10.1016/j.febslet.2004.12.006.

(202) Juan P. Liuzzi; Liuzzi, J. P.; Fikret Aydemir; Aydemir, F.; Hyeyoung Nam; Nam, H.; Mitchell D. Knutson; Knutson, M. D.; Robert J. Cousins; Robert J. Cousins; Cousins, R.; Robert J. Cousins; Robert J. Cousins. Zip14 (Slc39a14) Mediates Non-Transferrin-Bound Iron Uptake into Cells. *Proc. Natl. Acad. Sci. U. S. A.* **2006**, *103* (37), 13612–13617. https://doi.org/10.1073/pnas.0606424103.

(203) Jorge J. Pinilla-Tenas; Pinilla-Tenas, J. J.; Brian K. Sparkman; Sparkman, B. K.; Ali Shawki; Shawki, A.; Anthony C Illing; Illing, A. C.; C. J. Mitchell; Mitchell, C. J.; Ningning Zhao; Zhao, N.; Juan P. Liuzzi; Liuzzi, J. P.; Robert J. Cousins; Robert J. Cousins; Cousins, R.; Robert J. Cousins; Robert J. Cousins; Mitchell D. Knutson; Knutson, M. D.; Bryan Mackenzie; Mackenzie, B. Zip14 Is a Complex Broad-Scope Metal-Ion Transporter Whose Functional Properties Support Roles in the Cellular Uptake of Zinc and Nontransferrin-Bound Iron. *Am. J. Physiol.-Cell Physiol.* **2011**, *301* (4). https://doi.org/10.1152/ajpcell.00479.2010.

(204) Raimund Widhalm; Isabella Ellinger; Granitzer, S.; Forsthuber, M.; Bajtela, R.; Gelles, K.; Hartig, P.-Y.; Hengstschläger, M.; Zeisler, H.; Salzer, H.; Gundacker, C. Human Placental Cell Line HTR-8/SVneo Accumulates Cadmium by Divalent Metal Transporters DMT1 and ZIP14. *Metallomics* **2020**, *12* (11), 1822–1833. https://doi.org/10.1039/d0mt00199f.

(205) Masanari Taniguchi; Fukunaka, A.; Hagihara, M.; Watanabe, K.; Kamino, S.; Kambe, T.; Enomoto, S.; Hiromura, M. Essential Role of the Zinc Transporter ZIP9/SLC39A9 in Regulating the Activations of Akt and Erk in B-Cell Receptor Signaling Pathway in DT40 Cells. *PLOS ONE* **2013**, *8* (3). https://doi.org/10.1371/journal.pone.0058022.

(206) Yu, Y.; Wu, A.; Zhuzhen Zhang; Yan, G.; Zhang, F.; Lihong Zhang; Shen, X.; Hu, R.; Zhang, Y.; Keying Zhang; Fudi Wang. Characterization of the GufA Subfamily Member SLC39A11/Zip11 as a Zinc Transporter. *J. Nutr. Biochem.* **2013**, *24* (10), 1697–1708. https://doi.org/10.1016/j.jnutbio.2013.02.010.

(207) Monserrat Olea-Flores; Julia Kan; Alyssa Carlson; Sabriya A. Syed; Cat McCann; Varsha Mondal; Cecily Szady; Heather M. Ricker; Amy McQueen; Juan G. Navea; Leslie A. Caromile; Teresita Padilla-Benavides. ZIP11 Regulates Nuclear Zinc Homeostasis in HeLa Cells and Is Required for Proliferation and Establishment of

the Carcinogenic Phenotype. *Front. Cell Dev. Biol.* **2022**, *10*. https://doi.org/10.3389/fcell.2022.895433.

(208) Elizabeth Y Kim; Odette Verdejo-Torres; Karla Díaz-Rodríguez; Farah Hasanain; Leslie Caromile; Teresita Padilla-Benavides. Single Nucleotide Polymorphisms and Zn Transport by ZIP11 Shape Functional Phenotypes of HeLa Cells. *Metallomics* **2024**. https://doi.org/10.1093/mtomcs/mfae006.

(209) Gregor Grass; Marco D. Wong; Barry P. Rosen; Smith, R. L.; Rensing, C. ZupT Is a Zn(II) Uptake System in Escherichia Coli. *J. Bacteriol.* **2002**, *184* (3), 864–866. https://doi.org/10.1128/jb.184.3.864-866.2002.

(210) Gregor Grass; Grass, G.; Sylvia Franke; Franke, S.; Nadine Taudte; Taudte, N.; Dietrich H. Nies; Nies, D. H.; Lisa M. Kucharski; Kucharski, L. M.; Michael E. Maguire; Maguire, M. E.; Christopher Rensing; Rensing, C. The Metal Permease ZupT from Escherichia Coli Is a Transporter with a Broad Substrate Spectrum. *J. Bacteriol.* **2005**, *187* (5), 1604–1611. https://doi.org/10.1128/jb.187.5.1604-1611.2005.

(211) Taudte, N.; Grass, G. Point Mutations Change Specificity and Kinetics of Metal Uptake by ZupT from Escherichia Coli. *Biometals* **2010**, *23* (4), 643–656. https://doi.org/10.1007/s10534-010-9319-z.

(212) Yulia O. Korshunova; Korshunova, Y. O.; David J. Eide; Eide, D. J.; Eide, D. J.; William G. Clark; Clark, W. G.; Mary Lou Guerinot; Guerinot, M. L.; Himadri B. Pakrasi; Pakrasi, H. B. The IRT1 Protein from Arabidopsis Thaliana Is a Metal Transporter with a Broad Substrate Range. *Plant Mol. Biol.* **1999**, *40* (1), 37–44. https://doi.org/10.1023/a:1026438615520.

(213) Grégory Vert; Vert, G.; Natasha Grotz; Grotz, N.; Fabienne Dédaldéchamp; Dédaldéchamp, F.; Frédéric Gaymard; Gaymard, F.; Mary Lou Guerinot; Guerinot, M. L.; Jean François Briat; Briat, J.-F.; Catherine Curie; Curie, C. IRT1, an Arabidopsis Transporter Essential for Iron Uptake from the Soil and for Plant Growth. *Plant Cell* **2002**, *14* (6), 1223–1233. https://doi.org/10.1105/tpc.001388.

(214) Débora Silva Gomes; Fragoso, L. C.; Riger, C. J.; Panek, A. D.; Eleutherio, E. C. A. Regulation of Cadmium Uptake by Saccharomyces Cerevisiae. *Biochim. Biophys. Acta* **2002**, *1573* (1), 21–25. https://doi.org/10.1016/s0304-4165(02)00324-0.

(215) Rajakumar, S.; Ravi, C.; Nachiappan, V. Defect of Zinc Transporter ZRT1 Ameliorates Cadmium Induced Lipid Accumulation in Saccharomyces Cerevisiae. *Metallomics* **2016**, *8* (4), 453–460. https://doi.org/10.1039/c6mt00005c.

(216) Ting Han; Ting-Wei Tang; Peihong Zhang; Min Liu; Jing Zhao; Jia-Shi Peng; Shuan Meng. Cloning and Functional Characterization of SpZIP2. *Genes* **2022**, *13* (12), 2395–2395. https://doi.org/10.3390/genes13122395.

(217) Byung-Eun Kim; Kim, B.-E.; Fudi Wang; Wang, F.; Jodi Dufner-Beattie; Jodi Dufner-Beattie; Dufner-Beattie, J.; Glen K. Andrews; Andrews, G. K.; David J. Eide; Eide, D. J.; Eide, D. J.; Michael J. Petris; Petris, M. J. Zn2+-Stimulated Endocytosis of the mZIP4 Zinc Transporter Regulates Its Location at the Plasma Membrane. *J. Biol. Chem.* **2004**, *279* (6), 4523–4530. https://doi.org/10.1074/jbc.m310799200.

(218) Fudi Wang; Kim, B.-E.; Jodi Dufner-Beattie; Michael J. Petris; Andrews, G. K.; Eide, D. J. Acrodermatitis Enteropathica Mutations Affect Transport Activity, Localization and Zinc-Responsive Trafficking of the Mouse ZIP4 Zinc Transporter. *Hum. Mol. Genet.* **2004**, *13* (5), 563–571. https://doi.org/10.1093/hmg/ddh049.

(219) Wataru Matsuura; Tomohiro Yamazaki; Yamazaki, T.; Yuko Yamaguchi-Iwai; Masuda, S.; Nagao, M.; Andrews, G. K.; Kambe, T. SLC39A9 (ZIP9) Regulates Zinc Homeostasis in the Secretory Pathway: Characterization of the ZIP Subfamily I Protein in Vertebrate Cells. *Biosci. Biotechnol. Biochem.* **2009**, *73* (5), 1142–1148. https://doi.org/10.1271/bbb.80910.

(220) Tolunay Beker Aydemir; Aydemir, T. B.; Robert J. Cousins; Robert J. Cousins; Cousins, R.; Robert J. Cousins; Robert J. Cousins. The Multiple Faces of the Metal Transporter ZIP14 (SLC39A14). *J. Nutr.* **2018**, *148* (2), 174–184. https://doi.org/10.1093/jn/nxx041.

(221) Christopher Rensing; Bharati Mitra; Barry P. Rosen. The zntA Gene of Escherichia Coli Encodes a Zn(II)-Translocating P-Type ATPase. *Proc. Natl. Acad. Sci. U. S. A.* **1997**, *94* (26), 14326–14331. https://doi.org/10.1073/pnas.94.26.14326.

(222) Steven J. Beard; Rohani Hashim; Jorge Membrillo-Hernández; Martin N. Hughes; Poole, R. K. Zinc(II) Tolerance in Escherichia Coli K-12: Evidence That the zntA Gene (O732) Encodes a Cation Transport ATPase. *Mol. Microbiol.* **1997**, *25* (5), 883–891. https://doi.org/10.1111/j.1365-2958.1997.mmi518.x.

(223) Gregor Grass; Baochao Fan; Fan, B.; Barry P. Rosen; Sylvia Franke; Dietrich H. Nies; Rensing, C. ZitB (YbgR), a Member of the Cation Diffusion Facilitator Family, Is an Additional Zinc Transporter in Escherichia Coli. *J. Bacteriol.* **2001**, *183* (15). https://doi.org/10.1128/jb.183.15.4664-4667.2001.

(224) Silke I. Patzer; Hantke, K. The ZnuABC High-affinity Zinc Uptake System and Its Regulator Zur in Escherichia Coli. *Mol. Microbiol.* **1998**, *28* (6), 1199–1210. https://doi.org/10.1046/j.1365-2958.1998.00883.x.

(225) Shun Tamura; Etsuro Yoshimura. Promotion of Zn 2+ Uptake by Al 3+ in a Saccharomyces Cerevisiae Mutant That Lacks the ZRT1 Gene Encoding a High-Affinity Zn Transporter. *Biol. Trace Elem. Res.* **2008**, *124* (3), 262–268. https://doi.org/10.1007/s12011-008-8145-4.

(226) Linus Pauling. THE PRINCIPLES DETERMINING THE STRUCTURE OF COMPLEX IONIC CRYSTALS. *J. Am. Chem. Soc.* **1929**, *51* (4), 1010–1026. https://doi.org/10.1021/ja01379a006.

(227) Jenny P. Glusker. Structural Aspects of Metal Liganding to Functional Groups in Proteins. *Adv. Protein Chem.* **1991**, *42*, 1–76. https://doi.org/10.1016/s0065-3233(08)60534-3.

(228) Ralph G. Pearson. HARD AND SOFT ACIDS AND BASES. *J. Am. Chem. Soc.* **1963**, *85* (22), 3533–3539. https://doi.org/10.1021/ja00905a001.

(229) Kathryn L. Haas; Katherine J. Franz. Application of Metal Coordination Chemistry to Explore and Manipulate Cell Biology. *Chem. Rev.* **2009**, *109* (10), 4921–4960. https://doi.org/10.1021/cr900134a.

(230) Mikko Laitaoja; Jarkko Valjakka; Jänis, J. Zinc Coordination Spheres in Protein Structures. *Inorg. Chem.* **2013**, *52* (19), 10983–10991. https://doi.org/10.1021/ic401072d.

(231) Béatrice Milon; Milon, B.; Qin Wu; Wu, Q.; Jing Zou; Zou, J.; Leslie C. Costello; Costello, L. C.; Renty B. Franklin; Franklin, R. B. Histidine Residues in the Region between Transmembrane Domains III and IV of hZip1 Are Required for Zinc Transport across the Plasma Membrane in PC-3 Cells. *Biochim. Biophys. Acta* **2006**, *1758* (10), 1696–1701. https://doi.org/10.1016/j.bbamem.2006.06.005.

(232) Marie-Christine Franz; Alexandre Simonin; Graeter, S.; Hediger, M. A.; Gergely Kovács. Development of the First Fluorescence Screening Assay for the

SLC39A2 Zinc Transporter. *J. Biomol. Screen.* **2014**, *19* (6), 909–916. https://doi.org/10.1177/1087057114526781.

(233) Sagar Antala; Ovchinnikov, S.; Kamisetty, H.; Baker, D.; Robert E. Dempski. Computation and Functional Studies Provide a Model for the Structure of the Zinc Transporter hZIP4. *J. Biol. Chem.* **2015**, *290* (29), 17796–17805. https://doi.org/10.1074/jbc.m114.617613.

(234) Sunuwar, L.; Frkatović, A.; Sharapov, S. Zh.; Wang, Q.; Neu, H. M.; Wu, X.; Haritunians, T.; Fengyi Wan; Wan, F.; Michel, S. L. J.; Wu, S.; McGovern, D. P. B.; Lauc, G.; Donowitz, M.; Cynthia L. Sears; Melia, J. Pleiotropic ZIP8 A391T Implicates Abnormal Manganese Homeostasis in Complex Human Disease. *JCI Insight* **2020**, *5* (20). https://doi.org/10.1172/jci.insight.140978.

(235) Mealer, R. G.; Jenkins, B. G.; Chen, C.-Y.; Daly, M. J.; Ge, T.; Lehoux, S.; Marquardt, T.; Palmer, C. D.; Park, J. H.; Parsons, P. J.; Sackstein, R.; Williams, S. E.; Cummings, R. D.; Scolnick, E. M.; Smoller, J. W. The Schizophrenia Risk Locus in SLC39A8 Alters Brain Metal Transport and Plasma Glycosylation. *Sci. Rep.* **2020**, *10* (1), 13162. https://doi.org/10.1038/s41598-020-70108-9.

(236) Su Lin; Lin, S. J.; Valeria C. Culotta; Culotta, V. C. Suppression of Oxidative Damage by Saccharomyces Cerevisiae ATX2, Which Encodes a Manganese-Trafficking Protein That Localizes to Golgi-like Vesicles. *Mol. Cell. Biol.* **1996**, *16* (11), 6303–6312. https://doi.org/10.1128/mcb.16.11.6303.

(237) Kym M. Boycott; Boycott, K. M.; Chandree L. Beaulieu; Beaulieu, C. L.; Kristin D. Kernohan; Kernohan, K. D.; Ola H. Gebril; Gebril, O. H.; Aziz Mhanni; Mhanni, A.; Albert E. Chudley; Chudley, A. E.; David Redl; Redl, D.; Qiuyuan Wen; Qin, W.; Sarah E. Hampson; Hampson, S.; Sébastien Küry; Sébastien Küry; Küry, S.; Küry, S.; Martine Tétreault; Tétreault, M.; Erik G. Puffenberger; Puffenberger, E. G.; James N. Scott; Scott, J. N.; Stéphane Bézieau; Bézieau, S.; André Reis; Reis, A.; Steffen Uebe; Uebe, S.; Johannes Schumacher; Schumacher, J.; Robert A. Hegele; Hegele, R. A.; David McLeod; McLeod, D. R.; Marina Gálvez-Peralta; Gálvez-Peralta, M.; Jacek Majewski; Majewski, J.; Vincent Ramaekers; Ramaekers, V.; Daniel W. Nebert; Nebert, D. W.; A. Micheil Innes; Innes, A. M.; Jillian S. Parboosingh; Parboosingh, J. S.; Rami Abou Jamra; Jamra, R. A. Autosomal-Recessive Intellectual Disability with Cerebellar Atrophy Syndrome Caused by Mutation of the Manganese and Zinc Transporter Gene SLC39A8. *Am. J. Hum. Genet.* **2015**, *97* (6), 886–893. https://doi.org/10.1016/j.ajhg.2015.11.002.

(238) Julien H. Park; Park, J. H.; Max Hogrebe; Hogrebe, M.; Marianne Grüneberg; Grüneberg, M.; Ingrid DuChesne; DuChesne, I.; Ava L. von der Heiden; von der Heiden, A. L.; Janine Reunert; Reunert, J.; Karl Peter Schlingmann; Schlingmann, K. P.; Kym M. Boycott; Boycott, K. M.; Chandree L. Beaulieu; Beaulieu, C. L.; Aziz Mhanni; Mhanni, A.; A. Micheil Innes; Innes, A. M.; Konstanze Hörtnagel; Hörtnagel, K.; Saskia Biskup; Biskup, S.; Eva Gleixner; Gleixner, E. M.; Gerhard Kurlemann; Kurlemann, G.; Barbara Fiedler; Fiedler, B.; Heymut Omran; Omran, H.; Frank Rutsch; Rutsch, F.; Yoshinao Wada; Wada, Y.; Konstantinos Tsiakas; Tsiakas, K.; René Santer; Santer, R.; Daniel W. Nebert; Nebert, D. W.; Stephan Rust; Rust, S.; Thorsten Marquardt; Marquardt, T. SLC39A8 Deficiency: A Disorder of Manganese Transport and Glycosylation. *Am. J. Hum. Genet.* **2015**, *97* (6), 894–903. https://doi.org/10.1016/j.ajhg.2015.11.003.

(239) Eun Kyung Choi; Choi, E. K.; Trang Tiffany Nguyen; Nguyen, T. T.; Neil Gupta; Gupta, N.; Shigeki Iwase; Iwase, S.; Young Ah Seo; Seo, Y. A. Functional Analysis of SLC39A8 Mutations and Their Implications for Manganese Deficiency and Mitochondrial Disorders. *Sci. Rep.* **2018**, *8* (1), 3163–3163. https://doi.org/10.1038/s41598-018-21464-0.

(240) Hitomi Fujishiro; Sara Miyamoto; Daigo Sumi; Taiho Kambe; Himeno, S. Effects of Individual Amino Acid Mutations of Zinc Transporter ZIP8 on Manganese- and Cadmium-Transporting Activity. *Biochem. Biophys. Res. Commun.* **2022**. https://doi.org/10.1016/j.bbrc.2022.05.068.

(241) Mengran Zhao; Zhou, B.; Bing Zhou. A Distinctive Sequence Motif in the Fourth Transmembrane Domain Confers ZIP13 Iron Function in Drosophila Melanogaster. *Biochim. Biophys. Acta* **2020**, *1867* (2), 118607–118607. https://doi.org/10.1016/j.bbamcr.2019.118607.

(242) Karin Tuschl; Esther Meyer; Meyer, E.; Leonardo E Valdivia; Ningning Zhao; Chris Dadswell; Alaa Abdul-Sada; Hung, C. Y.; Simpson, M. A.; Chong, W. K.; Thomas S. Jacques; Randy Woltjer; Woltjer, R. L.; Eaton, S.; Allison Gregory; Gregory, A.; Gregory, A.; Lynn Sanford; Sanford, L.; Eleanna Kara; Kara, E.; Henry Houlden; Houlden, H.; Stephan M. Cuno; Cuno, S. M.; Holger Prokisch; Prokisch, H.; Lorella Valletta; Valletta, L.; Lorella Valletta; Valeria Tiranti; Tiranti, V.; Rasha Younis; Younis, R.; Eamonn R. Maher; Maher, E. R.; John Spencer; Spencer, J.; Ania Straatman-Iwanowska; Straatman-Iwanowska, A.; Paul Gissen; Gissen, P.; Laila Selim; Selim, L. A.; Guillem Pintos-Morell; Pintos-Morell, G.; Wifredo Coroleu-Lletget; Coroleu-Lletget, W.; Shekeeb S. Mohammad; Mohammad, S. S.; Sangeetha Yoganathan; Yoganathan, S.; Russell C. Dale; Dale, R. C.; Maya Thomas; Thomas, M.; Jason Rihel; Rihel, J.; Olaf A. Bodamer; Bodamer, O.;

Caroline A. Enns; Enns, C. A.; Susan J. Hayflick; Hayflick, S. J.; Peter T. Clayton; Clayton, P. E.; Philippa B. Mills; Mills, P. B.; Manju A. Kurian; Kurian, M. A.; Kurian, M. A.; Stephen W. Wilson; Wilson, S. W. Mutations in SLC39A14 Disrupt Manganese Homeostasis and Cause Childhood-Onset Parkinsonism-Dystonia. *Nat. Commun.* **2016**, *7* (1), 11601–11601. https://doi.org/10.1038/ncomms11601.

(243) Gaurav Sharma; Kenneth M. Merz. Formation of the Metal-Binding Core of the ZRT/IRT-like Protein (ZIP) Family Zinc Transporter. *Biochemistry* **2021**, *60* (36), 2727–2738. https://doi.org/10.1021/acs.biochem.1c00415.

(244) Elizabeth E. Rogers; Rogers, E. E.; David J. Eide; Eide, D. J.; Mary Lou Guerinot; Guerinot, M. L. Altered Selectivity in an Arabidopsis Metal Transporter. *Proc. Natl. Acad. Sci. U. S. A.* **2000**, *97* (22), 12356–12360. https://doi.org/10.1073/pnas.210214197.

(245) Kell, D. B.; Swainston, N.; Pir, P.; Oliver, S. G. Membrane Transporter Engineering in Industrial Biotechnology and Whole Cell Biocatalysis. *Trends Biotechnol*, 2015, *33*, 237–246. https://doi.org/10.1016/j.tibtech.2015.02.001.

(246) van der Hoek, S. A.; Borodina, I. Transporter Engineering in Microbial Cell Factories: The Ins, the Outs, and the in-Betweens. *Curr Opin Biotechnol*, 2020, *66*, 186–194. https://doi.org/10.1016/j.copbio.2020.08.002.

(247) Jorgensen, M. E.; Xu, D.; Crocoll, C.; Ernst, H. A.; Ramirez, D.; Motawia, M. S.; Olsen, C. E.; Mirza, O.; Nour-Eldin, H. H.; Halkier, B. A. Origin and Evolution of Transporter Substrate Specificity within the NPF Family. *Elife*, 2017, *6*. https://doi.org/10.7554/eLife.19466.

(248) Clemens, S.; Palmgren, M. G.; Kramer, U. A Long Way Ahead: Understanding and Engineering Plant Metal Accumulation. *Trends Plant Sci*, 2002, *7*, 309–315. https://doi.org/10.1016/s1360-1385(02)02295-1.

(249) Pottier, M.; Oomen, R.; Picco, C.; Giraudat, J.; Scholz-Starke, J.; Richaud, P.; Carpaneto, A.; Thomine, S. Identification of Mutations Allowing Natural Resistance Associated Macrophage Proteins (NRAMP) to Discriminate against Cadmium. *Plant J*, 2015, *83*, 625–637. https://doi.org/10.1111/tpj.12914.

(250) Hoch, E.; Lin, W.; Chai, J.; Hershfinkel, M.; Fu, D.; Sekler, I. Histidine Pairing at the Metal Transport Site of Mammalian ZnT Transporters Controls Zn2+ over Cd2+ Selectivity. *Proc Natl Acad Sci U S A*, 2012, *109*, 7202–7207. https://doi.org/10.1073/pnas.1200362109.

(251) Nishida, S.; Mizuno, T.; Obata, H. Involvement of Histidine-Rich Domain of ZIP Family Transporter TjZNT1 in Metal Ion Specificity. *Plant Physiol Biochem*, 2008, *46*, 601–606. https://doi.org/10.1016/j.plaphy.2008.02.011.

(252) Takagishi, T.; Hara, T.; Fukada, T. Recent Advances in the Role of SLC39A/ZIP Zinc Transporters In Vivo. *Int. J. Mol. Sci.* **2017**, *18* (12), 2708. https://doi.org/10.3390/ijms18122708.

(253) Hu, J. Toward Unzipping the ZIP Metal Transporters: Structure, Evolution, and Implications on Drug Discovery against Cancer. *FEBS J*, 2020. https://doi.org/10.1111/febs.15658.

(254) Kambe, T.; Kathryn Mary Taylor; Taylor, K. M.; Dax Fu; Fu, D. Zinc Transporters and Their Functional Integration in Mammalian Cells. *J. Biol. Chem.* **2021**, *296*, 100320–100320. https://doi.org/10.1016/j.jbc.2021.100320.

(255) Dalton, T. P.; He, L.; Wang, B.; Miller, M. L.; Jin, L.; Stringer, K. F.; Chang, X.; Baxter, C. S.; Nebert, D. W. Identification of Mouse SLC39A8 as the Transporter Responsible for Cadmium-Induced Toxicity in the Testis. *Proc Natl Acad Sci U S A*, 2005, *102*, 3401–3406. https://doi.org/10.1073/pnas.0406085102.

(256) Himeno, S.; Yanagiya, T.; Fujishiro, H. The Role of Zinc Transporters in Cadmium and Manganese Transport in Mammalian Cells. *Biochimie*, 2009, *91*, 1218–1222. https://doi.org/10.1016/j.biochi.2009.04.002.

(257) He, L.; Girijashanker, K.; Dalton, T. P.; Reed, J.; Li, H.; Soleimani, M.; Nebert, D. W. ZIP8, Member of the Solute-Carrier-39 (SLC39) Metal-Transporter Family: Characterization of Transporter Properties. *Mol Pharmacol*, 2006, *70*, 171–180. https://doi.org/10.1124/mol.106.024521.

(258) Jenkitkasemwong, S.; Wang, C. Y.; Mackenzie, B.; Knutson, M. D. Physiologic Implications of Metal-Ion Transport by ZIP14 and ZIP8. *Biometals*, 2012, *25*, 643–655. https://doi.org/10.1007/s10534-012-9526-x.

(259) Boycott, K. M.; Beaulieu, C. L.; Kernohan, K. D.; Gebril, O. H.; Mhanni, A.; Chudley, A. E.; Redl, D.; Qin, W.; Hampson, S.; Kury, S.; Tetreault, M.; Puffenberger, E. G.; Scott, J. N.; Bezieau, S.; Reis, A.; Uebe, S.; Schumacher, J.; Hegele, R. A.; McLeod, D. R.; Galvez-Peralta, M.; Majewski, J.; Ramaekers, V. T.; Care4Rare Canada, C.; Nebert, D. W.; Innes, A. M.; Parboosingh, J. S.; Abou Jamra, R. Autosomal-Recessive Intellectual Disability with Cerebellar Atrophy Syndrome Caused by Mutation of the Manganese and Zinc Transporter Gene

SLC39A8. *Am J Hum Genet*, 2015, *97*, 886–893. https://doi.org/10.1016/j.ajhg.2015.11.002.

(260) Choi, E. K.; Nguyen, T. T.; Gupta, N.; Iwase, S.; Seo, Y. A. Functional Analysis of SLC39A8 Mutations and Their Implications for Manganese Deficiency and Mitochondrial Disorders. *Sci Rep*, 2018, *8*, 3163. https://doi.org/10.1038/s41598-018-21464-0.

(261) Daniel W. Nebert; Nebert, D. W.; Zijuan Liu; Liu, Z. SLC39A8 Gene Encoding a Metal Ion Transporter: Discovery and Bench to Bedside. *Hum. Genomics* **2019**, *13* (1), 1–21. https://doi.org/10.1186/s40246-019-0233-3.

(262) Jenkitkasemwong, S.; Akinyode, A.; Paulus, E.; Weiskirchen, R.; Hojyo, S.; Fukada, T.; Giraldo, G.; Schrier, J.; Garcia, A.; Janus, C.; Giasson, B.; Knutson, M. D. SLC39A14 Deficiency Alters Manganese Homeostasis and Excretion Resulting in Brain Manganese Accumulation and Motor Deficits in Mice. *Proc Natl Acad Sci U S A*, 2018, *115*, E1769–E1778. https://doi.org/10.1073/pnas.1720739115.

(263) McCabe, S.; Limesand, K.; Zhao, N. Recent Progress toward Understanding the Role of ZIP14 in Regulating Systemic Manganese Homeostasis. *Comput Struct Biotechnol J*, 2023, *21*, 2332–2338. https://doi.org/10.1016/j.csbj.2023.03.039.

(264) Aydemir, T. B.; Cousins, R. J. The Multiple Faces of the Metal Transporter ZIP14 (SLC39A14). *J Nutr*, 2018, *148*, 174–184. https://doi.org/10.1093/jn/nxx041.

(265) Korshunova, Y. O.; Eide, D.; Clark, W. G.; Guerinot, M. L.; Pakrasi, H. B. The IRT1 Protein from Arabidopsis Thaliana Is a Metal Transporter with a Broad Substrate Range. *Plant Mol Biol*, 1999, *40*, 37–44. https://doi.org/10.1023/a:1026438615520.

(266) Connolly, E. L.; Fett, J. P.; Guerinot, M. L. Expression of the IRT1 Metal Transporter Is Controlled by Metals at the Levels of Transcript and Protein Accumulation. *Plant Cell*, 2002, *14*, 1347–1357. https://doi.org/10.1105/tpc.001263.

(267) Dufner-Beattie, J.; Wang, F.; Kuo, Y. M.; Gitschier, J.; Eide, D.; Andrews, G. K. The Acrodermatitis Enteropathica Gene ZIP4 Encodes a Tissue-Specific, Zinc-Regulated Zinc Transporter in Mice. *J Biol Chem*, 2003, *278*, 33474–33481. https://doi.org/10.1074/jbc.M305000200.

(268) Kuliyev, E.; Zhang, C.; Sui, D.; Hu, J. Zinc Transporter Mutations Linked to Acrodermatitis Enteropathica Disrupt Function and Cause Mistrafficking. *J Biol Chem*, 2021, *296*, 100269. https://doi.org/10.1016/j.jbc.2021.100269.

(269) Franklin, R. B.; Ma, J.; Zou, J.; Guan, Z.; Kukoyi, B. I.; Feng, P.; Costello, L. C. Human ZIP1 Is a Major Zinc Uptake Transporter for the Accumulation of Zinc in Prostate Cells. *J Inorg Biochem*, 2003, *96*, 435–442. https://doi.org/10.1016/s0162-0134(03)00249-6.

(270) Lane, A.; Gokhale, A.; Werner, E.; Roberts, A.; Freeman, A.; Roberts, B.; Faundez, V. Sulfur- and Phosphorus-Standardized Metal Quantification of Biological Specimens Using Inductively Coupled Plasma Mass Spectrometry. *STAR Protoc*, 2022, *3*, 101334. https://doi.org/10.1016/j.xpro.2022.101334.

(271) Case, D. A.; Aktulga, H. M.; Belfon, K.; Ben-Shalom, I. Y.; Brozell, S. R.; Cerutti, D. S.; Cheatham, T. E.; Cruzeiro, I., V. W. D.; Darden, T. A.; Duke, R. E.; Giambasu, G.; Gilson, M. K.; Gohlke, H.; Goetz, A. W.; Harris, R.; Izadi, S.; Izmailov, S. A.; Jin, C.; Kasavajhala, K.; Kaymak, M. C.; King, E.; Kovalenko, A.; Kurtzman, T.; Lee, T. S.; LeGrand, S.; Li, P.; Lin, C.; Liu, J.; Luchko, T.; Luo, R.; Machado, M.; Man, V.; Manathunga, M.; Merz, K. M.; Miao, Y.; Mikhailovskii, O.; Monard, G.; Nguyen, H.; O'Hearn, K. A.; Onufriev, A.; Pan, F.; Pantano, S.; Qi, R.; Rahnamoun, A.; Roe, D. R.; Roitberg, A.; Sagui, C.; Schott-Verdugo, S.; Shen, J.; Simmerling, C. L.; Skrynnikov, N. R.; Smith, J.; Swails, J.; Walker, R. C.; Wang, J.; Wei, H.; Wolf, R. M.; Wu, X.; Xue, Y.; York, D. M.; Zhao, S.; Kollman, P. A. Amber 2020. *University of California: San Francisco.*, 2020.

(272) Jo, S.; Kim, T.; Iyer, V. G.; Im, W. CHARMM-GUI: A Web-Based Graphical User Interface for CHARMM. *J Comput Chem*, 2008, *29*, 1859–1865. https://doi.org/10.1002/jcc.20945.

(273) Loncharich, R. J.; Brooks, B. R.; Pastor, R. W. Langevin Dynamics of Peptides: The Frictional Dependence of Isomerization Rates of N-Acetylalanyl-N'-Methylamide. *Biopolymers*, 1992, *32*, 523–535. https://doi.org/10.1002/bip.360320508.

(274) Berendsen, H. J. C.; Postma, J. P. M.; Vangunsteren, W. F.; Dinola, A.; Haak, J. R. Molecular-Dynamics with Coupling to an External Bath. *Journal of Chemical Physics*, 1984, *81*, 3684–3690. https://doi.org/Doi 10.1063/1.448118.

(275) Miyamoto, S.; Kollman, P. A. Settle - an Analytical Version of the Shake and Rattle Algorithm for Rigid Water Models. *Journal of Computational Chemistry*, 1992, *13*, 952–962. https://doi.org/DOI 10.1002/jcc.540130805.

(276) Sengupta, A.; Seitz, A.; Merz, K. M. Simulating the Chelate Effect. *Journal of the American Chemical Society*, 2018, *140*, 15166–15169. https://doi.org/10.1021/jacs.8b09371.

(277) Pezza, J. A.; Choi, K. H.; Berardini, T. Z.; Beernink, P. T.; Allen, K. N.; Tolan, D. R. Spatial Clustering of Isozyme-Specific Residues Reveals Unlikely Determinants of Isozyme Specificity in Fructose-1,6-Bisphosphate Aldolase. *J Biol Chem*, 2003, *278*, 17307–17313. https://doi.org/10.1074/jbc.M209185200.

(278) Rago, F.; Saltzberg, D.; Allen, K. N.; Tolan, D. R. Enzyme Substrate Specificity Conferred by Distinct Conformational Pathways. *J Am Chem Soc*, 2015, *137*, 13876–13886. https://doi.org/10.1021/jacs.5b08149.

(279) Cimpean, A.; Stefan, C.; Gijsbers, R.; Stalmans, W.; Bollen, M. Substrate-Specifying Determinants of the Nucleotide Pyrophosphatases/Phosphodiesterases NPP1 and NPP2. *Biochem J*, 2004, *381*, 71–77. https://doi.org/10.1042/BJ20040465.

(280) Chun, H.; Tamara Korolnek; Korolnek, T.; Tamara Korolnek; Lee, C.-J.; Coyne, H. J.; Winge, D. R.; Kim, B.-E.; Petris, M. J. An Extracellular Histidine-Containing Motif in the Zinc Transporter ZIP4 Plays a Role in Zinc Sensing and Zinc-Induced Endocytosis in Mammalian Cells. *J. Biol. Chem.* **2019**, *294* (8), 2815–2826. https://doi.org/10.1074/jbc.ra118.005203.

(281) Hoch, E.; Levy, M.; Hershfinkel, M.; Sekler, I. Elucidating the H(+) Coupled Zn(2+) Transport Mechanism of ZIP4; Implications in Acrodermatitis Enteropathica. *Int J Mol Sci*, 2020, *21*. https://doi.org/10.3390/ijms21030734.

(282) Linscott, J. A.; Kapilashrami, K.; Wang, Z.; Senevirathne, C.; Bothwell, I. R.; Blum, G.; Luo, M. Kinetic Isotope Effects Reveal Early Transition State of Protein Lysine Methyltransferase SET8. *Proc Natl Acad Sci U S A*, 2016, *113*, E8369–E8378. https://doi.org/10.1073/pnas.1609032114.

(283) Antala, S.; Ovchinnikov, S.; Kamisetty, H.; Baker, D.; Dempski, R. E. Computation and Functional Studies Provide a Model for the Structure of the Zinc Transporter hZIP4. *J Biol Chem*, 2015, *290*, 17796–17805. https://doi.org/10.1074/jbc.M114.617613.

(284) Lin, W.; Chai, J.; Love, J.; Fu, D. Selective Electrodiffusion of Zinc Ions in a Zrt-, Irt-like Protein, ZIPB. *J Biol Chem*, 2010, *285*, 39013–39020. https://doi.org/10.1074/jbc.M110.180620.

(285) Mezei, M. The Finite-Difference Thermodynamic Integration, Tested on Calculating the Hydration Free-Energy Difference between Acetone and Dimethylamine in Water. *Journal of Chemical Physics*, 1987, *86*, 7084–7088. https://doi.org/Doi 10.1063/1.452357.

(286) Straatsma, T. P.; Berendsen, H. J. C. Free-Energy of Ionic Hydration - Analysis of a Thermodynamic Integration Technique to Evaluate Free-Energy Differences by Molecular-Dynamics Simulations. *Journal of Chemical Physics*, 1988, *89*, 5876–5886. https://doi.org/Doi 10.1063/1.455539.

(287) Mitchell, M. J.; Mccammon, J. A. Free-Energy Difference Calculations by Thermodynamic Integration - Difficulties in Obtaining a Precise Value. *Journal of Computational Chemistry*, 1991, *12*, 271–275. https://doi.org/DOI 10.1002/jcc.540120218.

(288) Kollman, P. Free-Energy Calculations - Applications to Chemical and Biochemical Phenomena. *Chemical Reviews*, 1993, *93*, 2395–2417. https://doi.org/DOI 10.1021/cr00023a004.

(289) Beutler, T. C.; Mark, A. E.; Vanschaik, R. C.; Gerber, P. R.; Vangunsteren, W. F. Avoiding Singularities and Numerical Instabilities in Free-Energy Calculations Based on Molecular Simulations. *Chemical Physics Letters*, 1994, *222*, 529–539. https://doi.org/Doi 10.1016/0009-2614(94)00397-1.

(290) Hummer, G.; Szabo, A. Calculation of Free-Energy Differences from Computer Simulations of Initial and Final States. *Journal of Chemical Physics*, 1996, *105*, 2004–2010. https://doi.org/Doi 10.1063/1.472068.

(291) Simonson, T.; Carlsson, J.; Case, D. A. Proton Binding to Proteins: pK(a) Calculations with Explicit and Implicit Solvent Models. *Journal of the American Chemical Society*, 2004, *126*, 4167–4180. https://doi.org/10.1021/ja039788m.

(292) Domingo, J.; Baeza-Centurion, P.; Lehner, B. The Causes and Consequences of Genetic Interactions (Epistasis). *Annu Rev Genomics Hum Genet*, 2019, *20*, 433–460. https://doi.org/10.1146/annurev-genom-083118-014857.

(293) Diallinas, G. Transporter Specificity: A Tale of Loosened Elevator-Sliding. *Trends Biochem Sci*, 2021, *46*, 708–717. https://doi.org/10.1016/j.tibs.2021.03.007.

(294) Qureshi, A. A.; Suades, A.; Matsuoka, R.; Brock, J.; McComas, S. E.; Nji, E.; Orellana, L.; Claesson, M.; Delemotte, L.; Drew, D. The Molecular Basis for Sugar Import in Malaria Parasites. *Nature*, 2020, *578*, 321–325. https://doi.org/10.1038/s41586-020-1963-z.

(295) Krezel, A.; Maret, W. The Biological Inorganic Chemistry of Zinc Ions. *Arch Biochem Biophys*, 2016, *611*, 3–19. https://doi.org/10.1016/j.abb.2016.04.010.

(296) Hirano, T.; Murakami, M.; Fukada, T.; Nishida, K.; Yamasaki, S.; Suzuki, T. Roles of Zinc and Zinc Signaling in Immunity: Zinc as an Intracellular Signaling Molecule. *Adv Immunol*, 2008, *97*, 149–176. https://doi.org/10.1016/S0065-2776(08)00003-5.

(297) Myers, S. A. Zinc Transporters and Zinc Signaling: New Insights into Their Role in Type 2 Diabetes. *Int J Endocrinol*, 2015, *2015*, 167503. https://doi.org/10.1155/2015/167503.

(298) Fukada, T.; Yamasaki, S.; Nishida, K.; Murakami, M.; Hirano, T. Zinc Homeostasis and Signaling in Health and Diseases: Zinc Signaling. *J Biol Inorg Chem*, 2011, *16*, 1123–1134. https://doi.org/10.1007/s00775-011-0797-4.

(299) Kim, A. M.; Vogt, S.; O'Halloran, T. V.; Woodruff, T. K. Zinc Availability Regulates Exit from Meiosis in Maturing Mammalian Oocytes. *Nat Chem Biol*, 2010, *6*, 674–681. https://doi.org/10.1038/nchembio.419.

(300) Kim, A. M.; Bernhardt, M. L.; Kong, B. Y.; Ahn, R. W.; Vogt, S.; Woodruff, T. K.; O'Halloran, T. V. Zinc Sparks Are Triggered by Fertilization and Facilitate Cell Cycle Resumption in Mammalian Eggs. *ACS Chem Biol*, 2011, *6*, 716–723. https://doi.org/10.1021/cb200084y.

(301) Bernhardt, M. L.; Kong, B. Y.; Kim, A. M.; O'Halloran, T. V.; Woodruff, T. K. A Zinc-Dependent Mechanism Regulates Meiotic Progression in Mammalian Oocytes. *Biol Reprod*, 2012, *86*, 114. https://doi.org/10.1095/biolreprod.111.097253.

(302) Kong, B. Y.; Duncan, F. E.; Que, E. L.; Kim, A. M.; O'Halloran, T. V.; Woodruff, T. K. Maternally-Derived Zinc Transporters ZIP6 and ZIP10 Drive the Mammalian

Oocyte-to-Egg Transition. *Mol Hum Reprod*, 2014, *20*, 1077–1089. https://doi.org/10.1093/molehr/gau066.

(303) Seeler, J. F.; Sharma, A.; Zaluzec, N. J.; Bleher, R.; Lai, B.; Schultz, E. G.; Hoffman, B. M.; LaBonne, C.; Woodruff, T. K.; O'Halloran, T. V. Metal Ion Fluxes Controlling Amphibian Fertilization. *Nat Chem*, 2021, *13*, 683–691. https://doi.org/10.1038/s41557-021-00705-2.

(304) Mendoza, A. D.; Sue, A.; Antipova, O.; Vogt, S.; Woodruff, T. K.; Wignall, S. M.; O'Halloran, T. V. Dynamic Zinc Fluxes Regulate Meiotic Progression in Caenorhabditis Elegansdagger. *Biol Reprod*, 2022, *107*, 406–418. https://doi.org/10.1093/biolre/ioac064.

(305) Lo, M. N.; Damon, L. J.; Wei Tay, J.; Jia, S.; Palmer, A. E. Single Cell Analysis Reveals Multiple Requirements for Zinc in the Mammalian Cell Cycle. *Elife*, 2020, *9*. https://doi.org/10.7554/eLife.51107.

(306) Rakshit, A.; Holtzen, S. E.; Lo, M. N.; Conway, K. A.; Palmer, A. E. Human Cells Experience a Zn(2+) Pulse in Early G1. *Cell Rep*, 2023, *42*, 112656. https://doi.org/10.1016/j.celrep.2023.112656.

(307) Xu, Z.; Zhou, J. Zinc and Myocardial Ischemia/Reperfusion Injury. *Biometals*, 2013, *26*, 863–878. https://doi.org/10.1007/s10534-013-9671-x.

(308) Hojyo, S.; Fukada, T. Roles of Zinc Signaling in the Immune System. *J Immunol Res*, 2016, *2016*, 6762343. https://doi.org/10.1155/2016/6762343.

(309) Portbury, S. D.; Adlard, P. A. Zinc Signal in Brain Diseases. *Int J Mol Sci*, 2017, *18*. https://doi.org/10.3390/ijms18122506.

(310) Chakraborty, M.; Hershfinkel, M. Zinc Signaling in the Mammary Gland: For Better and for Worse. *Biomedicines*, 2021, *9*. https://doi.org/10.3390/biomedicines9091204.

(311) Allouche-Fitoussi, D.; Breitbart, H. The Role of Zinc in Male Fertility. *Int J Mol Sci*, 2020, *21*. https://doi.org/10.3390/ijms21207796.

(312) Foresta, C.; Garolla, A.; Cosci, I.; Menegazzo, M.; Ferigo, M.; Gandin, V.; De Toni, L. Role of Zinc Trafficking in Male Fertility: From Germ to Sperm. *Hum Reprod*, 2014, *29*, 1134–1145. https://doi.org/10.1093/humrep/deu075.

(313) Chen, Y. Y.; Chen, S.; Ok, K.; Duncan, F. E.; O'Halloran, T. V.; Woodruff, T. K. Zinc Dynamics Regulate Early Ovarian Follicle Development. *J Biol Chem*, 2023, *299*, 102731. https://doi.org/10.1016/j.jbc.2022.102731.

(314) Eide, D. J. Transcription Factors and Transporters in Zinc Homeostasis: Lessons Learned from Fungi. *Crit Rev Biochem Mol Biol*, 2020, *55*, 88–110. https://doi.org/10.1080/10409238.2020.1742092.

(315) Küry, S.; Dréno, B.; Bézieau, S.; Giraudet, S.; Kharfi, M.; Kamoun, R.; Moisan, J. P. Identification of SLC39A4, a Gene Involved in Acrodermatitis Enteropathica. *Nat Genet*, 2002, *31*, 239–240. https://doi.org/10.1038/ng913.

(316) Li, M.; Zhang, Y.; Bharadwaj, U.; Zhai, Q. J.; Ahern, C. H.; Fisher, W. E.; Brunicardi, F. C.; Logsdon, C. D.; Chen, C.; Yao, Q. Down-Regulation of ZIP4 by RNA Interference Inhibits Pancreatic Cancer Growth and Increases the Survival of Nude Mice with Pancreatic Cancer Xenografts. *Clin Cancer Res*, 2009, *15*, 5993–6001. https://doi.org/10.1158/1078-0432.CCR-09-0557.

(317) Chen, Q. G.; Zhang, Z.; Yang, Q.; Shan, G. Y.; Yu, X. Y.; Kong, C. Z. The Role of Zinc Transporter ZIP4 in Prostate Carcinoma. *Urol Oncol*, 2012, *30*, 906–911. https://doi.org/10.1016/j.urolonc.2010.11.010.

(318) Lin, Y.; Chen, Y.; Wang, Y.; Yang, J.; Zhu, V. F.; Liu, Y.; Cui, X.; Chen, L.; Yan, W.; Jiang, T.; Hergenroeder, G. W.; Fletcher, S. A.; Levine, J. M.; Kim, D. H.; Tandon, N.; Zhu, J. J.; Li, M. ZIP4 Is a Novel Molecular Marker for Glioma. *Neuro Oncol*, 2013, *15*, 1008–1016. https://doi.org/10.1093/neuonc/not042.

(319) Fan, Q.; Cai, Q.; Li, P.; Wang, W.; Wang, J.; Gerry, E.; Wang, T. L.; Shih, I. M.; Nephew, K. P.; Xu, Y. The Novel ZIP4 Regulation and Its Role in Ovarian Cancer. *Oncotarget*, 2017, *8*, 90090–90107. https://doi.org/10.18632/oncotarget.21435.

(320) Ishida, S.; Kasamatsu, A.; Endo-Sakamoto, Y.; Nakashima, D.; Koide, N.; Takahara, T.; Shimizu, T.; Iyoda, M.; Shiiba, M.; Tanzawa, H.; Uzawa, K. Novel Mechanism of Aberrant ZIP4 Expression with Zinc Supplementation in Oral Tumorigenesis. *Biochem Biophys Res Commun*, 2017, *483*, 339–345. https://doi.org/10.1016/j.bbrc.2016.12.142.

(321) Fan, Q.; Zhang, W.; Emerson, R. E.; Xu, Y. ZIP4 Is a Novel Cancer Stem Cell Marker in High-Grade Serous Ovarian Cancer. *Cancers (Basel)*, 2020, *12*. https://doi.org/10.3390/cancers12123692.

(322) Zhu, B.; Huo, R.; Zhi, Q.; Zhan, M.; Chen, X.; Hua, Z. C. Increased Expression of Zinc Transporter ZIP4, ZIP11, ZnT1, and ZnT6 Predicts Poor Prognosis in Pancreatic Cancer. *J Trace Elem Med Biol*, 2021, *65*, 126734. https://doi.org/10.1016/j.jtemb.2021.126734.

(323) Ma, C.; Gong, C. Expression, Purification and Characterization of a ZIP Family Transporter from Desulfovibrio Vulgaris. *Protein J*, 2021, *40*, 776–785. https://doi.org/10.1007/s10930-021-10008-7.

(324) Grass, G.; Franke, S.; Taudte, N.; Nies, D. H.; Kucharski, L. M.; Maguire, M. E.; Rensing, C. The Metal Permease ZupT from Escherichia Coli Is a Transporter with a Broad Substrate Spectrum. *J Bacteriol*, 2005, *187*, 1604–1611. https://doi.org/10.1128/JB.187.5.1604-1611.2005.

(325) Merriman, C.; Huang, Q.; Rutter, G. A.; Fu, D. Lipid-Tuned Zinc Transport Activity of Human ZnT8 Protein Correlates with Risk for Type-2 Diabetes. *J Biol Chem*, 2016, *291*, 26950–26957. https://doi.org/10.1074/jbc.M116.764605.

(326) Gaither, L. A.; Eide, D. J. The Human ZIP1 Transporter Mediates Zinc Uptake in Human K562 Erythroleukemia Cells. *J Biol Chem*, 2001, *276*, 22258–22264. https://doi.org/10.1074/jbc.M101772200.

(327) Jiang, Y.; Li, Z.; Sui, D.; Sharma, G.; Wang, T.; MacRenaris, K.; Takahashi, H.; Merz, K.; Hu, J. Rational Engineering of an Elevator-Type Metal Transporter ZIP8 Reveals a Conditional Selectivity Filter Critically Involved in Determining Substrate Specificity. *Commun Biol*, 2023, *6*, 778. https://doi.org/10.1038/s42003-023-05146-w.

(328) Richardson, C. E. R.; Nolan, E. M.; Shoulders, M. D.; Lippard, S. J. A Sensitive, Nonradioactive Assay for Zn(II) Uptake into Metazoan Cells. *Biochemistry*, 2018, *57*, 6807–6815. https://doi.org/10.1021/acs.biochem.8b01043.

(329) Richardson, C. E. R.; Cunden, L. S.; Butty, V. L.; Nolan, E. M.; Lippard, S. J.; Shoulders, M. D. A Method for Selective Depletion of Zn(II) Ions from Complex Biological Media and Evaluation of Cellular Consequences of Zn(II) Deficiency. *J Am Chem Soc*, 2018, *140*, 2413–2416. https://doi.org/10.1021/jacs.7b12897.

(330) Cho, Y. E.; Lomeda, R. A.; Ryu, S. H.; Lee, J. H.; Beattie, J. H.; Kwun, I. S. Cellular Zn Depletion by Metal Ion Chelators (TPEN, DTPA and Chelex Resin) and Its Application to Osteoblastic MC3T3-E1 Cells. *Nutr Res Pract*, 2007, *1*, 29–35. https://doi.org/10.4162/nrp.2007.1.1.29.

(331) Suhy, D. A.; Simon, K. D.; Linzer, D. I.; O'Halloran, T. V. Metallothionein Is Part of a Zinc-Scavenging Mechanism for Cell Survival under Conditions of Extreme Zinc Deprivation. *J Biol Chem*, 1999, *274*, 9183–9192. https://doi.org/10.1074/jbc.274.14.9183.

(332) Elia, G. Biotinylation Reagents for the Study of Cell Surface Proteins. *Proteomics*, 2008, *8*, 4012–4024. https://doi.org/10.1002/pmic.200800097.

(333) Maryon, E. B.; Molloy, S. A.; Ivy, K.; Yu, H.; Kaplan, J. H. Rate and Regulation of Copper Transport by Human Copper Transporter 1 (hCTR1). *J Biol Chem*, 2013, *288*, 18035–18046. https://doi.org/10.1074/jbc.M112.442426.

(334) Zhuang, H.; Matsunami, H. Evaluating Cell-Surface Expression and Measuring Activation of Mammalian Odorant Receptors in Heterologous Cells. *Nat Protoc*, 2008, *3*, 1402–1413. https://doi.org/10.1038/nprot.2008.120.

(335) Mao, X.; Kim, B. E.; Wang, F.; Eide, D. J.; Petris, M. J. A Histidine-Rich Cluster Mediates the Ubiquitination and Degradation of the Human Zinc Transporter, hZIP4, and Protects against Zinc Cytotoxicity. *J Biol Chem*, 2007, *282*, 6992–7000. https://doi.org/10.1074/jbc.M610552200.

(336) Schilling, K.; Harris, A. L.; Halliday, A. N.; Schofield, C. J.; Sheldon, H.; Haider, S.; Larner, F. Investigations on Zinc Isotope Fractionation in Breast Cancer Tissue Using in Vitro Cell Culture Uptake-Efflux Experiments. *Front Med (Lausanne)*, 2021, *8*, 746532. https://doi.org/10.3389/fmed.2021.746532.

(337) Guo, Y.; Smith, K.; Lee, J.; Thiele, D. J.; Petris, M. J. Identification of Methionine-Rich Clusters That Regulate Copper-Stimulated Endocytosis of the Human Ctr1 Copper Transporter. *J Biol Chem*, 2004, *279*, 17428–17433. https://doi.org/10.1074/jbc.M401493200.

(338) Zhang, X.; Wright, S. H. Transport Turnover Rates for Human OCT2 and MATE1 Expressed in Chinese Hamster Ovary Cells. *Int J Mol Sci*, 2022, *23*. https://doi.org/10.3390/ijms23031472.

(339) Peter, D.; Jimenez, J.; Liu, Y.; Kim, J.; Edwards, R. H. The Chromaffin Granule and Synaptic Vesicle Amine Transporters Differ in Substrate Recognition and Sensitivity to Inhibitors. *J Biol Chem*, 1994, *269*, 7231–7237.

(340) Yin, J.; Duan, H.; Shirasaka, Y.; Prasad, B.; Wang, J. Atenolol Renal Secretion Is Mediated by Human Organic Cation Transporter 2 and Multidrug and Toxin

Extrusion Proteins. *Drug Metab Dispos*, 2015, *43*, 1872–1881. https://doi.org/10.1124/dmd.115.066175.

(341) Gu, H.; Wall, S. C.; Rudnick, G. Stable Expression of Biogenic Amine Transporters Reveals Differences in Inhibitor Sensitivity, Kinetics, and Ion Dependence. *J Biol Chem*, 1994, *269*, 7124–7130.

(342) Trinco, G.; Arkhipova, V.; Garaeva, A. A.; Hutter, C. A. J.; Seeger, M. A.; Guskov, A.; Slotboom, D. J. Kinetic Mechanism of Na(+)-Coupled Aspartate Transport Catalyzed by Glt(Tk). *Commun Biol*, 2021, *4*, 751. https://doi.org/10.1038/s42003-021-02267-y.

(343) Gadsby, D. C. Ion Channels versus Ion Pumps: The Principal Difference, in Principle. *Nat Rev Mol Cell Biol*, 2009, *10*, 344–352. https://doi.org/10.1038/nrm2668.

(344) Keith M. Erikson; Aschner, M. Manganese: Its Role in Disease and Health. *Met. Ions Life Sci.* **2019**, *19*, 253–266. https://doi.org/10.1515/9783110527872-016.

(345) Nazanin Abbaspour; Richard Hurrell; Hurrell, R. F.; Roya Kelishadi. Review on Iron and Its Importance for Human Health. *J. Res. Med. Sci.* **2014**, *19* (2), 164–174.

(346) Keiko Yamada; Yamada, K. Cobalt: Its Role in Health and Disease. *Met. Ions Life Sci.* **2013**, *13*, 295–320. https://doi.org/10.1007/978-94-007-7500-8_9.

(347) Zamble, D. Introduction to the Biological Chemistry of Nickel. *Biological Chemistry of Nickel*, 2017, *10*, 1–11. https://doi.org/Book_Doi 10.1039/9781788010580.

(348) Festa, R. A.; Thiele, D. J. Copper: An Essential Metal in Biology. *Curr Biol*, 2011, *21*, R877-83. https://doi.org/10.1016/j.cub.2011.09.040.

(349) Mendel, R. R.; Bittner, F. Cell Biology of Molybdenum. *Biochim Biophys Acta*, 2006, *1763*, 621–635. https://doi.org/10.1016/j.bbamcr.2006.03.013.

(350) Nelson, N. Metal Ion Transporters and Homeostasis. *EMBO J*, 1999, *18*, 4361–4371. https://doi.org/10.1093/emboj/18.16.4361.

(351) Ma, Z.; Jacobsen, F. E.; Giedroc, D. P. Coordination Chemistry of Bacterial Metal Transport and Sensing. *Chem Rev*, 2009, *109*, 4644–4681. https://doi.org/10.1021/cr900077w.

(352) Narayanan, N.; Beyene, G.; Chauhan, R. D.; Gaitan-Solis, E.; Gehan, J.; Butts, P.; Siritunga, D.; Okwuonu, I.; Woll, A.; Jimenez-Aguilar, D. M.; Boy, E.; Grusak, M. A.; Anderson, P.; Taylor, N. J. Biofortification of Field-Grown Cassava by Engineering Expression of an Iron Transporter and Ferritin. *Nat Biotechnol*, 2019, *37*, 144–151. https://doi.org/10.1038/s41587-018-0002-1.

(353) Stanton, C.; Sanders, D.; Kramer, U.; Podar, D. Zinc in Plants: Integrating Homeostasis and Biofortification. *Mol Plant*, 2022, *15*, 65–85. https://doi.org/10.1016/j.molp.2021.12.008.

(354) Yang, Z.; Yang, F.; Liu, J. L.; Wu, H. T.; Yang, H.; Shi, Y.; Liu, J.; Zhang, Y. F.; Luo, Y. R.; Chen, K. M. Heavy Metal Transporters: Functional Mechanisms, Regulation, and Application in Phytoremediation. *Sci Total Environ*, 2022, *809*, 151099. https://doi.org/10.1016/j.scitotenv.2021.151099.

(355) Kozminska, A.; Wiszniewska, A.; Hanus-Fajerska, E.; Muszynska, E. Recent Strategies of Increasing Metal Tolerance and Phytoremediation Potential Using Genetic Transformation of Plants. *Plant Biotechnol Rep*, 2018, *12*, 1–14. https://doi.org/10.1007/s11816-017-0467-2.

(356) Navarro, C. A.; von Bernath, D.; Jerez, C. A. Heavy Metal Resistance Strategies of Acidophilic Bacteria and Their Acquisition: Importance for Biomining and Bioremediation. *Biol Res*, 2013, *46*, 363–371. https://doi.org/10.4067/S0716-97602013000400008.

(357) Antonucci, I.; Gallo, G.; Limauro, D.; Contursi, P.; Ribeiro, A. L.; Blesa, A.; Berenguer, J.; Bartolucci, S.; Fiorentino, G. Characterization of a Promiscuous Cadmium and Arsenic Resistance Mechanism in Thermus Thermophilus HB27 and Potential Application of a Novel Bioreporter System. *Microb Cell Fact*, 2018, *17*, 78. https://doi.org/10.1186/s12934-018-0918-7.

(358) He, G.; Tian, W.; Qin, L.; Meng, L.; Wu, D.; Huang, Y.; Li, D.; Zhao, D.; He, T. Identification of Novel Heavy Metal Detoxification Proteins in Solanum Tuberosum: Insights to Improve Food Security Protection from Metal Ion Stress. *Sci Total Environ*, 2021, *779*, 146197. https://doi.org/10.1016/j.scitotenv.2021.146197.

(359) Lee, J.; Bae, H.; Jeong, J.; Lee, J. Y.; Yang, Y. Y.; Hwang, I.; Martinoia, E.; Lee, Y. Functional Expression of a Bacterial Heavy Metal Transporter in Arabidopsis Enhances Resistance to and Decreases Uptake of Heavy Metals. *Plant Physiol*, 2003, *133*, 589–596. https://doi.org/10.1104/pp.103.021972.

(360) Jeong, J.; Walker, J. M.; Wang, F.; Park, J. G.; Palmer, A. E.; Giunta, C.; Rohrbach, M.; Steinmann, B.; Eide, D. J. Promotion of Vesicular Zinc Efflux by ZIP13 and Its Implications for Spondylocheiro Dysplastic Ehlers-Danlos Syndrome. *Proc Natl Acad Sci U S A*, 2012, *109*, E3530-8. https://doi.org/10.1073/pnas.1211775110.

(361) Jiang, Y.; MacRenaris, K.; O'Halloran, T. V.; Hu, J. Determination of Metal Ion Transport Rate of Human ZIP4 Using Stable Zinc Isotopes. *bioRxiv*, 2024. https://doi.org/10.1101/2024.05.20.594990.

(362) Arnold, F. H. Innovation by Evolution: Bringing New Chemistry to Life (Nobel Lecture). *Angew Chem Int Ed Engl*, 2019, *58*, 14420–14426. https://doi.org/10.1002/anie.201907729.